OUKA
The University of Osaka
Institutional Knowledge Archive

Title	In-situ Monitoring of GaN Synthesis Parameters in the Na-flux Method using Electroresistometry
Author(s)	Tandryo, Ricksen
Citation	大阪大学, 2023, 博士論文
Version Type	VoR
URL	https://doi.org/10.18910/92951
rights	
Note	

The University of Osaka Institutional Knowledge Archive : OUKA

https://ir.library.osaka-u.ac.jp/

The University of Osaka

Doctoral Dissertation

In-situ Monitoring of GaN Synthesis Parameters in the Na-flux Method using Electroresistometry

Ricksen Tandryo

June 2023

Graduate School of Engineering
Osaka University

Abstract

Gallium Nitride (GaN) is a wide bandgap semiconductor that has attracted considerable interest as a potential cornerstone for the next generation of semiconductors. It is widely employed in optoelectronic devices like Light-Emitting Diodes (LEDs) and Laser Diodes (LDs). Furthermore, GaN's excellent physical properties, including high breakdown field and high saturation velocity, make it a perfect fit for high-voltage and high-frequency power device applications. However, the synthesis of bulk GaN crystals is both costly and challenging, with immature technology leading to less than perfect crystal quality. Significant progress in creating high-quality, affordable GaN substrates is eagerly awaited as a crucial milestone that will enable the rapid dissemination of GaN-based devices.

The Na-flux method, which uses a Ga-Na liquid metal mixture for GaN crystallization, has garnered attention due to the high structural quality, low defects, and impurities of the resulting GaN crystal. However, the high temperature, high pressure, and corrosive nature of Ga and Na preclude direct observation of the growth process in the Na-flux growth system. This has resulted in the Na-flux system being referred to as a "black box", and improving crystal quality is a systematic and time-consuming process. To shed light on this "black box", the dissertation presents an in-depth study of innovative in-situ technology, electroresistometry, designed for process monitoring during GaN synthesis using the Na-flux method.

Chapter 1 outlines the potential of wide-bandgap semiconductors for energy-saving strategies, and the challenges facing the widespread implementation of GaN due to issues related to material availability and synthesis difficulties. The need for in-situ technologies to aid in semiconductor material development is highlighted.

Chapter 2 discusses the current status of bulk GaN crystal growth, focusing on growth mechanisms, technological advancements, and existing challenges in the Na-flux method. The author highlights the difficulties in producing high-quality bulk GaN crystals and discusses current solutions and techniques.

Chapter 3 introduces electroresistometry, an in-situ monitoring technique for the Na-flux method, which measures the electrical resistance of the Ga-Na solution used in GaN crystal growth. Preliminary electroresistometry experiments are performed to verify the accuracy of the system.

Chapter 4 explores the fundamental behaviors of the Ga-Na solution through electroresistometry, studying the dissolution of nitrogen and the impact of adding carbon to the solution.

Chapter 5 applies the insights gained from electroresistometry to monitor GaN crystal growth in the Na-flux method, introducing a dipping method for precise control over crystal positioning and observing changes in resistance during the growth process.

Chapter 6 demonstrates potential applications of the insights obtained from in-situ electroresistometry of the Ga-Na solution. Using a novel proposed temperature profile based on the insights from electroresistometry, improvement in growth rate, nucleation, and effective process time in the Na-flux GaN crystal growth was achieved. Additionally, the utilization of electroresistometry as a tool to investigate the effect of impurity on the Ga-Na solution was also demonstrated.

Chapter 7 provides a summary of the dissertation and a discussion on the future development and potential applications of electroresistometry.

Acknowledgements

This dissertation is the result of my Ph.D. studies conducted at Osaka University, Japan, and I am deeply grateful to all the individuals who have supported and encouraged me throughout this journey.

First, I would like to express my sincere gratitude to Professor Yusuke Mori for his invaluable advice, sincere encouragement and motivation, and inspiring research philosophy. I am indebted to direct guidance of Associate Professor Masayuki Imanishi for this research topic. Without his tireless encouragement and inspiring advice, I would not be able to write this dissertation. I am also grateful for insightful, critical, and constructive advices and comments from Professor Kazunobu Kojima and Visiting Professor Shoichi Mitsui through refereeing this dissertation.

I would like to express my gratitude for valuable advices and stimulating comments from Professor Mihoko Maruyama, Professor Masashi Yoshimura, Assistant Professor Shigeyoshi Usami through fruitful discussion.

During my study at Osaka University, I would like to express my gratitude for guidance from Professor Mitsuhiro Katayama, Professor Ryuji Katayama, Professor Masahiko Kondou, Professor Masanori Ozaki, Emeritus Professor Yagi Tetsuya, Emeritus Professor Toshimichi Ito, Professor Nobuya Mori, Professor Tetsuya Hirose, Professor Masayoshi Tonouchi and all other professors in the Division of Electrical Electronics and Infocommunications.

I would like to express my thanks to individuals who cooperated and involved in this study. I am indebtful for the cooperation from Dr. Kosuke Murakami. With his help, I can construct the electroresistometry apparatus as designed. He also taught me about programming, automating data acquisition, and 3D-CAD for designing the measurement system. I am grateful for the insightful, constructive advice and fruitful discussion with Dr. Hitoshi Kubo. Recognizing the difficulty of measuring low-resistive liquid materials, number of advices coming from his expertise in electrical circuits have helped me improve the measurement system with lesser noise. I would also express my gratitude to Mr. Koichi Itozawa, Mr. Junpei Fujiwara as fellow in-situ monitoring group members. Development of the electroresistometry technique would not have been achievable without their cooperation.

I would like to express my gratitude to Mr. Eisuke Sawai of Frontier Alliance, LLC for his help in slicing and polishing the crystal sample.

I would like to express my thanks to numbers of assistance and cooperation from wide-bandgap group researchers, Ms. Tomoko Kitamura, Ms. Kanako Okumura, Mr. Keisuke Kakinouchi, Mr. Kosuke Nakamura, Mr. Yuki Sakamoto, Mr. Norifumi Murashima, Mr. Kenichi Kawabata, Mr. Keisuke Hosokawa, Mr. Tatsuo Ozeki, Mr. Toshihide Takagaki, Mr. Akira Kitamoto, Mr. Haruya Kobayashi, Mr. Takahiro Oshiba, Ms. Ritsuko Higashiyama, Ms. Miyuki Kagawa.

My special thanks to fellow members of wide-bandgap group Dr. Takumi Yamada, Mr. Ryusei Kuramoto, Mr. Masatoshi Hayashi, Mr. Yohei Yamaguchi, Mr. Kim Do Hun, Mr. Yoshikazu Gunji, Mr. Yuki Sawada, Mr. Naoki Takeda, Mr. Endo Kiyoto, Mr. Shintaro Tsuno, Mr. Keiju Ishibashi, Mr. Hyoga Yamauchi, Mr. Ayumu Shimizu, Mr. Hiroaki Mifune Mr. Itsuki Kawanami, Mr. Keisuke Takiwaki, Ms. Hibiki Takahashi, Mr. Haruki Kitano, Mr. Shogo Washida, Ms. Bhavpreeta Pratap Charan, Mr. Yuki Sakurai, Ms. Masami Aihara, Mr. Yu Sumitani, Mr. Tomohiro Shiraishi, Mr. Daisuke Yamada, Mr. Masashi Sekine, Mr. Tsubasa Nakazono, Mr. Ryoutaro Sasaki, Mr. Takumi Miyamoto, Mr. Pan Jinchi.

I would like to express my thanks to members of other groups in Mori Lab, Dr. Yoshinori Takahashi, Dr. Ryota Murai, Dr. Kazuhisa Matsumoto, Mr. Hideo Takazawa, Ms. Keiko Hino, Mr. Jun Tanikawa, Mr. Kentaro Ueda, Mr. Keita Shikata, Mr. Kosuke Nii, Mr. Taishi Fukuhara, Mr. Riki Fujimoto, Mr. Haruka Ogawa, Mr. Koichi Sawada, Dr. Yasunori Tanaka, Dr. Yuka Tsuri, Ms. Nana Inaoka, Mr. Yutaka Maegaki, Ms. Yuriko Takahashi, Mr. Youta Ishihara, Mr. Kouta Sekigawa, Mr. Yoshiki Tada, Mr. Ryo Noguchi, Mr. Yuto Matsumi, Mr. Uta Michibata, Mr. Nagi Yamamoto, Mr. Yuga Ono, Mr. Yoshihiro Kataoka, Mr. Taiki Watanabe, Mr. Kyousuke Shimada, Mr. Tomoya Hatakeyama.

I would like to express my gratitude to my fellow colleague in Mori Lab, Mr. Kuniaki Atagi, Mr. Ryosuke Ishikawa, Mr. Hiromi Sugishima, Mr. Shota Kusumi, Mr. Masahiro Kamiyama, Mr. Tatsuhiko Nakajima, and Mr. Kazuma Hamada whom I spent sharing pleasant time in our laboratory life, along with numerous meals, drinks and chats. My special thanks to Mr. Tatsuhiko Nakajima and Mr. Kazuma Hamada for sharing laboratory life as Ph.D. students.

I would like to express my thanks to lab secretary Ms. Saori Kataoka, Ms. Sachiko Okamoto, Ms. Yurie Ishii, Ms. Kubo Yumi, Ms. Reiko Otsuki, Ms. Megumi Tanaka, Ms. Kazumi Shimada who made the necessary arrangement and kindly supported the conduct of research and completion of this work.

I would like to express my gratitude and acknowledge the financial support and scholarship from MEXT (2014–2019) and Matsuda Yosaichi Scholarship (2019–2020). This work was supported in part by the Japanese Society for the Promotion of Science through the Grant-in-Aid for Research Fellow (Project No. 21J201580, 2021–2024).

I sincerely wish to thank individuals who give their heartful encouragement, and warmful support through the prayers. I would like to thank my family for their understanding, and yet far from overseas give me support and heartfelt encouragement through their prayers.

Ricksen Tandryo

Osaka, June 2023

Contents

Abstract **i**

Acknowledgements **iii**

Contents **ix**

List of Figures **xvi**

List of Tables **xvii**

Chapter 1: Introduction **1**

1.1 Wide-bandgap semiconductors 2
1.2 Gallium Nitride: A versatile compound semiconductor 4
1.2.1 Optical devices 6
1.2.2 Power devices 9
1.2.3 Challenges from the material synthesis point of view 11
1.3 In-situ monitoring in semiconductor crystal growth 14
1.4 Purpose and outline of this study 15
References 18

Chapter 2: GaN crystal growth by Na-flux Method **23**

2.1 Na-flux compared to other methods 24
2.2 Growth mechanism of Na-flux growth 29
2.2.1 Driving force of Na-flux growth 29
2.2.2 Role of Na in the Ga-Na solution 30
2.3 Na-flux growth technology and its recent progress 31
2.3.1 Carbon additive for nucleation control 31
2.3.2 Liquid Phase Epitaxy (LPE) growth 33
2.3.3 Point seed and coalescence growth technique 33
2.3.4 Flux-film-coated (FFC) technology 37
2.4 Attempts on elucidating growth mechanism 39
2.5 Summary 40
References 41

Chapter 3: Design of electroresistomtery system **45**
3.1 Electroresistometry as inspection tool 45
3.2 Electrical resistance measurement method in the Na-flux growth 46
3.2.1 Technical considerations for accurate measurement 47
3.2.2 Materials consideration: electrode 49
3.2.3 Probe design 51
3.2.4 Final design and measurement method 51
3.3 Operational test: Preliminary experiments 52
3.3.1 Testing Procedure 53
3.3.2 Measurement of pure Ga 53
3.3.3 Measurement of pure Na 55
3.3.4 Measurement of the Ga-Na solution 56
3.4 Summary 59
References 59

Chapter 4: Nitrogen dissolution process in Ga-Na solution **61**
4.1 Homogenization of Ga-Na solution 62
4.1.1 Measurement in Ar atmosphere 62
4.1.2 Interpretation on increasing electrical resistance curve 63
4.1.3 Investigation on Homogenization velocity 66
4.2 Kinetics of nitrogen dissolution in Ga-Na solution 71
4.2.1 Measurement in nitrogen atmosphere 71
4.2.2 Interpretation on linear increase in resistance 72
4.2.3 Time dependence 74
4.2.4 Temperature dependence 80
4.3 Effect of carbon addition in the Ga-Na solution 86
4.3.1 Measurement of carbon-added Ga-Na solution 86
4.3.2 Volume dependence 87
4.3.3 Nitrogen pressure dependence 88
4.3.4 Measurement in argon atmosphere 89
4.3.5 Signification of peak 92
4.4 Summary 93
References 95

Chapter 5: In-situ monitoring of GaN growth via electroresistometry **97**
5.1 In-situ monitoring system set up for Na flux growth 97
5.2 Demonstration of in-situ growth monitoring via electroresistometry 98
5.2.1 Experimental procedure 98
5.2.2 Changes in electrical resistance during growth sequence 99
5.2.3 Steep changes by substrate immersion 100

5.2.4 Monotonous decrease in electrical resistance during GaN growth . . 101
5.3 In-situ electroresistometry of Na flux growth with various growth rate . . . 102
5.3.1 In-situ growth monitoring on varying N_2 pressure 102
5.4 Discussion 107
5.5 Summary 112
References 113

Chapter 6: Application of insights from in-situ electroresistometry 115
6.1 Dynamic temperature growth for enhanced nitrogen dissolution 115
6.1.1 Improvement in growth rate 116
6.1.2 Investigation of desorption properties 120
6.1.3 Shortening the pre-growth holding period 122
6.1.4 Improvement in nucleation 124
6.2 Inspection tool for impurity effect 126
6.2.1 Promotive impurity 127
6.2.2 Inhibitive impurity 127
6.3 Summary 131
References 132

Chapter 7: Conclusions 133
7.1 Conclusions 133
7.2 Future outlooks 136

Appendix A: Lesson from Innovation Design Course 139
A.1 Review on in-situ electroresistometry technology 139
A.1.1 Background 140
A.1.2 Understanding the essence and application of the in-situ electroresistometry 141
A.1.3 Identifying the customers (user) of in-situ electroresistometry . . . 142
A.1.4 Potential Competitors 142
A.1.5 Vision and goal of in-situ electroresistometry 142
A.2 Direct discussion with industry professionals (mentors) 143
A.2.1 Improving reproducibility: monitoring of impurity in Ga-Na solution 144
A.2.2 Other Applications 146
A.3 Summary 147
References 148

List of Publication 149

List of Figures

1.1 The unipolar limits of Si, SiC, and GaN 5
1.2 Crystal structure of hexagonal GaN. 6
1.3 Bandgap and a-axis lattice constant of III-Nitrides (AlN, GaN, InN) semiconductor. 7
1.4 Comparison of wafer and epitaxy costs (per area) and the mainstream and trending diameters of different wafer structures for power devices 12
1.5 Proposed in-situ monitoring technique for Na-flux method by electroresistometry of the Ga-Na solution. Electrical resistance of the solution contained valuable information such as homogeneity and the amount of dissolved GaN. 16

2.1 Schematic illustration of ammonothermal (a) basic, (b) acidic growth reactor. 26
2.2 Schematic illustration of solubility of GaN, solubility of N, and supersaturation concept in Na-flux method. 30
2.3 (a) Schematic drawing of LPE growth in the Na-flux method. (b) Dependence of LPE and polycrystal yield on the addition of carbon. Reprinted from [48] with permission. 32
2.4 (a) Schematic illustration of LPE sample for TEM observation. (b) Cross-sectional TEM image taken around the interface between MOCVD-GaN and LPE-GaN. (c) Enlarged view of TEM from Fig. 2.4b [56]. 34
2.5 Schematic illustration of two-step dislocation reduction [58]. 35
2.6 (a) Schematic drawing of point seed technique growth by mounting on sapphire mask [59]. (b) Photograph of well-faceted bulk GaN crystal grown with point-seed technique. 35
2.7 Schematic illustration of coalescence growth process on a multi-point seed (MPS) GaN substrate. 36
2.8 Schematic illustration of growth process combined multi-point seed and flux-film coated (MPS-FFC) technology [67, 68]. 38
2.9 (a) Cross-sectional cathodoluminescence image of crystal grown with multi-point seed and flux-film coated (MPS-FFC) technique. (b) Schematic drawing of Fig. 2.9a [67]. 38

3.1 Configuration of two-point probe resistance measurement. 47

3.2 Configuration of four-point probe resistance measurement. 48
3.3 (a) Schematic drawing of 4-point probe design for electrical resistance measurement in the Na-flux method. (b) Photograph of the prepared probe. . 51
3.4 Elecroresistometry system for in-situ monitoring of Ga-Na solution in the Na-flux method. 52
3.5 Temperature dependence of electrical resistivity of Ga measured in crucible with inner diameter 17 mm. 54
3.6 Temperature dependence of electrical resistivity of Ga measured in crucible with inner diameter 10 mm. 55
3.7 Temperature dependence of electrical resistivity of Na. 56
3.8 (a) Electrical resistance of Ga-Na and the corresponding temperature profile. (b) Resistance versus temperature plot from Fig. 3.8a. 58
3.9 Ga-Na phase diagram. Reprinted from [18] with permission. 58

4.1 Systematic analysis for interpreting the electrical resistance of Ga-Na solution. 62
4.2 Measurement and temperature sequence of electroresistometry experiments. Electrical resistance measurement starts when the vessel reach its target temperature. 63
4.3 Changes of electrical resistance of the Ga-Na solution subjected to a constant argon atmosphere at 870 °C. 64
4.4 Repeated measurement of Ga-Na solution (with reference to Fig. 4.3). . . . 64
4.5 Changes of electrical resistance of liquid Ga and Na subjected to a constant argon atmosphere at 870 °C. 65
4.6 Changes of electrical resistance of the Ga-Na solution with Ga:Na composition of 27:73 mol %. 67
4.7 Changes of electrical resistance of the Ga-Na solution with Ga:Na composition of 20:80 mol %. 68
4.8 Changes of electrical resistance of the Ga-Na solution with Ga:Na composition of 13:87 mol %. 69
4.9 Arrhenius plot of homogenization reaction rate constant of Ga-Na solution. 70
4.10 Changes of electrical resistance of the Ga-Na solution subjected to a constant nitrogen atmosphere at 870 °C. 72
4.11 Schematic illustration of comparison between the normalized resistance of Ga-Na solution measured in argon and nitrogen atmosphere. Residual linear increase in electrical resistance when measured in the nitrogen atmosphere is assumed to indicate the amount of dissolved nitrogen in the solution. 73

4.12 (a) Schematic drawing of the pattern of multi-point seed substrate and (b) temperature sequence used for ex-situ crystal growth investigation. 74
4.13 Scanning electron microscope images of GaN crystal grown on a MPS substrate at 870 °C with various pre-growth holding period. 75
4.14 Pre-growth holding period dependence of yield and thickness of the GaN crystal growth in Ga-Na solution. 76
4.15 Illustration of nitrogen dissolution process and captures of Ga free electron by formation of Ga-N bonding. 77
4.16 Backpressure profile monitored during (a) measurement of electrical resistance of Ga-Na solution in argon atmosphere and (b) during heating of an empty pressure-resistant vessel. 78
4.17 Nitrogen pressure decay during measurement of electrical resistance of Ga-Na solution in nitrogen atmosphere (Fig. 4.10). Total absorption of N_2 (green) was calculated from pressure decay by applying ideal gas law. . . . 79
4.18 Changes of electrical resistance of the Ga-Na solution in nitrogen atmosphere at 840 °C. 81
4.19 Changes of electrical resistance of the Ga-Na solution in nitrogen atmosphere at 870 °C. 82
4.20 Changes of electrical resistance of the Ga-Na solution in nitrogen atmosphere at 900 °C. 82
4.21 Changes of electrical resistance ratio of Ga-Na solution over time at different temperature. 83
4.22 Scanning electron microscope images of GaN crystal grown on a MPS substrate at 900 °C with various pre-growth holding period. 84
4.23 Evaluation of width and thickness of GaN crystals grown at 870 °C and 900 °C. Thickness was measured as the height of truncated hexagonal pyramid. Width was measured as the distance between opposing *m*-plane facets. The dashed lines indicate the guideline. 84
4.24 Changes of electrical resistance of the Ga-Na solution added with carbon. . 87
4.25 Changes of electrical resistance of the Ga-Na-C-N solution at liquid level of (a) 18 mm and (b) 24 mm. 88
4.26 Changes of electrical resistance of the Ga-Na solution and pressure dependence of the peaks appearing in the Ga-Na-C-N system. 90
4.27 Changes of electrical resistance of the Ga-Na-C solution measured in the argon atmosphere. Inset photograph shows the graphite that was recovered post-measurement. The graphite remained solid, the same state as that before the melting process. 91

4.28 Scanning electron microscope images of GaN crystal grown on a MPS substrate in carbon added Ga-Na solution at 870 °C with various pre-growth holding period. 93

4.29 Pre-growth holding period dependence of yield and thickness of the GaN crystal growth in carbon-added Ga-Na solution. 94

5.1 (a) Schematic diagram of four-point probe electrical resistance measurement used in Chapter 4. (b) Integration of dipping technique into electroresistometry which allows individual and abritrary control of probe and seed crystal position. 98

5.2 The sequence for in-situ monitoring of GaN crystal growth. 99

5.3 (a) Changes of electrical resistance of Ga-Na solution during crystal growth of GaN. Substrate was immersed at the timing pointed by orange arrow. (b) Photograph of the grown crystal retrieved after measurement. 100

5.4 Changes of electrical resistance of the Ga-Na solution during immersion and pulling of sapphire substrate. 101

5.5 (a) Changes of electrical resistance of Ga-Na solution during in-situ monitoring with various sample. (b) Extract of the graph from Fig. 5.5a after the immersion of substrate. Monotonous decrease in electrical resistance was consistently observed in all samples. (c) Photograph of the GaN crystal retrieved after in-situ monitoring. LPE Yield and the corresponding Ga shifts were calculated. 103

5.6 Two-grid plots showing electrical resistance and nitrogen pressure profile during in-situ electroresistometry (a) without and (b) with the presence seed crystal growth. Extract of the plot from (c) Fig. 5.6a and (d) Fig. 5.6b around the time when experiencing change in pressure. Changes in decreasing rate of electrical resistance (slope) were evident and evaluated with simple linear regression line. (e) Photograph of the crystal grown after in-situ monitoring growth. 105

5.7 Negative derivative plot of electrical resistance from Fig. 5.6d. 106

5.8 Panchromatic cathodoluminescence (CL) cross-section image of the sample (Fig. 5.6e) post in-situ growth monitoring. The white dashed lines delineate regions of distinct CL intensities, highlighting four different zones. 107

5.9 Schematic illustration of Ga consumption during GaN growth. GaN synthesis process consequently resulted in the the decrease of Ga/Na ratio. . . 108

5.10 Na fraction dependence of the electrical resistance of the Ga-Na solution. The observed trend shows a decreasing electrical resistance with increasing Na fraction. All measurements were carried out in an Ar environment, thus eliminating the contribution of nitrogen on the electrical resistance of Ga-Na solution. 109

5.11 (a) Illustrative representation of the increasing growth surface area (indicated by the yellow region) due to the progression of both thick and lateral growth expansion, as modeled from the final crystal shape of the sample in Fig. 5.6e. (b) Cross-sectional representation of how the surface area estimation at a specific crystal thickness (indicated by the black dashed line) is scaled from the final crystal shape. 111

6.1 Temperature sequence of conventional static and dynamic temperature profile. 116

6.2 SEM images of GaN crystal grown with conventional and dynamic temperature growth. 118

6.3 Evaluation of crystal size of GaN grown on point-seed in Ga-Na solution with conventional and dynamic temperature profile. 119

6.4 Changes of electrical resistance ratio of Ga-Na solution measured with conventional and dynamic temperature profile. 121

6.5 Schematic illustration temperature sequence to investigate desorption properties of nitrogen. 122

6.6 Average thickness and width of the grown GaN crystal as the function of second pre-growth holding period. Temperature sequence used for the corresponding growth is shown in Fig. 6.5. 123

6.7 Scanning electron microscope images of GaN crystal grown with short pre-growth holding period. 124

6.8 Scanning electron microscope images of GaN crystal grown on small point seed. 126

6.9 Changes of electrical resistance of the Ga-Na solution in comparison with the added with Li and C. 128

6.10 (a) Changes of electrical resistance ratio of Ga-Na solution incorporated with Si and O. (b) Pressure decay measurement on corresponding solution. 129

6.11 (a) Photograph of the Ga-Na alloy after measurement. Ga-Na solution incorporated with Si precipitated black residue on the surface of alloy. (b) Scanning electron microscope image of the black residue. 130

6.12 Powder X-ray Diffraction (PXRD) analysis of the residue collected from Fig. 6.11a. XRD matches with the pattern of Si_2N_2O. 131

A.1 Schematic illustration of the stages involved in mass production of GaN substrates for subsequent device processing. 141
A.2 Objective and Key Results for development of in-situ electroresistometry technology. 143
A.3 Reproducibility in the Na-flux growth. 144
A.4 Objective and Key Results to achieve improved reproducibility in the Na-flux growth. 145

List of Tables

1.1 Physical properties of major semiconductor materials (basic parameters at room temperature). 3
1.2 Lattice parameters, coefficient of thermal expansion (CTE), and thermal conductivity of substrate materials and their mismatch with GaN. 13

2.1 Comparison of leading techniques for bulk GaN crystal growth. 28

3.1 Candidates for electrode materials. 50

4.1 Measurement conditions of Ga-Na solution. 62
4.2 Measurement conditions and fitted reaction rate constant for investigation of homogenization velocity. 67
4.3 Measurement conditions of Ga-Na solution in nitrogen atmosphere. 71
4.4 Measurement conditions of Ga-Na solution heated at various temperature. 81
4.5 Measurement conditions of Ga-Na solution. 86
4.6 Amount of recovered solid graphite post-melting of Ga-Na-C solution. . . . 92

5.1 Growth parameters for in-situ experiments. 99
5.2 Post-run analysis of compositional shift in comparison to electrical resistance. 112

6.1 Growth parameters for dynamic temperature growth experiment. 117

Chapter 1

Introduction

The world of electronics was revolutionized by the invention of the first point-contact transistor, developed by John Bardeen and Walter H. Brattain [1], followed by invention of junction transistor by William Shockley [2]. This breakthrough led to the development of semiconductor industries, which paved the way for the digital era. The electronics industry, one of the largest in the world, will undoubtedly continue to significantly impact the economy, society, and politics. However, with the rise of big data and Internet of Things (IoT), the demand for energy is increasing, and the energy crisis has become a pressing issue. Despite advances in renewable energy technology, energy production still falls short of meeting demands. While nuclear power has been a clean option for developed countries, the threat of nuclear disasters has raised concerns [3]. As a result, fossil fuels remain the primary energy source, producing harmful CO_2 emissions that have negative environmental effects and contribute to global warming. While everybody is hoping that technological improvement and renewable energy can outpace the increasing demand for energy, the use of fossil fuels and its environmental consequences requires immediate attention to be resolved. A parallel approach by enhancing efficiency or replacing traditional electronics with energy-saving options can help moderate the overall energy consumption.

Semiconductors not only serve as a foundation for computers and modern electronic devices but are also used in the field of power electronics, where they are utilized to convert and control the electrical power. Semiconductors devices used as a switch or rectifiers for power electronics applications are commonly called “power devices”. These devices are recognized for their speed, compactness, and efficiency. The effectiveness of power conversion is largely influenced by the performance of these devices. Currently, when converting electricity, the technology achieves an efficiency rate of around 85–95 %. However, the remaining energy is lost as heat. While this may seem like a high efficiency rate at first glance, when considering the number of devices operating globally, the total energy loss is significant. As such, there is still ample opportunity to improve reducing energy consumption by enhancing the efficiency of power electronics [4].

Nowadays, most power devices are made with silicon (Si) due to advanced technology that produces high-quality wafers with large diameters. The advancement of Si power devices has reached its physical limitation. Nevertheless, the limited critical electric field and poor electric transport properties of Si impede the effectiveness of current power electronic systems and make them bulky. Researchers and engineers have been working hard to overcome the limitations of Si power devices through innovative device structures. However, enhancing their performance remains a challenging task. As a result, there is increasing interest in exploring new semiconductor materials. In recent decades, there has been significant progress in the development of "wide-bandgap" semiconductors, which are considered to be the future of power device materials.

1.1 Wide-bandgap semiconductors

Materials with a band gap larger than 2 electronvolt (eV) are generally known as wide-bandgap semiconductors. This is in contrast to conventional semiconductors like Si, Gallium Arsenide (GaAs), and germanium (Ge), which have bandgaps in the range of 0.6–1.5 eV. Examples of wide-bandgap materials can be found in the IV group, such as diamond and silicon carbide (SiC), the III-V group, such as gallium nitride (GaN) and aluminum nitride (AlN), or the II-VI group, such as gallium oxide (Ga_2O_3). Table 1.1 shows the physical properties of major semiconductor materials. Wide-bandgap semiconductors were not given much attention in comparison to conventional semiconductors until the late 20th century. However, in recent years, wide-bandgap semiconductors have become increasingly popular due to their superior physical properties and potential applications in various fields where Si cannot be used.

- Wide-bandgap permits devices to perform at higher operating temperatures [5] as they can withstand bandgap narrowing with increasing temperature which is problematic for conventional semiconductors. Si-based devices reliably operate only up to 125 °C, whereas wide-bandgap semiconductor devices can operate up to 200 °C as long as the device package can tolerate this.

- Wide-bandgap results in a higher critical electric field allowing the device to operate at a higher voltage application without experiencing breakdown or device failure.

- Most wide-bandgap semiconductors exhibit excellent electrical transport properties, including high electron mobility and high saturation velocity. These properties allow the devices to operate at higher frequencies, achieving higher performance in speed and power efficiency.

The performance of wide-bandgap semiconductor devices is often evaluated using a figure of merit and compared to those made with Si. Baliga's figure of merit is commonly

Table 1.1: Physical properties of major semiconductor materials (basic parameters at room temperature).

Property	Si	GaAs	4H-SiC	GaN
Crystal Structure	Diamond	Zinc blende	4H polytype	Wurtzite
Bandgap E_g [eV]	1.12	1.42	3.26	3.42
Band structure	Indirect	Direct	Indirect	Direct
Electron saturation velocity v_{sat} [$\times 10^7$ cm/s]	1.0	1.0	2.2	2.7
Electron mobility μ [$\mathrm{cm^2/(V\,s)}$]	1350	8500	1000 ($\perp c$) 1200 ($\parallel c$)	1470 (bulk) 2000 (2DEG)
Critical electric field E_{cr} [MV/cm]	0.3	0.3	2.8	3.3
Relative dielectric constant ε_s	11.9	12.9	9.7 ($\perp c$) 10.0 ($\parallel c$)	9.5 ($\perp c$) 10.4 ($\parallel c$)
Thermal conductivity [W/(cm K)]	1.5	0.46	4.9	2.0
Relative Baliga's Figure of Merit $\varepsilon_s \mu E_{cr}^3$	1	6.8	490	1157

used in power electronics applications to depict a material's unipolar limit [6] which is defined by the trade-off relationship between specific on-resistance ($R_{\text{on_sp}}$) and breakdown voltage (V_B). The unipolar limit is usually calculated by the following equation

$$R_{\text{on_sp}} = \frac{4V_B^2}{\varepsilon_s \mu E_{\text{cr}}^3} \tag{1.1}$$

Here, ε_s is the dielectric constant, μ is the mobility, E_{cr} is the critical electric field of the semiconductor. Fig. 1.1 shows the unipolar limit of silicon (Si) [6] in comparison to two potential wide-bandgap alternatives for power electronics, silicon carbide (SiC) [7] and gallium nitride (GaN) [8]. SiC and GaN have a high critical electric field of approximately ~3 MV/cm, which is roughly ×10 greater than that of Si. As a result, based on equation Equation (1.1), the specific-on-resistance limit can be reduced to ×1/1000. SiC and GaN have the potential to create devices that are ten times smaller due to their low specific on-resistance at higher breakdown voltage. This allows fabrication of simplified and miniaturized devices. Additionally, heat dissipation from the intrinsic resistance of the semiconductor is minimized, resulting in power electronics efficiency closer to ~99 %. SiC and GaN have been actively researched since 2000 and have experienced rapid growth around the 2010s. They are considered the next generation of energy-saving devices.

1.2 Gallium Nitride: A versatile compound semiconductor

GaN is a type of compound semiconductor that is known for its unique and highly desirable material properties. One of the most notable features of GaN is its large bandgap, which is measured at 3.42 eV. This is significantly higher than the bandgap of other commonly used semiconductors such as Si, which has a bandgap of only 1.12 eV, and 4H-SiC, which has a bandgap of 3.26 eV. Another key advantage of GaN is that it has a direct bandgap, which is shared by other materials in the III-Nitride family such as Aluminum Nitride (AlN) and Indium Nitride (InN). In addition, GaN has a stable structure known as wurtzite (Fig. 1.2), which is also found in AlN and InN. This allows for alloying and heterostructure, making it ideal for optoelectronics applications such as light-emitting diode (LED) and laser diode (LD). Today, GaN-based materials are mainly used for optical devices. In 2014, Akasaki, Amano, and Nakamura were awarded the Nobel Prize in Physics "for the invention of efficient blue light-emitting diodes which has enabled bright and energy-saving white light sources" [9–11]. The combination of GaN-based blue LEDs and yellow phosphorescence creates white lighting that now illuminates our world with up to 90 % more energy efficiency than traditional bulbs.

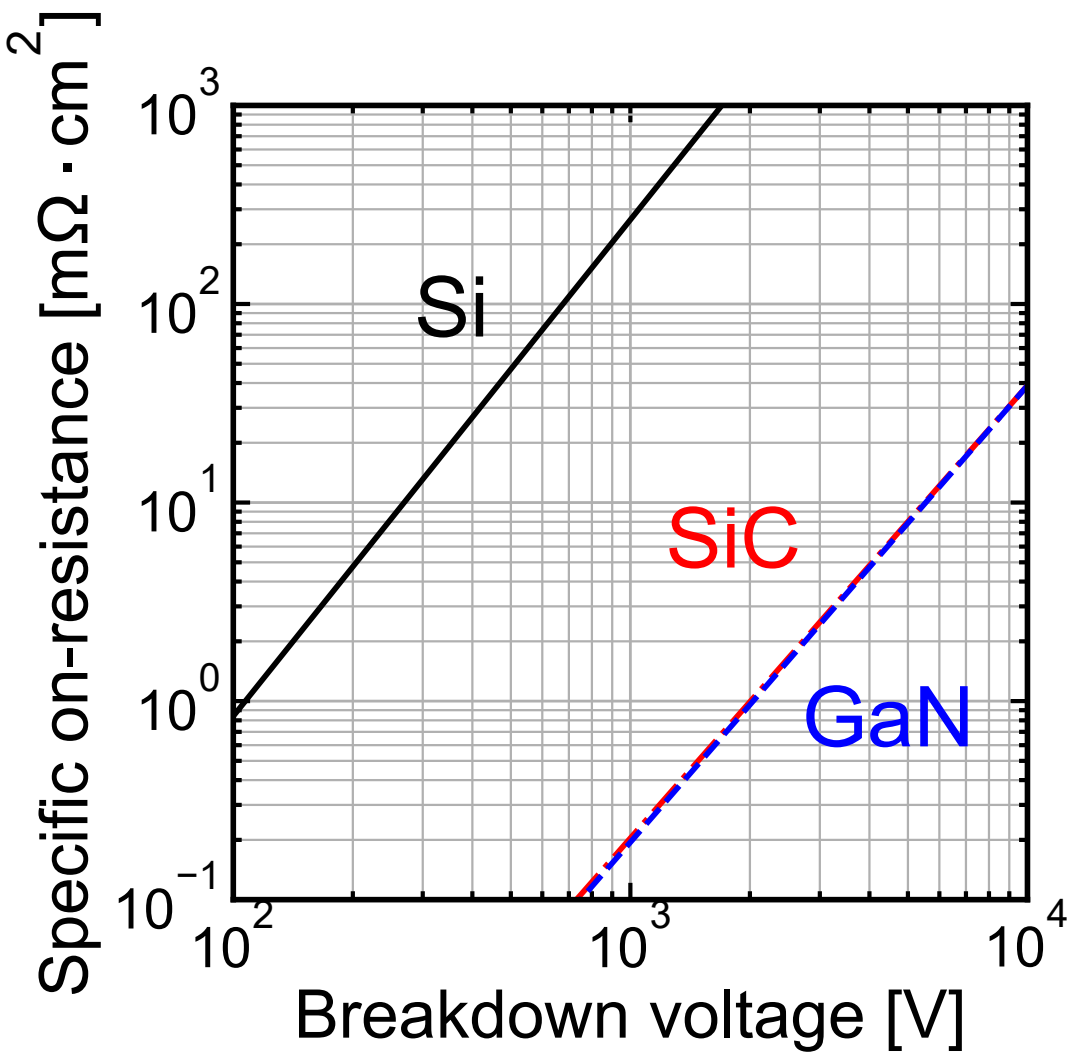

Figure 1.1: Trade-off relationship between specific-on resistance and breakdown voltage in Si [6], SiC, and GaN unipolar devices. The unipolar limit of SiC [7] and GaN [8] is drawn using recently reported updated relationship.

III-Nitrides semiconductors possess exceptional electrical properties due to their unique feature of availability for alloying and heterostructure. The AlGaN/GaN interface generates a two-dimensional electron gas (2DEG) [12] owing to the combination of internal spontaneous and stress-induced piezoelectric polarization fields and band offsets [13]. This structure is known as the high electron mobility transistor (HEMT) [14] which was in-

vented on AlGaAs/GaAs heterostructure. AlGaN/GaN HEMT was initially introduced by Asif Khan *et al.* [15]. In recent years, the performance of AlGaN/GaN HEMTs has considerably enhanced, making them ideal for high-frequency and power-related applications. Furthermore, they are being studied for potential use in power switching, biological [16], and sensor applications [17] at lower frequencies.

Although GaN devices have a wide range of applications, their early fabrication was greatly hampered by the challenge of materials synthesis. Due to the unavailability of a suitable substrate, they were mainly fabricated on a lattice-mismatched substrate, resulting in poor device performance. However, in the early 2000s, researchers started actively working on creating high-quality GaN substrates, which have now led to the development of various device structures that require such substrates, including laser diodes and vertical structure power devices.

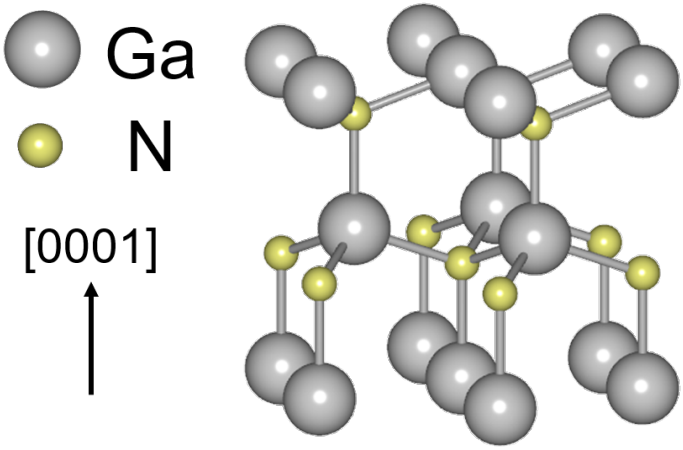

Figure 1.2: Crystal structure of hexagonal GaN.

1.2.1 Optical devices

Figure 1.3 plots the lattice constant and bandgap relationship of AlN, GaN, InN. These III-Nitride materials possess a direct bandgap and share the same stable crystal structure known as wurtzite. By utilizing ternary alloys like AlGaN and InGaN, the bandgap can be adjusted accordingly [18]. This allows for the creation of materials with light-emitting or absorbing properties that can cover a broad spectrum of wavelengths ranging from 200 to 1800 nm. The blue LED was considered to be the final element required for the creation of energy-efficient white lighting. During the late 1960s, efforts to develop blue-emitting devices began to gain momentum. However, GaN, which was believed to be the perfect material for the task, faced significant challenges during its early stages of research. The synthesis process was particularly difficult due to a lack of lattice-match substrate, and as a result, the crystal growth of GaN had to be performed on substrates with a significant lattice mismatch.

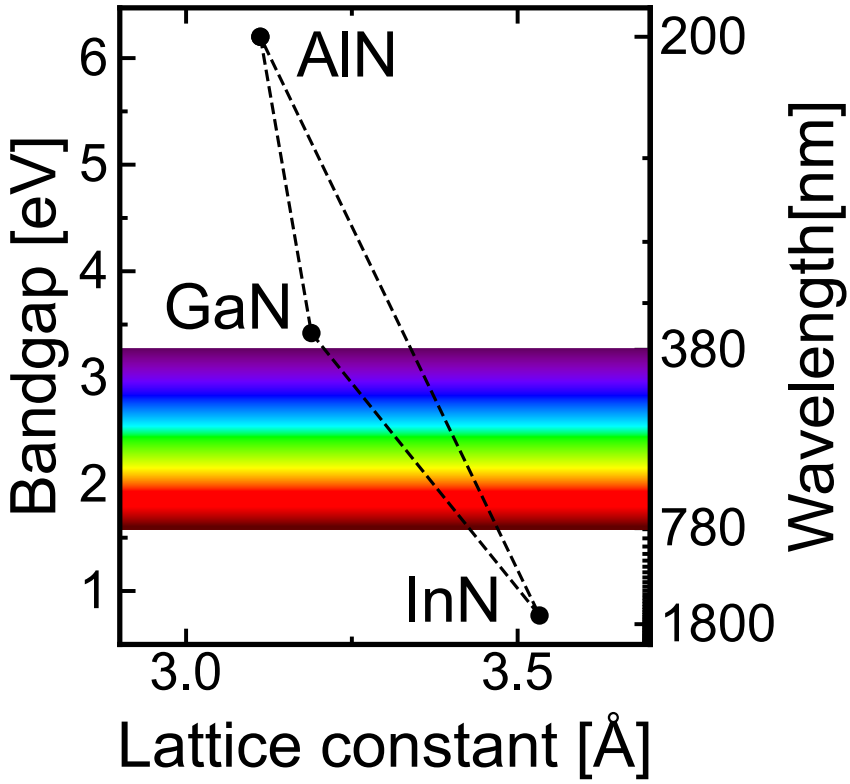

Figure 1.3: Bandgap and a-axis lattice constant of III-Nitrides (AlN, GaN, InN) semiconductor.

Early research

In 1969, Maruska and Tietjen reported the first preparation of a large area of single-crystal GaN layer on a sapphire substrate using hydride vapor phase epitaxy [19]. At that time, the GaN layer exhibited a high defect density and the surface morphology was very poor. Additionally, the high n-type background doping and the deep-ionization levels of common acceptors posed a challenge in growing p-type materials. The first blue electroluminescence was observed by Pankove *et al.* on insulating Zn-doped GaN [20]. Maruska *et al.* used Mg as a luminescent center in a metal-insulating semiconductor (MIS) M-i-n violet LED [21]. Despite the demonstration of LED, luminescence efficiency was very poor.

The problem began to be overcome in the late 1980s. In 1986, Amano *et al.* obtained high-quality GaN layer grown on sapphire substrates by metal organic chemical vapor deposition (MOCVD) following the deposition of AlN buffer layers at low temperature [22]. GaN layer had fairly excellent structural quality and optically flat. Later, Nakamura used the GaN buffer layers to facilitate the growth of high-quality GaN film [23].

Once the quality of the GaN layer was enhanced, the focus shifted towards growing the p-type layer. Unfortunately, the doping of the Mg resulted in an undesirable low doping efficiency. It was only after Amano *et al.* stumbled upon the discovery that low energy electron beam irradiation (LEEBI) [24] treatment could enhance the doping efficiency, which lead to the development of the first GaN UV LED with a p-n junction [24]. Nakamura *et al.* later found that annealing GaN:Mg in N_2 or a vacuum resulted in the material turning into conducting p-type [25]. The Mg acceptor was passivated by a hydrogen atom to form a Mg:H complex [26]. The hydrogen can be released from the complex through the energy of an electron beam or annealing in N_2 or vacuum.

Owing to these findings, Nakamura *et al.* was able to demonstrate high-brightness blue LEDs through the use of a double-heterostructure of InGaN/AlGaN [27]. The InGaN quantum well (active layer) played a significant role in enhancing recombination, resulting in a notable increase in luminescence efficiency. At that time, researchers wondered why the LED could be brightly lit despite the fact that GaN film still included high defect (dislocation) densities of 10^8–$10^{10}\,\mathrm{cm}^{-2}$. In other semiconductor materials, dislocations can impose a deleterious effect on the efficiency of electroluminescence [28, 29]. Moreover, dislocations are also found to act as non-radiative recombination centers (NRCs)[30]. Chichibu *et al.* shed light on the dislocation-insensitive nature of In-containing nitrides. This is due to localized states [31] associated with In-N atomic condensates and the extremely short diffusion length in InGaN, which allow for radiative recombinations to occur before encountering the dislocation-related NRCs [31, 32].

Thanks to these major breakthroughs in technology, GaN-based LEDs are now available for commercial use. These LEDs are primarily made using a GaN-on-Sapphire sub-

strate, which despite having a high level of dislocation, still offer a satisfactory level of luminescence efficiency. However, when it comes to GaN-based LDs, dislocations have been found to shorten the device lifetime of the laser [33, 34]. To create LDs with high power and long lifetimes, a high-quality bulk GaN substrate became necessary. This has become the driving force for the development of bulk GaN.

Even though *c*-plane GaN quality has improved, GaN-based optical devices still face issues due to intrinsic properties like spontaneous polarization, which is a result of the wurtzite structure's asymmetric bonding and stress-induced piezoelectric fields from compounds like InGaN. These properties cause the quantum-confined stark effect [35], which reduces recombination probability, narrows the effective bandgap, and results in the light-emitting devices' drive-current-dependent emission wavelength. To solve this, using a non-polar or semipolar plane with no or a smaller induced electric field is being considered. However, progress in this area is limited by substrate technology, as the fact that high semipolar GaN can only be obtained by slicing from a bulk *c*-plane GaN, which limits the available substrate area. A strategy is being developed to fabricate large-diameter, high-quality GaN on patterned foreign substrates [36].

1.2.2 Power devices

GaN is widely recognized for its excellent properties, such as high critical electric field, high saturation velocity, and high mobility, making it a promising choice for power electronics applications. In the optoelectronics field, nitride semiconductors stand out as the only semiconductor material capable of producing highly bright blue LEDs. However, when it comes to power electronics, GaN faces tough competition from the incumbent Si, which already has low-cost Power MOSFETs and Insulate Gate Bipolar Transistors (IGBTs) available for power applications. To make a mark in this field, GaN must prove to be cost-effective and offer improved performance compared to Si. GaN devices are commonly grown on foreign substrates such as sapphire, Si, and SiC due to the absence of low-cost bulk GaN substrates. GaN on foreign substrates are highly defective due to differences in lattice constant and coefficient of thermal expansion with the underlying material, requiring buffer layers and strain-engineering for device processing.

GaN-on-SiC

As high resistive SiC substrates become available, GaN-on-SiC power devices are becoming increasingly popular for their high-frequency capabilities and suitability for lateral structures [37], due to the electrical insulating properties and excellent thermal conductivity of the underlying SiC substrate. However, issues have been identified with the epitaxial growth. Thermal boundary resistance arises between GaN, AlN nucleation layer, and SiC substrate interfaces, which can cause temperature increases in the device layers [38]. To

reduce threading dislocations in the GaN layers, the thickness must be increased, which requires doping with acceptors such as carbon to suppress parasitic conduction below the conducting channel layer [39]. Unfortunately, this introduces charge trapping and leads to a current collapse at the device, which is a major factor limiting output radio frequency (RF) power. To address current collapse, the thickness of the GaN layer needs to be reduced, making the quality of the AlN nucleation layer crucial [40].

GaN-on-SiC vertical structure power devices are also built on conducting SiC substrates [41–43], but the number of reports become few after GaN substrates became available.

GaN-on-Si

Si is particularly attractive because of its low cost and large wafer diameter (200 mm and higher). However, epitaxy on Si substrate poses various challenges, including large lattice and thermal mismatch. Eutectic etching of Si can be caused by Ga, which requires the deposition of AlN buffer layers [44]. These layers also help to alleviate the stress caused by lattice and thermal expansion mismatch. GaN-on-Si lateral AlGaN/GaN HEMT [45] is increasingly becoming the preferred device for medium power applications due to its ability to provide high power conversion efficiency, reduced form factor, and attractive price, thereby facilitating a broader adoption in the market [46]. Today, 600V-class of GaN-on-Si power transistors are commercially available [47].

Although buffer technology can produce high-quality layers, threading dislocation is still a major concern that leads to current leakage in the vertical structure. However, several research groups have attempted to fabricate vertical GaN-on-Si power devices as vertical structure is excellent for high power application [48–56]. Performance has to be compromised due to reverse leakage current. Control of the carrier concentration to achieve high breakdown voltage is also difficult due to inevitable diffusion of Si from substrate to the device layers [57].

GaN-on-Sapphire

Unlike Si and SiC, epitaxial process on Sapphire substrates is relatively mature due to development in optoelectronics field. It does not require the deposition of thick buffer layers that would add extra cost and processing challenges. Additionally, the insulating property of sapphire is attractive for HEMT structure. However, due to its poor heat transport, the underlying sapphire thickness must be reduced for better thermal resistance [58]. Recently, GaN HEMT on sapphire with the blocking voltage 1200 V was reported [58].

GaN-on-GaN

The high cost and issues with the quality of bulk GaN still hinder the commercialization of the GaN-on-GaN power devices, but progress in material synthesis has enabled bulk GaN, which allowed for the research and demonstration of vertical GaN power devices [59–71]. Recent notable reports include the demonstration of GaN-on-GaN p-n diode with breakdown voltage of 5 kV and on-resistance 1.2 $m\Omega\,cm^2$ reported by Ohta *et al.* [64], 4.9 kV and on-resistance 0.9 $m\Omega\,cm^2$ p-n diode reported by Talesara *et al.* [67], 1.2 kV and on-resistance 0.2 $m\Omega\,cm^2$ vertical FinFET transistor reported by Zhang *et al.* [71].

GaN-on-GaN undoubtedly have superior performance and are quickly approaching their physical limits. Although the fabrication process of the devices are simpler, they are not yet widely available at a low cost. Conversely, GaN-on-Si devices have also seen improved performance through advancements and tricks in epitaxy and processing technology, and have already been adopted in the market. While the potential for further improvements in GaN-on-Si technology remains uncertain, GaN-on-GaN technology seems to be the clear choice for achieving optimal performance and simpler device processing. The main obstacle to developing GaN-on-GaN technology is the limited availability of affordable and acceptable quality GaN substrates.

1.2.3 Challenges from the material synthesis point of view

Material availability is a critical factor in the development of semiconductor devices. Unlike the mainstream semiconductor Si, GaN crystals cannot be grown using the melt growth process. This is because GaN undergoes thermal decomposition before reaching its melting state, which occurs at extremely high temperatures. It has been reported that a nitrogen pressure exceeding 6 GPa is necessary to prevent thermal decomposition and achieve congruent melting [72]. However, such extreme conditions are not practically achievable or economically viable for large-scale production. As a result, GaN is synthesized with other alternative methods. Since the first synthesis by Johnson *et al.* in 1932 [73], and by Juza and Hahn in 1938 [74] who passed ammonia over hot Ga, various GaN crystal growth methods have now been developed [19, 73–77]. Although there have been notable advancements in materials, the existing technology for synthesizing GaN falls short in producing cost-effective high-quality GaN substrates. As a result, as depicted in the Fig. 1.4, the majority of GaN are grown as a thin film on foreign substrates due to their appealing low-cost. Regrettably, the significant lattice mismatch and differences in the coefficient of thermal expansion (CTE) (see Table 1.2) have led to a crystal with a high number of dislocations, crystallographic bowing, and cracks. As a result, GaN on foreign substrates suffer not only from the deteriorated device performance, but they also encounter various challenges in the subsequent device fabrication process as mentioned in the previous section. Development in crystal technology led by three major bulk

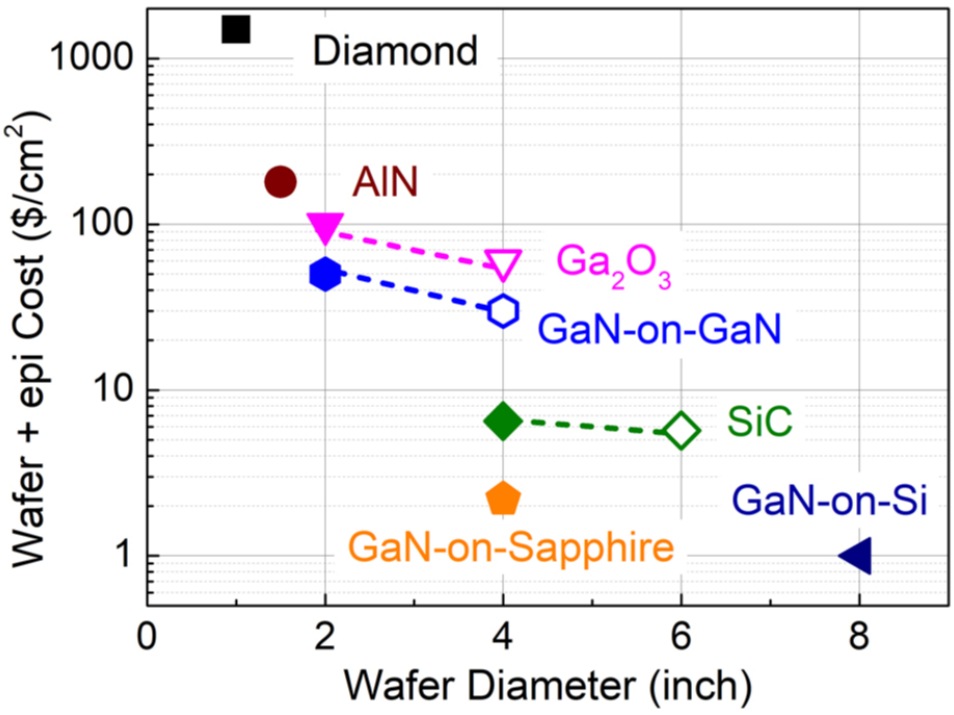

Figure 1.4: Comparison of wafer and epitaxy costs (per area) and the mainstream and trending diameters of different wafer structures for power devices. The solid symbols represent the current mainstream costs, while the dashed lines and hollow symbols indicate the expected or trending costs. Reprinted from [57] with permisson.

crystal growth technique, hydride vapor phase epitaxy (HVPE), ammonothermal, and Na-flux (detailed in the next chapter) have made bulk GaN substrates available. Now, HVPE-GaN substrates are commercially available but as they are obtained through the crystallization using GaN epilayer on the foreign substrate as the seeds, there are still issues remaining.

- Dislocation densities

  Dislocation acts as a non-radiative recombination [30] center as well as lifetime killer in LDs [33, 34]. In power devices, threading dislocation induces current leakage [78] and dislocation densities of the available GaN substrates are ranging from 10^4–10^7 cm^{-2}, which is still too high compared to Si and SiC substrates. Dislocation must be reduced to exhibit the true performance of GaN devices. Dislocation reduction through thick growth is a long challenging process. Reduction mechanisms are more advanced in liquid phase growth such as the ammonothermal and Na-flux method.

- Crystallographic bowing

  The problem of crystallographic bowing is a significant factor in the variation of substrate orientation, specifically the offcut angle. It is crucial to maintain a uniform offcut angle to ensure the consistent epitaxial growth and uniform doping incor-

Table 1.2: Lattice parameters, coefficient of thermal expansion (CTE), and thermal conductivity of substrate materials and their mismatch with GaN.

Property	GaN	Si	6H-SiC	Sapphire
Lattice constant [Å]	$a = 3.189$ $c = 5.186$	$a = 3.84$ (converted to (111))	$a = 3.082$ $c = 15.112$	$a = 4.758$ $c = 12.991$
Lattice Mismatch [%]	0	-17	3.5	16
CTE [10^{-6}/K]	$\Delta a/a = 5.59$ $\Delta c/c = 3.17$	$\Delta a/a = 3.59$	$\Delta a/a = 4.3$ $\Delta c/c = 4.7$	$\Delta a/a = 7.5$ $\Delta c/c = 8.5$
CTE mismatch [%]	0	55.7	33.1	-25.5
Thermal conductivity [W/(cm K)]	2.3	1.5	4.9	0.3-0.5

poration in the epitaxial layer. For a 2-inch GaN wafer, the radius of curvature (ROC) should be at least 15 m [79]. The ROC of GaN wafers produced by HVPE still falls between 5–10 m, while that of ammonothermal and Na-flux methods meet the requirements.

- Purity or controlled doping

  Control of impurities is vital in acquiring the required electrical properties of GaN substrates, especially when considering a specific application or device structure. In the case of vertical power structure devices, it is fundamental to use a conducting substrate (n-type GaN), whereas for lateral structure devices, the use of semi-insulating GaN substrates are typically favored. Therefore, it is preferable to have a controlled doping the process to achieve uniform doping in the substrates. Growth in an ambient with high purity is preferred as the presence of unwanted or parasitic impurities in the growth system can pose serious problems. These could result in an undesirable increase in carrier concentration or lead to the formation of unanticipated deep-level states.

- Cost

  Currently, the cost of GaN substrates remains higher than that of Si or SiC. In order to make them more accessible, manufacturing expenses need to be reduced without compromising quality. This can be achieved through scaling in both lateral

(increasing diameter) and vertical (thickening) GaN wafer size, which is a difficult but promising approach to mass production. Additionally, growth rate is a crucial factor to consider from an economic standpoint.

Meeting the aforementioned requirements not only enhances GaN device performance but also aids in boosting device yield and mitigating issues experienced during epitaxial growth on foreign substrates. This is expected to result in cost reduction for epitaxial growth and subsequent processes. High-quality bulk GaN development will now focus on the crystallization on native bulk GaN as seeds. The task will rely on liquid phase growth methods: ammonothermal and Na-flux methods, as they are excellent for the growth of high-quality GaN crystal. In particular, the Na-flux method, which involves the high-temperature synthesis of GaN in a Ga-Na metal solution under N_2 gas over-pressure, has gained interest due to its world-record 6-inch diameter high-quality GaN substrate [80]. Consistent high-quality production and reproducibility become crucial for the Na-flux method. Realtime observation and access to control important parameters of growth process are ideal for this purpose. However, observing the growth process in the Na-flux growth system is not possible. Due to the adverse conditions of elevated temperature, pressure, and corrosive materials, the Na-flux growth takes place in an enclosed opaque pressure-resistant vessel, preventing optical access inside the vessel. This lack of direct observation limits the process control capability, making it difficult to achieve reproducible industry production. Additionally, the current study of the Na-flux method is restricted to time-consuming ex-situ investigations and simulations, which do not provide a comprehensive understanding of the growth process.

1.3 In-situ monitoring in semiconductor crystal growth

Crystal growth is a multifactor process in which the control of various synthesis parameters (both monitored and unmonitored) is crucial to achieve desired result.

In the crystal growth of semiconductors, the parameters to be monitored can be categorized as follows [81]:

(1) Heating element parameters: voltage, current, and heater power.

(2) Equipment parameters: chamber temperature, chamber pressure, mass-flow parameters, crystal rotation and pulling rates.

(3) Complex parameters: related to heat and mass transfer, including the shape and position of the growth interface, the surface tension and viscosity of the melt, and solution concentration.

(4) Parameters related to characteristics of the crystal, such as its composition, structure, and defects.

The complexities of monitoring and the number of information become larger from (1) to (4). Monitoring (1) and (2) is usually an easy task and a common practice for crystal growers. However, monitoring (3) and (4) requires extra effort, specialized equipment, and dedicated space within the laboratory environment. Despite the tangible challenges, they are an integral part of ensuring the quality and consistency of the crystal growth process.

The development of monitoring techniques has significantly contributed to the progress of semiconductor crystal growth technology. For instance, in the case of Si crystal growth, the use of necking growth can lead to dislocation-free single crystals of Si [82]. However, the crystal's diameter is a crucial factor that needs to be carefully considered. Real-time monitoring of crystal diameter with optical metrology or crystal weighing [83] has resulted in increased crystal yield and minimized diameter loss of Si ingots [84, 85]. In sublimation growth of SiC crystal, Kato *et al.* observed a high density of dislocations using X-ray topography [86]. These dislocations appeared immediately above seeds, highlighting the importance of dislocation and nucleation control during initial growth. Nakamura *et al.* used the interference effect to observe the growth morphology of GaN film on MOCVD growth. The information obtained from this monitoring was utilized to optimize the thickness of the GaN buffer layer [87].

The topic of in-situ technology is relatively new for the Na-flux method, but it is crucial in improving the synthesis process to meet the prescribed requirements for GaN devices. Additionally, much of the potential of the Na-flux method remains untapped due to a limited understanding of its complex parameters, such as solution concentration and uniformity, even after 20 years since its discovery. With an aim to advance our knowledge in this area, the author has delved into the implementation of in-situ technology, recognizing its potential to enhance the synthesis process and crystal yield to meet the required criteria for GaN wafers. The author initially attempted to monitor in-situ Na-flux growth process by evaluating the homogeneity of the Ga-Na solution via measurement of its electrical resistance. After conducting several experiments and systematic analysis, the author discovered that the electrical resistance of the Ga-Na solution not only provides information on homogeneity but also strongly correlates with the nitrogen concentration in the solution, which is a crucial parameter for GaN synthesis [88].

1.4 Purpose and outline of this study

The author proposes the use of electrical resistance measurement (electroresistometry) of Ga-Na solution as a new in-situ monitoring method and investigates the complex parameters involved in GaN. Toward this purpose, first, the author constructs the basis model for interpretation of electrical resistance data and demonstrates how it correlates with GaN synthesis process through systematic measurement and analysis. Based on the

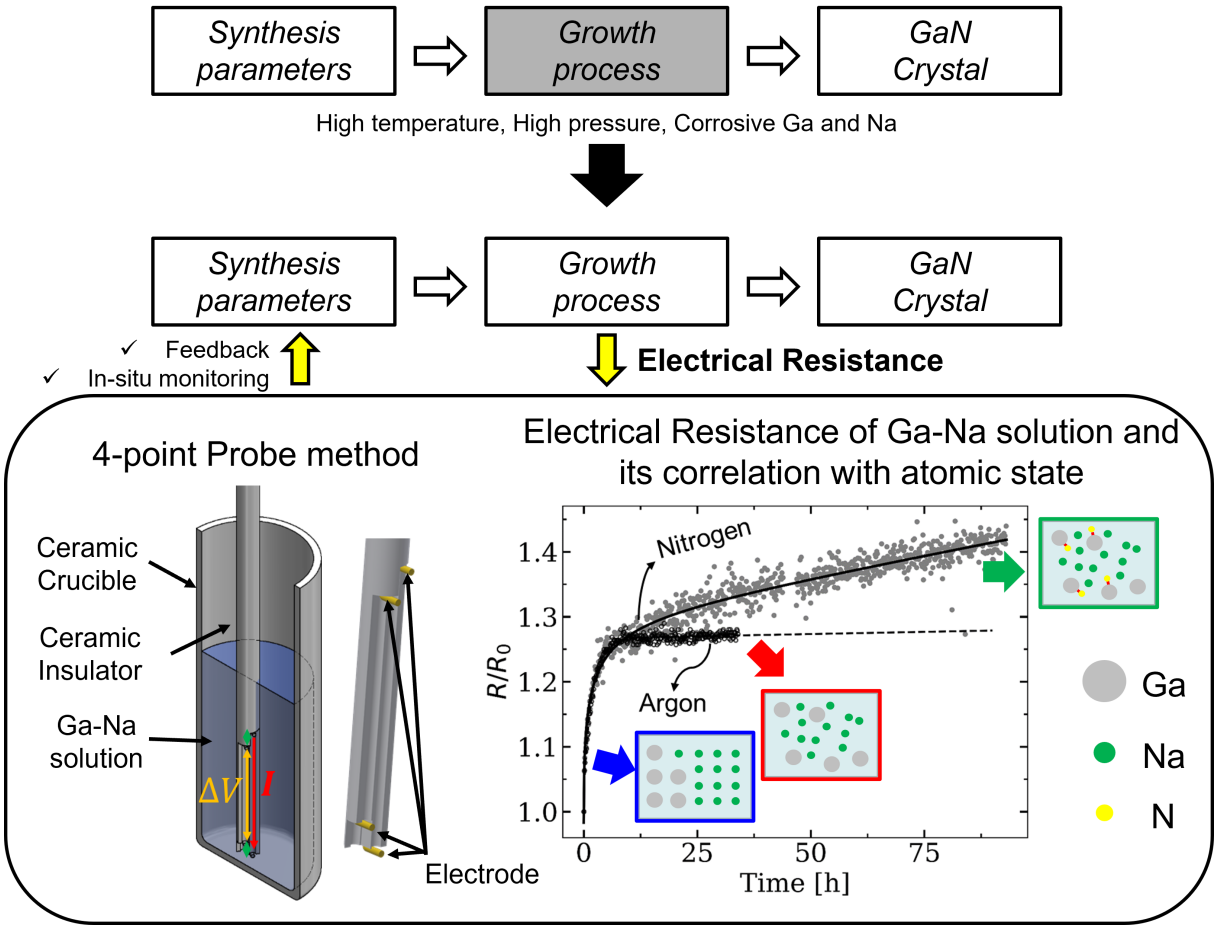

Figure 1.5: Proposed in-situ monitoring technique for Na-flux method by electroresistometry of the Ga-Na solution. Electrical resistance of the solution contained valuable information such as homogeneity and the amount of dissolved GaN.

model, the author studied the process parameters involved in the synthesis of GaN and utilized the new insights for improved GaN crystal growth. Finally, in-situ monitoring of GaN crystal growth is attempted while simultaneously varying the growth parameters.

In Chapter 2, the author describes the status of bulk GaN crystal growth. In particular, the growth mechanism, technological progress, and the challenges in the Na-flux method will be detailed.

In Chapter 3, the author introduces the electroresistometry as a novel in-situ monitoring technique for Na-flux method which involves measuring the electrical resistance of Ga-Na solution used as the solvent to grow GaN crystal. The author first designs the concept of the measurement and performs preliminary electroresistometry experiments by measuring the electrical resistance of pure Ga and Na, comparing the values with literature to test the system's accuracy.

In Chapter 4, the author uses electroresistometry to study the fundamental behavior of Ga-Na solution from its electrical resistance. Starting with the measurement in an argon atmosphere, the author observed the homogenization process of Ga-Na. The author then investigates the parameters in N_2 atmosphere. The author found that the dissolution of nitrogen in Ga-Na solution led to an increase in resistance. With regard to measurement of carbon-added Ga-Na solution, the author describes the finding of peculiar signals related to the formation CN which signifies the state of readiness for GaN synthesis.

In Chapter 5, with the insights obtained and described in Chapter 4, the author advances to use electroresistometry for monitoring of crystal growth process of GaN in the Na-flux method. The author integrates the dipping methods into electroresistometry system, which allows the arbitrary control of the crystal position. Electrical resistance of Ga-Na solution was simultaneously measured during the crystal growth of GaN. The changes in electrical resistance when altering the growth parameters are also observed.

In Chapter 6, the author demonstrates the application of the new insights obtained from the in-situ electroresistometry of Ga-Na solution. The author focuses on the slow nitrogen desorption properties of Ga-Na solution and utilized it to achieve a high-supersaturated solution. By using a newly proposed temperature profile that enhances the nitrogen dissolution, the author achieved the improved growth rate, improved nucleation, and able to shorten the growth process.

Additionally, the author also demonstrates the investigation of impurity effect that enhances (such as Li) and inhibits (such as O, Si) the nitrogen dissolution process on Ga-Na solution using electroresistometry.

In Chapter 7, the author summarizes this dissertation and discusses the future development and applications of electroresistometry.

References

[1] J. Bardeen and W. H. Brattain, Phys. Rev. **74**, 230 (1948).

[2] W. Shockley, Bell Syst. Tech. J. **28**, 435 (1949).

[3] A. Ohtsuru, K. Tanigawa, A. Kumagai, O. Niwa, N. Takamura, S. Midorikawa, K. Nollet, S. Yamashita, H. Ohto, R. K. Chhem, and M. Clarke, Lancet **386**, 489 (2015).

[4] B. K. Bose, IEEE Trans. Ind. Electron. **60**, 2638 (2013).

[5] P. R. Chalker, Thin Solid Films **343-344**, 616 (1999).

[6] B. J. Baliga, *Fundamentals of Power Semiconductor Devices*, Springer International Publishing, (2019).

[7] T. Kimoto, Jpn. J. Appl. Phys. **58**, 018002 (2019).

[8] T. Maeda, PhD thesis (Kyoto University, 2020).

[9] I. Akasaki, Rev. Mod. Phys. **87**, 1119 (2015).

[10] H. Amano, Rev. Mod. Phys. **87**, 1133 (2015).

[11] S. Nakamura, Rev. Mod. Phys. **87**, 1139 (2015).

[12] M. A. Khan, J. N. Kuznia, J. M. Van Hove, N. Pan, and J. Carter, Appl. Phys. Lett. **60**, 3027 (1992).

[13] F. Bernardini, V. Fiorentini, and D. Vanderbilt, Phys. Rev. B **56**, R10024 (1997).

[14] T. Mimura, S. Hiyamizu, T. Fujii, and K. Nanbu, Jpn. J. Appl. Phys. **19**, L225 (1980).

[15] M. Asif Khan, A. Bhattarai, J. N. Kuznia, and D. T. Olson, Appl. Phys. Lett. **63**, 1214 (1993).

[16] G. Steinhoff, B. Baur, G. Wrobel, S. Ingebrandt, A. Offenhäusser, A. Dadgar, A. Krost, M. Stutzmann, and M. Eickhoff, Appl. Phys. Lett. **86**, 033901 (2005).

[17] M. Stutzmann, G. Steinhoff, M. Eickhoff, O. Ambacher, C. Nebel, J. Schalwig, R. Neuberger, and G. Müller, Diam. Relat. Mater. **11**, 886 (2002).

[18] H. Morkoç, *Handbook of Nitride Semiconductors and Devices*, Wiley, (2008).

[19] H. P. Maruska and J. J. Tietjen, Appl. Phys. Lett. **15**, 327 (1969).

[20] J. I. Pankove, E. A. Miller, and J. E. Berkeyheiser, J. Lumin. **5**, 84 (1972).

[21] H. Maruska, D. Stevenson, and J. Pankove, Appl. Phys. Lett. **22**, 303 (1973).

[22] H. Amano, N. Sawaki, I. Akasaki, and Y. Toyoda, Appl. Phys. Lett. **48**, 353 (1986).

[23] S. Nakamura, Jpn. J. Appl. Phys. **30**, L1705 (1991).

[24] H. Amano, M. Kito, K. Hiramatsu, and I. Akasaki, Jpn. J. Appl. Phys. **28**, L2112 (1989).

[25] S. Nakamura, T. Mukai, M. S. Masayuki Senoh, and N. I. Naruhito Iwasa, Jpn. J. Appl. Phys. **31**, L139 (1992).

[26] J. A. V. Vechten, J. D. Zook, R. D. Horning, and B. Goldenberg, Jpn. J. Appl. Phys. **31**, 3662 (1992).

[27] S. Nakamura, T. Mukai, and M. Senoh, Appl. Phys. Lett. **64**, 1687 (1994).

[28] A. Herzog, D. Keune, and M. Craford, J. Appl. Phys. **43**, 600 (1972).

[29] W. A. Brantley, O. G. Lorimor, P. D. Dapkus, S. E. Haszko, and R. H. Saul, J. Appl. Phys. **46**, 2629 (1975).

[30] T. Sugahara, H. Sato, M. Hao, Y. Naoi, S. Kurai, S. Tottori, K. Yamashita, K. Nishino, L. T. Romano, and S. Sakai, Jpn. J. Appl. Phys. **37**, L398 (1998).

[31] S. Chichibu, T. Azuhata, T. Sota, and S. Nakamura, Appl. Phys. Lett. **69**, 4188 (1996).

[32] S. F. Chichibu, A. Uedono, T. Onuma, B. A. Haskell, A. Chakraborty, T. Koyama, P. T. Fini, S. Keller, S. P. DenBaars, J. S. Speck, U. K. Mishra, S. Nakamura, S. Yamaguchi, S. Kamiyama, H. Amano, I. Akasaki, J. Han, and T. Sota, Nat. Mater. **5**, 810 (2006).

[33] S.-i. Nagahama, N. Iwasa, M. Senoh, T. Matsushita, Y. Sugimoto, H. Kiyoku, T. Kozaki, M. Sano, H. Matsumura, H. Umemoto, K. Chocho, and T. Mukai, Jpn. J. Appl. Phys. **39**, L647 (2000).

[34] S. Tomiya, H. Nakajima, K. Funato, T. Miyajima, K. Kobayashi, T. Hino, S. Kijima, T. Asano, and M. Ikeda, Phys. Status Solidi **188**, 69 (2001).

[35] D. A. B. Miller, D. S. Chemla, T. C. Damen, A. C. Gossard, W. Wiegmann, T. H. Wood, and C. A. Burrus, Phys. Rev. Lett. **53**, 2173 (1984).

[36] Y. Hashimoto, K. Yamane, N. Okada, and K. Tadatomo, Phys. Status Solidi Basic Res. **253**, 36 (2016).

[37] R. S. Pengelly, S. M. Wood, J. W. Milligan, S. T. Sheppard, and W. L. Pribble, IEEE Trans. Microw. Theory Tech. **60**, 1764 (2012).

[38] A. Manoi, J. W. Pomeroy, N. Killat, and M. Kuball, IEEE Electron Device Lett. **31**, 1395 (2010).

[39] E. Bahat-Treidel, F. Brunner, O. Hilt, E. Cho, J. Wurfl, and G. Trankle, IEEE Trans. Electron Devices **57**, 3050 (2010).

[40] J.-T. Chen, J. Bergsten, J. Lu, E. Janzén, M. Thorsell, L. Hultman, N. Rorsman, and O. Kordina, Appl. Phys. Lett. **113**, 041605 (2018).

[41] D. Yoo, J. B. Limb, J.-H. Ryou, W. Lee, and R. D. Dupuis, J. Electron. Mater. **36**, 353 (2007).

[42] A. Nishikawa, K. Kumakura, and T. Makimoto, Jpn. J. Appl. Phys. **46**, 2316 (2007).

[43] A. Nishikawa, K. Kumakura, T. Akasaka, and T. Makimoto, J. Cryst. Growth **298**, 819 (2007).

[44] A. Krost and A. Dadgar, Mater. Sci. Eng. B **93**, 77 (2002).

[45] S. L. Selvaraj, A. Watanabe, A. Wakejima, and T. Egawa, IEEE Electron Device Lett. **33**, 1375 (2012).

[46] T. J. Anderson, S. Chowdhury, O. Aktas, M. Bockowski, and J. K. Hite, Electrochem. Soc. Interface **27**, 43 (2018).

[47] P. Parikh, Y. F. Wu, and L. K. Shen, Mater. Sci. Forum **778-780**, 1174 (2014).

[48] X. Zou, X. Zhang, X. Lu, C. W. Tang, and K. M. Lau, IEEE Electron Device Lett. **37**, 636 (2016).

[49] S. Mase, Y. Urayama, T. Hamada, J. J. Freedsman, and T. Egawa, Appl. Phys. Express **9**, 111005 (2016).

[50] S. Mase, T. Hamada, J. J. Freedsman, and T. Egawa, IEEE Electron Device Lett. **38**, 1720 (2017).

[51] X. Zhang, X. Zou, X. Lu, C. W. Tang, and K. M. Lau, IEEE Trans. Electron Devices **64**, 809 (2017).

[52] K. Zhang, S. Mase, K. Nakamura, T. Hamada, and T. Egawa, Electron. Lett. **53**, 1610 (2017).

[53] R. Abdul Khadar, C. Liu, L. Zhang, P. Xiang, K. Cheng, and E. Matioli, IEEE Electron Device Lett. **39**, 401 (2018).

[54] Y. Zhang, M. Yuan, N. Chowdhury, K. Cheng, and T. Palacios, IEEE Electron Device Lett. **39**, 715 (2018).

[55] C. Liu, R. Abdul Khadar, and E. Matioli, IEEE Electron Device Lett. **39**, 71 (2018).

[56] R. A. Khadar, C. Liu, R. Soleimanzadeh, and E. Matioli, IEEE Electron Device Lett. **40**, 443 (2019).

[57] Y. Zhang, A. Dadgar, and T. Palacios, J. Phys. D. Appl. Phys. **51**, 273001 (2018).

[58] G. Gupta, M. Kanamura, B. Swenson, D. Bisi, B. Romanczyk, C. Neufeld, S. Wienecke, T. Ogino, Y. Miyazaki, K. Imanishi, J. Ikeda, M. Kamiyama, J. Guerrero, M. Labrecque, R. Prejdova, B. Cruse, J. McKay, G. Bolante, Z. Wang, T. Hosoda, Y. Wu, P. Parikh, R. Lal, and U. Mishra, in 2022 IEEE 34th Int. Symp. Power Semicond. Devices ICs, Vol. 2022-May (May 2022), pp. 349–352.

[59] I. C. Kizilyalli, A. P. Edwards, H. Nie, D. Bour, T. Prunty, and D. Disney, IEEE Electron Device Lett. **35**, 247 (2014).

[60] H. Ohta, N. Kaneda, F. Horikiri, Y. Narita, T. Yoshida, T. Mishima, and T. Nakamura, IEEE Electron Device Lett. **36**, 1180 (2015).

[61] K. Nomoto, Z. Hu, B. Song, M. Zhu, M. Qi, R. Yan, V. Protasenko, E. Imhoff, J. Kuo, N. Kaneda, T. Mishima, T. Nakamura, D. Jena, and H. G. Xing, in 2015 IEEE Int. Electron Devices Meet. Vol. 2016-Febru (Dec. 2015), pp. 9.7.1–9.7.4.

[62] K. Nomoto, B. Song, Z. Hu, M. Zhu, M. Qi, N. Kaneda, T. Mishima, T. Nakamura, D. Jena, and H. G. Xing, IEEE Electron Device Lett. **37**, 161 (2016).

[63] Y. Hatakeyama, K. Nomoto, A. Terano, N. Kaneda, T. Tsuchiya, T. Mishima, and T. Nakamura, Jpn. J. Appl. Phys. **52**, 028007 (2013).

[64] H. Ohta, K. Hayashi, F. Horikiri, M. Yoshino, T. Nakamura, and T. Mishima, Jpn. J. Appl. Phys. **57**, 04FG09 (2018).

[65] H. Fujikura, K. Hayashi, F. Horikiri, Y. Narita, T. Konno, T. Yoshida, H. Ohta, and T. Mishima, Appl. Phys. Express **11**, 045502 (2018).

[66] V. Talesara, Y. Zhang, Z. Chen, H. Zhao, and W. Lu, Phys. Status Solidi - Rapid Res. Lett. **16**, 2100599 (2022).

[67] V. Talesara, Y. Zhang, V. G. T. Vangipuram, H. Zhao, and W. Lu, Appl. Phys. Lett. **122**, 123501 (2023).

[68] T. Oka, Y. Ueno, T. Ina, and K. Hasegawa, Appl. Phys. Express **7**, 021002 (2014).

[69] H. Nie, Q. Diduck, B. Alvarez, A. P. Edwards, B. M. Kayes, M. Zhang, G. Ye, T. Prunty, D. Bour, and I. C. Kizilyalli, IEEE Electron Device Lett. **35**, 939 (2014).

[70] C. Gupta, C. Lund, S. H. Chan, A. Agarwal, J. Liu, Y. Enatsu, S. Keller, and U. K. Mishra, IEEE Electron Device Lett. **38**, 353 (2017).

[71] Y. Zhang, M. Sun, D. Piedra, J. Hu, Z. Liu, Y. Lin, X. Gao, K. Shepard, and T. Palacios, in 2017 IEEE Int. Electron Devices Meet. (Dec. 2017), pp. 9.2.1–9.2.4.

[72] W. Utsumi, H. Saitoh, H. Kaneko, T. Watanuki, K. Aoki, and O. Shimomura, Nat. Mater. **2**, 735 (2003).

[73] W. C. Johnson, J. B. Parson, M. C. Crew, J. B. Parsons, and M. C. Crew, J. Phys. Chem. **36**, 2651 (1932).

[74] R. Juza and H. Hahn, Zeitschrift für Anorg. und Allg. Chemie **239**, 282 (1938).

[75] J. Karpiński, J. Jun, and S. Porowski, J. Cryst. Growth **66**, 1 (1984).

[76] R. Dwiliński, J. Baranowski, M. Kamińska, R. Doradziński, J. Garczyński, and L. Sierzputowski, Acta Phys. Pol. A **90**, 763 (1996).

[77] H. Yamane, M. Shimada, S. J. Clarke, and F. J. DiSalvo, Chem. Mater. **9**, 413 (1997).

[78] P. Kozodoy, J. P. Ibbetson, H. Marchand, P. T. Fini, S. Keller, J. S. Speck, S. P. DenBaars, and U. K. Mishra, Appl. Phys. Lett. **73**, 975 (1998).

[79] R. Kucharski, T. Sochacki, B. Lucznik, and M. Bockowski, J. Appl. Phys. **128**, 050902 (2020).

[80] *Toyoda Gosei Succeeds in Making Larger GaN Substrates for Next-Generation Power Devices | News | Toyoda Gosei Co., Ltd.* https://www.toyoda-gosei.com/news/details.php?id=306.

[81] É. L. Lube, in *Growth cryst.* Vol. 13 (Springer US, Boston, MA, 1986), pp. 353–363.

[82] W. C. Dash, J. Appl. Phys. **30**, 459 (1959).

[83] N. Abrosimovi, Prog. Cryst. Growth Charact. Mater. **46**, 1 (2003).

[84] W. Zulehner, Mater. Sci. Eng. B **4**, 1 (1989).

[85] J. Winkler, M. Neubert, and J. Rudolph, Acta Phys. Pol. A **124**, 181 (2013).

[86] T. Kato, N. Oyanagi, H. Yamaguchi, S.-i. Nishizawa, M. Nasir Khan, Y. Kitou, and K. Arai, J. Cryst. Growth **222**, 579 (2001).

[87] S. Nakamura, T. Mukai, and M. Senoh, J. Appl. Phys. **71**, 5543 (1992).

[88] R. Tandryo, K. Murakami, T. Kitamura, M. Imanishi, and Y. Mori, Appl. Phys. Express **12**, 065502 (2019).

Chapter 2

GaN crystal growth by Na-flux Method

The Czochralski (Cz) [1, 2] method, also called the pulling method, is the most widely used technique for growing bulk single crystals of electronic and optical materials. This method is particularly useful for producing high-quality silicon ingots [3], which are crucial for manufacturing reliable and affordable electronics. In fact, most electronics materials today are grown using the Cz method. With the integration of advanced monitoring systems, the Cz method has reached a new level of maturity, advancing to control and automate the crystal growth process [4].

Unfortunately for the crystallization of GaN, it is not possible to adopt the Cz growth technology due to the difficulty in obtaining stoichiometric congruent melting of GaN. This is caused by the decomposition process that occurs at high temperatures prior to melting, resulting in high vapor pressure of nitrogen [5]. Utsumi *et al.* determined that the pressure required for congruent melting is 6 GPa [6], which is not suitable for industrial purposes. In the 1990s and 2000s, the high nitrogen pressure solution (HNPS) method was developed as the first approach for high-quality synthesis of GaN. This method involves growing GaN crystals in a solution of liquid Ga and dissolved N at a growth temperature of 1500 °C and N_2 pressure of about 1 GPa. Although high-quality GaN crystals can be obtained using this technique, it did not advance to an industrial stage due to its extremely harsh growth parameters.

Various methods are employed to synthesize GaN crystals at lower pressure. Currently, three primary techniques are utilized to produce bulk GaN crystals, namely halide vapor phase epitaxy (HVPE), ammonothermal, and Na-flux. HVPE involves the crystallization of GaN from the vapor phase, while ammonothermal and Na-flux are classified as high-pressure solution growth methods. These approaches are capable of producing GaN crystals with a diameter of up to 4 inches. However, the properties of the resulting GaN crystal such as structural quality, purity, and electrical properties are influenced by the growth method and parameters as well as the seed used in the growth process. Among

them, Na-flux is the most attractive option Na-flux, as it offers economic advantages with its comparatively milder process conditions compared to the other two. This allows for the production of large-diameter GaN crystals. Additionally, the grown GaN crystals exhibit high-structural quality, high purity and excellent electrical properties.

The following chapter will discuss the growth characteristics of Na-flux and other methods, as well as delve into the growth mechanism and recent advancements in Na-flux technology.

2.1 Na-flux compared to other methods

HVPE

The process of halide vapor phase epitaxy (HVPE) involves the crystallization of GaN by the reaction of GaCl (as the precursor of Ga) and ammonia (NH_3). The HVPE growth reactor has two zones [7]. The first one is the source zone where Ga precursors (GaCl) are synthesized at temperatures ranging from 800–900 °C by reacting with HCl gases

$$\mathrm{Ga_{(l)}} + \mathrm{HCl_{(g)}} \rightleftharpoons \mathrm{GaCl_{(g)}} + \frac{1}{2}\,\mathrm{H_{2(g)}} \tag{2.1}$$

GaCl gas flows with carrier gas into the growth zone where the temperature range from 1000–1100 °C. In this zone, it reacts with NH_3 to synthesize GaN.

$$\mathrm{GaCl_{(g)}} + \mathrm{NH_{3(g)}} \rightleftharpoons \mathrm{GaN_{(s)}} + \mathrm{HCl_{(g)}} + \mathrm{H_{2(g)}} \tag{2.2}$$

Supersaturation, the driving force of crystal growth, is created by the difference between the equilibrium partial pressure of GaCl and the sum of input partial pressures of GaCl at the given temperature of the reaction. GaN is usually crystallized on a native or foreign substrate, for example, sapphire or GaAs substrates, to perform growth on a large diameter wafer.

Compared with other methods, HVPE has the longest history, having been first reported by Maruska and Tietjen in 1969 [8]. It is advantageous in terms of growth rate (in bulk direction) owing to the high reactivity between GaCl and NH_3. Growth rate is typically between 200–400 µm/h but the highest can reach 1870 µm/h [9]. Owing to its high growth rate, it is the leading technique for the production of commercial GaN substrate. Unfortunately, obstacles have been encountered that impede the successful implementation of thick GaN layer growth in HVPE.

- Dislocation reduction and cracking

  HVPE GaN is usually grown on foreign seed substrates and the threading dislocation densities of the grown GaN are typically between 10^7–$10^8\,\mathrm{cm^{-2}}$. Reducing

the dislocation density solely through HVPE thick growth is a challenging task. Moreover, thick GaN growth resulted in a crack due to a difference in thermal coefficient expansion. To tackle this issue, HVPE crystal growers are employing various technologies to effectively reduce dislocations. Back in 1997, Usui *et al.* successfully accomplished the growth of a thick layer of GaN without any cracks on a 2-inch sapphire substrate, utilizing the epitaxial lateral overgrowth (ELO) technique, thereby reducing the dislocation density to $10^7\,\mathrm{cm}^{-2}$ [10]. Selective GaN growth on the opening of SiO_2 mask promotes the development of facet-plane as the inclined facet-plane greatly bends propagation of the threading dislocations thus accelerating the annihilation of dislocations [11, 12]. Following this finding, several variations of the ELO technique have been developed to promote the growth of facet structures and minimize dislocation in GaN. These include hetero ELO (HELO) [13], dislocation by epitaxial growth with inverse-pyramidal pits (DEEP) [14], void-assisted separation(VAS) [15, 16], facet-controlled ELO (FACELO) [17]. More recently, there have been maskless ELO approaches such as random-island FIELO (r-FIELO) [18] and maskless-3D method [19] further reduced the dislocation to 10^5–$10^6\,\mathrm{cm}^{-2}$, eliminating the dislocation-dense regions that were present with the conventional ELO methods.

- Crystallographic bowing

  When HVPE GaN is grown on a foreign seed substrate, the crystallographic plane often becomes severely deformed or bowed due to differences in lattice constants and thermal expansion coefficients with the underlying substrates. This issue is especially pronounced in comparison to ammonothermal and Na-flux growth processes due to the higher temperature required for HVPE growth. Achieving uniform orientation of the crystallographic plane is crucial for subsequent epitaxial growth processes. The best solution is to use high-quality native GaN as seed crystals, which can be prepared using ammonothermal or Na-flux grown GaN crystals. Sochacki *et al.* and Imanishi *et al.* have both demonstrated successful homoepitaxial HVPE growth on GaN seed crystals produced by ammonothermal [20] and Na-flux [21], respectively. The grown GaN layers are crystallographically flat, with a low dislocation density ($\sim 10^5\,\mathrm{cm}^{-2}$) and exhibit high structural quality. By using this hybrid growth process, it is possible to mass-produce high-quality GaN crystals with thick growth using HVPE, making it a promising and cost-effective method for producing GaN substrates.

- Exhaust clogging by NH_4Cl solid-ash

  The residual gases from reaction Eq. (2.1) and Eq. (2.2) are pumped to exhaust. However, the remaining NH_3 and HCl can react to form solid NH_4Cl by-product.

Exhaust clogging due to NH_4Cl solid-ash limits the available growth time. One possible solution to this problem is to utilize or produce different forms of Ga precursor. Halide-free [22] or oxide [23] precursors are viable options as they do not result in the formation of solid byproducts from residual gas.

Ammonothermal method

The ammonothermal method is a process similar to hydrothermal crystallization [24] of quartz or oxide crystals, but instead of water, supercritical ammonia is used to dissolve and crystallize GaN. The process requires a high pressure of ammonia ranging from 100–600 MPa and a growth temperature of 400–750 °C. Due to the high pressure, a specially designed high-pressure autoclave is necessary to contain the supercritical ammonia, typically made of thick-wall nickel-based superalloy. Dwiliński *et al.* first demonstrated the synthesis of GaN using ammonothermal in 1996, and it was found that mineralizers are crucial in improving the solubility of GaN [25]. Hence, mineralizers are added to the ammonia solution to enhance the solubility of GaN or gallium in ammonia [26]. Depending on the mineralizer used, the ammonothermal growth method can be classified as either basic ammonothermal (ammonobasic) or acidic ammonothermal (ammonoacidic) method. As shown in Fig. 2.1, in the ammonothermal growth system, there are two separate zones: the dissolving zone for placing GaN feedstock, and the growing zone for placing the seed crystals. The temperature in each zone varies depending on the type of mineralizer used.

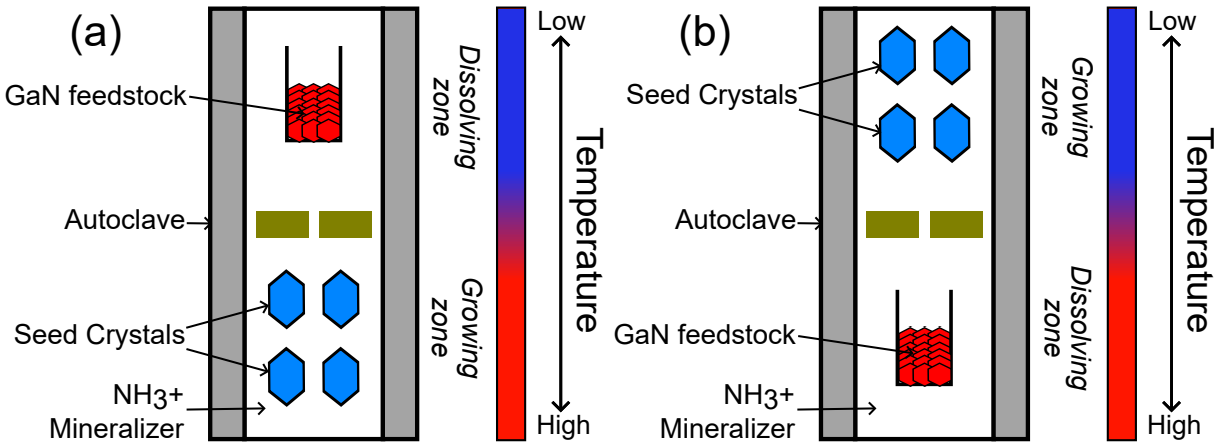

Figure 2.1: Schematic illustration of ammonothermal (a) basic, (b) acidic growth reactor.

Basic ammonothermal

In the process of ammonobasic growth, mineralizers made up of alkali metals or their amides (such as $LiNH_2$ [25], KNH_2 [27], $NaNH_2$ [28]) are utilized. The solubility of GaN in ammonia with basic mineralizers exhibit retrograde solubility (with the exception of $NaNH_2$ which exhibits positive temperature coefficient at temperature lower than 550 °C), meaning that the solubility of GaN increases as the temperature decreases. Consequently, as depicted in Fig. 2.1a, the GaN feedstock is placed at a lower temperature, and the growth of GaN crystals occurs at a higher temperature where the solubility of GaN is lower. Ammonobasic growth has achieved GaN crystal with low dislocation density ($\sim 10^3\,cm^{-2}$) and radius of curvature of several hundred meters for 2-inch-diameter GaN [29]. In terms of structural quality, thickness, and lateral size of the crystals, the best results were obtained with the growth using $NaNH_2$ as mineralizer [30, 31]. Typically, basic mineralizers contribute minimally to the increase in GaN solubility, leading to a higher requirement for ammonia pressure (>200 MPa) for growth. As a result, the inner diameter of the ammonobasic autoclave is limited due to the need for a thick-wall structure to withstand high pressure. This negatively affects the effectiveness of mass production and growth of large diameter substrates.

Acidic ammonothermal

In the process of ammonoacidic growth, ammonia halides (such as NH_4F [32, 33], NH_4I [34], NH_4Cl [35]) are used as mineralizers. In contrast to basic mineralizers, the use of acidic mineralizers results in the typical orthodromic solubility of GaN(with the exception of NH_4F in which the solubility curve becomes retrograde at temperature higher than 500 °C [32]), meaning that solubility of GaN increases as the temperature increases. As illustrated in Fig. 2.1b, the growth configuration is reversed compared to ammonobasic growth. In this case, the GaN feedstock is placed at a higher temperature, and the growth of GaN crystals occurs at a lower temperature. Among the acidic mineralizers, the use of NH_4F highlights a significant improvement in growth rate, although it is still limited to ~200 µm/h [32]. The growth in other crystallographic directions is also favorable. In particular, growth in the *m*-direction is higher than that of the *c*-direction [32]. As acidic mineralizers improve the solubility of GaN higher than basic mineralizers, growth pressure can be reduced to approximately 100 MPa. This particular ammonoacidic growth with low pressure is categorized as LPAAT (low-pressure acidic ammonothermal) [36]. This method is advantageous in terms of mass-production and large-scale crystallization.

Na-flux method

The first synthesis of GaN crystals using Na-flux method was first reported in 1997 by Yamane *et al.* [37]. When working with the synthesis of new ternary Ga containing

nitrides [38], Yamane *et al.* observed some hexagonal transparent crystals, which were identified as GaN. They found that GaN could be synthesized with reactions in the system containing Na, Ga, and N. Although ternary Na-Ga-N were not found in the study, synthesis of single-phase GaN was achieved at temperature of 600–800 °C with a N_2 pressure requirement of around 2–4 MPa, which was almost three orders significantly lower than that of High Nitrogen Pressure Solution (HNPS). Due to its mild process conditions, the Na-flux method attracts interest for its potential economic benefits in producing GaN crystals. Today, this method has advanced and is used to prepare bulk GaN crystal growth on foreign seeds with diameters up to 6 inches. The lateral growth rate of GaN in the Na-flux growth is typically high (more than 50 µm/h), but it is not suitable for thick-layer growth as its growth rate in *c*-direction is only 10 µm/h, much slower compared to HVPE.

Brief comparison

Table 2.1: Comparison of leading techniques for bulk GaN crystal growth.

Growth method	HVPE	Ammonothermal	Na-flux
Growth Temperature [°C]	1000–1100	400–700	600–900
Pressure [MPa]	0.1	100–600	2–4
Growth rate [µm/h]	> 200	10	10–40
Dislocation density [cm^{-2}]	10^5–10^6	10^3–10^6	10^2–10^5
Wafer size [inch]	4	2	6
Radius of curvature [m]	< 10	1000	100

Table 2.1 shows the brief comparison of bulk GaN crystal growth by HVPE, ammonothermal, and the Na-flux method. HVPE-GaN wafers are now commercially available owing to its advantage high growth rate. However, dislocation densities are still high and the radius of curvature of wafer fails to meet the required recommendation. On the other hand, the liquid phase growth: ammonothermal and the Na-flux method, can achieve low dislocation densities and crystallographically flat wafer but the production of this method is greatly hindered due to slow growth rate in *c*-direction. HVPE probably will not develop further with growth on foreign seeds, and the GaN substrate technology will focus with the crystallization on native GaN seeds. Both ammonothermal and Na-flux are promising methods for providing high-quality GaN seeds. The Na-flux method, in

particular, has shown promising results by successfully producing 6-inch GaN substrates and is currently advancing towards the development of an 8-inch substrate. This advancement is significant as mass production of large-diameter GaN wafers via hybrid growth of HVPE and Na-flux would potentially be beneficial from an economic standpoint.

2.2 Growth mechanism of Na-flux growth

2.2.1 Driving force of Na-flux growth

The Na-flux process follows the same growth mechanism as the HNPS method but with the addition of Na in the system, which reduces the required pressure for growth. GaN growth via HPNS can be considered as growth in the Ga self-flux, as GaN does not form a congruent melt with the HPNS process conditions. However, the HPNS growth method differs significantly from commonly used flux methods that rely on the solvent's large solubility. If the self-flux concept is applied, the nitrogen concentration can be expressed as approximately equal to the solubility of GaN. This is because a minor amount of GaN molecules dissolved in a large amount of Ga melt has a negligible effect on the increase of Ga element.

The Na-flux method involves two processes related to GaN synthetic reaction. The first process is the dissolution of GaN into the Ga-Na solution. The solubility of GaN follows a typical solubility curve and is dependent on temperature [39]. The second process is the dissolution of nitrogen through the application of pressure in the Ga-Na solution. The amount of dissolved nitrogen follows Sieverts' law and is proportional to the square root of the partial pressure applied [40]. It is important to note that the solubility of nitrogen also depends on temperature. Fig. 2.2 illustrates the solubility curves for GaN and solubility curves for N at a given temperature T. At temperature T, GaN has a solubility of S_0 [mol %]. Equilibrium holds with a pressure of p_0, which has an equivalent solubility of N at S_0 [mol %]. At this condition, neither crystal growth nor melting will occur. If pressure p_1 is applied to the Ga-Na solution, which is lower than the equilibrium pressure p_0, the solution becomes undersaturated, causing GaN to dissolve. On the other hand, if applied with the pressure p_2, which exceeds the equilibrium pressure, the solubility of N increases to S_2, exceeding the equilibrium solubility of GaN. In this case, the solubility of GaN becomes excessive at temperature T, based on the concept that nitrogen concentration is equivalent to the solubility of GaN. This leads to crystal growth occurring with a supersaturation σ, which is created by the difference between the concentration of nitrogen S and the solubility of GaN S_0 at the given temperature T. Supersaturation σ can be described by the following equation

$$\sigma = \frac{S - S_0}{S_0} \tag{2.3}$$

Morishita *et al.* determined the solubility of nitrogen from the threshold pressure and the equity relation between the solubility of GaN and solubility of N [41]. The solubility of nitrogen in the Ga-Na solubility was in the range of ~0.02 at.%. Consequently, nitrogen concentration becomes the determining parameter in Ga-Na solution due to the small amount of dissolved nitrogen and GaN compared to the amount of Ga.

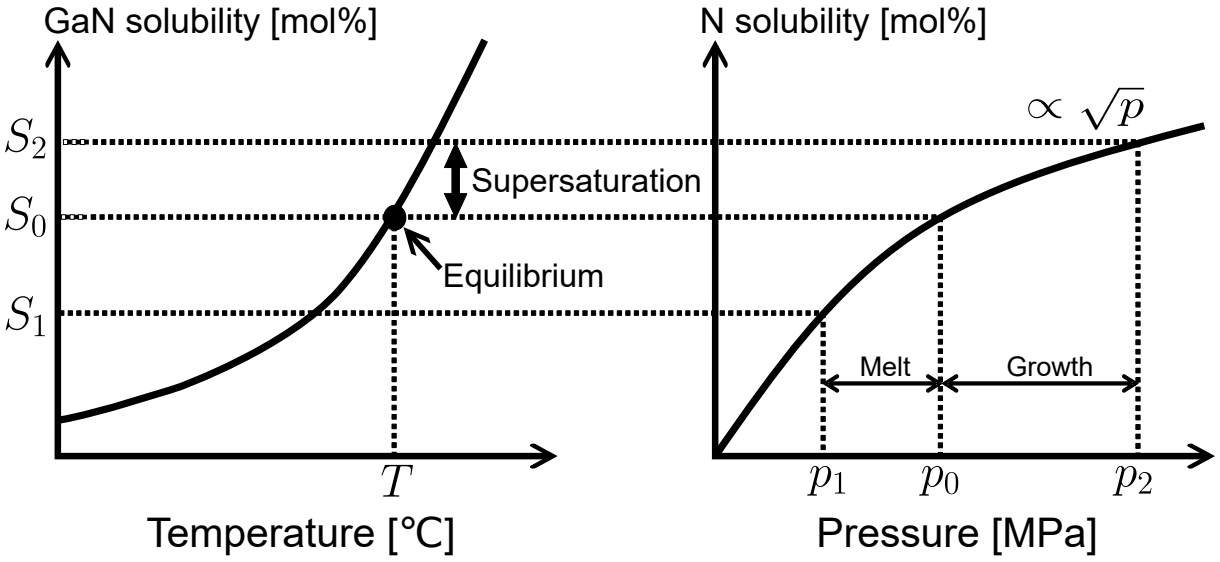

Figure 2.2: Schematic illustration of solubility of GaN, solubility of N, and supersaturation concept in Na-flux method.

2.2.2 Role of Na in the Ga-Na solution

Karpiński *et al.* examined the equilibrium pressure of N_2 over GaN and determined the thermal stability curve of the GaN and N_2 system [5]. At the temperature and pressure range used for Na-flux growth, GaN is stable. While it is thermodynamically possible to generate GaN, it is, however, challenging to grow GaN from a Ga melt due to the nitrogen solubility being extremely small. Although Na has low nitrogen solubility, the mixture with Ga significantly enhances nitrogen solubility to approximately 0.02 mol %. This conclusion is based on the growth threshold pressure investigation in the Na-flux growth [39, 41]. Similarly, improved nitrogen solubility in liquid Na is observed in the Na-Ba-N system reported by Addison *et al.* [42], leading to the use of Na-fluxes for ternary crystal growth by Yamane and DiSalvo [38]. This indicates the crucial role played by Na in improving nitrogen when alloyed with other metals.

The process of nitrogen dissolution in liquid metal involves a following series of reactions.

(1) Dissociation of nitrogen molecules and absorption of radicalized nitrogen into liquid

(2) Diffusion of radicalized nitrogen in the liquid

(3) Recombination of nitrogen and desorption into gas

The final solubility of nitrogen is determined by the equilibrium of these reactions. In the case of nitrogen dissolution in molten Fe, the addition of small amounts of metal additives like Ti, Zr, or V can significantly improve the dissolution rate of nitrogen [43]. This is likely due to the enhanced dissociation process that occurs as a result of the introduction of these impurities. Similar catalytic effects have been observed in the nitridation of silicon surfaces covered by Na at high temperatures [44]. To increase the solubility of nitrogen in Ga-Na solutions, Na is considered to play a similar role in improving the dissociation process of nitrogen. However, since both Ga and Na have low nitrogen solubility, other reactions must be involved in increasing the solubility of nitrogen. In reaction (3), the desorption process depends on recombination and the chemical potential difference between the gas and the liquid. Adding Ca or Li to the Ga-Na solution can significantly improve the solubility of nitrogen owing to the fixation of nitrogen by Ca and Li [41]. This lowers the activity of nitrogen, thereby lowering its chemical potential in the liquid. As a result, nitrogen desorption is prevented, and solubility is increased. In Ga-Na solutions, Ga considerably provides a strong host for radicalized nitrogen, preventing desorption.

Kawahara *et al.* approached Na's role in improving solubility from a first-principle calculation, presenting a different view [45, 46]. In a Ga-Na solution, specifically a Ga-rich solution, Ga and Na atoms tend to segregate and form a zintl liquid where p-block elements create polyhedral clusters within alkali metals [47]. In this structure, Ga atoms are strongly interacting with each other and cannot react with nitrogen. However, in a Na-rich solution, Ga atoms exist in isolation or form a small cluster comprising only a few Ga atoms. Isolated Ga atoms have weaker Ga-Ga interactions, making it easier to form bonds with nitrogen [45]. This results in a decrease in nitrogen activity in the liquid, leading to an increase in the solubility of nitrogen in a Ga-Na solution. Therefore, the solubility of nitrogen in a Ga-Na solution depends on the ratio of Ga:Na composition [46].

2.3 Na-flux growth technology and its recent progress

2.3.1 Carbon additive for nucleation control

In the industrial application of crystal growth, high-growth rate is desirable. However, the Na-flux method, while advantageous in dissolving nitrogen at lower pressure, presents a challenge in controlling spontaneous nucleation. The nitrogen supply tends to concentrate and cause excess supersaturation at the gas-liquid interface, leading to parasitic nucleation in the form of GaN polycrystals. Such polycrystals consume the dissolved nitrogen, resulting in a lower growth rate and hindering the potential for liquid phase epitaxial growth (see Fig. 2.3a).

Kawamura *et al.* discovered that adding carbon to the Ga-Na solution could significantly suppress the generation of polycrystals [48]. Figure 2.3b shows the effect of carbon additive on suppressing polycrystal generation during growth with nitrogen pressure of 50 atm and temperature of 750–800 °C. Growth without carbon additive results in mostly polycrystalline GaN with low yield on LPE seeded growth. With the addition of carbon, these polycrystals are suppressed, and mostly LPE-GaN is yielded. Later, Imade *et al.* investigated the effect of carbon and found that it also enhances the growth rate. Furthermore, adding carbon to the Ga-Na solution does not result in carbon being incorporated into the crystal as an impurity [48], nor does it have a harmful effect on the structural quality of the grown GaN [49]. Ainsley *et al.* reported that carbon is hardly

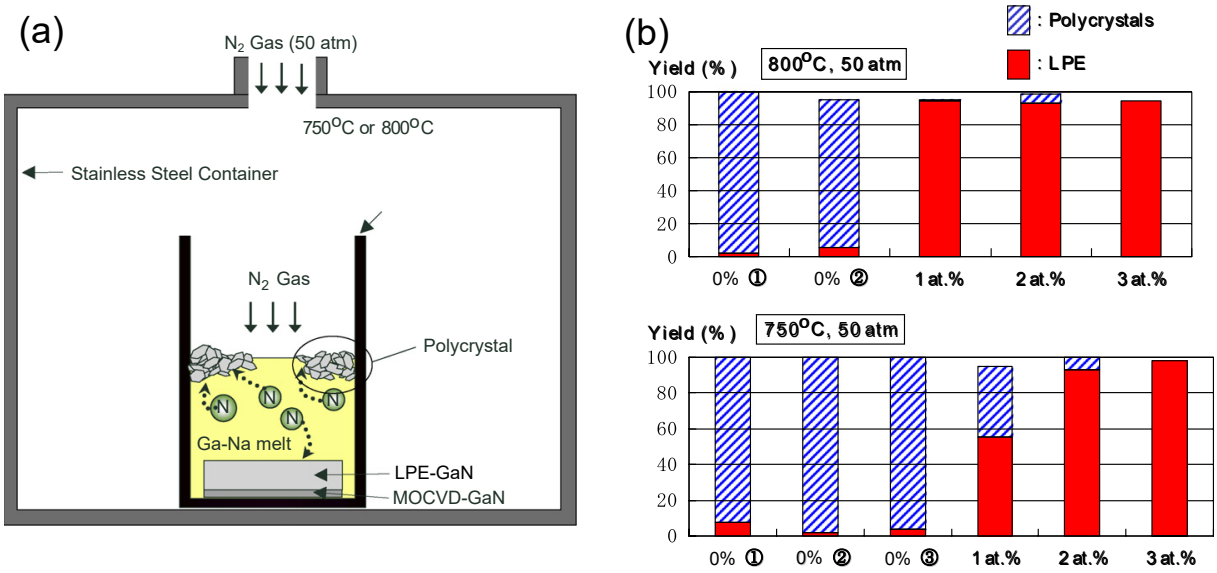

Figure 2.3: (a) Schematic drawing of LPE growth in the Na-flux method. (b) Dependence of LPE and polycrystal yield on the addition of carbon. Reprinted from [48] with permission.

soluble in liquid Na, but in the nitrogen ambient, it dissolves in the form of CN^- ion [50, 51]. Therefore, the CN^- ion is significantly associated with the controlled nucleation mechanism of GaN in the Ga-Na solution. The mechanism was clarified by calculating the free energies for the formation and dissociation of C-N bonds [52]. It is revealed that in the Ga-Na solution, the energy required to form C-N bonding is low, and the energy for their dissociation is high, making the C-N bond highly stable compared to the Ga-N bond. Interestingly, the stability of the C-N bond weakened when the Ga atoms existed around the N atom [52]. Furthermore, the C-N bonding could easily dissociate at the kink of the GaN surface [53], and dissociation energy further lowered with the excess of Ga near the kink of the GaN surface [54]. With the Ga-N bonding more stable, the dissociated C-N promotes the GaN growth by nitrogen transportation mediated by CN^- [54].

Adding carbon to the Ga-Na solution has two favorable effects: suppressing the generation of polycrystals and enhancing GaN growth. These are ideal for industrial large-scale production of GaN crystal and open up the opportunity for selective GaN growth on a prepared seed crystal in the Na-flux growth, known as liquid phase epitaxial growth.

2.3.2 Liquid Phase Epitaxy (LPE) growth

To improve the quality of GaN crystals, liquid-phase epitaxy (LPE) growth with the Na-flux method has been utilized. This involves performing epitaxial growth on a GaN template (GaN-on-Sapphire) that was prepared using metal-organic chemical vapor deposition (MOCVD). The practice of LPE growth started in 2003, with Kawamura *et al.* first report [55]. The LPE-grown layer was found to have extremely low dislocation density around $10^4\,\mathrm{cm}^{-2}$, while the MOCVD-GaN substrate originally had 10^8–$10^9\,\mathrm{cm}^{-2}$ dislocation densities. A mechanism that significantly reduces dislocations was identified through cross-sectional TEM observation, as shown in Fig. 2.4 [56]. During the initial LPE growth process, dislocations from MOCVD-GaN disappeared as they were bent and concentrated following the development of $\{10\bar{1}1\}$ facets. As the growth continues, the development of the *c*-plane becomes preferential, and dislocation reduction to $10^4\,\mathrm{cm}^{-2}$ cannot be explained by this mechanism alone. It was noted that propagating dislocations form a staircase structure as bunched steps proceed, and their propagation directions are redirected obliquely [57]. This process led to further bundling of dislocations and resulted in a remarkable reduction in dislocation density, down to approximately 10^4–$10^5\,\mathrm{cm}^{-2}$, as depicted in a schematic representation Fig. 2.5 and reported by Kawamura *et al.* [58]. The initial dislocation reduction in the LPE-GaN layer reduced the dislocation to $10^6\,\mathrm{cm}^{-2}$, which is the same as achieved by HVPE by artificial processes. Further thickening of LPE-GaN layer reduces the dislocation to 10^4–$10^5\,\mathrm{cm}^{-2}$. This unique feature in the Na-flux growth makes the Na-flux method promising for improving GaN crystal quality.

2.3.3 Point seed and coalescence growth technique

Point seed technique

The LPE growth technique mentioned earlier is a promising method for enhancing crystal quality through its spontaneous dislocation reduction mechanism. However, reducing dislocation density to less than $10^4\,\mathrm{cm}^{-2}$ has been proven to be challenging. Moreover, using GaN templates prepared by the MOCVD method has led to severe crystallographic bowing or cracking due to thermal stress caused by the mismatch with the underlying sapphire. Native GaN seed crystal prepared by HVPE is not crystallographically flat, and this has resulted in bowing in the LPE-GaN. To address these issues, A new technique

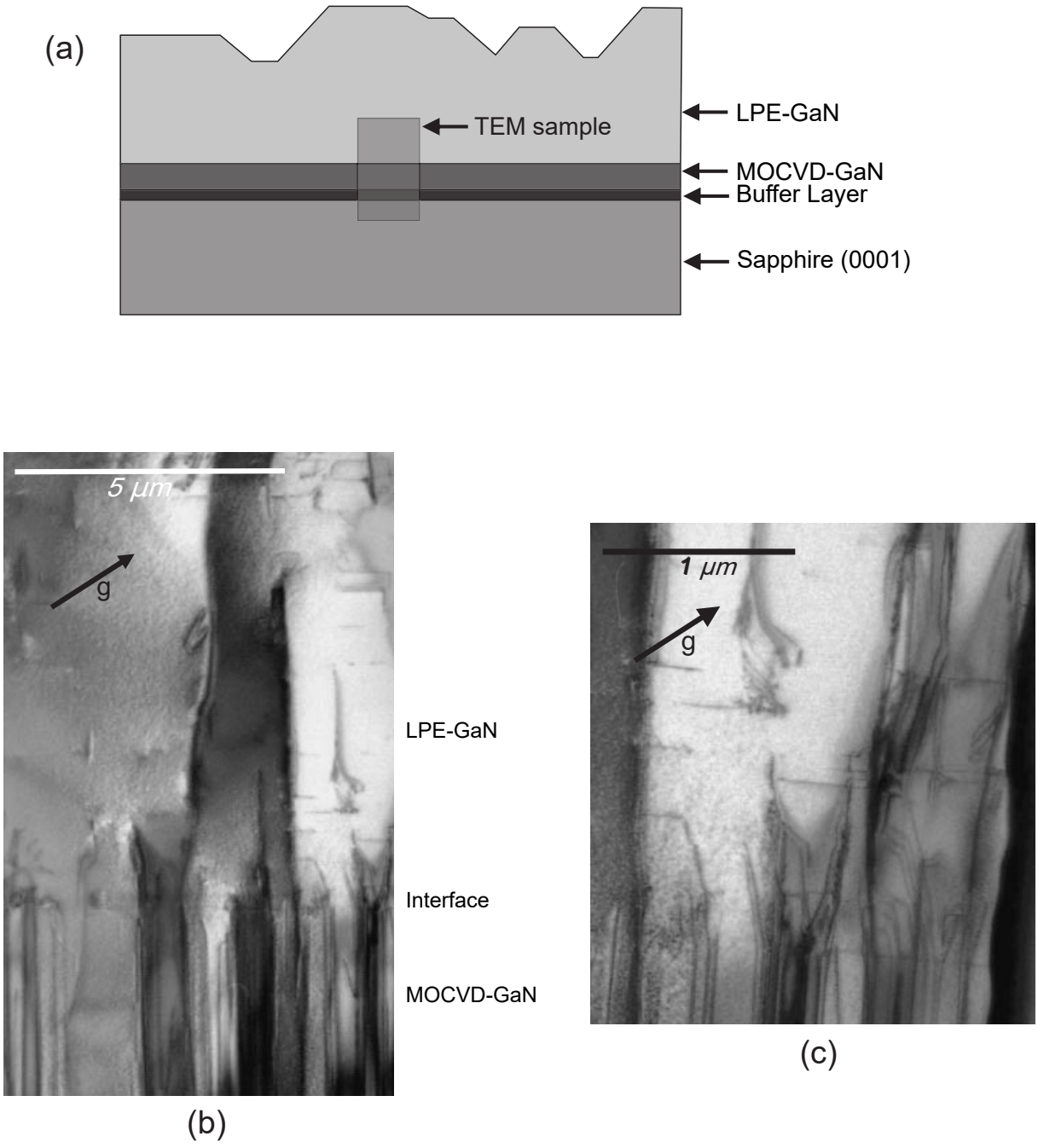

Figure 2.4: (a) Schematic illustration of LPE sample for TEM observation. (b) Cross-sectional TEM image taken around the interface between MOCVD-GaN and LPE-GaN. (c) Enlarged view of TEM from Fig. 2.4b [56].

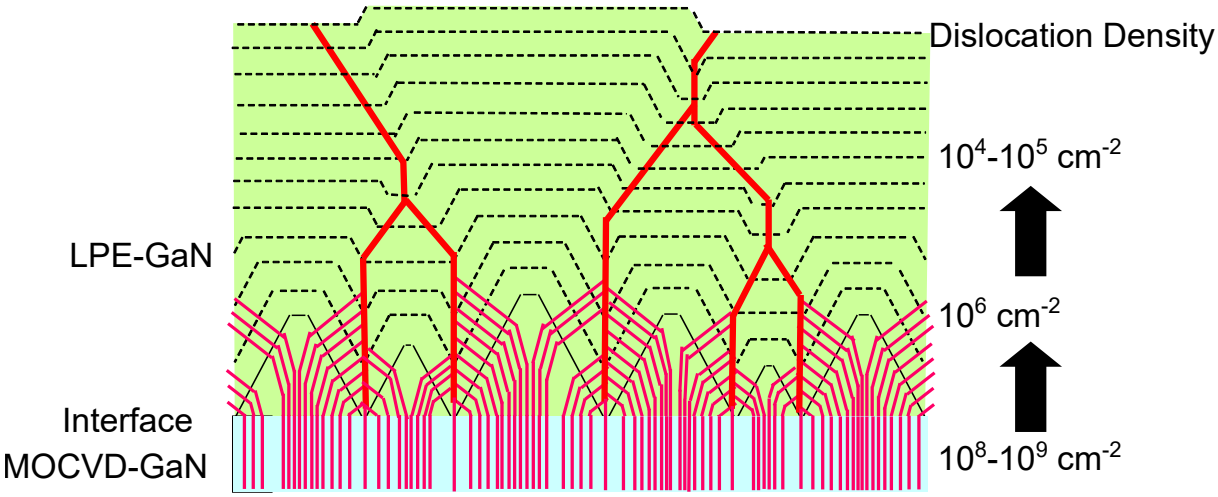

Figure 2.5: Schematic illustration of two-step dislocation reduction [58].

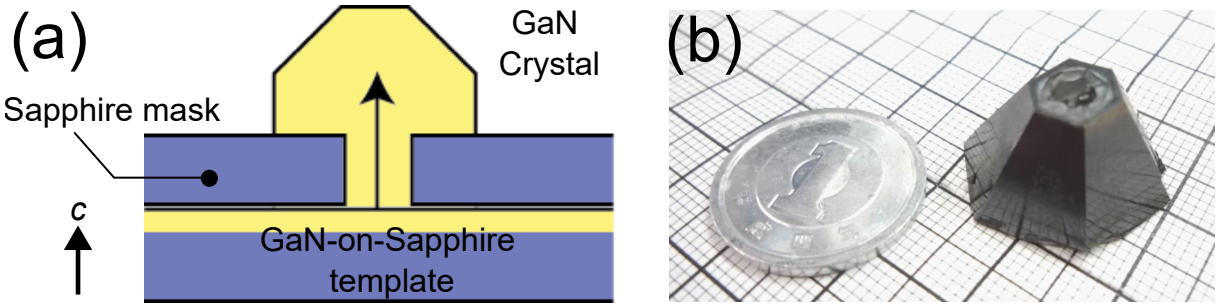

Figure 2.6: (a) Schematic drawing of point seed technique growth by mounting on sapphire mask [59]. (b) Photograph of well-faceted bulk GaN crystal grown with point-seed technique.

called "point seed" [59] was proposed, which is similar to the necking method used for growing dislocation-free silicon crystals [3].

Imade *et al.* reported the first variant of the point seed technique by mounting a sapphire mask on a GaN template [59], as shown in Fig. 2.6a. The use of a mask is similar to the ELO technique in HVPE, but in the Na-flux method, dislocation reduction also occurs in the mask opening, unlike the HVPE method where dislocations appear from the mask opening. Dislocations propagate perpendicular to the growth direction, and the development of $\{10\bar{1}1\}$ facets drive the dislocation to propagate in lateral directions. In the conventional LPE method, the dislocations that go in lateral directions usually remain in the crystal while in this necking technique, the directed dislocations terminate at the sapphire sidewall. The photograph in Fig. 2.6b shows a well-faceted GaN crystal grown using the point seed technique, which had no dislocations observed at the opening. The structural quality measured with the Spring-8 facility obtained the full-width half maximum (FWHM) of X-ray rocking curve to be 2.1 arcsecs, near the theoretical value of

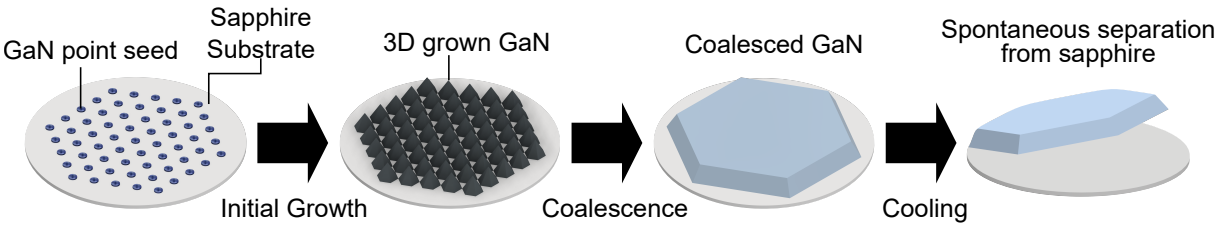

Figure 2.7: Schematic illustration of coalescence growth process on a multi-point seed (MPS) GaN substrate.

2.0 arcsecs. This indicated that the grown sample crystal had perfect structural quality. Although this technique demonstrates the growth of a perfect GaN crystal, it is unfortunately not employed for industrial use since it is difficult to grow large-scale crystals using this technique.

Coalescence growth and Multi-point seed (MPS) technique

In 2013, an improved version of the point seed technique called the Multi-Point Seed (MPS) Technique was introduced. This approach involves merging crystals grown on multiple point seeds to form a larger GaN crystal. However, aligning the coalescence process to prevent misfits at the junction is a crucial challenge in this technique. Its successful execution requires precise adjustment of both growth parameters and point-seed configuration. Preliminary research by Imanishi *et al.* has identified several critical aspects necessary for the advancement of MPS technology:

- The behavior of misfits and dislocations during the coalescence of point seeds at a junction depends on the crystal planes involved. When crystals merge in the *m*-direction, many dislocations are generated, while coalescence in the *a*-direction minimizes misfits [60, 61].

- The conventional point-seed approach struggles to deliver nitrogen into the mask opening, particularly if the mask opening size is configured small. A mesa-shaped point seed created through etching of GaN template has been suggested as a solution.

- Using a smaller diameter point seed not only helps to reduce pre-existing dislocations, but it also encourages a pyramidal growth habit that leads to a significant reduction in dislocations [62].

Based on the findings, the MPS technique growth requires arranging point seeds on the MPS substrate in a hexagonal pattern and is configured so that the crystal coalesce in *a*-direction [63, 64]. The original crystallographically bent GaN template's strain is relieved after patterning (etching) to the MPS substrate [64]. The coalescence growth

process is illustrated in Fig. 2.7, starting with 3D pyramidal growth on individual point seeds which significantly reduces the dislocations. Then, the crystals coalesce in the later growth stage forming a coalesced GaN crystal. Upon cooling, thermal stresses occur at the GaN/Sapphire interface, but due to a small contact area, weak adhesion between GaN and sapphire resulted in spontaneous separation instead of bending [64]. The MPS technique not only produces low-dislocation density crystals but also results in a crystallographically flat and free-standing GaN substrate, thanks to the spontaneous separation process.

2.3.4 Flux-film-coated (FFC) technology

Although a solution for producing high-quality and large-diameter GaN crystals exists [64], the slow growth rate in the bulk direction (c-direction) is a hindrance to mass production in the Na-flux method. In the case of ammonothermal, where the growth rate is also slow, a quick route to mass production of high-quality GaN is proposed through the use of high-quality ammonothermal-GaN as a seed substrate for subsequent thick growth by HVPE, known as hybrid growth [20]. The same approach can be utilized with Na-flux GaN as a seed crystal. However, Imanishi *et al.* identified a critical problem where GaN wafers grown by Na-flux have expanded lattice constant due to high oxygen incorporation in $\{10\bar{1}1\}$-facet that always appears for crystal grown using point seed technique [21]. Consequently, incompatibility arises with cracking or dislocations generated after HVPE growth due to lattice mismatch [21]. The solution to this issue is to grow GaN point-seed crystals with a surface fully composed by c-plane. In HVPE growth, the growth habit and facet structure can be controlled by tuning the growth parameters, such as temperature or V/III ratio [65]. Meanwhile, Na-flux growth can achieve a 2D-flat growth mode with expanded c-plane with high supersaturation [66]. However, supersaturation cannot be drastically altered from the growth parameters alone.

Back in Section 2.3.1, it was mentioned that nitrogen tends to concentrate at the gas-liquid interface, resulting in a high supersaturation. This phenomenon was utilized by Imanishi *et al.* through the flux-film-coat (FFC) method, which involves applying a thin film of Ga-Na solution to the surface of the crystal [67]. This technique was initially attempted in 2003 by Kawamura *et al.* for LPE-growth [69], but it was unsuccessful due to the use of c-plane GaN and the inability of the Ga-Na solution to properly wet and form a thin film on the flat c-plane. However, the execution of FFC can be improved with the use of pyramidal-shaped crystals grown on a MPS substrate, and the advancement of the dipping technique which allows the precise control of the crystal position through the dipping-pulling mechanism [70]. Figure 2.8 illustrates the FFC growth process when growing a crystal with the MPS technique. This growth process involves three stages of growth. First, the 3D pyramidal growth process occurs in the initial growth stage. Second, after the pyramidal crystals are formed, the crystal surface is flattened by repeatedly

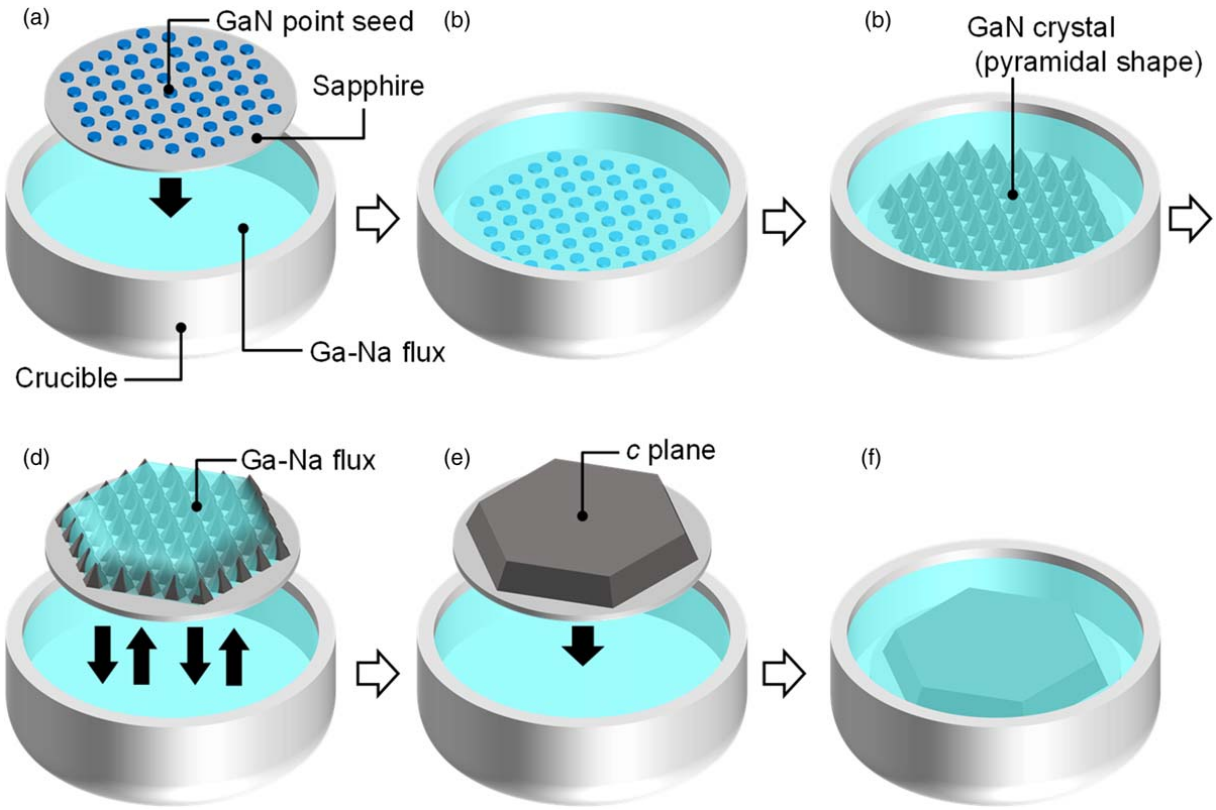

Figure 2.8: Schematic illustration of growth process combined multi-point seed and flux-film coated (MPS-FFC) technology [67, 68].

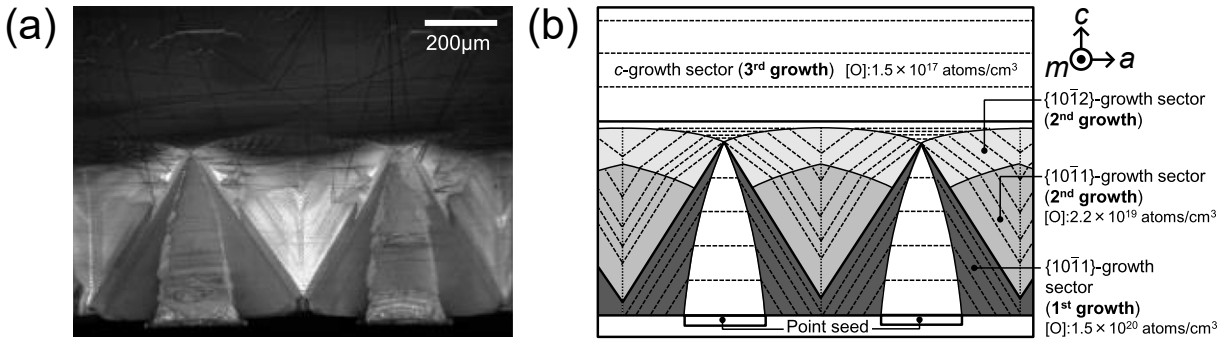

Figure 2.9: (a) Cross-sectional cathodoluminescence image of crystal grown with multi-point seed and flux-film coated (MPS-FFC) technique. (b) Schematic drawing of Fig. 2.9a [67].

dipping the crystal into the solution and pulling it out of the solution in the crucible. When the crystal is pulled out of the solution, the residual Ga-Na solution forms a thin film and is retained on the V-shaped valley between the pyramidal. Not only is the residual solution highly concentrated with nitrogen, but it also restricts growth in the vertical direction, promoting growth in the lateral direction and expanding the *c*-plane. As Ga sources do not last long in the thin film of Ga-Na solution during this growth process, the crystal is dipped and pulled again to extract the growing sources and retain the growth process. This process is repeated until the surface becomes flat and fully composed of *c*-plane. After the surface is flattened, the third growth process involves the final thick growth of the crystal with the last dipping of the crystal into the Ga-Na solution. Observation of cathodoluminescence images and investigation through SIMS (Fig. 2.9) have revealed that the surface of the resulting GaN crystal is uniformly composed of *c*-plane with low oxygen concentration. The obtained GaN layers demonstrated good lattice matching with HVPE, while the structural quality was excellent and uniform across the surface. Furthermore, the crystallographic flatness was satisfactory, establishing the GaN crystal obtained through this method as a high-quality native seed for HVPE growth.

Although the MPS-FFC technique produces crystal with a very low threading dislocation density (TDD), ranging between 10^3–$10^4\,\mathrm{cm}^{-2}$, there are still some regions where TDD is relatively high, exceeding $10^5\,\mathrm{cm}^{-2}$ [71]. These high-density regions are found at triple junctions, where three adjacent GaN crystals merge. The number of dislocations formed at these junctions varies, possibly due to misfit arising from the asymmetry of the crystals' shape or variation in growth rate of the three surrounding GaN crystals. Consequently, challenges remain in achieving consistent quality of GaN wafers.

2.4 Attempts on elucidating growth mechanism

The Na-flux technique has made notable advancements by using carbon to control nucleation and implementing advanced methods like point seed and flux-film coated technology. This approach has shown great promise in producing excellent quality GaN wafers. However, although there have been significant technological improvements, much remains to be understood about the growth mechanisms, and there have been no recent new insights in this area. There have been limited reports on the growth mechanism and kinetics of the Na-flux method, in comparison to the HVPE or ammonothermal methods. HVPE uses thermodynamic analysis to predict the system's reaction [72], while in-situ reflectivity is utilized to directly monitor the growth [73, 74]. The ammonothermal method, on the other hand, employs techniques such as UV-vis spectroscopy, video optical measurements, and X-ray observation for in-situ monitoring [75, 76]. Numerical simulations and modeling of ammonothermal growth have also been reported [77, 78].

Studying the growth process directly in Na-flux is challenging due to the harsh conditions of high temperature, high pressure, and corrosive nature of Ga and Na. Therefore, the study of mechanisms is limited to only a few reports using ex-situ investigations, first-principle calculations, and molecular dynamics simulations. Ex-situ investigations are time-consuming and lack information about the growth process, while simulations can only predict the equilibrium state. There are some differences between the predicted mechanism and the actual process that have been identified. For example, Kawahara *et al.* calculated that the solubility of nitrogen was determined by the composition and structure of the liquid, but in reality, the growth materials are prepared with pure Ga and Na. Similarly, Kawamura simulated the effect of carbon by CN ions in enhancing growth, but the process actually begins with solid graphite added to the starting materials. Therefore, it is essential to monitor the state of the Ga-Na solution to bridge the gap between the predicted mechanism and the actual process. In-situ monitoring in the Na-flux method has been attempted using surface X-ray diffractivity by Jong *et al.* [79, 80] and the group from the University of California Santa Barbara (UCSB) through pressure decay measurement [81]. Real-time in-situ monitoring methods have enabled access to growth systems and research opportunities for the mechanistic study of GaN synthesis using the Na-flux method. This is expected to provide better control over critical aspects of the process.

2.5 Summary

This chapter delved into the three primary techniques utilized for the bulk growth of GaN crystals, namely HVPE, ammonothermal, and Na-flux. The author provided a particular focus on an in-depth discussion of the growth mechanisms and technological advancements achieved through the Na-flux approach. The study of the growth mechanisms was limited to ex-situ, first-principle calculations, and molecular dynamics simulations. Consequently, progress in the Na-flux method primarily centered on the introduction of advanced techniques such as the point seed and flux-film coated technology.

In the next chapter, the author acknowledges the potential for research in understanding the growth mechanism in Na-flux and introduces a new technique for in-situ monitoring using electroresistometry of Ga-Na solution. Through this study, the author aims to clarify the kinetic processes involved in the growth chamber, with the goal of gaining new insights and improving control over important synthesis parameters for GaN growth using the Na-flux method.

References

[1] J. Czochralski, Zeitschrift für Phys. Chemie **92**, 219 (1918).

[2] P. E. Tomaszewski, J. Cryst. Growth **236**, 1 (2002).

[3] W. C. Dash, J. Appl. Phys. **30**, 459 (1959).

[4] J. Winkler, M. Neubert, and J. Rudolph, Acta Phys. Pol. A **124**, 181 (2013).

[5] J. Karpiński, J. Jun, and S. Porowski, J. Cryst. Growth **66**, 1 (1984).

[6] W. Utsumi, H. Saitoh, H. Kaneko, T. Watanuki, K. Aoki, and O. Shimomura, Nat. Mater. **2**, 735 (2003).

[7] M. Bockowski, M. Iwinska, M. Amilusik, M. Fijalkowski, B. Lucznik, and T. Sochacki, Semicond. Sci. Technol. **31**, 093002 (2016).

[8] H. P. Maruska and J. J. Tietjen, Appl. Phys. Lett. **15**, 327 (1969).

[9] T. Yoshida, Y. Oshima, K. Watanabe, T. Tsuchiya, and T. Mishima, Phys. Status Solidi **8**, 2110 (2011).

[10] A. Usui, H. Sunakawa, A. Sakai, and A. A. Yamaguchi, Jpn. J. Appl. Phys. **36**, L899 (1997).

[11] A. Sakai, H. Sunakawa, and A. Usui, Appl. Phys. Lett. **73**, 481 (1998).

[12] A. Sakai, H. Sunakawa, A. Kimura, and A. Usui, Appl. Phys. Lett. **76**, 442 (2000).

[13] K. Motoki, T. Okahisa, N. Matsumoto, M. Matsushima, H. Kimura, H. Kasai, K. Takemoto, K. Uematsu, T. Hirano, M. Nakayama, S. Nakahata, M. Ueno, D. Hara, Y. Kumagai, A. Koukitu, and H. Seki, Jpn. J. Appl. Phys. **40**, L140 (2001).

[14] K. Motoki, T. Okahisa, R. Hirota, S. Nakahata, K. Uematsu, and N. Matsumoto, J. Cryst. Growth **305**, 377 (2007).

[15] Y. Oshima, T. Eri, M. Shibata, H. Sunakawa, and A. Usui, en, Phys. Status Solidi **194**, 554 (2002).

[16] Y. Oshima, T. Eri, M. Shibata, H. Sunakawa, K. Kobayashi, T. Ichihashi, and A. Usui, Jpn. J. Appl. Phys. **42**, L1 (2003).

[17] K. Hiramatsu, K. Nishiyama, M. Onishi, H. Mizutani, M. Narukawa, A. Motogaito, H. Miyake, Y. Iyechika, and T. Maeda, J. Cryst. Growth **221**, 316 (2000).

[18] H. Geng, H. Sunakawa, N. Sumi, K. Yamamoto, A. Atsushi Yamaguchi, and A. Usui, J. Cryst. Growth **350**, 44 (2012).

[19] T. Yoshida and M. Shibata, Jpn. J. Appl. Phys. **59**, 071007 (2020).

[20] T. Sochacki, Z. Bryan, M. Amilusik, R. Collazo, B. Lucznik, J. L. Weyher, G. Nowak, B. Sadovyi, G. Kamler, R. Kucharski, M. Zajac, R. Doradzinski, R. Dwilinski, I. Grzegory, M. Bockowski, and Z. Sitar, Appl. Phys. Express **6**, 075504 (2013).

[21] M. Imanishi, T. Yoshida, T. Kitamura, K. Murakami, M. Imade, M. Yoshimura, M. Shibata, Y. Tsusaka, J. Matsui, and Y. Mori, Cryst. Growth Des. **17**, 3806 (2017).

[22] D. Nakamura and T. Kimura, Appl. Phys. Express **11**, 065502 (2018).

[23] J. Takino, T. Sumi, Y. Okayama, M. Nobuoka, A. Kitamoto, M. Imanishi, M. Yoshimura, and Y. Mori, Jpn. J. Appl. Phys. **58**, SC1043 (2019).

[24] K. Byrappa and M. Yoshimura, in *Handb. hydrothermal technol.* (Elsevier, 2001), pp. 1–52.

[25] R. Dwiliński, J. Baranowski, M. Kamińska, R. Doradziński, J. Garczyński, and L. Sierzputowski, Acta Phys. Pol. A **90**, 763 (1996).

[26] D. Ehrentraut and M. Bockowski, in *Handb. cryst. growth*, Vol. 2 (Elsevier, 2015), pp. 577–619.

[27] R. Dwiliński, R. Doradziński, J. Garczyński, L. Sierzputowski, A. Puchalski, Y. Kanbara, K. Yagi, H. Minakuchi, and H. Hayashi, J. Cryst. Growth **310**, 3911 (2008).

[28] T. Hashimoto, M. Saito, K. Fujito, F. Wu, J. S. Speck, and S. Nakamura, J. Cryst. Growth **305**, 311 (2007).

[29] R. Dwiliński, R. Doradziński, J. Garczyński, L. Sierzputowski, R. Kucharski, M. Zajac, M. Rudziński, R. Kudrawiec, W. Strupiński, and J. Misiewicz, Phys. Status Solidi A **208**, 1489 (2011).

[30] R. Kucharski, T. Sochacki, B. Lucznik, and M. Bockowski, J. Appl. Phys. **128**, 050902 (2020).

[31] K. Grabianska, R. Kucharski, A. Puchalski, T. Sochacki, and M. Bockowski, J. Cryst. Growth **547**, 125804 (2020).

[32] Q. Bao, M. Saito, K. Hazu, K. Furusawa, Y. Kagamitani, R. Kayano, D. Tomida, K. Qiao, T. Ishiguro, C. Yokoyama, and S. F. Chichibu, Cryst. Growth Des. **13**, 4158 (2013).

[33] S. Schimmel, M. Koch, P. Macher, A.-C. L. Kimmel, T. G. Steigerwald, N. S. Alt, E. Schlücker, and P. Wellmann, J. Cryst. Growth **479**, 59 (2017).

[34] D. Tomida, Y. Kagamitani, Q. Bao, K. Hazu, H. Sawayama, S. Chichibu, C. Yokoyama, T. Fukuda, and T. Ishiguro, J. Cryst. Growth **353**, 59 (2012).

[35] Y. Kagamitani, D. Ehrentraut, A. Yoshikawa, N. Hoshino, T. Fukuda, S. Kawabata, and K. Inaba, Jpn. J. Appl. Phys. **45**, 4018 (2006).

[36] K. Kurimoto, Q. Bao, Y. Mikawa, K. Shima, T. Ishiguro, and S. F. Chichibu, Appl. Phys. Express **15**, 055504 (2022).

[37] H. Yamane, M. Shimada, S. J. Clarke, and F. J. DiSalvo, Chem. Mater. **9**, 413 (1997).

[38] H. Yamane and F. J. DiSalvo, J. Solid State Chem. **119**, 375 (1995).

[39] F. Kawamura, M. Morishita, K. Omae, M. Yoshimura, Y. Mori, and T. Sasaki, J. Mater. Sci. Mater. Electron. **16**, 29 (2005).

[40] A. Sieverts, Zeitschrift für Met. **21**, 37 (1929).

[41] M. Morishita, F. Kawamura, M. Kawahara, M. Yoshimura, Y. Mori, and T. Sasaki, J. Cryst. Growth **284**, 91 (2005).

[42] C. C. Addison, G. K. Creffield, P. Hubberstey, and R. J. Pulham, J. Chem. Soc. Dalt. Trans. **2**, 1105 (1976).

[43] H. Ono, K. Morita, and N. Sano, Metall. Mater. Trans. B **26**, 991 (1995).

[44] T. L. Bush, D. O. Hayward, and T. S. Jones, Surf. Sci. **313**, 179 (1994).

[45] M. Kawahara, F. Kawamura, M. Yoshimura, Y. Mori, T. Sasaki, S. Yanagisawa, and Y. Morikawa, J. Appl. Phys. **101**, 6 (2007).

[46] M. Kawahara, F. Kawamura, M. Yoshimura, Y. Mori, T. Sasaki, S. Yanagisawa, and Y. Morikawa, J. Cryst. Growth **303**, 34 (2007).

[47] H. Schäfer, B. Eisenmann, and W. Müller, Angew. Chemie Int. Ed. English **12**, 694 (1973).

[48] F. Kawamura, M. Morishita, M. Tanpo, M. Imade, M. Yoshimura, Y. Kitaoka, Y. Mori, and T. Sasaki, J. Cryst. Growth **310**, 3946 (2008).

[49] M. Imade, Y. Hirabayashi, Y. Konishi, H. Ukegawa, N. Miyoshi, M. Yoshimura, T. Sasaki, Y. Kitaoka, and Y. Mori, Appl. Phys. Express **3**, 075501 (2010).

[50] R. Ainsley, L. P. Hartlib, P. Holroyd, and G. Long, J. Nucl. Mater. **52**, 255 (1974).

[51] R. Pulham and P. Hubberstey, J. Nucl. Mater. **115**, 239 (1983).

[52] T. Kawamura, Y. Yamada, H. Imabayashi, M. Maruyama, M. Imade, M. Yoshimura, Y. Mori, and Y. Morikawa, Jpn. J. Appl. Phys. **9**, 08JA04 (2010).

[53] T. Kawamura, H. Imabayashi, M. Maruyama, M. Imade, M. Yoshimura, Y. Mori, and Y. Morikawa, Phys. Status Solidi B **252**, 1084 (2015).

[54] T. Kawamura, H. Imabayashi, M. Maruyama, M. Imade, M. Yoshimura, Y. Mori, and Y. Morikawa, Appl. Phys. Express **9**, 015601 (2016).

[55] F. Kawamura, T. Iwahashi, K. Omae, M. Morishita, M. Yoshimura, Y. Mori, and T. Sasaki, Jpn. J. Appl. Phys. **42**, L4 (2003).

[56] F. Kawamura, H. Umeda, M. Morishita, M. Kawahara, M. Yoshimura, Y. Mori, T. Sasaki, and Y. Kitaoka, Jpn. J. Appl. Phys. **45**, L1136 (2006).

[57] F. Kawamura, M. Morishita, N. Miyoshi, M. Imade, M. Yoshimura, Y. Kitaoka, Y. Mori, and T. Sasaki, J. Cryst. Growth **311**, 4647 (2009).

[58] F. Kawamura, M. Tanpo, N. Miyoshi, M. Imade, M. Yoshimura, Y. Mori, Y. Kitaoka, and T. Sasaki, J. Cryst. Growth **311**, 3019 (2009).

[59] M. Imade, K. Murakami, D. Matsuo, H. Imabayashi, H. Takazawa, Y. Todoroki, A. Kitamoto, M. Maruyama, M. Yoshimura, and Y. Mori, Cryst. Growth Des. **12**, 3799 (2012).

[60] M. Imanishi, K. Murakami, H. Imabayashi, H. Takazawa, Y. Todoroki, D. Matsuo, M. Maruyama, M. Imade, M. Yoshimura, and Y. Mori, Appl. Phys. Express **5**, 095501 (2012).

[61] M. Imanishi, K. Murakami, H. Imabayashi, H. Takazawa, Y. Todoroki, D. Matsuo, M. Maruyama, M. Imade, M. Yoshimura, and Y. Mori, Phys. Status Solidi C **10**, 400 (2013).

[62] M. Imanishi, Y. Todoroki, K. Murakami, D. Matsuo, H. Imabayashi, H. Takazawa, M. Maruyama, M. Imade, M. Yoshimura, and Y. Mori, J. Cryst. Growth **427**, 87 (2015).

[63] M. Imade, M. Maruyama, M. Yoshimura, and Y. Mori, Jpn. J. Appl. Phys. **53**, 05FA06 (2014).

[64] M. Imade, M. Imanishi, Y. Todoroki, H. Imabayashi, D. Matsuo, K. Murakami, H. Takazawa, A. Kitamoto, M. Maruyama, M. Yoshimura, and Y. Mori, Appl. Phys. Express **7**, 035503 (2014).

[65] S. Goubara, T. Matsubara, K. Yukizane, N. Arita, S. Fujimoto, T. Ezaki, R. Inomoto, K. Yamane, N. Okada, and K. Tadatomo, J. Cryst. Growth **478**, 123 (2017).

[66] H. Yamane, M. Aoki, T. Yamada, M. Shimada, H. Goto, T. Goto, H. Makino, T. Yao, S. Sarayama, H. Iwata, and F. J. DiSalvo, Jpn. J. Appl. Phys. **44**, 3157 (2005).

[67] M. Imanishi, K. Murakami, T. Yamada, K. Kakinouchi, K. Nakamura, T. Kitamura, K. Okumura, M. Yoshimura, and Y. Mori, Appl. Phys. Express **12**, 045508 (2019).

[68] Y. Mori, M. Imanishi, K. Murakami, and M. Yoshimura, Jpn. J. Appl. Phys. **58**, SC0803 (2019).

[69] F. Kawamura, M. Morishita, K. Omae, M. Yoshimura, Y. Mori, and T. Sasaki, Jpn. J. Appl. Phys. **42**, L879 (2003).

[70] T. Sato, K. Nakamura, M. Imanishi, K. Murakami, H. Imabayashi, H. Takazawa, Y. Todoroki, D. Matsuo, M. Imade, M. Maruyama, M. Yoshimura, and Y. Mori, Jpn. J. Appl. Phys. **54**, 105501 (2015).

[71] M. Imanishi, K. Okumura, K. Nakamura, T. Kitamura, K. Kakinouchi, K. Murakami, M. Yoshimura, Y. Fujita, Y. Tsusaka, J. Matsui, and Y. Mori, Appl. Phys. Express **13**, 085510 (2020).

[72] A. Koukitu, S. I. Hama, T. Taki, and H. Seki, Japanese J. Appl. Physics, Part 1 Regul. Pap. Short Notes Rev. Pap. **37**, 762 (1998).

[73] D. Martin, J. F. Carlin, V. Wagner, H. J. Bühlmann, and M. Ilegems, Phys. Status Solidi A **194**, 520 (2002).

[74] D. Martin, J. Napierala, H. J. Bühlmann, and M. Ilegems, Phys. Status Solidi C **2**, 2053 (2005).

[75] N. Alt, E. Meissner, E. Schlücker, and L. Frey, Phys. status solidi c **9**, 436 (2012).

[76] S. Schimmel, U. Künecke, H. Baser, T. G. Steigerwald, B. Hertweck, N. S. Alt, E. Schlücker, W. Schwieger, and P. Wellmann, Phys. Status Solidi **11**, 1439 (2014).

[77] S. Schimmel, D. Tomida, M. Saito, Q. Bao, T. Ishiguro, Y. Honda, S. Chichibu, and H. Amano, Crystals **11**, 254 (2021).

[78] S. Schimmel, D. Tomida, T. Ishiguro, Y. Honda, S. Chichibu, and H. Amano, Crystals **11**, 356 (2021).

[79] A. de Jong, V. Vonk, V. Honkimäki, B. Gorges, H. Vitoux, and E. Vlieg, J. Cryst. Growth **420**, 84 (2015).

[80] A. E. De Jong, V. Vonk, M. Ruat, M. Boćkowski, G. Kamler, I. Grzegory, V. Honkimäki, and E. Vlieg, J. Cryst. Growth **448**, 70 (2016).

[81] P. Von Dollen, S. Pimputkar, M. A. Alreesh, S. Nakamura, and J. S. Speck, J. Cryst. Growth **456**, 67 (2016).

Chapter 3

Design of electroresistomtery system

3.1 Electroresistometry as inspection tool

Electrical resistivity is a physical quantity of material that indicates how strongly it resists the electric current. From its electrical resistivity, material can be classified into three categories: conductor (10^{-8}–$10^{-2}\,\Omega\,\mathrm{m}$), semiconductor ($10^{-3}$–$10^{8}\,\Omega\,\mathrm{m}$), and insulator ($10^{7}$–$10^{20}\,\Omega\,\mathrm{m}$). Theoretical measures of electrical resistivity essentially involve the derivation of resistivity using the properties and behaviors of the material at a microscopic or atomic level. This encompasses the use of various theories, models, and equations. Two fundamental measures of electrical resistivity on a theoretical basis include the Drude model and the Quantum Mechanical Model (or Band Theory).

- Drude model [1, 2]

  This is a classical model for calculating resistivity in metallic conductors. It treats the solid as a 'gas' of free electrons, where the electrons are scattered by the immobile ions in the metal that obstructs the movement of electrons. According to this model, resistivity (ρ) can be given by:

  $$\rho = \frac{m^*}{ne^2\tau} \tag{3.1}$$

  where: m^* is the effective mass of the charge carrier (electron), n is the number of conduction electrons per unit volume, e is the elementary charge, τ is the mean time between collisions (scattering time).

- Quantum Mechanical Model (Band Theory)

  Band theory introduces the concept of energy bands and band gaps, distinguishing between conductors, semiconductors, and insulators. In semiconductors, resistivity can be theoretically calculated using complex formulae involving factors like the effective mass of the charge carriers, temperature, and the band gap energy.

The resistivity of a material provides not only information about its electrical properties, but also its structural and chemical bonding state. While the classical Drude model

is limited in explaining the behavior of semiconductors and insulators, Eq. (3.1) offers a simple understanding that the electrical resistivity is influenced by the scattering time τ, which is closely related to the microstructure of the material and the average time between electron collisions within it. Moreover, the measurement of electrical resistivity is also affected by the number of conduction electrons n, which makes it strongly associated with chemical bonding [3] and its reactivity. This is because the material can gain, lose, or share electrons with other atoms during specific reactions, altering its electronic structure. Therefore, electrical resistivity is a structure-sensitive and chemical-sensitive property that can be used as an indicator to gain insight about the state or condition of material.

Electrical resistivity measurement is commonly used in geophysical applications to predict soil parameters such as water content, degree of soil compaction, and others [4]. It is also used to monitor the purity of water where electrical resistivity of pure water is 18.18 MΩ cm at 25 °C. In materials science, Azumi *et al.* used resistometry to monitor the hydrogen absorption in Ti (titanium) and study the hydrogen embrittlement effect [5]. In the crystal growth process, Sánchez-Valdés *et al.* studied the growth rate on epitaxial $YBa_2Cu_3O_7$ (YBCO) film by means of in-situ electroresistometry [6].

Although electroresistometry is a valuable inspection tool in various applications, it is not commonly used for monitoring the crystal growth process in semiconductors. This is primarily because of the challenge in linking the measurement data with crucial parameters in the crystal growth process. Accurately measuring and interpreting the results, as well as correlating them with crystal growth, presents a challenge toward In-situ monitoring the growth process. This chapter details the design of an electroresistometry system for accurate measurement of electrical resistance, specifically for Na-flux growth.

3.2 Electrical resistance measurement method in the Na-flux growth

In this study, the author aims to investigate the state of the Ga-Na solution through its electrical resistance. Both pure Ga and pure Na themselves are metals which have very low resistivity, and measuring low resistances (1 Ω and lower) has a variety of technical challenges. Here, the author describes several considerations when designing electroresistometry system in the Na-flux growth

3.2.1 Technical considerations for accurate measurement

Conquering errors from wire resistance

Figure 3.1 shows the two-point probe method, where the test current flows through the wire R_w and the resistance R being measured. The voltmeter then calculates the resistance value by measuring the voltage across the resistance through the same set of test wire. However, low-resistance measurements pose a challenge as the total resistance of wire R_w gets added to the measurement. This is because the test current I causes a small but significant voltage drop across the wire resistances, resulting in a voltage measured by the meter V as

$$V = V_R + 2IR_w \tag{3.2}$$

which is different from the voltage V_R ($V_R = IR$) directly across the specimen resistance R. Typical wire resistances range between 10–100 mΩ. This is not an issue when the specimen resistance is larger than wire resistance ($R >> R_w$). However, if the specimen resistance is much lower ($R << R_w$), the effect of voltage drop by wire resistance can lead to significant errors, or can even bury the desired signal V_R.

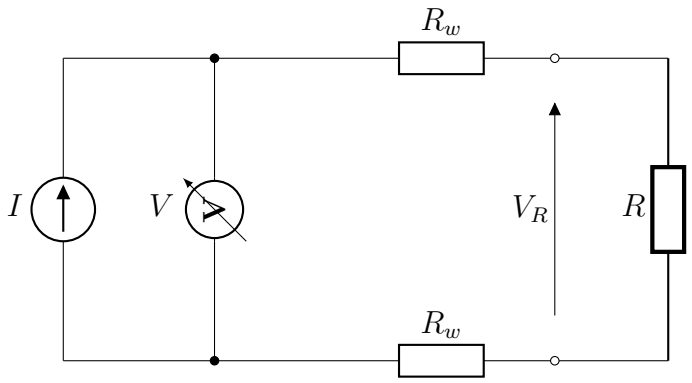

Figure 3.1: Configuration of two-point probe resistance measurement.

Wenner encountered the problem of two-point probe resistance measurement while he was trying to measure the electrical resistivity of the earth [7]. He then proposed a measurement using four wires to minimize the error contributions from wire and/or contact resistance. Valdes then used this idea to measure the resistivity of Ge and this measurement become widely known as four-point probe method [8].

Let us then compare the two-point probe method with four-point probe method as shown in Fig. 3.2. A current I is passed through a test resistance R using one set of wires, while another set is used to measure the voltage V across the specimen. The input resistance of the voltmeter is high enough to ensure that the current flowing through the sense wires is negligible and does not affect the voltage measurement. This means that the voltage drop across the sense wires is negligible, and the voltmeter can measure the voltage V almost the same as the voltage V_R across the resistance R. This four-point

probe method is advantageous for low-resistance measurement and minimizes errors from wire resistances. As such, the author chose the four-point probe method for measuring the electrical resistance of low-resistive Ga-Na solution.

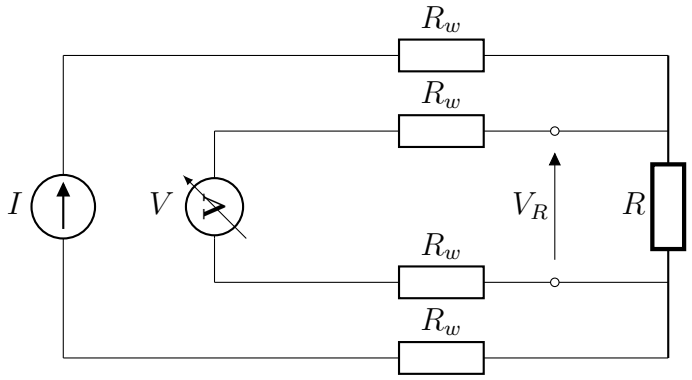

Figure 3.2: Configuration of four-point probe resistance measurement.

Cancelling thermoelectric voltages

When two conductors made of different metals are connected in a loop, and one of the junctions has a higher temperature than the other, an electrical current flow through the loop. Upon opening such a loop, a thermoelectric voltage appears across the open ends. The occurrence of this phenomenon is dependent on the type of metals used and the temperature difference between the junctions. The junction between the two metals generates thermoelectric voltage. As the electrical resistance measurement of the Ga-Na solution will be conducted at elevated temperatures of around 900 °C, the thermoelectric effect can be problematic, causing an error in reading. Thermoelectric effect can be canceled by obtaining two readings: with, and without passing the current. Without passing the current, the voltmeter will read the thermoelectric voltage E_{emf} present in the specimen

$$V_1 = E_{emf} \tag{3.3}$$

then, the other reading by passing the current to the specimen includes the voltage drop across the resistance.

$$V_2 = E_{emf} + IR \tag{3.4}$$

Taking the difference between Eq. (3.3) and Eq. (3.4) yield.

$$V_2 - V_1 = IR \tag{3.5}$$

$$R = \frac{V_2 - V_1}{I} \tag{3.6}$$

Note that E_{emf} is not always constant and could possibly be mounted with electrical noise from surrounding. Therefore the differential of the readings may yield

$$R = \frac{V_2 - V_1}{I} + \frac{\delta E_{emf}}{I} \tag{3.7}$$

where δE_{emf} is captured as the noise causing variation in measured electrical resistance. From Equation (3.7), increasing the test current I can improve the signal-to-noise ratio of resistance reading by reducing the effect of δE_{emf}.

Heating of specimen

The test currents used in low-resistance measurements are usually much higher (>0.1 A), so passing the current could result in considerable power dissipation (Joule heating) given by this formula.

$$P = I^2 R \tag{3.8}$$

where P is amount of dissipated power, I is the current, and R is the resistance of specimen.

To cancel the thermoelectric effect, the current source has to be alternated between on and off to obtain the resistance reading. As such, the most straightforward way to minimize the specimen heating effect is to perform the measurement by passing a narrow pulsed current only during measurement acquisition with specific cycles.

3.2.2 Materials consideration: electrode

When measuring electrical resistance at elevated temperatures and pressures, the choice of electrode material is crucial. Here are some important criteria to consider:

1. High-melting point and thermal stability

   For the Na-flux growth process, which typically occurs at temperatures ranging from 750–900 °C, it is essential to use a thermally stable electrode with a high melting point.

2. Chemically inert in the system

   The electrode should not react with Ga or Na. Alloying with any melt constituent will prevent the stability of the measurement. Additionally, electrode is preferred to be chemically inert with N.

3. Electrical conductivity

   The electrode material should have good electrical conductivity to ensure accurate resistance measurements

4. No inhibitory effect on GaN crystal growth

Considering the future use of electroresistometry method for in-situ monitoring of crystal growth, electrode materials (or its impurity) must not exert any growth inhibitory effect on the GaN crystal growth.

Among the high-melting point and corrosive-resistant electrodes, criteria (2) narrows the selection to only a few metals, as Ga forms alloys with most metals. Here, three types of metal wire tungsten (W), tantalum (Ta), and molybdenum (Mo) were considered. Considering the future application as a monitoring method for Na-flux growth, the materials were examined from the crystal growth standpoint. Comparison of these materials are summarized in Table 3.1

The use of W was opted out because the presence of W in the Ga-Na solution did not result in the GaN growth.

Transparent GaN can grow when Ta wires are added to the Ga-Na solution [9]. There were concerns with the use of Ta due to the possibility of reacting with Ga at high temperatures (400 °C higher than its liquidus (melting) temperature). However, tantalum can be applied as an electrode for a Ga-alloy since its liquidus temperature rises at low Ga content, and it tends to be inactive, as reported by Fujinaga and Murakami [10]. This makes it suitable for Na flux growth, which uses Ga-Na alloys melt with low Ga content. In the study, four pieces of Ta wire weighing 0.3895 g initially were immersed in the Ga-Na solution (Ga:Na composition 27:73 mol %) at 870 °C for 72 h. The weight changed to 0.3899 g, which is negligible and does not indicate any significant weight reduction that could suggest electrode deterioration.

Mo was also reported to be used as a seed holder or thermowell by Von Dollen *et al.* in which no major degradation was observed [11]. However, the resulting GaN crystals were black or gray colored [11, 12] and it was not clear whether the presence of Mo influenced it or if it was due to suboptimal growth parameters.

Considering the above criteria, the author used Ta for the measurement of Ga-Na solution. For some special cases and testing procedures, the author also experimented with other electrodes for comparison.

Table 3.1: Candidates for electrode materials.

Material	Melting Point[°C]	Resistivity [nΩ m]	GaN Crystal Growth
Tungsten (W)	3420	52.8	No Growth
Tantalum (Ta)	3020	131	Growth[9]
Molybdenum (Mo)	2623	49.9	Growth[11,12] (coloration)

3.2.3 Probe design

To successfully execute 4-point probe methods, the specimen (liquid metals or alloys) has to be probed with 4 electrodes and each electrode must be electrically insulated from each other. Inspired by the four-point probe measurement apparatus reported by [13], the author designed the specific 4-point probes for measurement in the Na-flux method as shown in the Fig. 3.3. Metal wires were inserted into an alumina (α-Al_2O_3) tube insulator (sheath) with equally spaced four rounded holes, with each end bent into an L-shape to serve as the electrode. The electrode at the top and the bottom serve as probes for passing test current and the two electrodes that are placed in between them serve as probes for sensing voltage.

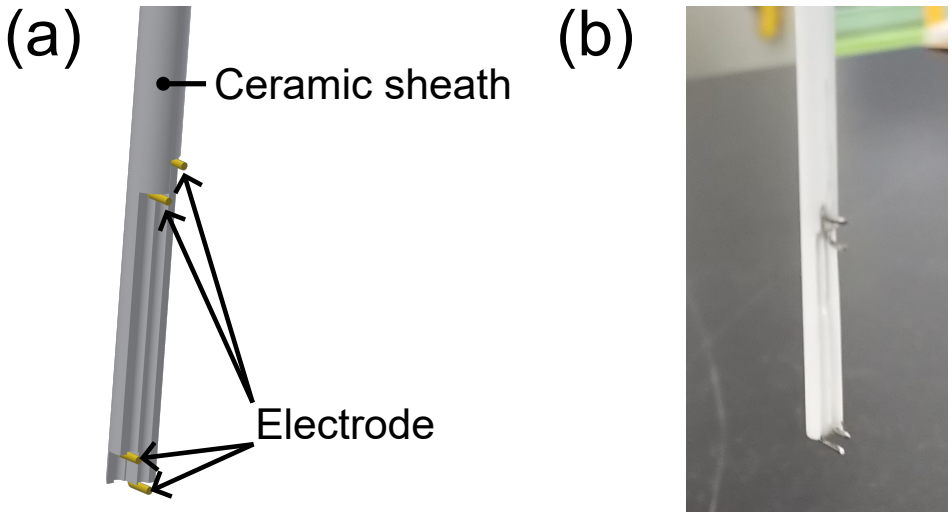

Figure 3.3: (a) Schematic drawing of 4-point probe design for electrical resistance measurement in the Na-flux method. (b) Photograph of the prepared probe.

3.2.4 Final design and measurement method

After carefully considering technical aspects, materials, and probe design, the author determined the optimal electroresistometry system and measurement method, as illustrated in Fig. 3.4 and outlined below:

1. The probe shown in Fig. 3.3 is prepared typically using Ta wires as electrode, then attached to a cable-feedthrough inside a pressure-resistant vessel used for growth. The materials (Ga and/or Na) and the crucible were prepared in a glovebox then loaded in the vessel. At this point, the probe is positioned above the crucible.

2. After placing the vessel in the reactor, the cable that is wired to the probe was connected to nanovoltmeter (Keithley 2182A) and constant DC power supply (GW-

Instek PSS-2005 or Kikusui). These instruments were connected to a PC for data acquisition.

3. The vessel was then heated with an electric furnace (resistive heater) for around 1 h until it reached the target temperature. After the materials were molten (Ga-Na solution with Ga:Na composition 27:73 mol % typically melts at ~600 °C), the probe was immersed into the solution and continuity tests were performed to ensure each electrode was immersed.

4. Electrical resistance measurement started after the electric furnace reached its target temperature. The measurement was performed by acquiring voltage reading without and with pulsed current sequentially (as described in Eqs. (3.3) to (3.5)) every one minute. The testing pulse current was between 0.1~2 A, with 1 A being typically used. The amount of current did not affect the measurement result or influence the interpretation, but a larger current was helpful when measuring low-resistive materials. Other equipment parameters, such as gas pressure value and temperature, were monitored with a pressure transducer and thermocouple placed near the vessel.

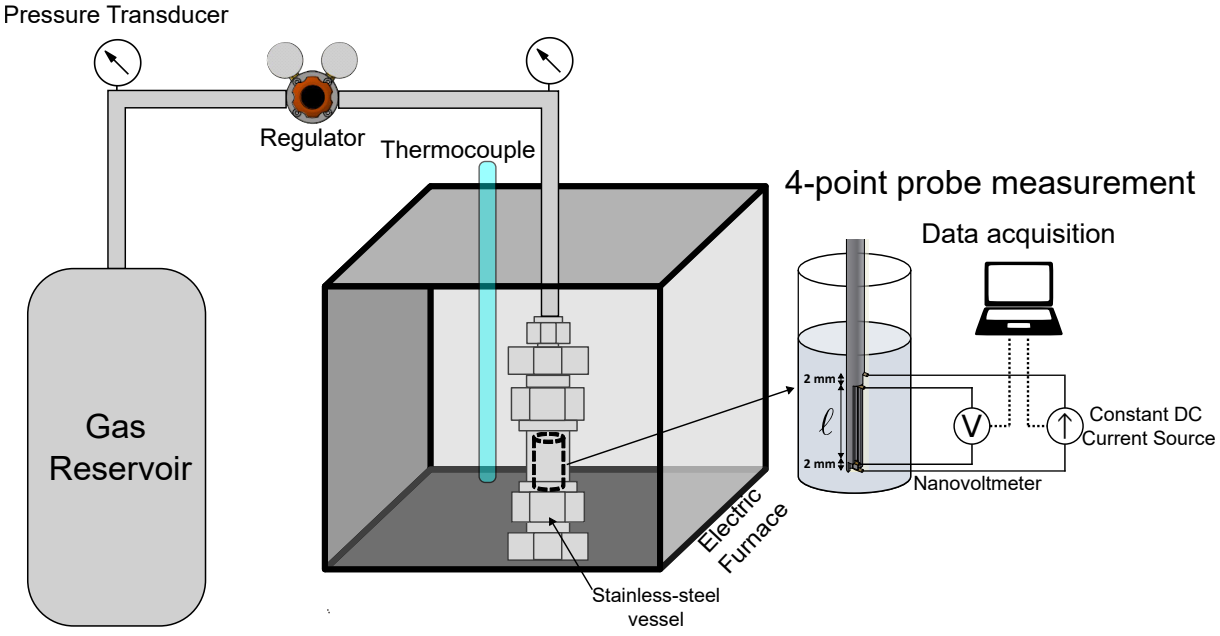

Figure 3.4: Elecroresistometry system for in-situ monitoring of Ga-Na solution in the Na-flux method.

3.3 Operational test: Preliminary experiments

To validate the functionality and accuracy of the designed 4-point probe measurements, initial experiments were conducted to measure the electrical resistance of pure Ga,

pure Na, and the Ga-Na solution. The resulting resistivity temperature coefficients were then compared with values reported in the literature.

For liquid Ga, there were many research reporting its resistivity. These values are both accurate and demonstrate a high degree of consistency across different studies [14–16].

On the other hand, for Na, reported literature values exhibit discrepancies [17], potentially attributable to the reactive nature of Na and the challenges in controlling impurity contributions.

No literature reports were found describing the temperature characteristics of Ga-Na alloy resistivity. Therefore, for potential observed phase transitions during the experiment, the phase diagram of the Ga-Na binary system will be referred to as a reference [18].

3.3.1 Testing Procedure

The starting materials (Ga and/or Na) were prepared in an Ar-filled glove box then placed in an alumina (α-Al_2O_3) crucible with an inner diameter of 17 mm. The amount of materials were adjusted so that when the metal melted, it filled the crucible with liquid height of about 24 mm.

3.3.2 Measurement of pure Ga

For the measurement of liquid Ga, Re-W (Re 3 at.%) wires were used instead of Ta to avoid alloying of Ta with Ga. Ga pellets were melted at 30 °C then the probe was immersed into the liquid Ga and verified the immersion of all electrodes with an electrical continuity test. The Ga was then heated to 300 °C (heating rate 2.5 °C/min) while simultaneously measuring the electrical resistance every minute. Test current I was 2 A to obtain appreciable signal as the resistance of the liquid during measurement was very low (~0.03 mΩ). Electrical resistance was calculated according to Ohm'w law as described in Eq. (3.5). Then electrical resistivity ρ of the gallium was calculated according to Pouillet's law

$$\rho = R\frac{A}{\ell} \tag{3.9}$$

where A is the cross-sectional area of the current path, which was the base area of the melted Ga filling the crucible. ℓ is the distance of the voltage probe, which was 18.23 mm. Considering the presence of alumina insulator in the melt, A was calculated as follows [13]:

$$A = \frac{\pi d_1^2}{4} - \frac{\pi d_2^2}{8} \tag{3.10}$$

where d_1 is the inner diameter of crucible and d_2 is the outer diameter of the alumina crucible.

Figure 3.5 plots the resistivity versus temperature of Ga measured with the proposed electroresistometry system. Resistivity showed a typical positive temperature coefficient

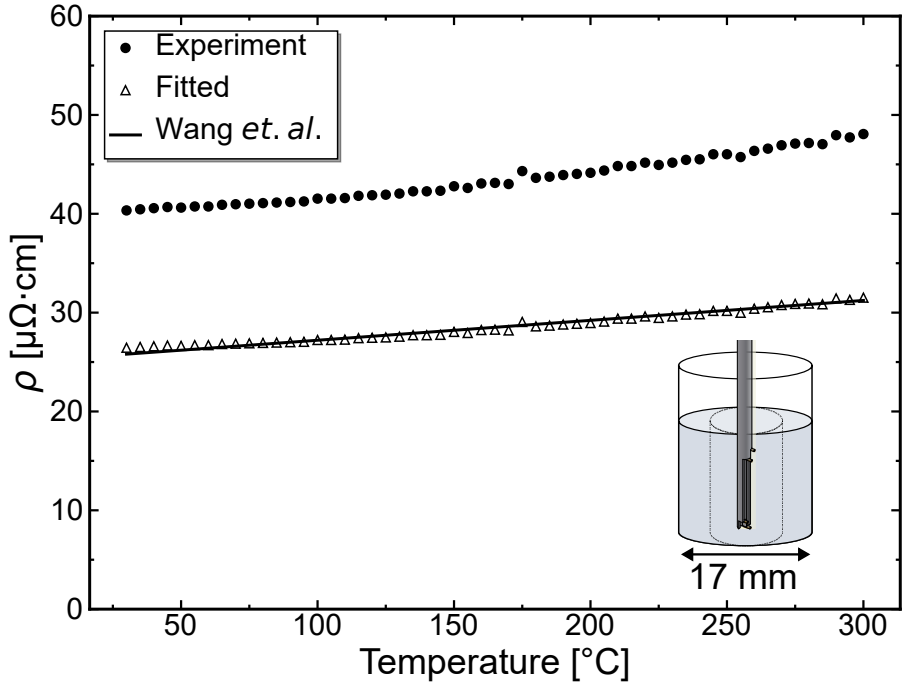

Figure 3.5: Temperature dependence of electrical resistivity of Ga measured in crucible with inner diameter 17 mm.

as reported for Ga; however, the obtained values of the resistivities were discrepant with data reported by Wang *et al.* [14], which shows good agreement with some other literature [15, 16].

Geometric Factor Correction

The reason for this discrepancy was the resistivity not being correctly calculated with Eq. (3.9), as Pouillet's law of deriving resistivity only valid if the sample shape is close to a 1D wire [19]. Here, geometric correction factor C was used with Eq. (3.9) such that resistivity ρ was calculated as follows [13]:

$$\rho = CR\frac{A}{\ell} \tag{3.11}$$

Then, the correction factor C was determined by fitting the measured resistivity with the reported literature values. C was 0.656, and the resistivity well-fitted with that of literature values, indicating that the calculated resistivities were indeed scaled by factor C. Assuming that the test current I did not spread evenly across the area A, based on the fitted value, the effective current spreading area was d_1' calculated by multiplying C into A and reverse calculating the inner diameter of the crucible d_1. The obtained value d_1' was 13.99 mm, which then could be hypothesized as the effective current spreading

area. Note that this value is the estimation and not the actual method to calculate the effective spreading area.

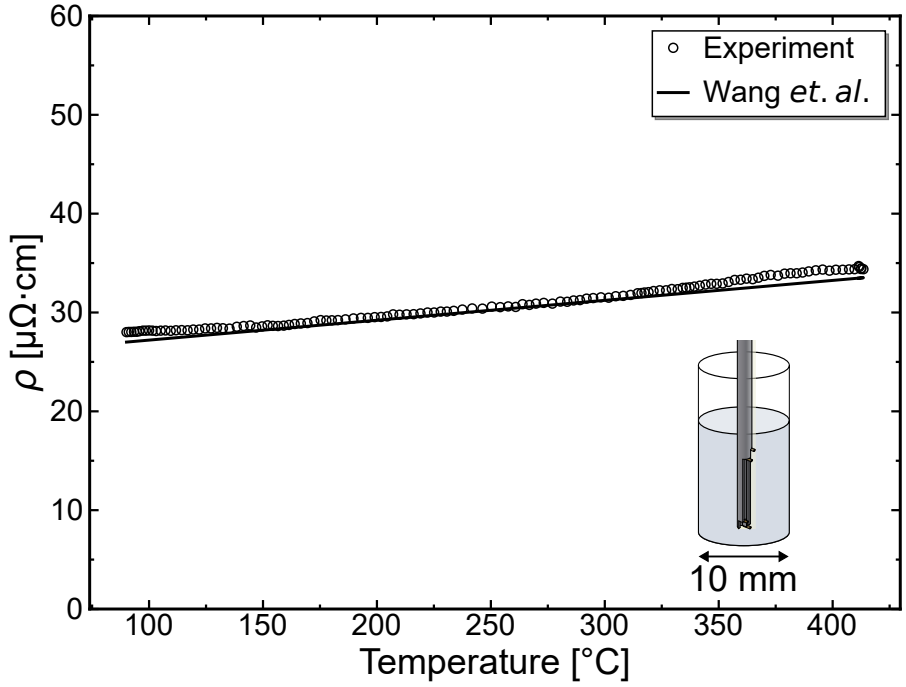

Figure 3.6: Temperature dependence of electrical resistivity of Ga measured in crucible with inner diameter 10 mm.

The experiment was repeated using a crucible with an inner diameter of 10 mm. Resistivities were calculated using Eq. (3.9). As shown in the Fig. 3.6, the calculated resistivities were close (slightly high) to the reported values. In fact, Murashima *et al.* analyzed the correction factors for the four-point probe measurement on cylindrical shape, and conclude that Eq. (3.9) valids when ratio of ℓ/A is large. Here, decreasing the inner diameter of the crucible decreased the A and brought the correction factor C closer to unity (1).

3.3.3 Measurement of pure Na

The pure Na was first melted around 150 °C (above melting point 97.8 °C), then the probe was immersed into the melted Na and underwent a cooling and solidification at room temperature. Starting from the solid state, a similar measurement procedure with that of Ga was conducted. Measurement was performed using Ta wires as electrodes in an alumina crucible with an inner diameter of 17 mm. Resistivity (calculated with Eq. (3.9)) - Temperature characteristics of the Na was plotted in Fig. 3.7 along with the resistivity reported by Addison *et al.* [17].

At its melting point, Na exhibits a sharp rise in resistance, leading to a distinct separation in resistivity characteristics between its solid state and liquidus. A similar

increase in resistance was observed, however at a temperature of approximately 150 °C. This observed lag can be attributed to the incomplete melting of Na during the heating process, resulting in low measurement values due to conduction through the remaining solid Na, which has a low resistivity. Eventually, upon complete melting, the resistivity of Na increases to that of its liquidus state.

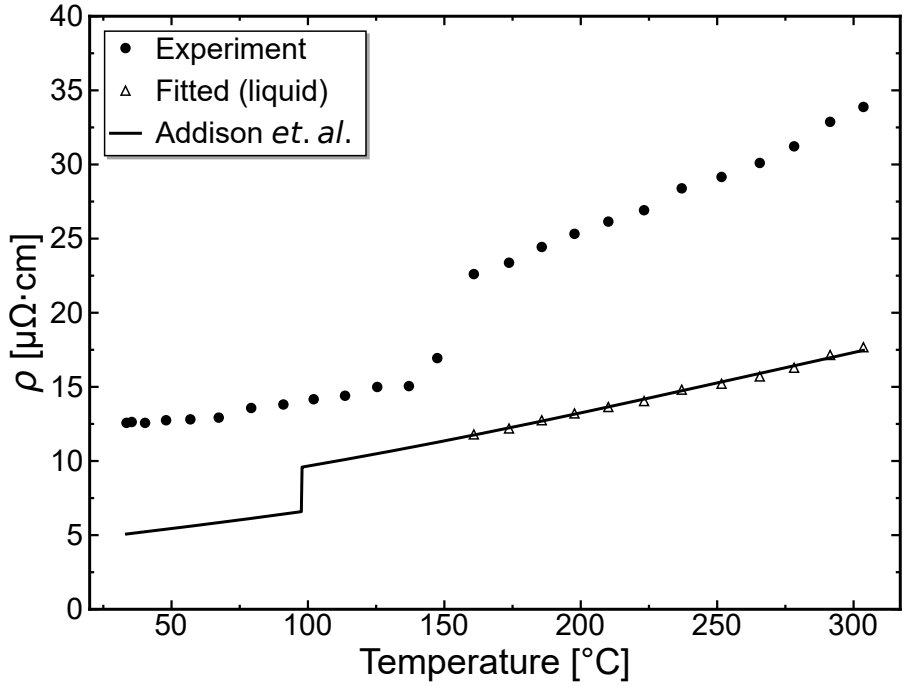

Figure 3.7: Temperature dependence of electrical resistivity of Na.

Again, the discrepancies were observed between calculated resistivities obtained from the experiment with resistivity provided by empirical equation reported by Addison *et al.* [17]. Fitting the resistivities data of the liquidus part to the empirical equation yields the correction factor of C to be 0.522. The calculated d_1' was 12.62 mm. The value was different from the one experimented with Ga due to uncertainty in the resistivities of Na, or possibly the volumetric expansion of Na that affect the measurement of resistivity.

3.3.4 Measurement of the Ga-Na solution

The Ga-Na solution (composed of Ga:Na in a 27:73 mol % ratio) was initially melted by heating it to 800 °C. Ga-Na generally melts around approximately 600 °C. Upon melting, the probe was immersed into the solution and the successful melting process was verified by a continuity test of the probe. The Ga-Na solution, with the probe still immersed, was then allowed to cool.

Fig. 3.8a shows the electrical resistance and temperature profile during the measurement of the Ga-Na alloy. The electrical resistance was measured from room temperature, followed by a heating phase to 900 °C over the course of 1 hour. The temperature was maintained at this level for a duration of 10 hours. Subsequently, the temperature was decreased from 900 °C to 600 °C over a period of 2 hours, and then from 600 °C to 400 °C over a 10-hour period. Finally, it was allowed to cool naturally to room temperature. From Fig. 3.8a, Resistance versus temperature $R-T$ diagram was constructed as shown in Fig. 3.8b.

Heating process

The electrical resistance exhibited an abrupt increase around a temperature of 300 °C, which is consistent with the transformation of solid Na to liquid Na as observed in Fig. 3.7. The observed transformation occurred at a higher temperature due to the elevated heating rate (14.5 °C/min). The resistance continued to increase with temperature within a certain range, until a significant rise in resistance was observed at approximately 600 °C. This transition to a higher resistance value signifies the molten state of the Ga-Na alloy.

At a constant temperature of 900 °C, the electrical resistance showed an increasing resistance curve behavior during the early stages of measurement. This suggests the occurrence of a homogenization process, which will be discussed further in Chapter 4.

Cooling process

In the cooling process from 900 °C to 600 °C, the electrical resistance exhibited an abrupt decrease followed by an increase. This trend is not straightforward to interpret, but could potentially be attributed to fluctuations in concentration due to liquidus phase separation around ~700 °C, as depicted in the phase diagram in Fig. 3.9 [18]. Itami *et al.* reported a negative temperature coefficient of electrical resistivity ($d\rho/dT$) for Na compositions around 50 %.

Around ~500 °C, a sharp transition in electrical resistance was observed, corresponding to the phase line of Ga_4Na. Below this temperature, the decreasing rate of resistance with respect to temperature accelerated, likely due to the formation of solid Ga_4Na. The observed curve in the resistance-temperature ($R-T$) plot from 400 °C to 550 °C suggests a transformation process to Ga_4Na alloy.

The resistance decrease with respect to temperature became steady. Finally, at 98 °C, an abrupt drop was observed, corresponding to the melting point of Na.

In conclusion, the resistance values obtained during the cooling process reflect the changing states of the Ga-Na alloy. At temperatures below 98 °C, both Na and the Ga_4Na alloy were in solid form. At temperatures between 98 °C and 500 °C, Na transitioned into the liquid phase while Ga_4Na remained solid. Above 500 °C, all constituents were molten.

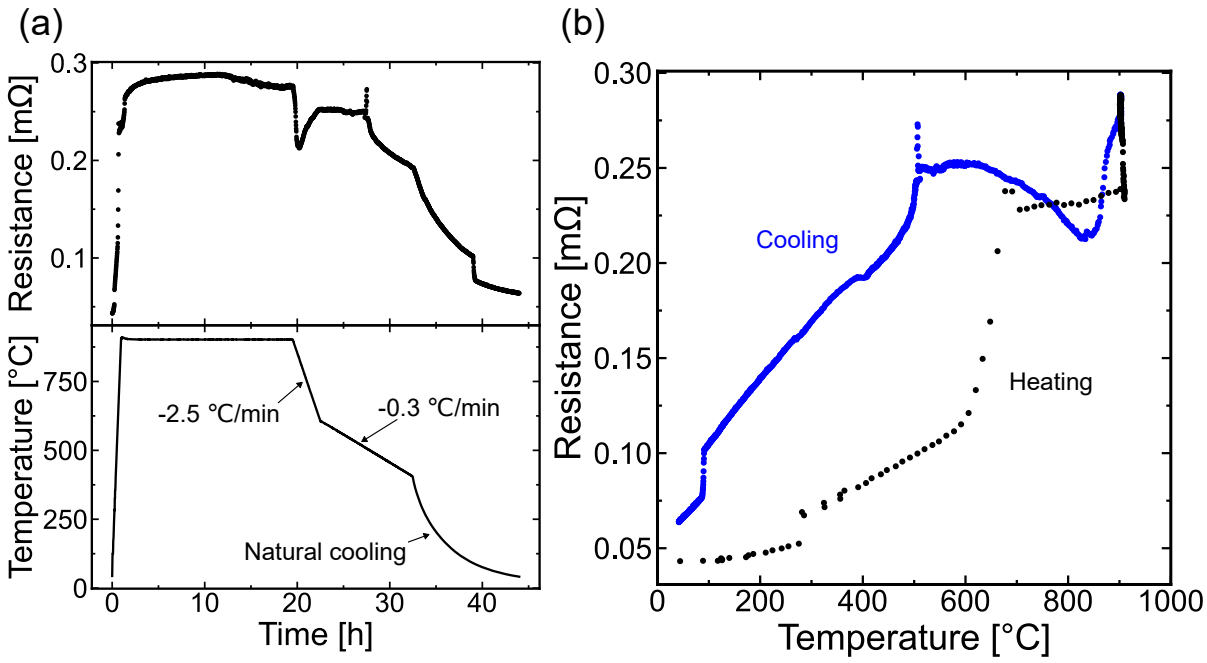

Figure 3.8: (a) Electrical resistance of Ga-Na and the corresponding temperature profile. (b) Resistance versus temperature plot from Fig. 3.8a.

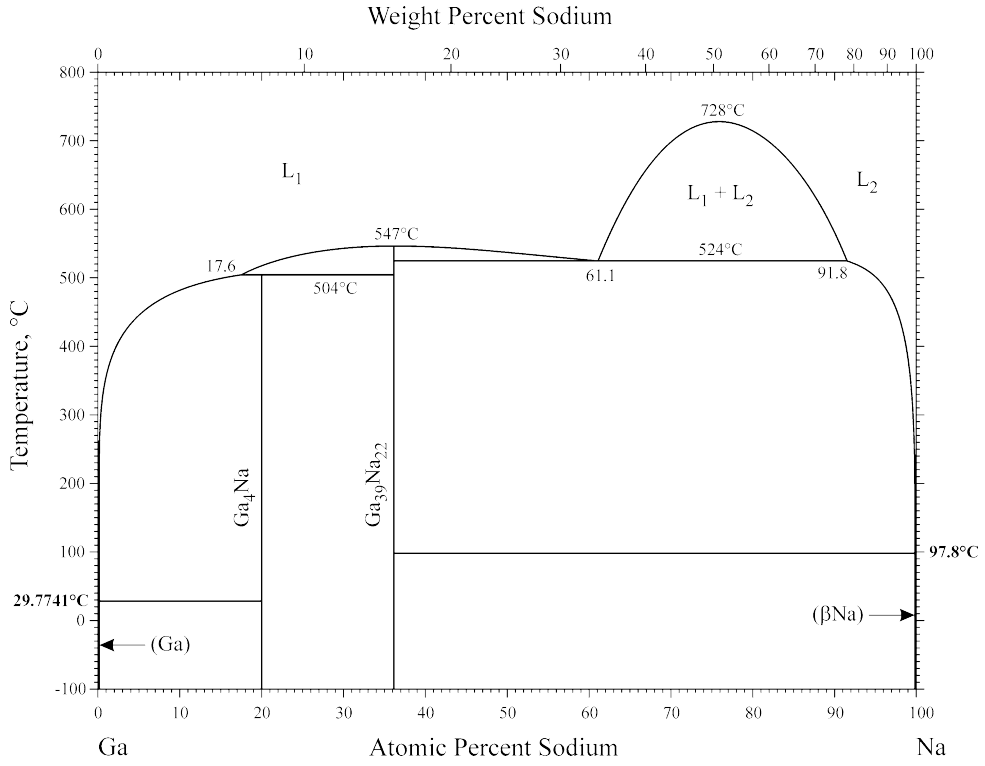

Figure 3.9: Ga-Na phase diagram. Reprinted from [18] with permission.

3.4 Summary

In summary, the author designed an electroresistometry method and validated the operation of this measurement technique by measuring the electrical resistance of Ga, Na, and the Ga-Na solution. The accuracy of these electrical resistance measurements was confirmed from the temperature characteristic of electrical resistivity and identifying phase transitions in the Ga-Na solution.

Unfortunately, due to geometric factors and the correction factor not being unity for a crucible with a 17 mm inner diameter and the current probe configuration, the electrical resistivity could not be measured accurately. The effective measurement area was estimated to be around the radius of 6–7 mm surrounding the probe position.

Consequently, the measured electrical resistance cannot be straightforwardly converted into electrical resistivity unless a specifically shaped container is used for measurement, such as a crucible with a smaller diameter. However, this would mean performing the measurement in a system different from the actual Na-flux growth system. In the following chapter, the author uses crystal growth as a means to validate the interpretation of the electrical resistance of the Ga-Na system, which requires the measurement to be conducted under the same conditions as the growth conditions. Therefore, the author chose to measure the electrical resistance in a 17 mm crucible without converting it into resistivity. Consequently, the resistance values will be challenging to compare from one experiment to another due to the significant uncertainty. Instead, the focus of the analysis will be on the changes in electrical resistance and its unique behaviors.

References

[1] P. Drude, Ann. Phys. **308**, 369 (1900).

[2] N. W. Ashcroft and N. D. C. N. .-. Q. . Mermin, *Solid state physics*, Holt, Rinehart and Winston, (1976).

[3] W.-K. Rhim and T. Ishikawa, Rev. Sci. Instrum. **69**, 3628 (1998).

[4] M. Lech, Z. Skutnik, M. Bajda, and K. Markowska-Lech, Appl. Sci. **10**, 2263 (2020).

[5] K. Azumi, Y. Asada, T. Ueno, M. Seo, and T. Mizuno, J. Electrochem. Soc. **149**, B422 (2002).

[6] C. F. Sánchez-Valdés, T. Puig, and X. Obradors, en, Supercond. Sci. Technol. **28**, 024006 (2015).

[7] F. Wenner, Bull. Bur. Stand. **12**, 469 (1916).

[8] L. Valdes, Proc. IRE **42**, 420 (1954).

[9] K. Itozawa, Bachelor Thesis (Osaka University, 2020).

[10] Y. Fujinaga and Y. Murakami, Mater. Trans. **44**, 377 (2003).

[11] P. Von Dollen, S. Pimputkar, M. A. Alreesh, H. Albrithen, S. Suihkonen, S.

Nakamura, and J. S. Speck, J. Cryst. Growth **456**, 58 (2016).

[12] P. Von Dollen, S. Pimputkar, M. A. Alreesh, S. Nakamura, and J. S. Speck, J. Cryst. Growth **456**, 67 (2016).

[13] R. Endo, S. Maeda, Y. Jinnai, R. Lan, M. Kuwahara, Y. Kobayashi, and M. Susa, Jpn. J. Appl. Phys. **49**, 065802 (2010).

[14] Q. Wang, X.-M. Chen, and K.-Q. Lu, J. Phys. Condens. Matter **13**, 8445 (2001).

[15] G. Ginter, J. G. Gasser, and R. Kleim, Philos. Mag. B **54**, 543 (1986).

[16] M. Pokorny and H. U. Astrom, J. Phys. F Met. Phys. **6**, 559 (1976).

[17] C. C. Addison, G. K. Creffield, P. Hubberstey, and R. J. Pulham, J. Chem. Soc. A Inorganic, Phys. Theor., 1482 (1969).

[18] H. Okamoto, J. Phase Equilibria Diffus. **31**, 206 (2010).

[19] I. Miccoli, F. Edler, H. Pfnür, and C. Tegenkamp, J. Phys. Condens. Matter **27**, 223201 (2015).

[20] S. Murashima, H. Kanamori, and F. Ishibashi, Jpn. J. Appl. Phys. **9**, 58 (1970).

[21] T. Itami, M. Shimoji, J. Meijer, G. Vinke, C. Van Der Marel, and W. Van Der Lugt, Phys. B+C **142**, 145 (1986).

Chapter 4

Nitrogen dissolution process in Ga-Na solution

In Chapter 3, the author designed the electroresistometry system and demonstrated the electrical resistance measurement of Ga, and Ga-Na solution. The designed system is capable of correctly measuring the resistance of the solution. The author aimed to use the electroresistometry to monitor the electrical resistance of the Ga-Na solution, and also for in-situ monitoring of GaN growth in the Na-flux method. However, electrical resistance incorporates various information such as temperature, chemical bonding state and structural information in a single value of electrical resistance. To derive meaningful and interpretable data from the measured electrical resistance, it is essential to understand and correlate this property with the dynamic phenomena occurring within the Na-flux process. The process of synthesizing GaN in the Na-flux growth involves preparing a Ga-Na solution supersaturated with nitrogen. This commences from the melting of Ga and Na at high temperatures which forms the Ga-Na solution through a homogenization process, followed by dissolution of nitrogen with pressurized nitrogen gas.

This chapter delves into the systematic investigation of interpreting electrical resistance by measuring the electrical resistance of Ga-Na solution in various solution systems: Ga-Na system, Ga-Na-N system, and Ga-Na-C-N system, as shown in Fig. 4.1.

The electrical resistances of Ga-Na solutions were initially measured in an inert gas argon (Ar) atmosphere. By measuring it in an Ar atmosphere, the occurring process was limited to homogenization only, which allowed the effect of nitrogen to be distinguished and obtain the baseline measurement of the Ga-Na solution. Specific behavior related to the nitrogen dissolution process was then identified from the measurement in nitrogen atmosphere and comparison with the measurement in Ar atmosphere. Finally, the characteristic behavior of carbon was also studied by adding it to the Ga-Na solution.

The analysis primarily focuses on the change of electrical resistance of Ga-Na solution measured isothermally and its unique behavior in the corresponding solution system.

Through this study, an interpretation of how electrical resistance can describe the state of the Ga-Na solution is aimed to be provided.

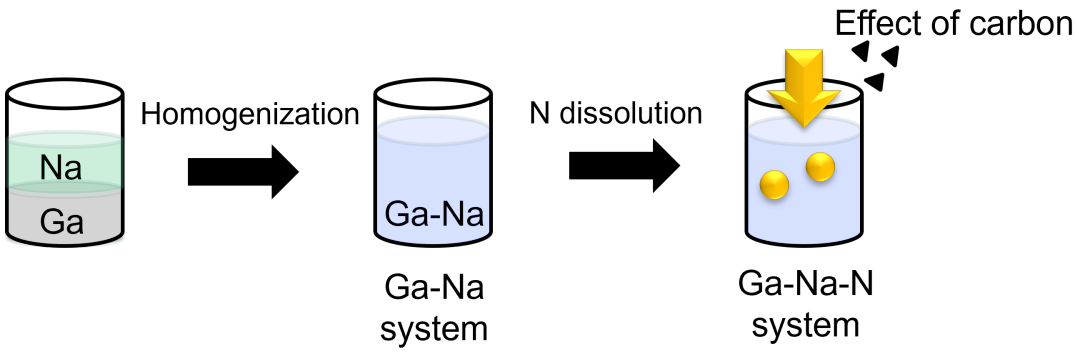

Figure 4.1: Systematic analysis for interpreting the electrical resistance of Ga-Na solution.

4.1 Homogenization of Ga-Na solution

4.1.1 Measurement in Ar atmosphere

Electrical resistance of the Ga-Na solution (Ga:Na composition 27:73 mol %) was measured with 4-point probe as shown in Fig. 3.3 using Ta wires as electrode. The pressure-resistant vessel containing the Ga-Na solution was filled with 4 MPa of argon. The vessel was heated in the electric furnace to 870 °C over 1 h, then the temperature was kept constant over the measurement period. Electrical resistance measurement commenced when the temperature reach 870 °C with the procedure and measurement algorithm described in Section 3.2.4. The test current was 0.1 A and the resistance measurements were performed every minute. For comparison, the measurements with pure liquid Ga and Na were also experimented with a test current of 1 A. The liquid level of the solution/melt in the crucible were adjusted to 24 mm, with voltage probe distance ℓ being 16 mm. Table 4.1 summarizes the measurement condition and Fig. 4.2 depicts the temperature sequence of the experiment.

Table 4.1: Measurement conditions of Ga-Na solution.

Temperature [°C]	Gas / Pressure [MPa]	Ga:Na [mol %]	Test Current [A]
870	Ar / 4	27:73	0.1
870	Ar / 4	100:0	1
870	Ar / 4	0:100	1

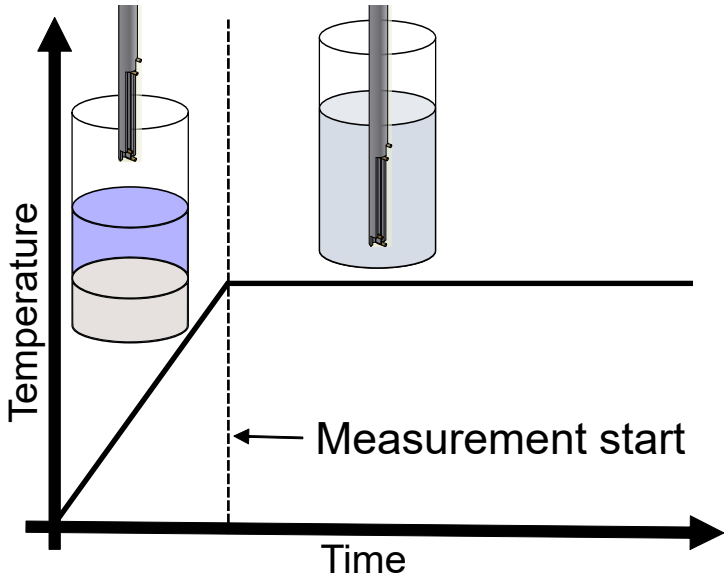

Figure 4.2: Measurement and temperature sequence of electroresistometry experiments. Electrical resistance measurement starts when the vessel reach its target temperature.

Figure 4.3 plots the changes of electrical resistance of the Ga-Na solution over a 35-hour period of measurement. The value of the resistance was initially low, then increased monotonically and eventually reached saturation after 10 hours. The resistance curve can be expressed as a function of time (t) and a well-fitted curve can be obtained by incorporating R_0, ΔR, K, n into the following equation.

$$R(t) = R_0 + \Delta R(1 - e^{-Kt^n}) \tag{4.1}$$

where R_0 denotes the initial resistance (at $t = 0$), ΔR is the increase of resistance. K and n are the rate constant and Avrami constant of the Avrami equation [1], respectively. Figure 4.4 shows the plot of repeated measurement of Ga-Na solution in the same condition. Despite the difference in the value of resistance, the increasing resistance curve phenomenon was also observed in the repeated measurement. On the other hand, the observed increasing resistance curve was not identified when measuring liquid Ga and Na individually as shown in Fig. 4.5. Electrical resistance of Ga and Na stay constant from the beginning over 30 hours of measurement. Additionally, the value of resistances were small (~0.05 mΩ) compared to 0.2 mΩ of the Ga-Na solution.

4.1.2 Interpretation on increasing electrical resistance curve

Residual resistivity by alloy scattering

The reason that the Ga-Na solution had higher measured resistance is due to residual scattering in alloy structure, namely alloy scattering. Electrical resistivity of the disor-

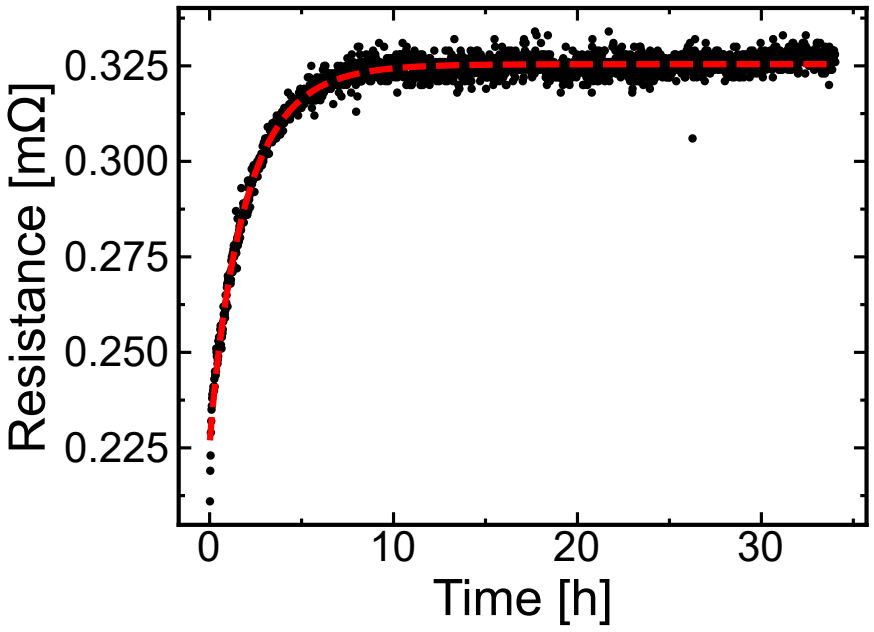

Figure 4.3: Changes of electrical resistance of the Ga-Na solution subjected to a constant argon atmosphere at 870 °C.

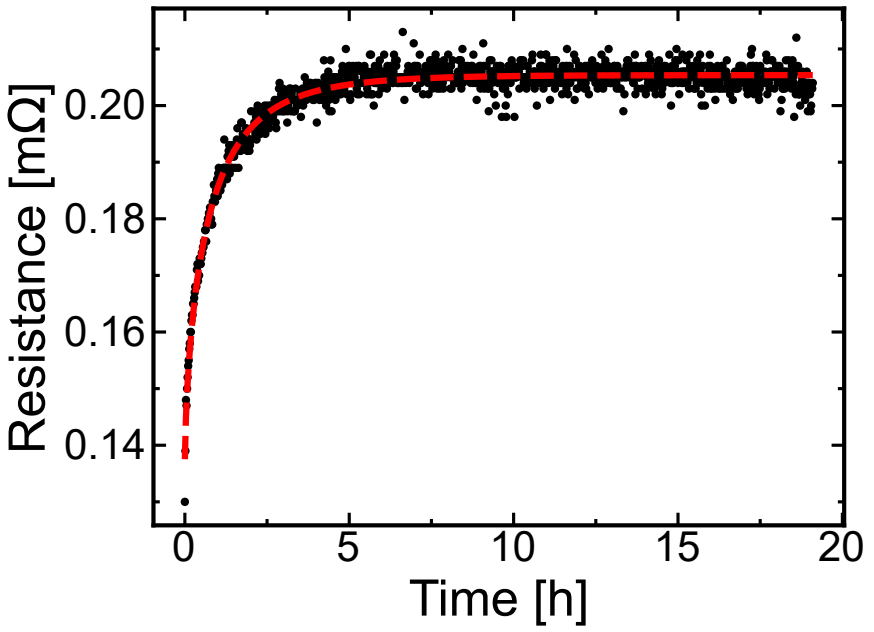

Figure 4.4: Repeated measurement of Ga-Na solution (with reference to Fig. 4.3).

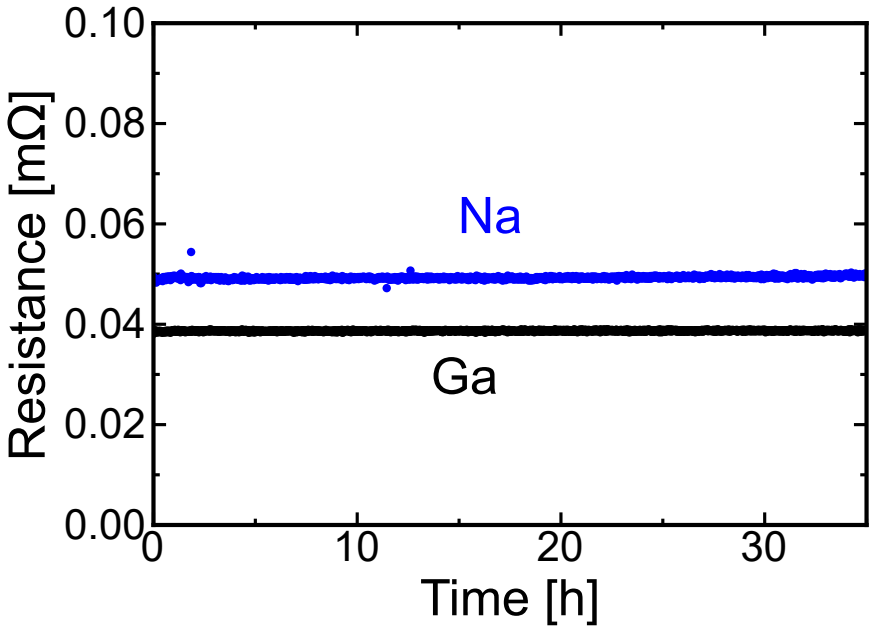

Figure 4.5: Changes of electrical resistance of liquid Ga and Na subjected to a constant argon atmosphere at 870 °C.

dered binary mixture of Ga-Na, according to Nordheim's rule [2], can be described as following

$$\rho = \rho_{Ga}\chi + \rho_{Na}(1-\chi) + \rho_{GaNa}\chi(1-\chi) \tag{4.2}$$

where ρ_{Ga} and ρ_{Na} are the resistivity of the pure Ga and Na, respectively. ρ_{GaNa} is the residual resistivity arising from the alloying of Ga and Na. χ denotes the fraction of Ga.

In fact, Itami *et al.* reported the composition dependence of the electrical resistivity of Ga-Na which shows the maximum at Na fraction composition of 50 %. This confirms that the alloy structure's disorder can significantly increase its resistance, thereby validating the presence and impact of alloy scattering.

Increasing resistance curve

Temporal increases in electrical resistance were observed in the electrical resistance measurement of Ga-Na, which can be described using Eq. (4.1). Exponential part in the second term of Eq. (4.1) is known as the Avrami exponent

$$X(t) = 1 - e^{-Kt^n} \tag{4.3}$$

where X shows the transformed fraction during solid-solid or liquid-solid transformation. This equation is often used in JMAK (Johnson-Mehl-Avrami-Kolmorogov) analysis to de-

scribe the kinetics of phase change [4] or crystallization kinetics [5]. Although there are several works that reported electrical resistivity time evolution on isothermal annealing that fits Avrami equation [6–8], there are no reported cases for liquid-liquid transformations. Consequently, it was not clear whether the Avrami equation could accurately describe a liquid-liquid transformation, as in the case of Ga-Na in the melt form. If the resistance increase is due to additional alloying scattering, as described previously, then the increase indicates the transformation of pure Ga and Na into a mixture of Ga-Na solution. The Avrami exponent could potentially describe the fractional progression of this process.

A similar temporal increase in electrical resistance was observed by Addison *et al.* during the dissolution of Ba into liquid Na. Resistance eventually plateaued, indicating that the Ba had completely dissolved into the Na, resulting in a homogenous solution [9]. Wang *et al.* observed the homogenization process in the electrical resistivity monitoring during the isothermal melting process of a semimetal Bi-Ga-Sn alloy. In that report, the electrical resistivity decreased towards a homogeneous transformation due to the lower resistivity of the semimetal Bi alloy compared to its metal/semimetal constituent.

Considering that the Ga-Na solution exhibited a higher resistivity, the increase in resistance implies a transformation towards a homogeneous Ga-Na solution, and saturation may signal complete homogenization. Therefore, the resistance increase curve could be analyzed to evaluate the time required for the Ga-Na solution to transform into a homogeneous solution. If the homogenization process leads to the even distribution of Ga atoms within the Ga-Na solution, it could potentially optimize the increase in nitrogen solubility in the Ga-Na solution [11]. The increasing resistance curve was not observed in the measurements of pure liquid Ga and Na, because pure metal did not undergo the process of homogenization.

4.1.3 Investigation on Homogenization velocity

In this section, the author investigates the parameters that are involved in the homogenization process by measuring the electrical resistance of Ga-Na solution and analyzing the resistance curve observed at the early stage of measurement. Here, the author alters two parameters: temperature, and composition of Ga-Na solution. The observed curve is fitted with the following equation

$$R(t) = R_0 + \Delta R(1 - e^{-kt}) \tag{4.4}$$

considering fitting with Avrami equation yield the value of n around 0.9~1.1, which can be treated as 1 for the sake of simplicity. Here, k is treated as the reaction rate to indicate how fast the homogenization occurs. Table 4.2 summarizes the measurement conditions

and the fitted value of k. Figures 4.6 to 4.8 shows the measured electrical resistance curve for Ga-Na solution with composition 27:73, 20:80, and 13:87 respectively.

Table 4.2: Measurement conditions and fitted reaction rate constant for investigation of homogenization velocity.

Temperature [°C]	Ga:Na [mol %]	k [h^{-1}]
700	27:73	0.409 ± 0.007
800		0.659 ± 0.009
900		1.704 ± 0.016
700	20:80	0.783 ± 0.008
800		1.129 ± 0.023
900		1.613 ± 0.078
700	13:87	1.773 ± 0.030
800		24.00 ± 7.476
900		1.776 ± 0.031

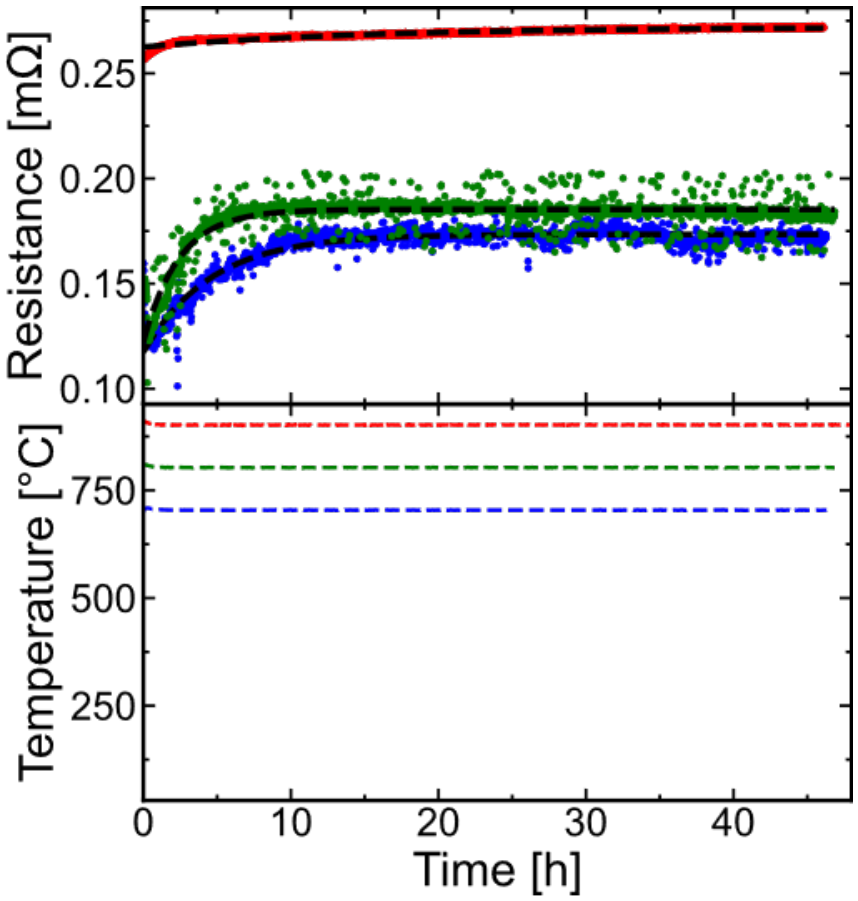

Figure 4.6: Changes of electrical resistance of the Ga-Na solution with Ga:Na composition of 27:73 mol %.

In Fig. 4.6, the resistance values measured at 900 °C are noticeably higher than those measured at 800 °C and 700 °C. This discrepancy can be attributed to variations in the

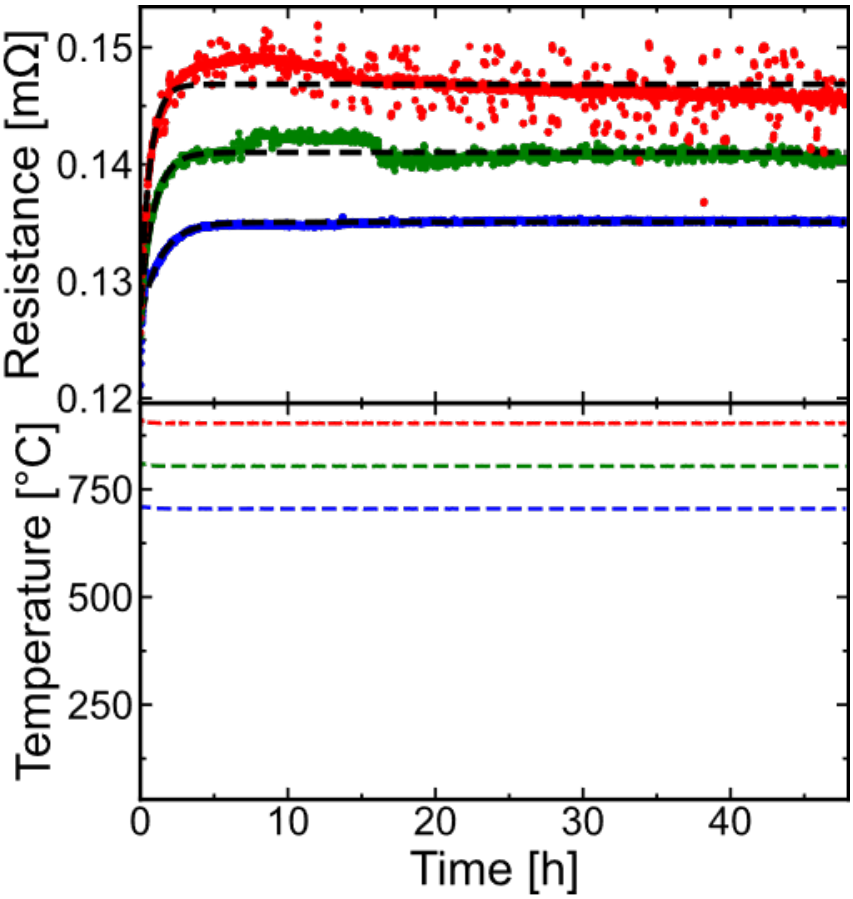

Figure 4.7: Changes of electrical resistance of the Ga-Na solution with Ga:Na composition of 20:80 mol %.

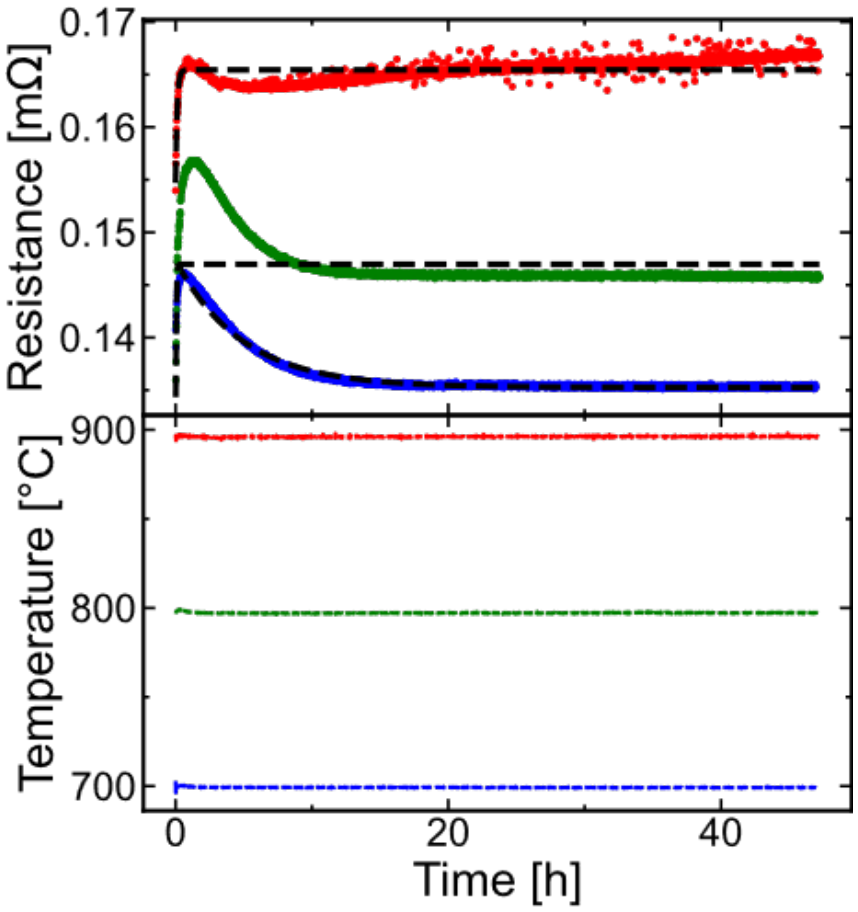

Figure 4.8: Changes of electrical resistance of the Ga-Na solution with Ga:Na composition of 13:87 mol %.

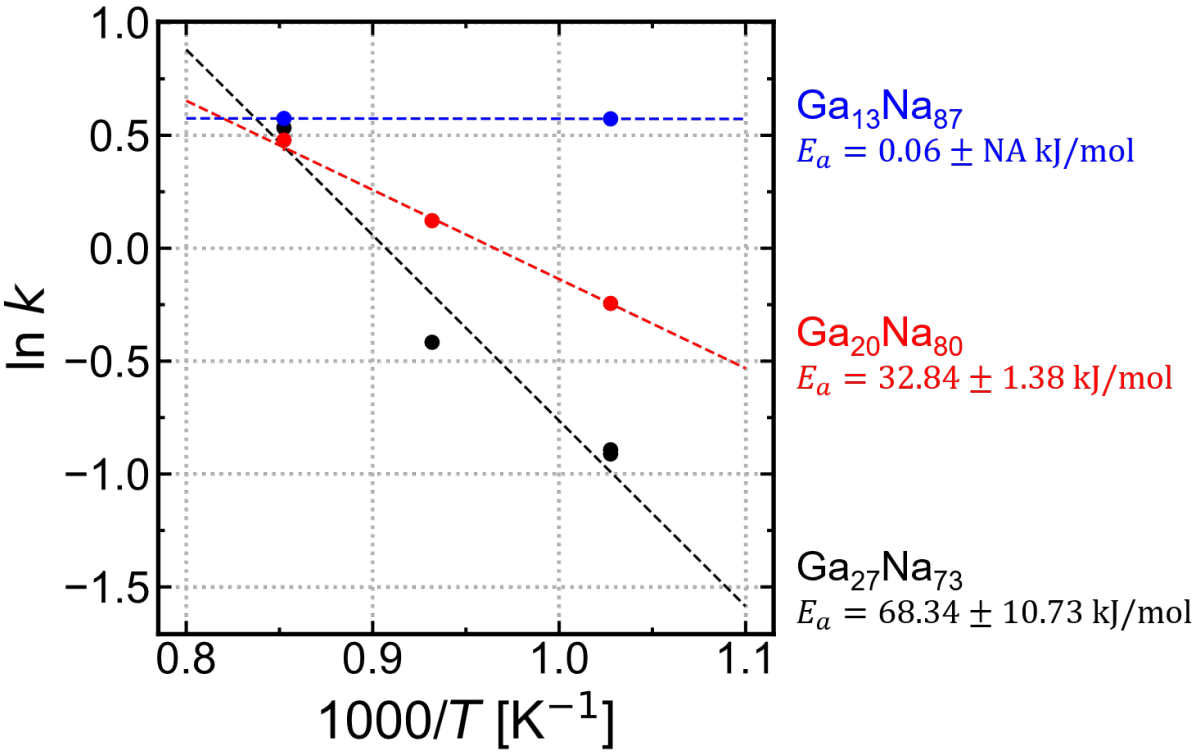

Figure 4.9: Arrhenius plot of homogenization reaction rate constant of Ga-Na solution.

probe position. Despite these discrepancies, reasonable k values were obtained from the curve fitting.

Measurements performed on the Ga-Na solution with a Ga:Na composition of 13:87 mol % presented some challenges. Most of the resistance curves showed a sharp overshoot, the cause of which remains unclear. Furthermore, changing the composition of the solution affects its physical properties, such as wettability, making the measurements more challenging. Specifically, the electrical resistance measured at 800 °C could not be satisfactorily fitted using Eq. (4.4), resulting in an anomalous k value. This result implies that other factors not accounted for in the analysis might be influencing the homogenization process at this temperature and composition.

The fitted values of k as summarized in Table 4.2 were used to construct the Arrhenius plot shown in Fig. 4.9. A simple linear regression fit was evident from the data points. Assuming that k follows the Arrhenius equation

$$k = Ae^{-\frac{E_a}{RT}} \tag{4.5}$$

where A is the pre-exponential factor, E_a is the activation energy, R is the gas constant, and T is the temperature, the activation energy is calculated E_a from the slope of the straight line in the Arrhenius plot. The calculated activation energy and its corresponding uncertainty range for the Ga-Na solutions with Ga:Na compositions of 27:73

mol %, 20:80 mol %, and 13:87 mol % are 68.34 ± 10.73 kJ/mol, 32.84 ± 1.38 kJ/mol, and 0.06 kJ/mol, respectively. Note that the electrical resistance curve for composition 13:87 mol % exhibited anomalous behavior, making the validity of the derived activation energy questionable.

The fact that k follows the Arrhenius equation likely suggests that the homogenization process primarily depends on mutual diffusion [10]. It has been reported that diffusion in Bi-Ga binary melts obeys the Arrhenius relationship [12], which further supports this interpretation. This indeed appeared to be the case in the absence of mechanical stirring.

Activation energy derived from this study could be seen as an indicator of the efficiency of the homogenization process. Higher activation energy values, such as those found in Ga:Na compositions of 27:73 mol %, suggest a slower homogenization process. Conversely, lower activation energy values found in Ga-Na solutions with lower Ga composition suggest a faster homogenization process. The activation energy of 68.34 ± 10.73 kJ/mol for Ga:Na 27:73 mol % was higher than that reported for Bi-Ga melt (27.175 ± 0.600 kJ/mol) [12]. However, it is worth noting that a rapid homogenization process can be achieved by conducting the melting process at higher temperatures.

4.2 Kinetics of nitrogen dissolution in Ga-Na solution

4.2.1 Measurement in nitrogen atmosphere

In this section, the electrical resistance of Ga-Na solution in a nitrogen atmosphere was investigated. The measurement condition is shown in Table 4.3.

Table 4.3: Measurement conditions of Ga-Na solution in nitrogen atmosphere.

Temperature [°C]	Gas / Pressure [MPa]	Ga:Na [mol %]	Test Current [A]
870	N_2 / 4	27:73	0.1

Fig. 4.10 shows the temporal evolution of electrical resistance of the Ga-Na solution when pressurized with nitrogen gas. At the initial stage of measurement, the similar increasing resistance curve when measured in argon atmosphere was also observed. However, at the later stage, the value of resistance did not saturate. Instead, it showed a continuous linear increase over more than 80 hours of measurement. Interestingly, this behavior can be well fitted into the following equation

$$R(t) = R_0 + \Delta R(1 - e^{-Kt^n}) + R't \tag{4.6}$$

This function is similar to Eq. (4.1) used for fitting the electrical resistance measured at argon, with an additional linear term $R't$ being added.

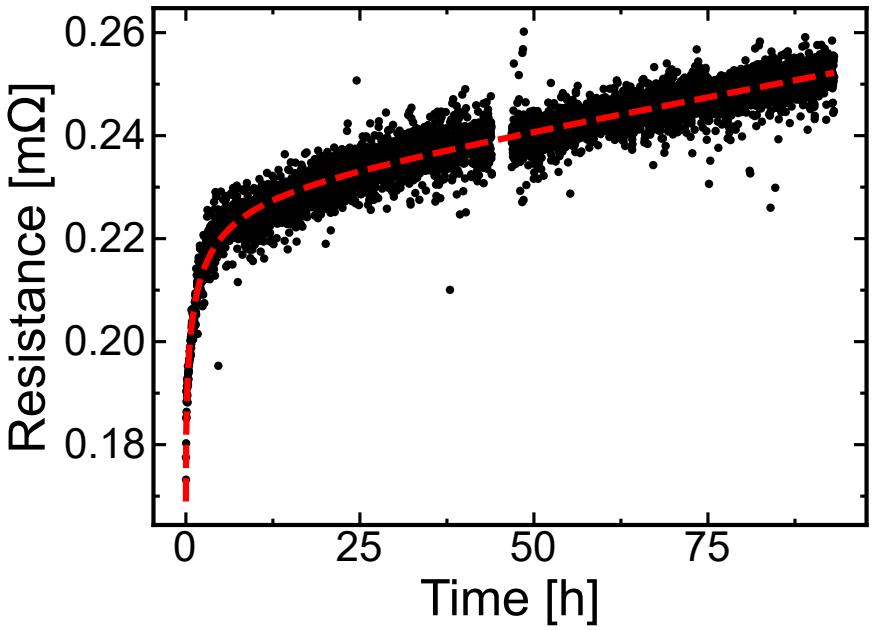

Figure 4.10: Changes of electrical resistance of the Ga-Na solution subjected to a constant nitrogen atmosphere at 870 °C.

4.2.2 Interpretation on linear increase in resistance

Comparing the electrical resistance measured in a nitrogen atmosphere with that measured in an argon atmosphere, it can be hypothesized that the linear increase ($R't$) is a phenomenon uniquely occurring in the nitrogen environment, suggesting that this might be the nitrogen dissolution process in the Ga-Na solution. Consequently, the high resistance implied high number of nitrogen being dissolved in the solution as depicted in Fig. 4.11 This observation is rather counter-intuitive, as the resistance continuously increased for over 80 hours, implying that nitrogen is not reaching its equilibrium (or saturation point). In the nitrogen dissolution of iron (Fe), the dissolution reaction occured much faster [13]. If the resistance increase was induced by other species, such as oxygen (potentially from decomposition of the alumina crucible), we would have expected to observe a similar increase in the electrical resistance measured in the argon atmosphere. However, this was not the case, suggesting that the contribution of oxygen to an increase in electrical resistance was either negligible or significantly smaller compared to that of nitrogen. This notion aligns with a report by Addison *et al.*, who reported that the contribution of oxygen to the electrical resistance of liquid Na was four times smaller than that of nitrogen [14]. Therefore, based on the electrical resistance data, it can be hypothesized that the concentration of nitrogen in the Ga-Na solution is gradually increasing.

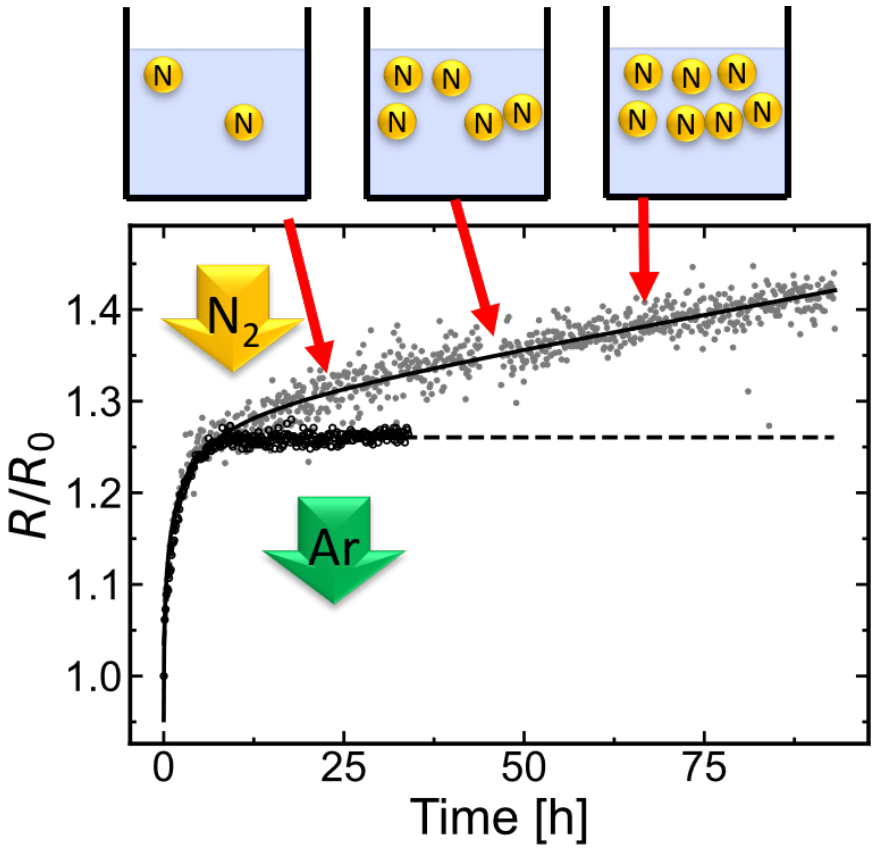
N
N
N

4.2.3 Time dependence

To confirm that nitrogen indeed continuously dissolves throughout the process period, two methods were employed for validation: ex-situ crystal growth investigation, and pressure decay monitoring.

Ex-situ crystal growth investigation

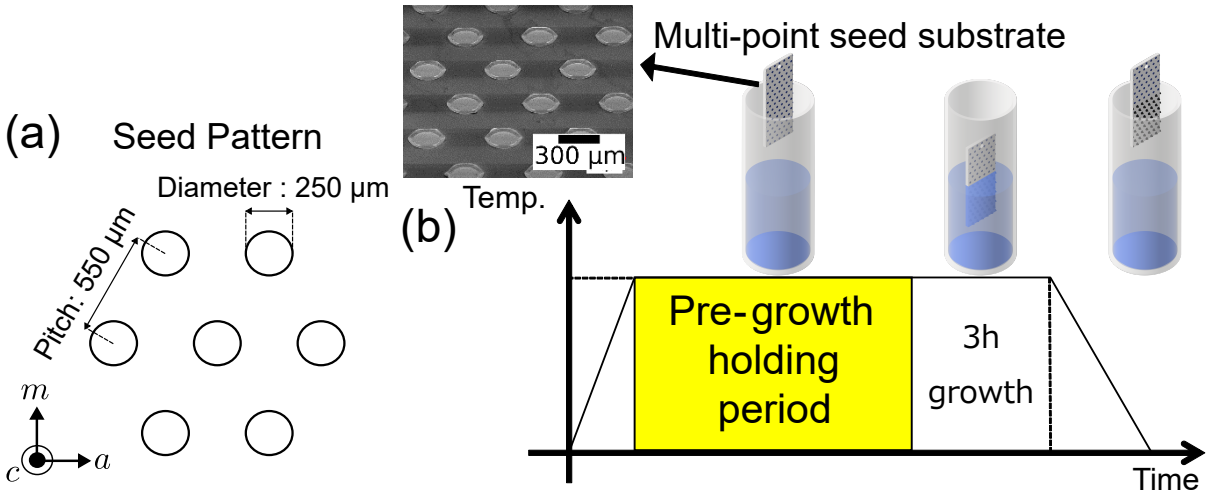

Figure 4.12: (a) Schematic drawing of the pattern of multi-point seed substrate and (b) temperature sequence used for ex-situ crystal growth investigation.

Nitrogen concentration in the Ga-Na solution was estimated from the size of the GaN crystal that grew on a multi-point seed (MPS) substrate [15] (point seed diameter: 250 µm, pitch: 550 µm) over a short growth period of three hours. The seed pattern and the temperature sequence used for the crystal growth are presented in Fig. 4.12. To investigate the time dependence of nitrogen dissolution, the dipping method [16] was employed. This allowed the positioning of the seed crystal and the initiation of growth at an arbitrary time.The MPS substrate was positioned above the crucible for a specific duration named as the pre-growth holding period (or pre-growth nitrogen dissolution period). This pre-growth holding period was varied to 24 hours, 48 hours, 72 hours, and 144 hours in different experiments to modify the nitrogen dissolution process period. Subsequently, the growth of GaN over the next three hours would reflect the supersaturation, or the nitrogen concentration, at the time when crystal growth commenced. The grown crystals were observed with a scanning electron microscope and their size (thickness) were evaluated using Keyence VK-9710 Laser Microscrope (resolution: 0.001 µm).

Figure 4.13 shows the scanning electron microscope images of the grown crystals. Here, it can be observed that the crystals grown over longer pre-growth holding periods

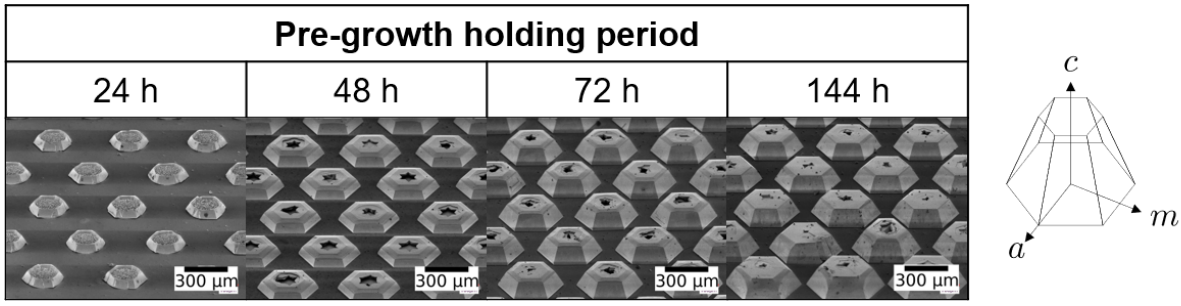

Figure 4.13: Scanning electron microscope images of GaN crystal grown on a MPS substrate at 870 °C with various pre-growth holding period.

were larger in size compared to those grown over shorter periods. This suggests that supersaturation increases with prolonged nitrogen dissolution periods.

The grown crystals were observed to have a hollow or void-shaped center. This is likely due to faster crystal growth at the edges compared to the center, a result of supersaturation differences, a phenomenon known as the Berg effect [17]. This could suggest that the slow mass transport of nitrogen in the liquid acts as a limiting factor, bottlenecking the nitrogen dissolution process toward its equilibrium.

Figure 4.14 presents both the yield and the average thickness of the GaN crystals. The data show an increasing trend in yield and thickness with longer pre-growth holding periods. Moreover, crystal growth with holding periods of 72 hours and 144 hours led to the formation of polycrystal growth (polyGaN) observed on the inner ring of the crucible. The total yield of seeded GaN growth decreased with a 144-hour holding period due to the consumption of nitrogen by the seed substrate being outpaced by the polycrystalline growth. As a result, the total yield of the GaN crystal growth cannot be used as a reliable reference due to high uncertainty, and accounting for polycrystalline growth would complicate the analysis.

Therefore, the author shifted the focus to the size of the grown crystal, which was measured from individual point seeds.

The observed increase in crystal size with longer pre-growth holding periods indicates an increase in supersaturation during the nitrogen dissolution process. This observation aligns well with the electrical resistance measurements, which also suggest an increase in nitrogen concentration with prolonged nitrogen dissolution periods.

These findings imply a surprising fact that nitrogen does not reach its equilibrium in the Ga-Na-N system during the Na-flux growth, even after 80 hours. Specific reasons behind this behavior remains unclear, but these measurements have revealed the time-dependent nature of the nitrogen dissolution process.

Formation of polyGaN in cases of prolonged pre-growth holding periods can be explained by the concept of the metastable region [18] and the time-dependent increase of nitrogen concentration. Polycrystalline growth did not nucleate, but seeded growth was

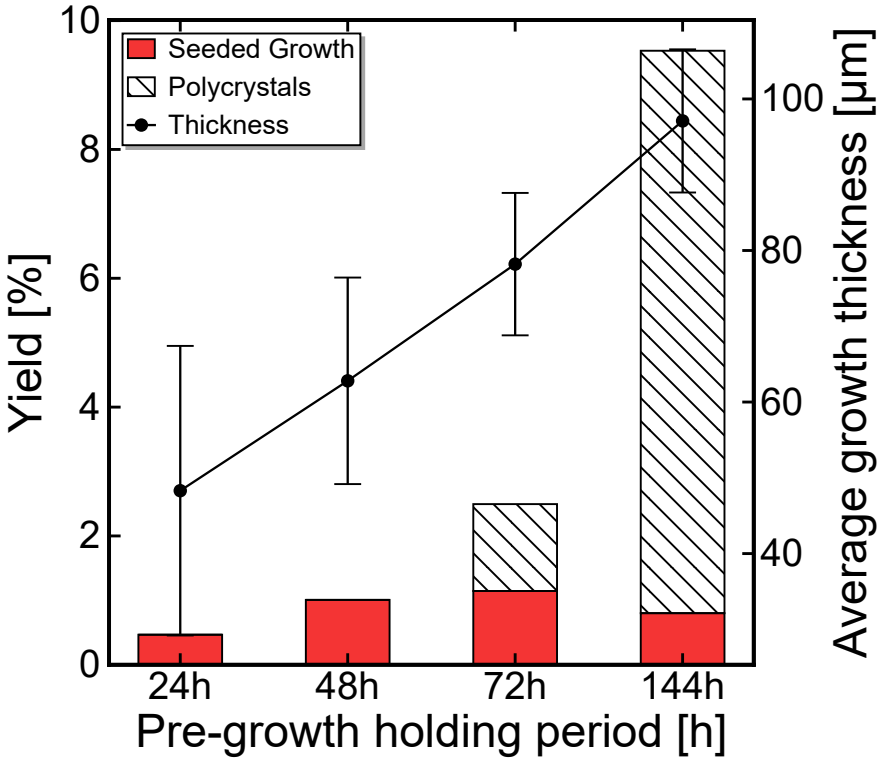

Figure 4.14: Pre-growth holding period dependence of yield and thickness of the GaN crystal growth in Ga-Na solution.

possible because nitrogen concentrations were in the metastable region. A longer dissolution period resulted in an increase in nitrogen concentration, leading to the occurrence of heterogeneous nucleation as the nitrogen concentration became superfluous.

Increase in electrical resistance due to nitrogen dissolution

What could be the possible mechanism that causes an increase in electrical resistance when nitrogen dissolves into the Ga-Na solution? Figure 4.15 presents a simple model that illustrates the increase in electrical resistivity due to the loss of free electrons in the Ga-Na solution.

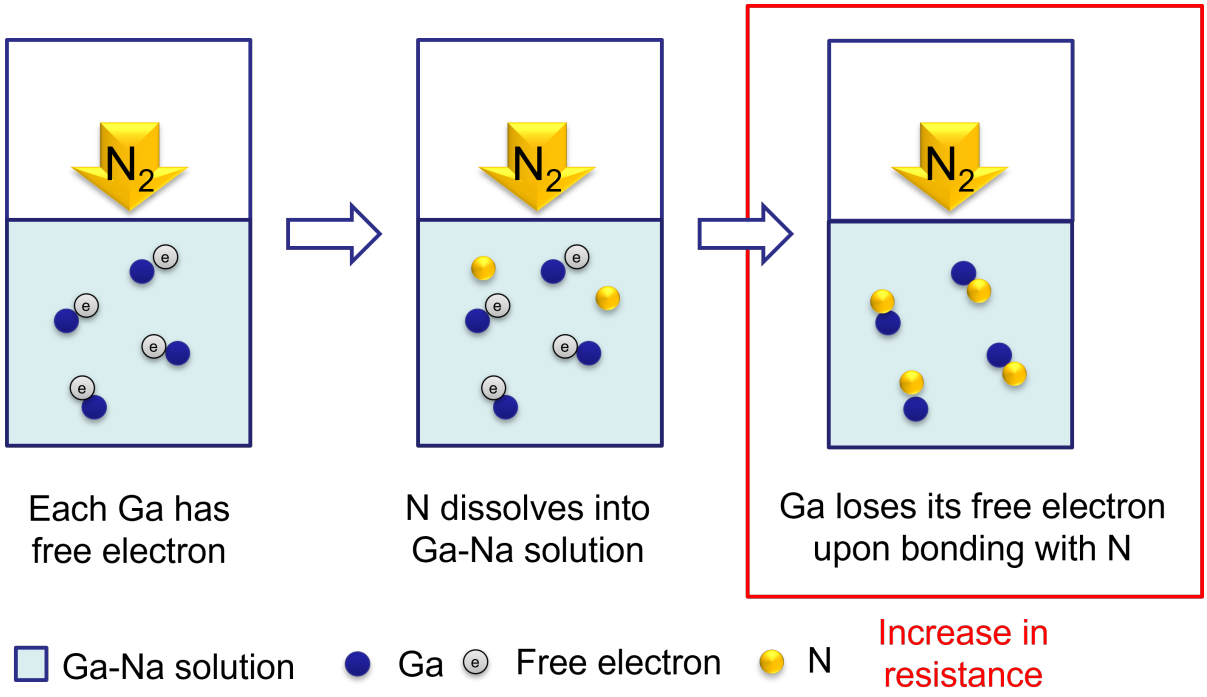

Figure 4.15: Illustration of nitrogen dissolution process and captures of Ga free electron by formation of Ga-N bonding.

Initially, Ga atoms in the Ga-Na solution carry free electrons. As nitrogen dissolves into the solution, it bonds with Ga atoms, leading to the formation of Ga-N. This bonding process results in the Ga atoms losing their free electrons [19, 20]. As described by the Drude model (Eq. (3.1)), electrical resistivity ρ is inversely proportional to the concentration of free electrons n. Therefore, the reduction in free electron concentration due to the formation of Ga-N bonds inherently leads to an increase in the electrical resistance of the Ga-Na solution.

Another potential mechanism is that nitrogen in the Ga-Na solution may act as a scattering center, similar to an impurity, which could disrupt the flow of electrons and thus lower the conductivity of the solution. However, the subsequent investigation using pressure decay monitoring seemed to be more consistent with the first model.

Pressure decay monitoring

Continuous dissolution of nitrogen may be inferred from the linear increase in electrical resistance, which happens as gallium atoms bond with nitrogen, leading to a decrease in free electrons. The author thus gathered further evidence to support this mechanism by examining its correlation with nitrogen pressure decay monitoring, which was proposed by Von Dollen *et al.* as a in-situ monitoring method for Na-flux growth [21].

As illustrated in Fig. 3.4, the experimental setup for electrical resistance measurement incorporates a pressure transducer installed at both the growth vessel and gas reservoir, enabling the monitoring of gas pressure. The gas filled into the growth vessel is regulated to a constant 4 MPa and is supplied from the gas reservoir. By recording the value of the backpressure (measured at the gas reservoir), it is possible to track pressure decay, which indicates the absorption of gases occurring within the Ga-Na solution system. Backpressure was recorded using NAGANO KEIKI GC16 pressure transducer (with an accuracy ± 0.035 MPa). To accurately interpret the pressure decay data, it is critical to first examine the baseline behavior of the backpressure, both when measured in an argon atmosphere, and when measured in a nitrogen atmosphere without the presence of a Ga-Na solution. This provides a baseline for understanding the unique pressure changes associated with the Ga-Na-N system.

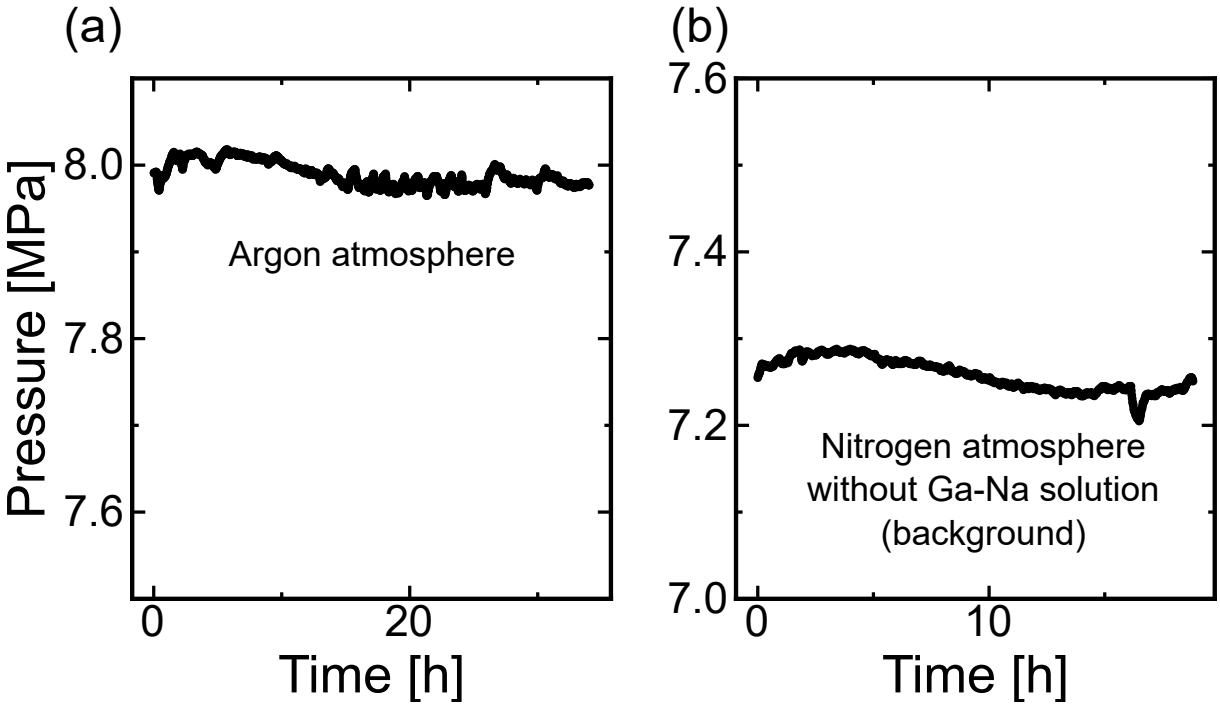

Figure 4.16: Backpressure profile monitored during (a) measurement of electrical resistance of Ga-Na solution in argon atmosphere and (b) during heating of an empty pressure-resistant vessel.

Figure 4.16a shows the backpressure values obtained during the measurement of electrical resistance of the Ga-Na solution in an argon atmosphere (Fig. 4.3). No significant reduction in pressure was observed, suggesting that argon was neither absorbed by the Ga-Na solution nor by the containing vessel or crucible. In Fig. 4.16b, the backpressure of nitrogen is shown during the heating of a stainless-steel vessel without the Ga-Na solution present. Changes in pressure were also small, indicating no significant absorption by the pressure-resistant vessel.

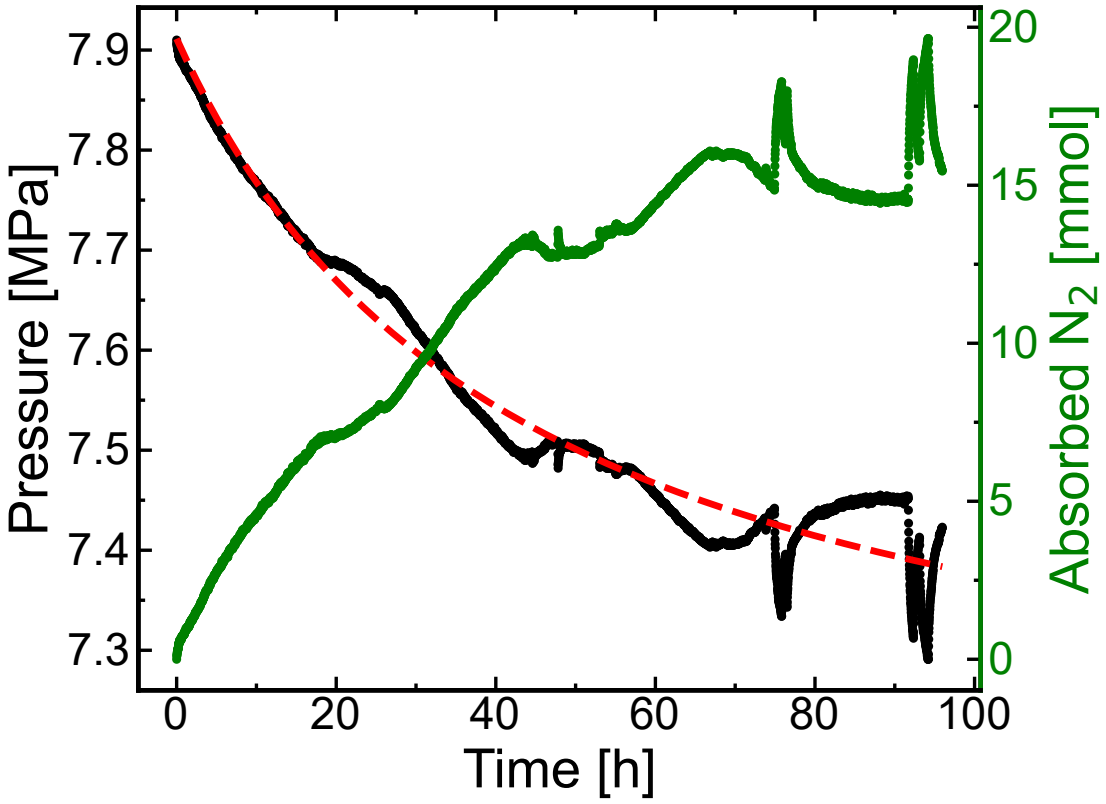

Figure 4.17: Nitrogen pressure decay during measurement of electrical resistance of Ga-Na solution in nitrogen atmosphere (Fig. 4.10). Total absorption of N_2 (green) was calculated from pressure decay by applying ideal gas law.

Figure 4.17 shows the nitrogen pressure decay during measurement of electrical resistance of Ga-Na solution in the nitrogen atmosphere (see Fig. 4.10). Compared to background measurement in Fig. 4.16b, the pressure decay curve indicates the nitrogen absorption in the Ga-Na solution, which decreased by about 0.6 MPa. The nitrogen pressure curve was converted into the total absorption of nitrogen in mmol by applying ideal gas law.

$$\Delta n = \frac{\Delta P V}{R T} \tag{4.7}$$

where Δn represents the total absorbed N_2 in moles, ΔP indicates the pressure drop, V corresponds to the volume of the gas reservoir (not considering the volume of the connecting pipe), T is the temperature of N_2 in the reservoir, and R is the ideal gas constant. The total absorption of N_2 was approximately 15 mmol. Assuming every molecule of N_2 dissociated into radicalized nitrogen N^*, the total amount of nitrogen in the Ga-Na-N system would be about 30 mmol. This is half of 62 mmol, the total moles of Ga initially prepared.

Based on models outlining the capture of free electrons by nitrogen, the quantity of free electrons in the solution over time, denoted as $N(t)$, is inversely proportional to electrical resistance. Consequently, if the electrical resistance rises linearly over time, the change in the number of free electrons as a function of time would correspond to an inverse function of this linear increase.

$$N(t) \propto \frac{1}{at + b} \tag{4.8}$$

The system compensates for the loss of nitrogen, which occurs due to its bonding with Ga atoms and subsequent absorption in the solution, through a corresponding decrease in pressure from the gas reservoir. Assuming that the quantity of nitrogen absorbed is directly proportional to the loss of free electrons from Ga, the pressure decay curve can be satisfactorily fitted using equation Eq. (4.8). This is confirmed by the pressure decay curve shown in Fig. 4.17, which is indeed well-aligned with the fit obtained from equation Eq. (4.8). This result supports the model that suggests an increase in resistance due to the capture of free electrons.

4.2.4 Temperature dependence

From the investigation described in the previous section, it was revealed that the electrical resistance can be utilized to monitor the amount of dissolved nitrogen in the form of increased resistance. The previous section has revealed the time-dependent nature of nitrogen dissolution in the Ga-Na system. Here, the author used this phenomenon to investigate the temperature dependence of nitrogen dissolution in Ga-Na solution by examining the behavior of electrical resistance of the Ga-Na solution subjected to different temperatures.

The measurement of electrical resistance was carried out following the same procedure outlined in the previous section. The Ga-Na solution was heated and maintained at target temperatures of 840 °C, 870 °C, and 900 °C, and the electrical resistance at these temperatures was investigated.

Figures 4.18 to 4.20 show the change in electrical resistance over time for a Ga-Na solution under 4 MPa of nitrogen gas pressure at temperatures of 840 °C, 870 °C, and 900 °C, respectively. In each instance, an increasing resistance curve is evident in the early stages of measurement, which suggests a homogenization process. In the later stages of

Table 4.4: Measurement conditions of Ga-Na solution heated at various temperature.

Temperature [°C]	Gas / Pressure [MPa]	Ga:Na [mol %]	Test Current [A]
840	N_2 / 4	27:73	1
870	N_2 / 4	27:73	1
900	N_2 / 4	27:73	1

measurement, a linear increase in resistance indicates the nitrogen dissolution process. The resistance measurements at 840 °C and 870 °C align well with Eq. (4.6). However, the increasing resistance observed at 900 °C deviates from linearity and shows a more complex, non-linear behavior.

A direct comparison of resistance values between experiments can be challenging due to significant uncertainties tied to geometric factors, such as probe position. Despite this, it is crucial to perform an analysis on these measured values. For this purpose, all resistance values are replotted in the figure using normalized values, expressing the increase as a resistance ratio. Here, discussion will focus on the behavior instead of the resistance values.

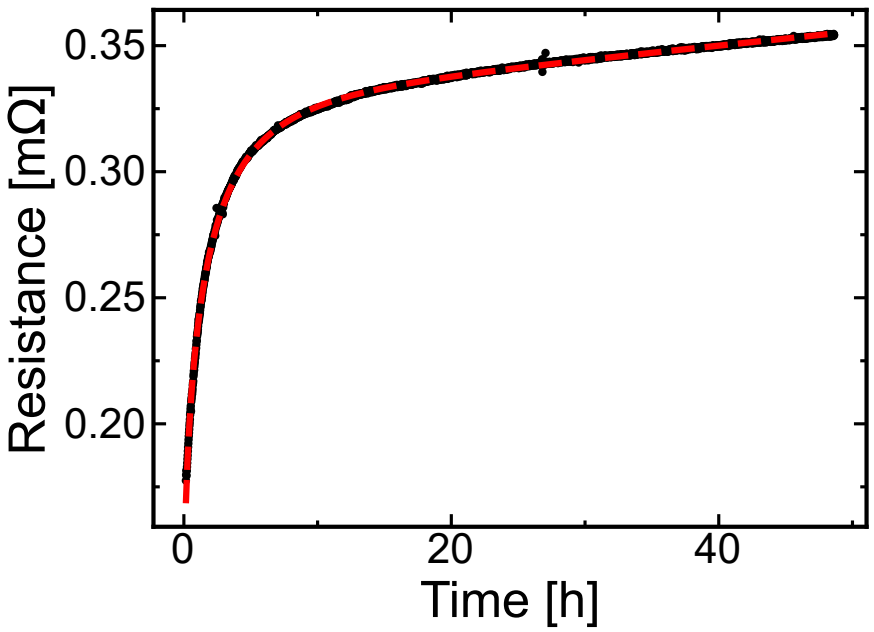

Figure 4.18: Changes of electrical resistance of the Ga-Na solution in nitrogen atmosphere at 840 °C.

As per Fig. 4.21, the linear increase in electrical resistance observed at 840 °C and 870 °C did not significantly differ. However, a notably steeper slope was observed for

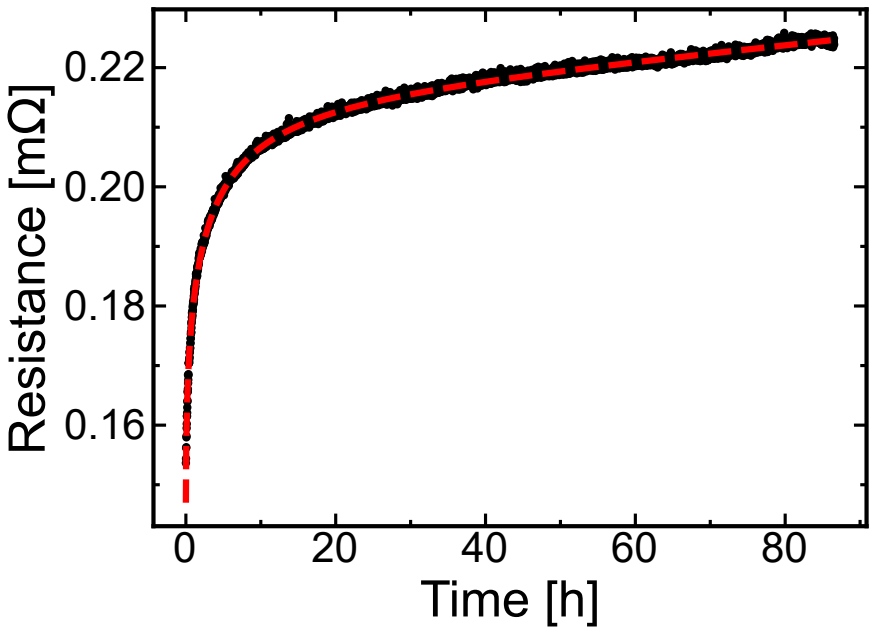

Figure 4.19: Changes of electrical resistance of the Ga-Na solution in nitrogen atmosphere at 870 °C.

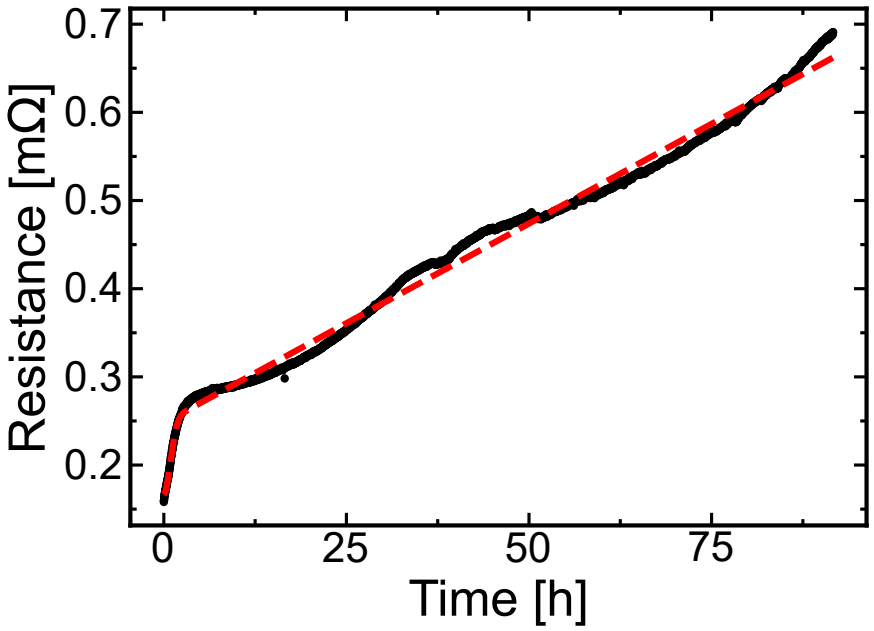

Figure 4.20: Changes of electrical resistance of the Ga-Na solution in nitrogen atmosphere at 900 °C.

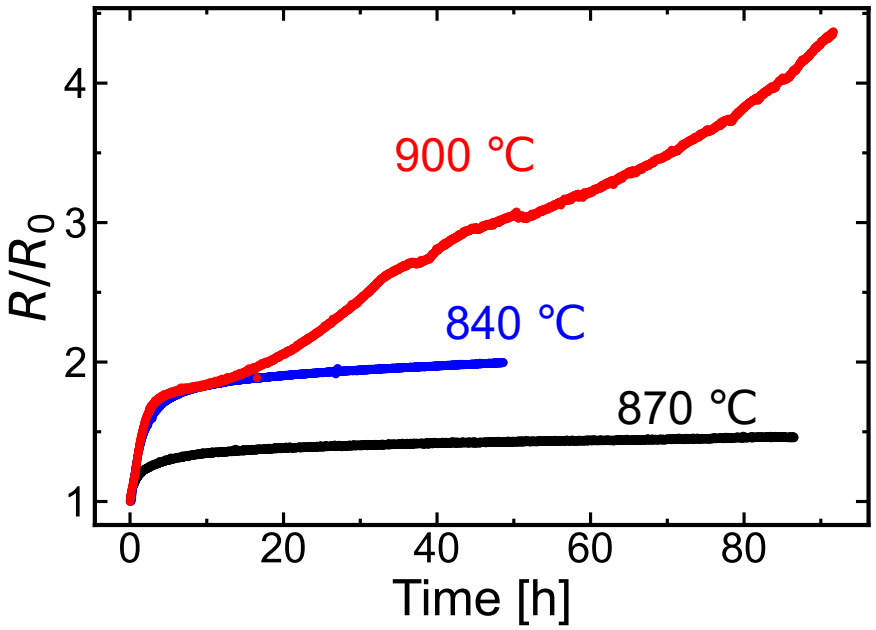

Figure 4.21: Changes of electrical resistance ratio of Ga-Na solution over time at different temperature.

resistance increase measured at 900 °C. By the end of the measurement, the electrical resistance value exceeds four times of its initial value. Unfortunately, further investigation beyond 80 hours was hindered due to the rupture of the stainless-steel vessel, resulting in nitrogen gas leakage.

If we interpret the electrical resistance as indicative of the amount of dissolved nitrogen, the measurements suggest that the nitrogen dissolution process is significantly enhanced at a higher temperature of 900 °C. To substantiate this, the author investigated the dependency of the pre-growth nitrogen dissolution period on the MPS GaN crystal, grown at 900 °C. Crystal was grown following the same seed pattern and temperature sequence as detailed in Fig. 4.12. Width and thickness of the samples were evaluated using a Keyence VK-9710 Laser microscope, which has a resolution of 0.001 µm. Here, "width" refers to the distance between two opposing *m*-plane facets, while "thickness" is defined as the height of the truncated hexagonal pyramid. The thickness was profiled across two opposing facets. These measurements, both width and thickness, were taken from 10 samples of the grown point seed.

Figure 4.22 shows the SEM images and pre-growth holding period dependence of the GaN crystal grown at 900 °C. The observation showed increasing crystal size with a longer pre-growth holding period, which is consistent with the predicted increase in nitrogen concentration from the increase in electrical resistance. However, the resulting GaN crystal did not appear to grow larger compared to SEM images provided in Fig. 4.13

The detailed evaluation of the crystal size (width and thickness) is shown in the Fig. 4.23. The crystals grown at a temperature of 900 °C were generally smaller than those grown at 870 °C. However, the crystal size showed a linear increase with extended pre-growth holding periods at 900 °C. In contrast, crystal growth at 870 °C appeared to reach a saturation point at around 72 h.

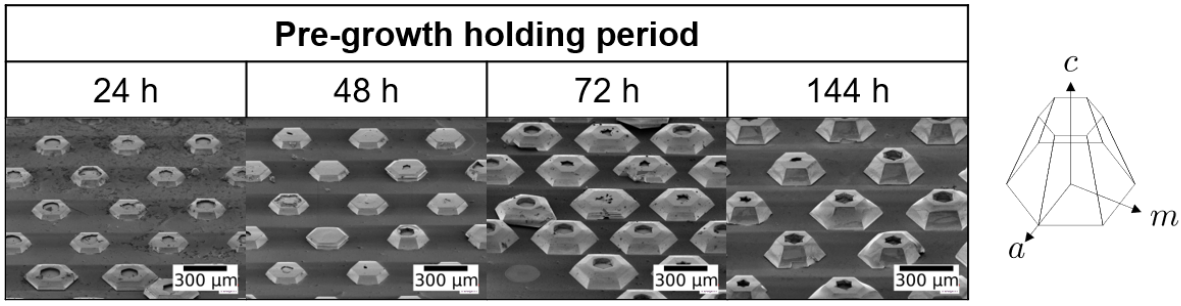

Figure 4.22: Scanning electron microscope images of GaN crystal grown on a MPS substrate at 900 °C with various pre-growth holding period.

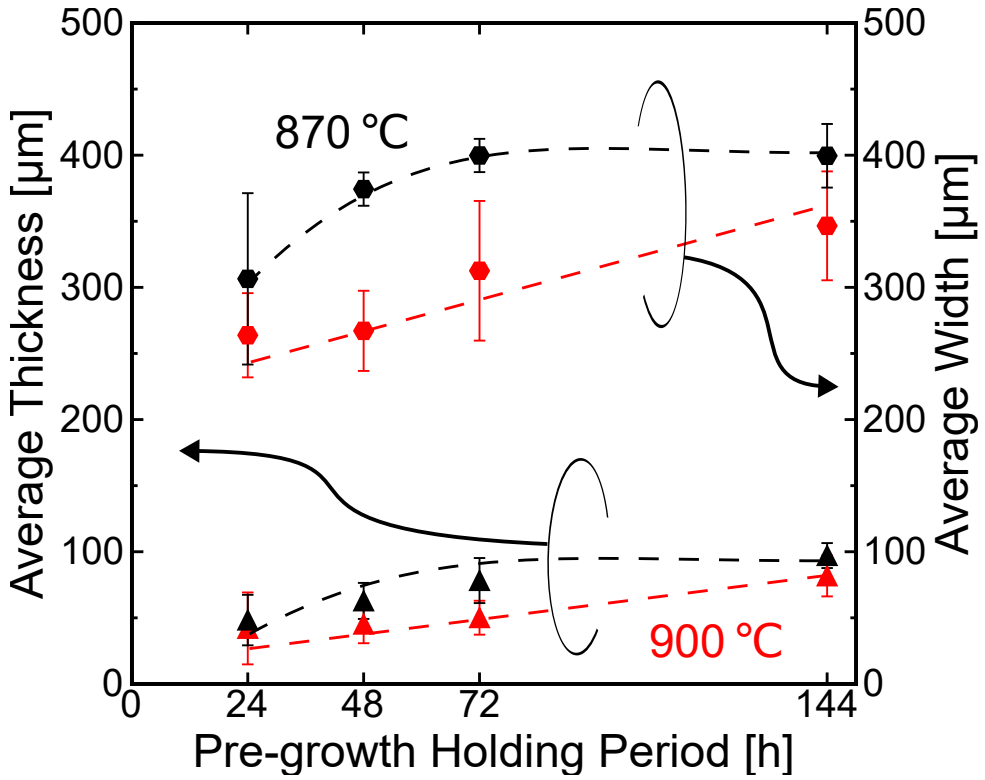

Figure 4.23: Evaluation of width and thickness of GaN crystals grown at 870 °C and 900 °C. Thickness was measured as the height of truncated hexagonal pyramid. Width was measured as the distance between opposing *m*-plane facets. The dashed lines indicate the guideline.

Discussion: effect of high solution temperature

As described in the previous section, the increase in electrical resistance indicate the process of nitrogen dissolution through formation of Ga-N bonds that resulted in the decrease of free electrons in the solution. The slope in Fig. 4.21 then shows how fast the electrons depleted, in other words the nitrogen dissolution rate. Hence, it can be hypothesized that nitrogen is enhanced at 900 °C, which is consistent with the fact that nitrogen dissociation reaction is an endothermic process [22]. Then, high growth rate (crystal size) could be expected from increased supersaturation of the Ga-Na solution with a greater amount of nitrogen concentration. Although the nitrogen dissolves faster at high temperatures, the overall growth rate at 900 °C was lower than that at 870 °C. As mentioned in Section 2.2.1, the supersaturation σ in the Na-flux growth is described with Eq. (2.3) ($\sigma = \frac{S-S_0}{S_0}$). While increasing the nitrogen concentration S at higher temperatures can enhance supersaturation, the increased temperature also leads to a higher solubility of GaN S_0, which reduces supersaturation both in the numerator and the denominator. As a result, supersaturation diminishes if the rise in GaN solubility is greater than the increase in nitrogen concentration. Referring to the solubility data reported by Morishita *et al.*, it was calculated that the solubility of nitrogen only increased by 2 %, which was significantly outpaced by a 37.7 % increase in GaN solubility when the temperature was increased from 870 °C to 900 °C. The net effect of these changes was a decrease in supersaturation from 35.6 % at the lower temperature to only 0.6 % at the higher temperature.

Despite the high solubility of GaN at 900 °C, the growth in crystal size in relation to the pre-growth holding period was linear and comparable to the growth observed at 870 °C. This suggests a more substantial increase in nitrogen concentration at a higher temperature. In essence, this points towards an enhanced rate of nitrogen dissolution at elevated temperatures. The enhancement in nitrogen dissolution at higher temperatures was confirmed through crystal growth experiments, aligning well with the electrical resistance measurements [24]. A higher solution temperature resulted in increased nitrogen solubility, and the resulting deviation from equilibrium appeared to drive the rate of nitrogen dissolution.

In Chapter 6, the author utilizes this newly acquired understanding of temperature effects to achieve a solution that is highly supersaturated with nitrogen by dissolving nitrogen at elevated temperatures and subsequently growing crystals at lower temperatures. The resulting process can facilitate a faster growth rate, enhance nucleation, and effectively shorten the overall growth process.

4.3 Effect of carbon addition in the Ga-Na solution

Without a doubt, carbon has had a pivotal role in the history of Na-flux growth. It has effectively solved issues concerning nucleation control [25], thereby enabling the progression of LPE growth and the continued development of Na-flux techniques. As a result, the use of carbon has become a standard practice in Na-flux growth. As mentioned in Section 2.3.1, studies have elucidated that CN^- ions play a significant role in preventing parasitic GaN nucleation [26–28]. However, given that carbon is incorporated into the Ga-Na solution in the form of solid graphite, one intriguing question arises: How long does it take for the added carbon to transform into CN^- in the Ga-Na solution? This question is of particular interest considering the lengthy process of homogenization (exceeding 10 hours) and the pseudo-equilibrium state of the nitrogen dissolution process.

4.3.1 Measurement of carbon-added Ga-Na solution

Measurement on Ga-Na solution added with carbon was attempted. The total amount of solid graphite about 0.5 mol % and 1.0 mol % were loaded together with starting materials Ga and Na (Ga:Na composition 27:73 mol %), then heated to 870 °C for electrical resistance measurement. Electrical resistance measurement follows the same procedure as described previously. Table 4.5 summarizes the measurement condition.

Table 4.5: Measurement conditions of Ga-Na solution.

Temperature [°C]	Gas / Pressure [MPa]	Ga:Na:C [mol %]	Test Current [A]
870	N_2 / 4	27:73:0	1
870	N_2 / 4	27:73:0.5	1
870	N_2 / 4	27:73:1.0	1

The plots in Figure 4.24 show the temporal evolution in electrical resistance for Ga-Na solutions supplemented with 0.0 mol %, 0.5 mol%, and 1.0 mol % of carbon. Electrical resistance of the Ga-Na solution appears to increase with the addition of more carbon. This increase in resistance could possibly suggest enhanced nitrogen dissolution due to the presence of carbon. However, the interpretation of the electrical resistance data comparison of the value per experiment measurement is quite uncertain due to geometric factors.

Another interesting, yet puzzling result is the appearance of peaks and valleys around 20 hours in the carbon-added Ga-Na solution (Ga-Na-C). These behaviors were not observed in the Ga-Na-N system. Moreover, these peaks and valleys only appeared temporarily in the Ga-Na-C-N system, and their occurrence varied significantly depending on the amount of carbon added. After the peaks and valleys, the electrical resistance

showed a linear increase and have the same behavior with Ga-Na-N system. At present, the reason for these carbon-related peaks and valleys is not understood, and no current model is available to explain this behavior. An observed behavior somewhat similar to this is the phenomenon of depolarization and hyperpolarization that occurs due to the poisoning of cell membranes by CN^- ions. This process results in abrupt increases or decreases in cell membrane resistance [29]. However, it remains questionable whether a similar mechanism could be at play in a high-temperature liquid metal solution.

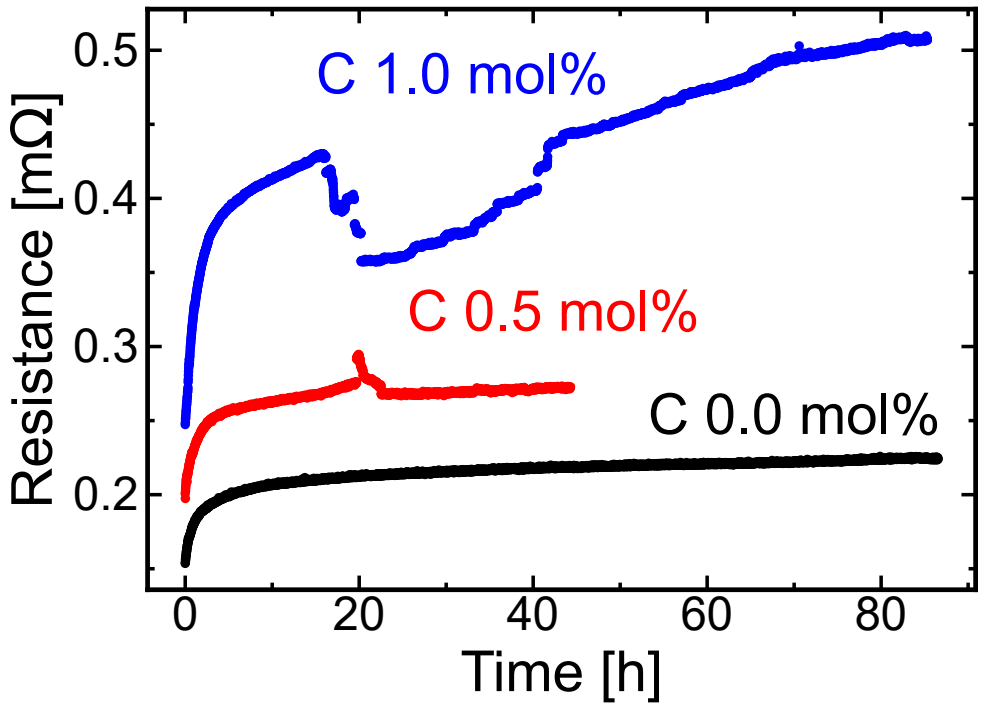

Figure 4.24: Changes of electrical resistance of the Ga-Na solution added with carbon.

Consequently, the author sought to understand the nature of these peaks and valleys by altering various process parameters and monitoring changes in electrical resistance. This approach aims to provide a better understanding of the potential influences that could trigger such variations in the resistance of the Ga-Na-C solution.

The author considered the effect of solution volume and nitrogen pressure which play a role in changing the behavior of peaks and valleys.

4.3.2 Volume dependence

The volume of the Ga-Na solution, in which 0.5 mol % of carbon was added, was changed. This led to different liquid levels in a 17 mm crucible with heights of 18 mm and 24 mm. The measured electrical resistances of these solutions were then plotted and can be seen in Fig. 4.25.

The solutions with a liquid level of 18 mm exhibited two observed peaks (at 3 hours and 14 hours) and valleys, whereas in the solution with a liquid level of 24 mm, only one

peak was observed, appearing at 20 hours. After the last peaks appeared, the electrical resistance stabilized and exhibited a linear increase. If this state was the equilibrium in the Ga-Na-C-N system, then the timing of the appearance of the last peaks becomes particularly important. Interestingly, the liquid level altered the timing of the appearance of the peaks.

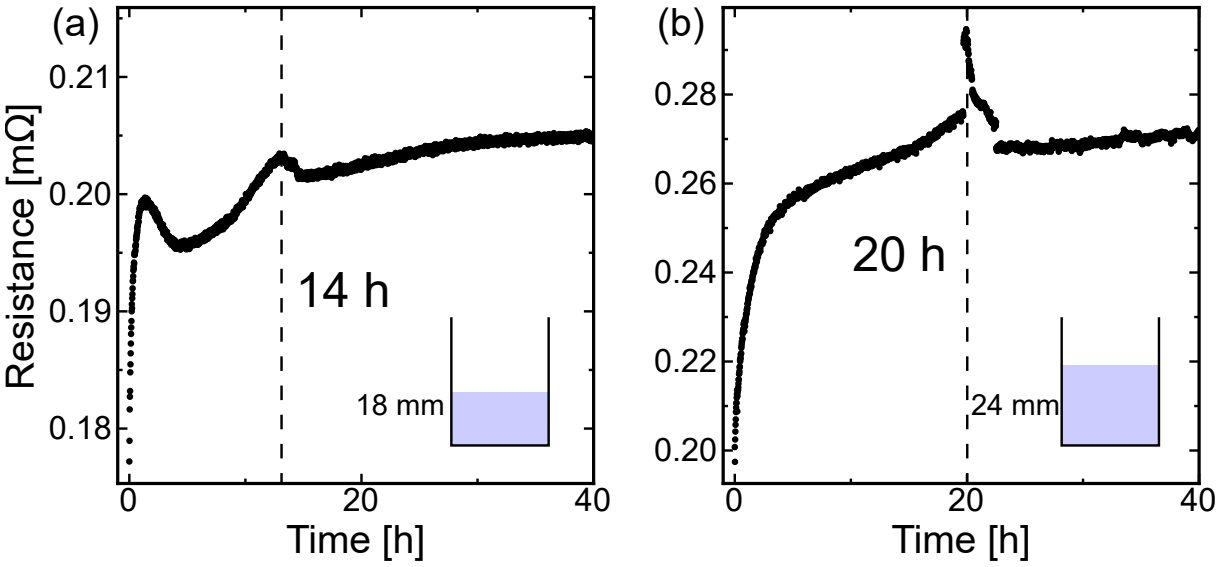

Figure 4.25: Changes of electrical resistance of the Ga-Na-C-N solution at liquid level of (a) 18 mm and (b) 24 mm.

The dependency of the results on the liquid level suggests that the peaks could be linked with reactions occurring at the surface of the liquid, specifically the dissolution process of nitrogen. The reaction rate at the liquid/gas interface is generally proportional to the surface area of the interface and inversely proportional to the volume of the liquid, as pointed out in earlier studies [13, 30]. As a consequence, an increase in volume led to an apparent decrease in the rate of increase in nitrogen concentration in the solution, despite the same amount of nitrogen being absorbed at the surface area. This slower reaction rate for the higher liquid level of 24 mm resulted in the peaks appearing significantly later (by approximately 6 hours) than those for the liquid level of 18 mm. Therefore, the peaks are presumably dependent on the nitrogen concentration. Based on these findings, the author decided to further investigate the dependence on nitrogen pressure and focus on the peak position.

4.3.3 Nitrogen pressure dependence

The electrical resistance of a Ga-Na solution added with 0.5 mol % of carbon, maintaining a liquid level of 18 mm, was examined under nitrogen pressures of 2 MPa, 3 MPa, and 4 MPa. This investigation aimed to ascertain the effect of varying nitrogen pressures

on the manifestations of electrical resistance peaks and valleys in the Ga-Na-C-N solution. The results are illustrated in Fig. 4.26. A Ga-Na solution pressurized with 2 MPa showed a peak appearing late at 19 h, with 3 MPa the peak appeared at 16.8 h, and the solution pressurized with 4 MPa showed the earliest peak at 14 h.

These findings suggest a clear relationship between nitrogen pressure and the timing of the peak electrical resistance. A higher nitrogen pressure appears to cause the peak in electrical resistance to occur earlier. This could potentially be attributed to a faster rate of nitrogen dissolution at higher pressures, resulting in an earlier appearance of peak electrical resistance. It is also worth noting that the pressure dependence of the peaks reinforces the previous hypothesis that these peaks are related to the nitrogen concentration in the solution.

4.3.4 Measurement in argon atmosphere

Previous experiments have indicated a strong relationship between the carbon-related peak and the nitrogen concentration. Then, what if the nitrogen was removed from the system? Figure 4.27 shows the electrical resistance of Ga-Na-C solution measured in the argon atmosphere. The appearance of peaks and valleys observed under nitrogen atmosphere was not replicated in the case of argon atmosphere, suggesting that both carbon and nitrogen are essential for these phenomena to occur. This implies that CN^- might be the species linked to the observed peaks and valleys. Moreover, it is worth noting that after the experiment, the solid graphite could be retrieved in the same state as before the experiment, despite undergoing a melting process in the Ga-Na solution over 50 hours. In experiments conducted in a nitrogen atmosphere, all added carbon appeared to have vanished, likely due to its conversion into CN^-.

Investigation on carbon state before and after the peaks

If the absence of peaks and valleys is associated with the presence of solid carbon, then it is possible that the carbon remained solid until the peaks appeared. To explore this further, the author performed an experiment in which the starting materials of the Ga-Na-C solution were melted over a brief period, and then the amount of residual solid carbon was measured. The result was summarized in Table 4.6. The results of this experiment can be understood in the context of the electrical resistance measurements plotted in Fig. 4.25a. In cases of short melting periods of 1 h and 5 h, almost all carbon could be recovered. In the case of a melting period of 10 h, only part of the carbon was recoverable, with the other half being lost, potentially during the cooling process. When the melting period was extended to 20 h, after which the peaks appear, carbon was not recoverable, implying its transformation into CN^-. Given these results, it can be suggested that the peaks in the electrical resistance are related to the presence of CN^- and that the timing

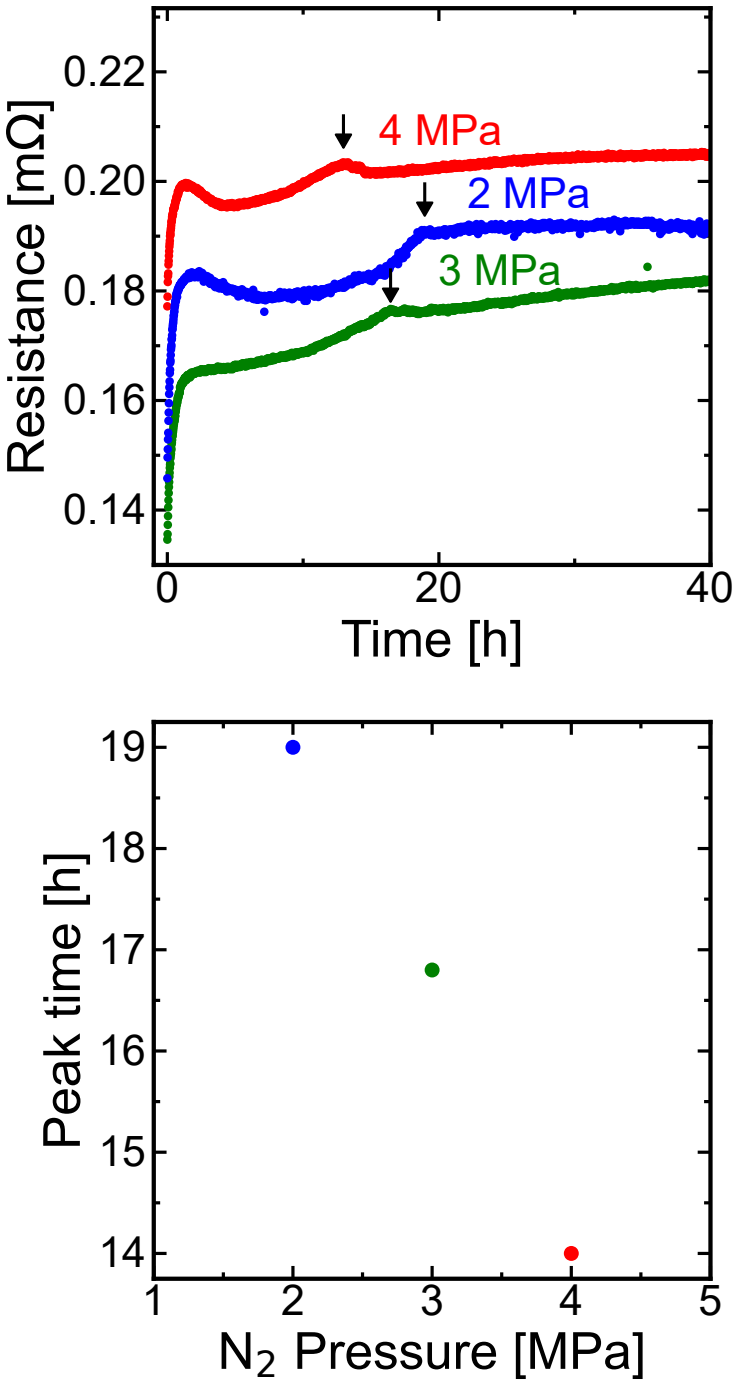

Figure 4.26: Changes of electrical resistance of the Ga-Na solution and pressure dependence of the peaks appearing in the Ga-Na-C-N system.

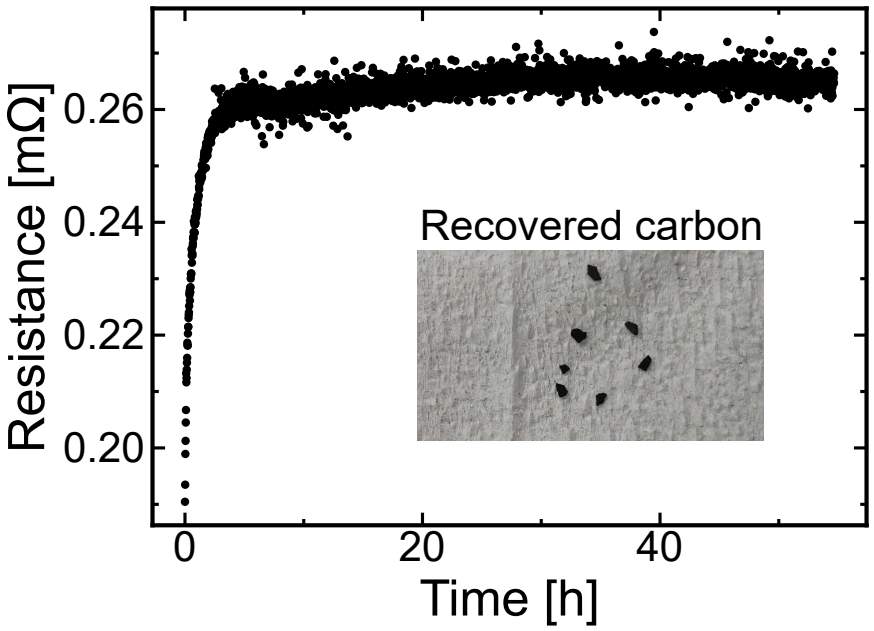

Figure 4.27: Changes of electrical resistance of the Ga-Na-C solution measured in the argon atmosphere. Inset photograph shows the graphite that was recovered post-measurement. The graphite remained solid, the same state as that before the melting process.

of the peaks indicates the transformation of carbon into CN^-. Carbon has been shown to have a very slow dissolution rate in liquid sodium [31]. However, this dissolution can be significantly enhanced through its reaction with nitrogen, leading to the formation of cyanide [32, 33].

Table 4.6: Amount of recovered solid graphite post-melting of Ga-Na-C solution.

Melting Period [h]	Amount of prepared carbon [g]	Amount of recovered carbon [g]
1	0.0104	0.0100
5	0.0102	0.0104
10	0.0103	0.0054
20	0.0102	0

4.3.5 Signification of peak

The investigation revealed that peculiar peaks and valleys signal the conversion of carbon into CN^-. What is the significance of detecting these peaks? The author attempted to investigate this by comparing the crystal growth commenced at the timing before and after the appearance of peaks. Crystal growth was performed using the same MPS substrate pattern and the temperature sequence as shown in Fig. 4.12. The pre-growth holding period was varied to 12 h, 18 h, 24 h, and 48 h.

Figure 4.28 shows the SEM images of GaN crystals grown in the Ga-Na-C solution. The yield of the crystal growth and the thickness of the GaN crystals are represented in Fig. 4.29. Crystals grown with a pre-growth holding period of 18 hours and beyond - which is after the appearance of peaks in Fig. 4.25a - resulted in significantly larger GaN crystals compared to those grown without carbon addition. It was reported that the incorporation of carbon into the Ga-Na solution enhances the growth rate [25, 28, 34].

In contrast, the crystals that were immersed prior to the appearance of peaks (pre-growth holding period of 12 hours) did not grow, despite the fact that crystals immersed at 18 hours developed into significantly larger sizes. The reason for this lack of growth remains unclear; it could be due to the undersaturated solution abruptly becoming supersaturated during the formation of CN^-, or possibly the presence of C (which had yet to be converted into CN^-) in the Ga-Na solution inhibits the synthesis of GaN. It is plausible that as long as carbon remain in the solution, the formation of C-N bonds becomes favored, thereby inhibiting the synthesis of Ga-N. This could potentially lead to a dead zone during this phase. Therefore, it is advisable to avoid the simultaneous presence of GaN seeds and carbon in the solution.

Nevertheless, the equilibrium of the Ga-Na-C can be reached after the peak signal, and beyond this point, a significant enhancement in growth rate and the desired effect of

controlled nucleation is observed. The peak signal can thus serve as an indicator that GaN can be readily synthesized in the solution. From another perspective, it can be inferred that the formation of CN^- becomes a limiting factor that dictates the required time until GaN can be synthesized in the solution.

The detection of peaks and valleys linked to CN^- is a significant and unique contribution arising from electroresistometry study of the Na-flux method. This new knowledge can potentially enable better process control and optimization in GaN crystal growth.

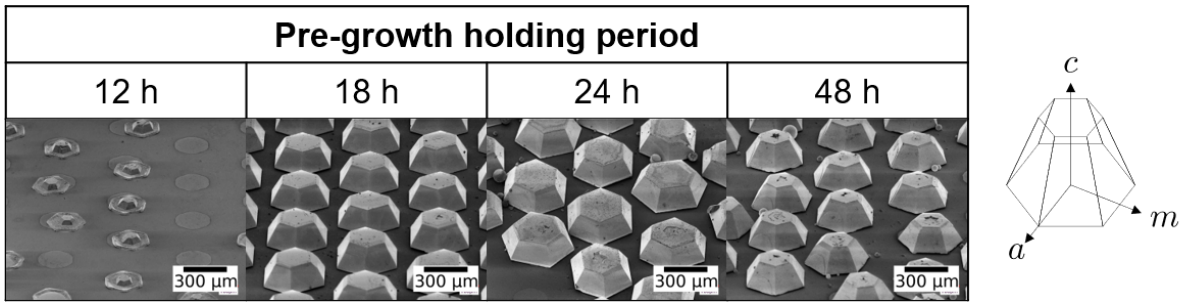

Figure 4.28: Scanning electron microscope images of GaN crystal grown on a MPS substrate in carbon added Ga-Na solution at 870 °C with various pre-growth holding period.

4.4 Summary

In this chapter, the author systematically performed electrical resistance measurements on three solution systems: Ga-Na, Ga-Na-N, and Ga-Na-C-N. The interpretation of each process toward the preparation of a supersaturated Ga-Na solution was described. These include:

1. Homogenization Process:

   This process is represented by the increasing resistance curve in the early stages of the measurement. Parameters involved in this processes are temperature and Ga:Na composition.

2. Nitrogen Dissolution Process:

   This process is identified by the linear increase of electrical resistance. The capturing process of free electrons due to the bonding of nitrogen makes it possible to monitor the nitrogen concentration in the Ga-Na solution via monitoring its electrical resistance. Nitrogen dissolution is a time-dependent process, indicating the pseudo-equilibrium state of the dissolution process, which was revealed for the first time with electrical resistance monitoring. Additionally, temperature also significantly enhances the nitrogen dissolution process based on the electrical resistance measurement.

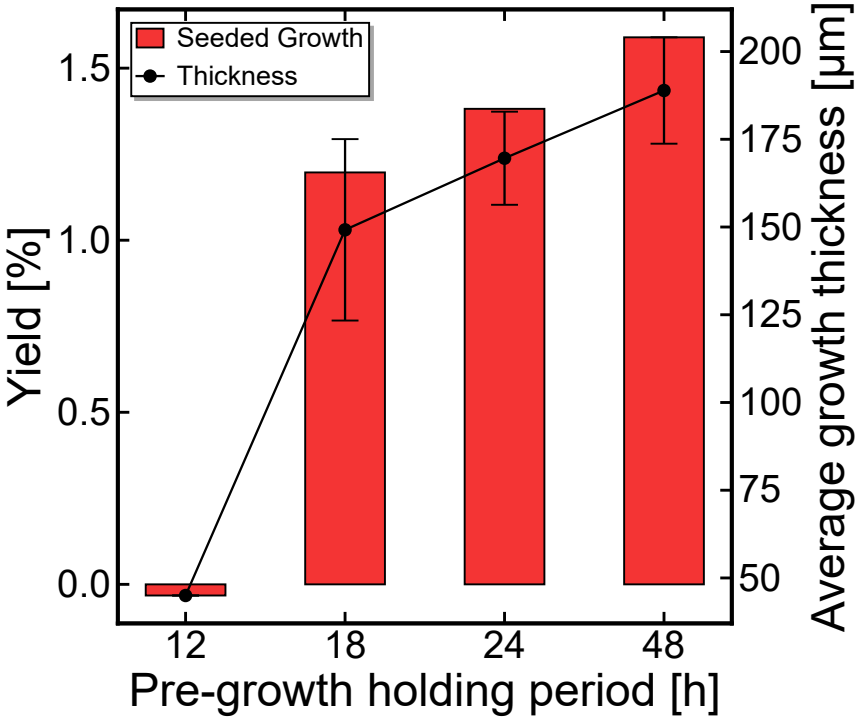

Figure 4.29: Pre-growth holding period dependence of yield and thickness of the GaN crystal growth in carbon-added Ga-Na solution.

3. Formation of CN^-:

   This process is identified through the appearance of peaks and valleys, with the last appearing peak indicating the conversion of solid carbon into CN^-. This peak is significant as it signals the timing when GaN can be readily synthesized. Parameters affecting the appearance of the signals are nitrogen pressure and solution volume.

References

[1] M. Avrami, J. Chem. Phys. **7**, 1103 (1939).

[2] C. Kittel, *Introduction to Solid State Physics*, Wiley, (2004).

[3] T. Itami, M. Shimoji, J. Meijer, G. Vinke, C. Van Der Marel, and W. Van Der Lugt, Phys. B+C **142**, 145 (1986).

[4] M. Avrami, J. Chem. Phys. **8**, 212 (1940).

[5] M. C. Weinberg, D. P. Birnie, and V. A. Shneidman, J. Non. Cryst. Solids **219**, 89 (1997).

[6] T. Car, N. Radić, J. Ivkov, and A. Tonejc, Appl. Phys. A Mater. Sci. Process. **80**, 1087 (2005).

[7] R. Shinoda, A. Fawzy, G. Graiss, and G. Saad, Solid State Commun. **84**, 335 (1992).

[8] J. van der Stel, H. B. van Veldhuizen, G. W. Koebrugge, J. Sietsma, and A. van den Beukel, Phys. Status Solidi A **112**, 35 (1989).

[9] C. C. Addison, G. K. Creffield, P. Hubberstey, and R. J. Pulham, J. Chem. Soc. A Inorganic, Phys. Theor. Chem., 1393 (1971).

[10] Z. Wang, Z. Sun, S. Jiang, and X. Wang, J. Mol. Liq. **237**, 10 (2017).

[11] M. Kawahara, F. Kawamura, M. Yoshimura, Y. Mori, T. Sasaki, S. Yanagisawa, and Y. Morikawa, J. Cryst. Growth **303**, 34 (2007).

[12] R. Khairulin, S. Stankus, and A. Sorokin, J. Non. Cryst. Solids **297**, 120 (2002).

[13] K. Ito, K. Amano, and H. Sakao, Trans. Iron Steel Inst. Japan **28**, 41 (1988).

[14] C. C. Addison, G. K. Creffield, P. Hubberstey, and R. J. Pulham, J. Chem. Soc. Dalt. Trans. **2**, 1105 (1976).

[15] M. Imade, K. Murakami, D. Matsuo, H. Imabayashi, H. Takazawa, Y. Todoroki, A. Kitamoto, M. Maruyama, M. Yoshimura, and Y. Mori, Cryst. Growth Des. **12**, 3799 (2012).

[16] T. Sato, K. Nakamura, M. Imanishi, K. Murakami, H. Imabayashi, H. Takazawa, Y. Todoroki, D. Matsuo, M. Imade, M. Maruyama, M. Yoshimura, and Y. Mori, Jpn. J. Appl. Phys. **54**, 105501 (2015).

[17] W. F. Berg and W. L. Bragg, Proc. R. Soc. London. Ser. A - Math. Phys. Sci. **164**, 79 (1938).

[18] F. Kawamura, M. Morishita, N. Miyoshi, M. Imade, M. Yoshimura, Y. Kitaoka, Y. Mori, and T. Sasaki, J. Cryst. Growth **311**, 4647 (2009).

[19] H. Kubo, *Private communication*, 2018.

[20] R. Tandryo, K. Murakami, T. Kitamura, M. Imanishi, and Y. Mori, Appl. Phys. Express **12**, 065502 (2019).

[21] P. Von Dollen, S. Pimputkar, M. A. Alreesh, S. Nakamura, and J. S. Speck, J. Cryst. Growth **456**, 67 (2016).

[22] G. Colonna, L. D. Pietanza, and M. Capitelli, J. Thermophys. Heat Transf. **22**, 399 (2008).

[23] M. Morishita, F. Kawamura, M. Kawahara, M. Yoshimura, Y. Mori, and T. Sasaki, J. Cryst. Growth **284**, 91 (2005).

[24] R. Tandryo, K. Murakami, K. Okumura, T. Yamada, T. Kitamura, M. Imanishi, M. Yoshimura, and Y. Mori, J. Cryst. Growth **535**, 125549 (2020).

[25] F. Kawamura, M. Morishita, M. Tanpo, M. Imade, M. Yoshimura, Y. Kitaoka, Y. Mori, and T. Sasaki, J. Cryst. Growth **310**, 3946 (2008).

[26] T. Kawamura, Y. Yamada, H. Imabayashi, M. Maruyama, M. Imade, M. Yoshimura, Y. Mori, and Y. Morikawa, Jpn. J. Appl. Phys. **9**, 08JA04 (2010).

[27] T. Kawamura, H. Imabayashi, M. Maruyama, M. Imade, M. Yoshimura, Y. Mori, and Y. Morikawa, Phys. Status Solidi B **252**, 1084 (2015).

[28] T. Kawamura, H. Imabayashi, M. Maruyama, M. Imade, M. Yoshimura, Y. Mori, and Y. Morikawa, Appl. Phys. Express **9**, 015601 (2016).

[29] W. P. Anderson, D. L. Hendrix, and N. Higinbotham, Plant Physiol. **54**, 712 (1974).

[30] C.-H. Eom, M.-H. Song, and D.-J. Min, ISIJ Int. **55**, 2694 (2015).

[31] B. Longson and A. W. Thorley, J. Appl. Chem. **20**, 372 (2007).

[32] R. Ainsley, L. P. Hartlib, P. Holroyd, and G. Long, J. Nucl. Mater. **52**, 255 (1974).

[33] R. Pulham and P. Hubberstey, J. Nucl. Mater. **115**, 239 (1983).

[34] M. Imade, Y. Hirabayashi, Y. Konishi, H. Ukegawa, N. Miyoshi, M. Yoshimura, T. Sasaki, Y. Kitaoka, and Y. Mori, Appl. Phys. Express **3**, 075501 (2010).

Chapter 5

In-situ monitoring of GaN growth via electroresistometry

Chapter 4 investigated the preparation process of the Ga-Na solution through an electroresistometry study. The electrical resistance offered three crucial pieces of information: homogeneity, the quantity of dissolved nitrogen, and the detection of CN^- formation. It is undeniable that electroresistometry has emerged as a valuable monitoring tool for investigating the characteristics of Ga-Na solutions [1, 2]. However, Na-flux growers could benefit further if the GaN crystal growth process itself could also be monitored via electroresistometry. Therefore, in this chapter, the author develops a new system that enables the simultaneous execution of crystal growth and electroresistometry. The in-situ monitoring of GaN crystal growth is demonstrated by measuring the electrical resistance of the Ga-Na solution.

5.1 In-situ monitoring system set up for Na flux growth

Dipping technology has allowed the arbitrary positioning of GaN crystal seed during growth process [3]. This proves essential as we learned in Section 4.3 that avoiding the simultaneous presence of carbon and seed crystal in the Ga-Na solution is crucial. It also paves the way for a strategic pause until the solution becomes supersaturated. This approach can effectively eliminate meltback, enabling a direct correlation between electrical resistance and growth during the analysis.

In response to these requirements, the author developed an apparatus that integrates dipping technology with the electroresistometry system. This novel setup allows for the individual positioning of the 4-point probe and the seed crystal. A schematic overview of this in-situ monitoring setup is provided in Fig. 5.1b, which is an advanced version of Fig. 5.1a previously employed for studying the Ga-Na solution. With this setup, the monitoring of the Ga-Na solution is conducted by immersing the probe into the solution, while

the substrate is positioned above the crucible. The initiation of crystal growth can be performed at desired timing by immersing the substrate into the solution. Crystal growth typically performed in a solution with liquid height of approximately 18 mm at a temperature 870 °C (total volume was 4.1 cm^3), as increasing rate of nitrogen concentration become higher with smaller solution volume.

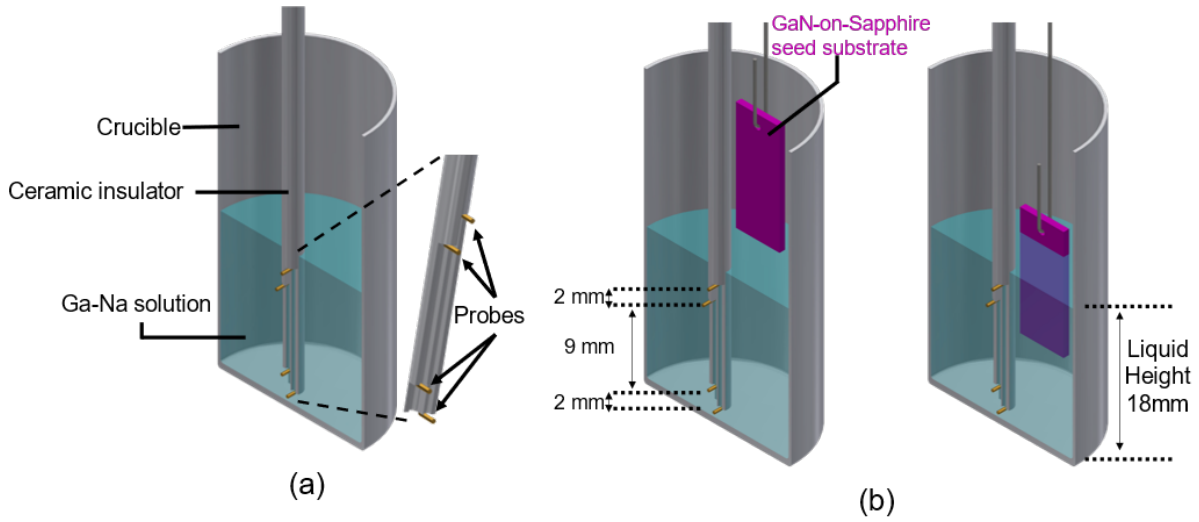

Figure 5.1: (a) Schematic diagram of four-point probe electrical resistance measurement used in Chapter 4. (b) Integration of dipping technique into electroresistometry which allows individual and abritrary control of probe and seed crystal position.

5.2 Demonstration of in-situ growth monitoring via electroresistometry

5.2.1 Experimental procedure

In this study, the growth of GaN on a *c*-plane GaN-on-Sapphire template was performed while simultaneously measuring the electrical resistance of the Ga-Na solution. The experimental procedure follows the standard preparation process in the Na-flux growth and electroresistometry experiments. The parameters for the growth experiments are summarized in Table 5.1. Commercially available GaN-on-Sapphire templates served as the seed substrates. These seed substrates were arranged in a dipping configuration inside the pressure vessel.

The sequence of the in-situ monitoring growth process is depicted in Fig. 5.2. The in-situ electroresistometry was initiated when the target temperature was reached, while the substrate remained above the crucible. After a pre-growth holding period of 24 hours, the seed substrate was immersed into the solution to initiate the crystal growth. Throughout

the growth process, the electroresistometry system continuously recorded the electrical resistance of the Ga-Na solution. In order to prevent any interference between the grown crystal and the 4-point probe, the *c*-face of the GaN template was oriented in the opposite direction to the probe.

In-situ monitoring of GaN growth was repeated several times to confirm the reproducibility as well as to identify the unique changes in electrical resistance associated with crystal growth.

Table 5.1: Growth parameters for in-situ experiments.

Seed	Temperature [°C]	N_2 pressure [MPa]	Ga:Na:C [mol %]
c-GaN template	870	4.0	27:73:0.5

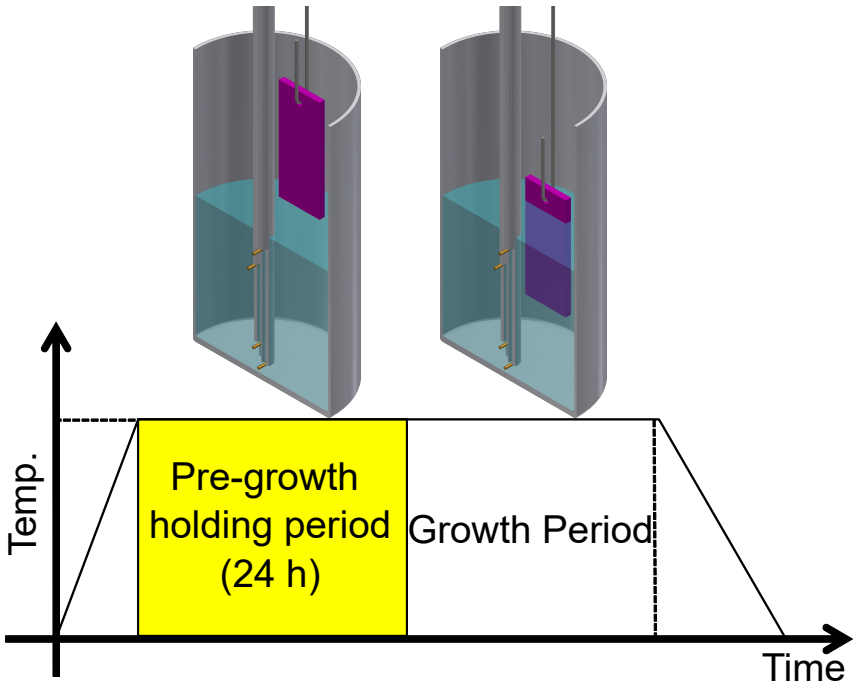

Figure 5.2: The sequence for in-situ monitoring of GaN crystal growth.

5.2.2 Changes in electrical resistance during growth sequence

The first demonstration of the in-situ monitoring of crystal growth is presented in Fig. 5.3. The corresponding electrical resistance during this process is shown in Fig. 5.3a. From the electrical resistance profile, one can observe the progression of the transformation of Ga-Na solution. This includes the increasing resistance curve indicating the homogenization process in the early stages of measurement.

Interestingly, peculiar peaks and valleys, corresponding to the formation of CN^-, were also observed, which appeared around 18 h. The seed crystal was immersed at 24 h, as indicated by the orange arrow. For comparative analysis, we can refer to the electrical resistance measured in Fig. 4.25a.

In contrast to the electrical resistance measured with only the Ga-Na solution, a different behavior was observed here. Specifically, a steep change in electrical resistance occurred around 24 h, coinciding with the immersion of the seed substrate into the solution. It can be hypothesized that this abrupt change in value is attributed to the disturbance of the Ga-Na solution caused by substrate immersion.

Following this discontinuity, the electrical resistance resumed its increase. However, at around 40 h, the resistance began to decrease monotonously, continuing this trend until the completion of the growth run. This decrease in electrical resistance was hypothesized to be driven by the GaN growth on the seed substrate.

Figure 5.3b shows the photograph of the crystal obtained after the in-situ growth run. Exposing the metal electrodes to the Ga-Na solution could introduce new impurities, which may influence, or possibly gave a detrimental effect on the GaN crystal growth. It appeared that transparent GaN crystal was grown successfully, as described in Chapter 3.

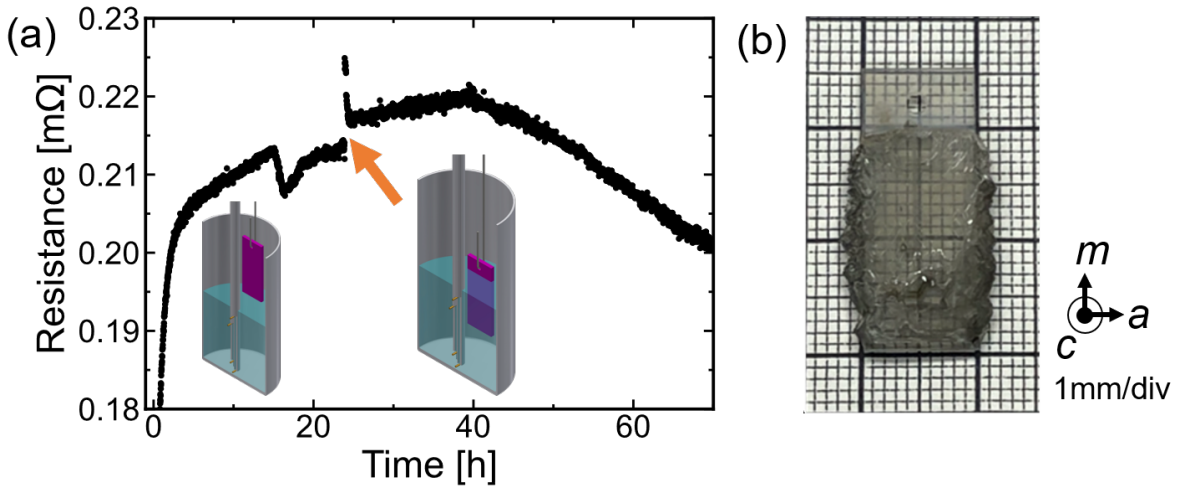

Figure 5.3: (a) Changes of electrical resistance of Ga-Na solution during crystal growth of GaN. Substrate was immersed at the timing pointed by orange arrow. (b) Photograph of the grown crystal retrieved after measurement.

5.2.3 Steep changes by substrate immersion

To differentiate between the effects causing the steep change and the monotonous decrease in resistance, an experiment was conducted wherein the electrical resistance of the Ga-Na solution was in-situ monitored during the immersion of a sapphire substrate.

The measured electrical resistance is shown in Fig. 5.4. After the sapphire substrate was immersed at 24 h, a steep decrease in resistance was observed. Following this, the electrical resistance resumed a linear increase. No monotonous decrease was evident in this case as there was no GaN seed crystal present to trigger the GaN growth. Upon pulling off the sapphire substrate at the 85 h, an increase in resistance was noted.

These results suggest that the steep change in electrical resistance is associated with the presence of the substrate, which potentially modifies the original conduction path through the solution. The abrupt change with the sapphire substrate's presence in this experiment was observed as a decrease, contrasting with the steep increase observed in Fig. 5.3. This discrepancy can be attributed to the relative geometric positioning of the substrate and the probe, specifically whether the substrate was immersed in front of or behind the probe.

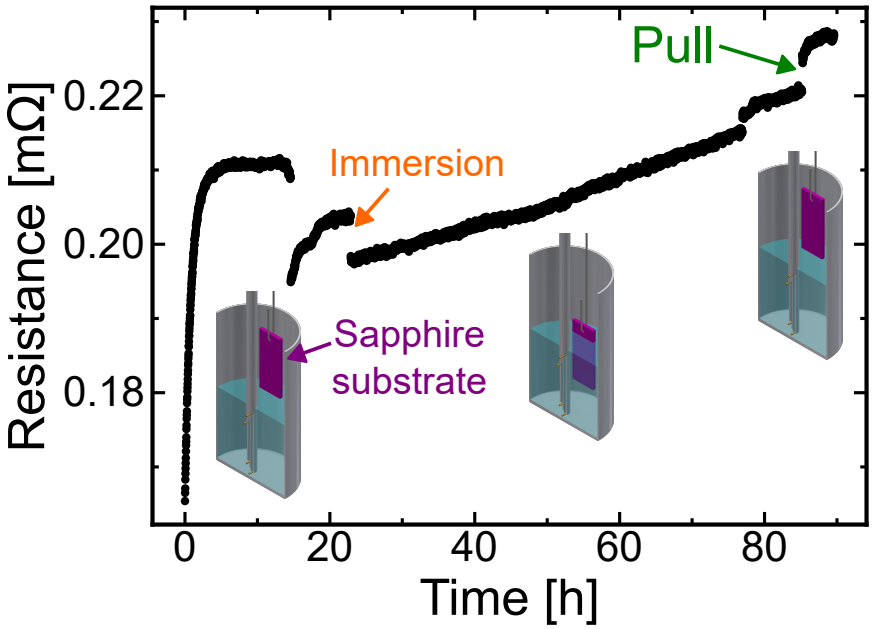

Figure 5.4: Changes of electrical resistance of the Ga-Na solution during immersion and pulling of sapphire substrate.

5.2.4 Monotonous decrease in electrical resistance during GaN growth

The previous investigation had also indicated that monotonous decrease in electrical resistance was uniquely observed only if GaN seed crystal was present in the solution. To confirm this, the author performed repeated experiments on the in-situ growth monitoring on *c*-GaN template. The growth parameters were the same as described in Table 5.1.

The electrical resistance of Ga-Na solutions during in-situ growth monitoring on *c*-GaN templates is shown in Fig. 5.5b. Each experiment consisted of immersing the templates for around 24 hours. As seen in the figure, there was an observed rapid increase in the electrical resistance, which had also been discussed in the previous section. The magnitude of this increase, however, varies significantly across different experiments, leading to a high level of uncertainty.

Following this sharp rise, a consistent decrease in resistance can be observed, as depicted in Fig. 5.5b. Precipitation of GaN was confirmed in all the experiments, as shown in Fig. 5.5c. This consistently coincided with the decrease in electrical resistance, supporting the hypothesis that GaN growth is associated with a reduction in electrical resistance. However, the precise mechanism by which GaN growth leads to a decrease in electrical resistance remains unclear based solely on the findings of the in-situ experiment.

5.3 In-situ electroresistometry of Na flux growth with various growth rate

The connection between GaN growth and a decrease in electrical resistance is not readily apparent. The current methodology, which only involves in-situ growth monitoring, does not provide enough insight to establish this correlation definitively. To better understand this connection, the author decided to alter the growth rate during the crystal growth experiment. If GaN growth directly influences the reduction in the Ga-Na solution's electrical resistance, observable changes in the rate of resistance reduction can be anticipated when the growth rate is altered.

As described in Section 2.2.1, in the Na-flux growth, the supersaturation is controlled by temperature and nitrogen pressure applied to the Ga-Na solution [4]. Due to the difficulty in comparing electrical resistance across separate experiments, growth parameters such as nitrogen (N_2) pressure or will be altered in the mid-experiment. This approach allows for comparative analysis within the confines of a single experiment.

5.3.1 In-situ growth monitoring on varying N_2 pressure

The author initially chose to adjust the nitrogen pressure to change the supersaturation, as the electrical resistance is also dependent on temperature, which could introduce additional complexity into the analysis.

The preparation of the experiment is the same as described in the previous section. Upon immersing the seed substrate and observing the monotonous decrease in electrical resistance (in line with the observations from the first in-situ measurement experiment), the nitrogen pressure was reduced from 4.0 MPa to 3.0 MPa, and then to 2.0 MPa. This was achieved by reducing the value on the pressure regulator and slowly releasing the

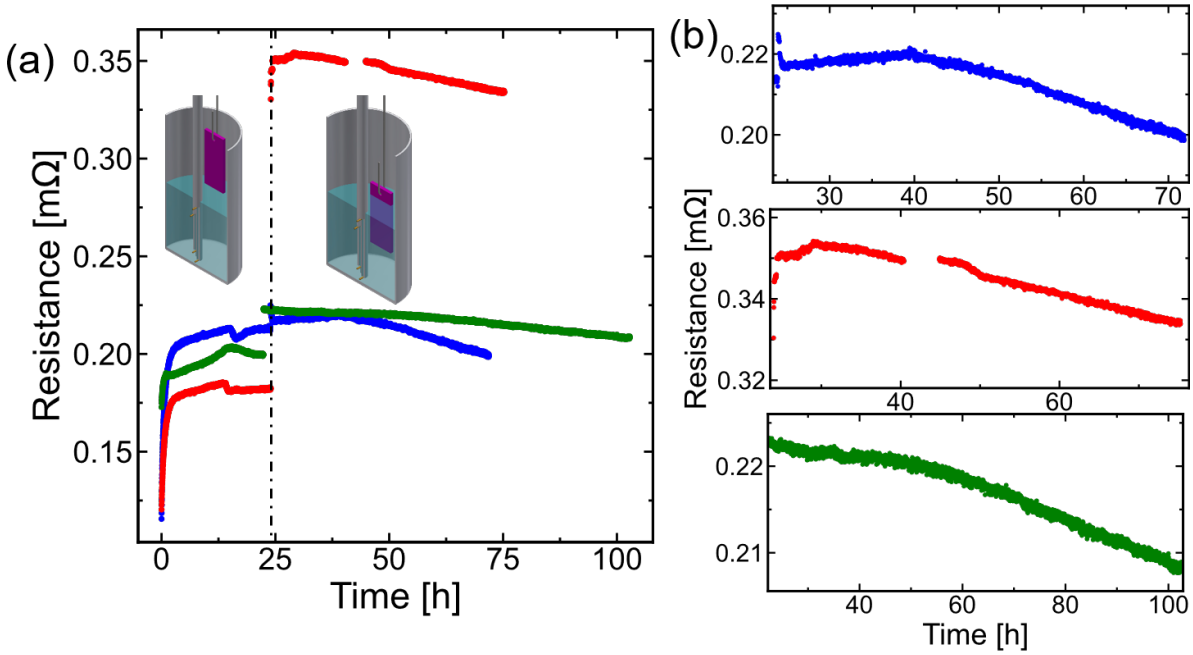

LPE Yield [mmol]	10.7847	12.3397	10.8325
Ga shifts [mol%]	27.0→22.0	27.0→21.4	27.0→22.0

Figure 5.5: (a) Changes of electrical resistance of Ga-Na solution during in-situ monitoring with various sample. (b) Extract of the graph from Fig. 5.5a after the immersion of substrate. Monotonous decrease in electrical resistance was consistently observed in all samples. (c) Photograph of the GaN crystal retrieved after in-situ monitoring. LPE Yield and the corresponding Ga shifts were calculated.

nitrogen gas into the environment. The growth process then continued for a further 24 h at each of these pressure (3.0 MPa and 2.0 MPa), after which the pressure was raised back to approximately 3.8 MPa for a final 10 h growth period. Nitrogen pressure values were recorded using a NAGANO KEIKI GC61 pressure transducer. Following the in-situ growth monitoring run, the sample was retrieved. A cross-sectional slice of the pre-treated sample (chemically mechanically polished) was examined with panchromatic cathodoluminescence (CL) imaging (HORIBA DF-100) to confirm any changes in the growth rate during the crystal growth process. For comparative and baseline analysis, electroresistometry was also performed without the crystal growth process.

Figures 5.6a and 5.6b present the two-grid plots, with the upper plot showing electrical resistance of Ga-Na solution and the lower plot showing the nitrogen pressure profile simultaneously taken during electroresistometry. Figure 5.6a shows the electrical resistance of the Ga-Na solution without a seed crystal present. Despite changes in the nitrogen filling pressure, the electrical resistance did not show significant changes, as also seen in the enlarged plots presented in Fig. 5.6c. In contrast, Fig. 5.6b shows that the electrical resistance of the Ga-Na solution with a GaN template seed present experienced a reduction upon substrate immersion at 24 h. The decreasing rate of the electrical resistance became pronounced and linear around 50 h. Figure 5.6d shows the electrical resistance of the Ga-Na solution during the decrease and its change following the reduction of nitrogen pressure. The original decreasing rate of $-3.90 \times 10^{-4}\,\mathrm{m\Omega/h}$ at 4.0 MPa decreased to $-3.31 \times 10^{-4}\,\mathrm{m\Omega/h}$ following the decrease in pressure to 3.0 MPa, then decreased to $-1.39 \times 10^{-4}\,\mathrm{m\Omega/h}$ following the further decrease to 2.0 MPa. Finally, the pressure was increased again to 3.8 MPa and the decreasing rate was increased to $-6.41 \times 10^{-4}\,\mathrm{m\Omega/h}$. Figure 5.6e shows the photograph of GaN crystal retrieved after undergoing the above-mentioned experiment process.

A more detailed analysis of the decreasing rate of the electrical resistance can be performed by plotting the negative of the first derivative of the electrical resistance, as demonstrated in Fig. 5.7. Since the data points were too noisy, the derivative plot was acquired after preprocessing with a locally weighted scatterplot smoothing technique [5]. The value of the derivative remained relatively constant for every growth pressure stage except after the pressure was raised to 3.8 MPa. A positive correlation can be observed between the pressure profile and the derivative of resistance. An exception was observed during the final growth stage at 3.8 MPa, where the derivative of the resistance was higher than that at the initial 4.0 MPa growth stage.

Four distinct luminescent regions were identified from the cross-sectional cathodoluminescence image of the grown crystal as shown in Fig. 5.8. Previous report showed that different growth rates in the Na-flux growth are observable from the different CL intensities [6]. If these regions correspond to the four distinct stages of nitrogen pressure, the growth rate can be estimated from the thickness of each luminescent layer.

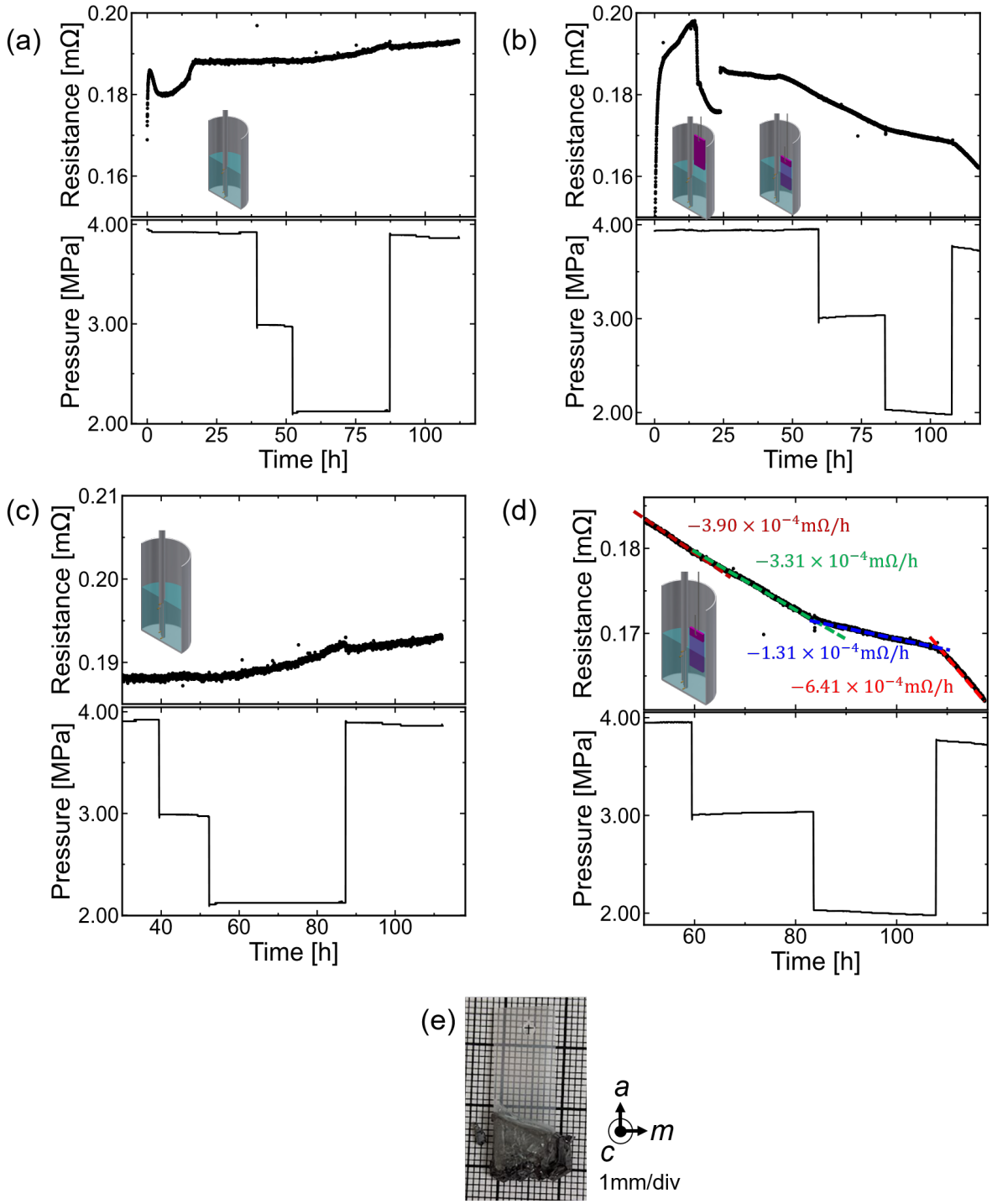

Figure 5.6: Two-grid plots showing electrical resistance and nitrogen pressure profile during in-situ electroresistometry (a) without and (b) with the presence seed crystal growth. Extract of the plot from (c) Fig. 5.6a and (d) Fig. 5.6b around the time when experiencing change in pressure. Changes in decreasing rate of electrical resistance (slope) were evident and evaluated with simple linear regression line. (e) Photograph of the crystal grown after in-situ monitoring growth.

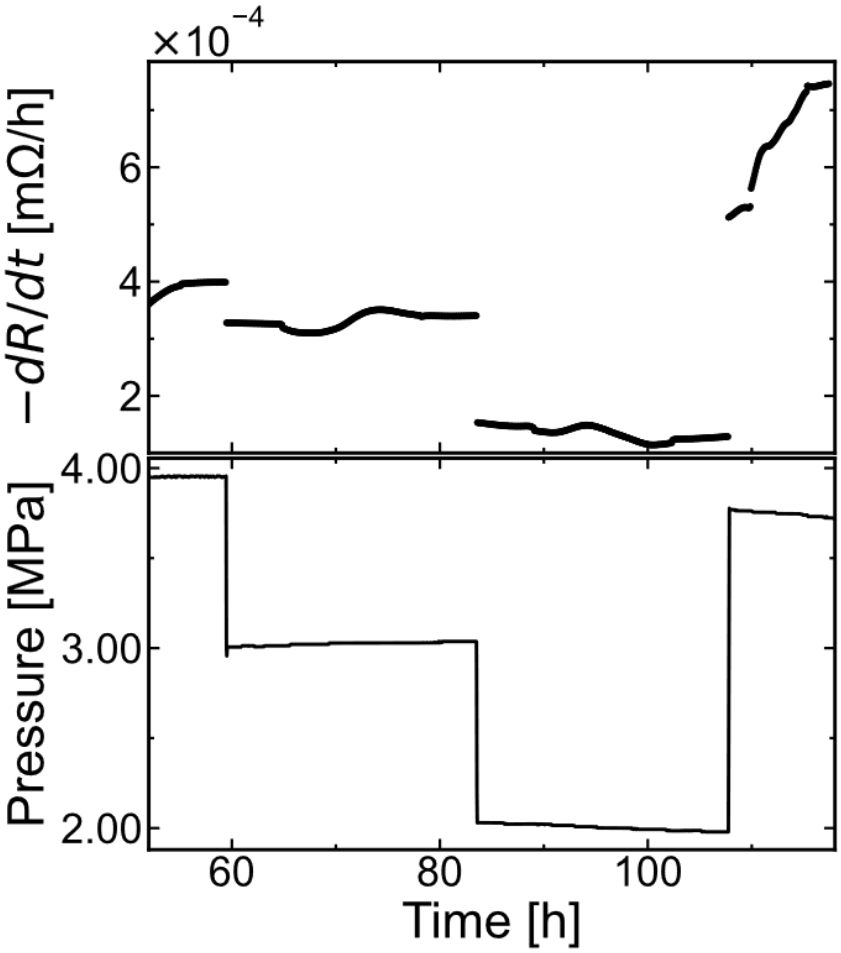

Figure 5.7: Negative derivative plot of electrical resistance from Fig. 5.6d.

The thickness of the growth layers during the stages of 3.8 MPa, 2.0 MPa, and 3.0 MPa (from top to bottom) were measured to be 155.2 µm, 101.2 µm, and 371.1 µm, respectively. The growth rate in the *c*-direction can be evaluated by dividing the thickness of each layer by its corresponding growth period. This results in estimated growth rates of 15.5 µm/h, 4.21 µm/h, and 15.4 µm/h for the stages of 3.8 MPa, 2.0 MPa, and 3.0 MPa, respectively.

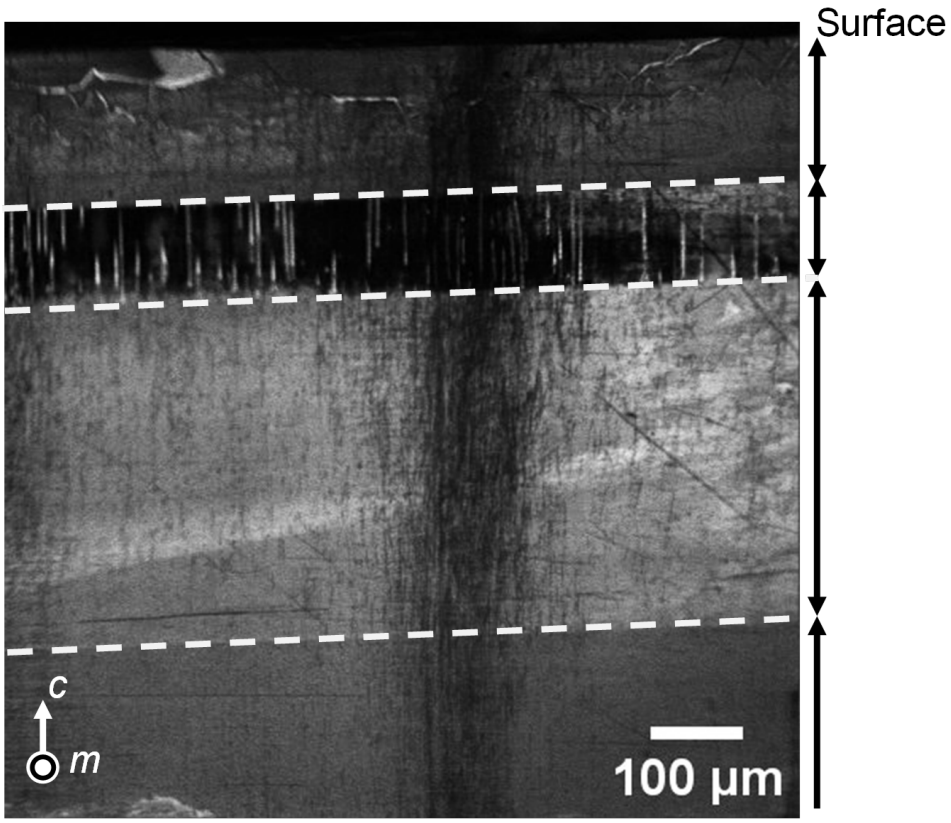

Figure 5.8: Panchromatic cathodoluminescence (CL) cross-section image of the sample (Fig. 5.6e) post in-situ growth monitoring. The white dashed lines delineate regions of distinct CL intensities, highlighting four different zones.

5.4 Discussion

Decreased in Ga/Na ratio during GaN growth

The consistently observed monotonous decrease of electrical resistance, exclusively when a seed crystal is present in the Ga-Na solution, strongly suggests a correlation between this resistance decrease and the crystal growth process. This monotonous decrease of electrical resistance, absent in the results from Chapter 4, indicates a unique property associated with the GaN synthesis process. The decrease itself is not straightforward to interpret. However, the electrical resistivity of the Ga-Na binary alloy has been reported to decrease following a reduction in the Ga/Na ratio [7]. In this context, the synthesis of

GaN presents a plausible scenario that could lead to a decrease in the Ga/Na ratio, as illustrated in Fig. 5.9. The crystal growth process of GaN consumes Ga from the Ga-Na solution, as Ga is one of the required elements for synthesis. As Ga is consumed, the composition of the remaining Ga-Na solution shifts towards a Na-rich solution. Given that the initial growth started from a Ga:Na composition of 27:73 mol %, further reduction in Ga will cause the solution's composition to shift closer to that of pure Na. According to Eq. (4.2), this shift will cause the solution to lose its residual alloy resistivity [8–10].

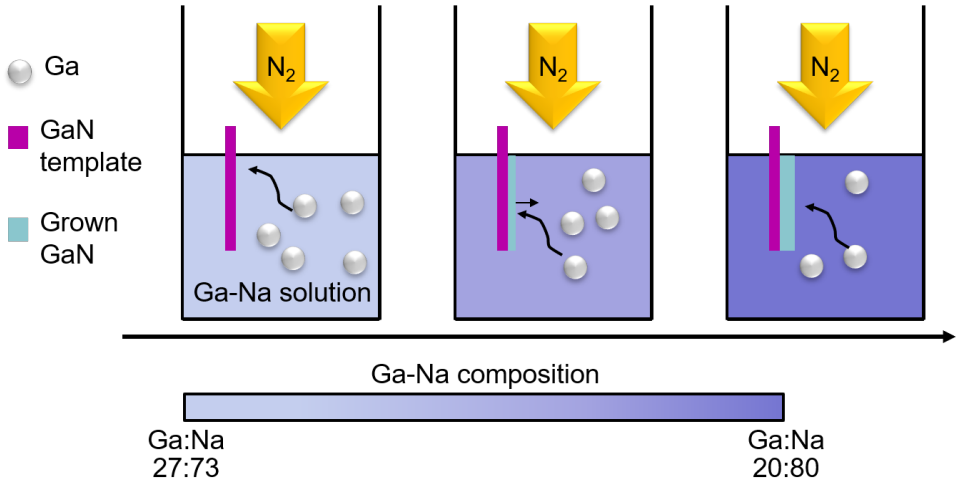

Figure 5.9: Schematic illustration of Ga consumption during GaN growth. GaN synthesis process consequently resulted in the the decrease of Ga/Na ratio.

The author has collected data on the electrical resistance of Ga-Na solutions with different Ga:Na compositions under typical Na-flux growth conditions. This was done in an argon environment. The results, which are plotted in Fig. 5.10 as resistance versus Na fraction, show a decreasing resistance trend towards high Na fractions. This trend aligns well with the resistivity report by Itami *et al.* [7]. Furthermore, the plot reveals a stronger dependency on composition compared to temperature. This suggests that the decrease in electrical resistance is primarily driven by changes in the Ga/Na ratio, rather than variations in temperature.

Based on the above analysis, it can be inferred that the monitoring of electrical resistance indirectly observes the growth of GaN through the consumption of Ga in the Ga-Na solution. The in-situ growth experiment with varying nitrogen pressure provides more robust evidence of this, as the rate of decrease in electrical resistance changes based on the nitrogen pressure (Fig. 5.6d). The nitrogen pressure on the Ga-Na solution determines the supersaturation and thus influences the GaN growth rate [4, 11]. A higher nitrogen pressure leads to a higher growth rate, and vice versa. A higher GaN growth rate implies faster Ga consumption from the Ga-Na solution, causing the Ga/Na ratio to decrease more quickly. This is reflected in the higher rate of decrease in electrical resistance at higher pressures. Conversely, when the pressure is lowered, the decreasing rate

of electrical resistance also drops due to the reduced growth rate. An increase in pressure back to 3.8 MPa raises the decreasing rate as the growth rate accelerates again. Thus, this confirms the hypothesis that the decrease in electrical resistance results from shifts in the Ga/Na ratio towards a Na-rich condition, which is a consequence of Ga consumption for GaN synthesis.

In some in-situ monitoring experiments, such as in Fig. 5.3a, a decrease in resistance was observed at later stages, rather than immediately after substrate immersion. This raises the question of whether the crystal grew immediately or not after immersion in the Ga-Na solution. While this is not definitively clear, it is crucial to remember that nitrogen dissolution also contributes to an increase in resistance. If the decrease in resistance due to growth is significantly smaller than the increase due to nitrogen dissolution, the overall electrical resistance will appear to rise. This makes it important to qualitatively assess the contributions of each of these factors to the electrical resistance. By understanding how both the growth process and nitrogen dissolution affect resistance, we can gain a more comprehensive view of the processes occurring during GaN crystal growth.

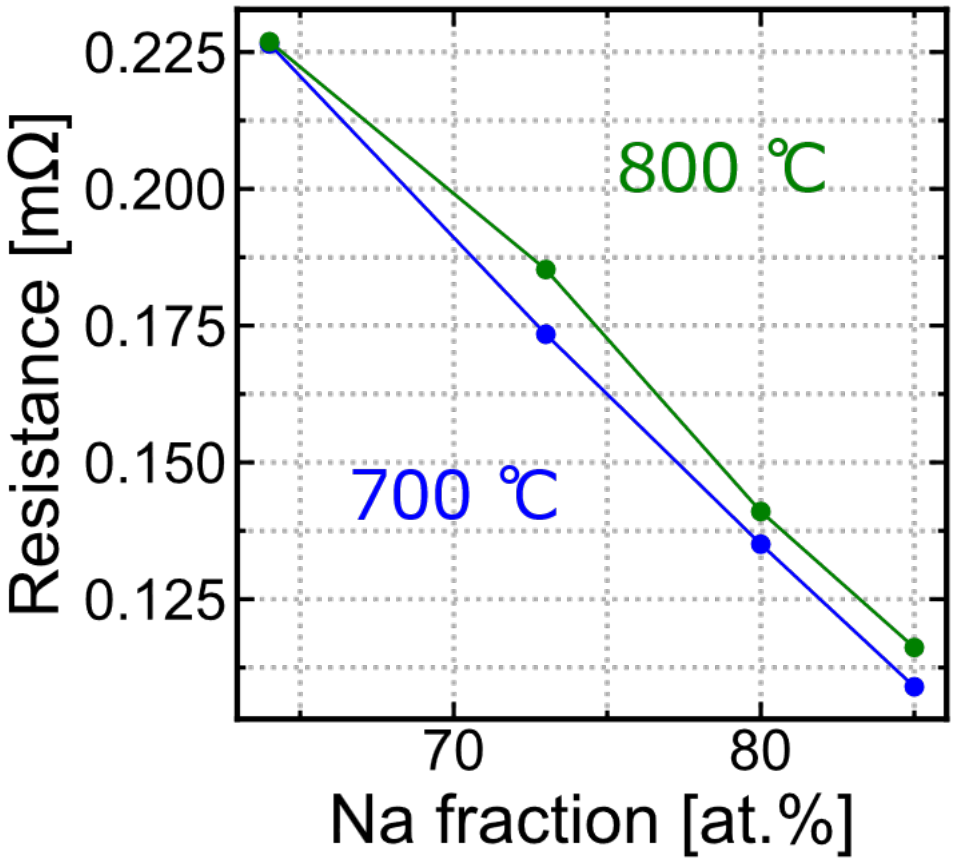

Figure 5.10: Na fraction dependence of the electrical resistance of the Ga-Na solution. The observed trend shows a decreasing electrical resistance with increasing Na fraction. All measurements were carried out in an Ar environment, thus eliminating the contribution of nitrogen on the electrical resistance of Ga-Na solution.

Decrease in electrical resistance as measure of volumetric growth rate

The discrepancy between the growth rates derived from electrical resistance measurements and from the cathodoluminescence (CL) image, assuming that the CL image accurately reflects the actual growth rate, raises interesting questions about the process. Notably, the growth rate during the 3.8 MPa growth pressure period appears high as evaluated from electrical resistance, while the CL intensity evaluation shows no difference compared to the growth rate during the 3.0 MPa growth pressure period.

The growth rate as predicted by electrical resistance is based on the consumption of Ga. It does not measure growth rate in a specific direction, but rather the volumetric growth rate, which is strongly influenced by the surface area of the crystal. As the growth process continues, more crystal surfaces will be exposed, resulting in a higher apparent rate of decrease in electrical resistance. This suggests that the electrical resistance is sensitive to the increased overall volume of GaN crystal being produced as the growth process continues, especially when the growth occurs over a larger surface area. This hypothesis could potentially provide an explanation for the observed increase in the rate of decrease in electrical resistance shown in Fig. 5.5b and during the 3.8 MPa growth stage in Fig. 5.6d.

In order to examine the effect of crystal surface area on growth, a simple geometric model was developed to estimate increases in the volumetric growth rate. The surface area was calculated from the model with the aid of Autodesk® Inventor® application. A boule observed in the grown crystal (Fig. 5.6e) was used as a model. Figure 5.11 depicts how the surface area of the grown crystal expanded as the growth process continued. The total available surface area (including the backside of the lateral overgrowth section) was determined to be 153.8 mm^2 and 207.1 mm^2 at thicknesses of 0.77 mm and 1.25 mm respectively, using scaling estimations from the final crystal shape. According to the contrast boundary shown in Fig. 5.8, these thicknesses correspond to the final stage of 4 MPa growth and the initial stage of 3.8 MPa growth respectively. Assuming that the total Ga consumption was directly proportional to the growth surface area, leading to a larger decrease rate of electrical resistance, the ratio of surface areas should resemble the ratio of decreasing rates of electrical resistance. The ratio between surface areas at thicknesses of 1.25 mm and 0.77 mm was found to be 1.35. This is approximately equal to the ratio of the decreasing rates of electrical resistance, as the value at 3.8 MPa (-5.40×10^{-4} mΩ/h, from Fig. 5.7) was 1.38 times greater than the value at 4.0 MPa (-3.90×10^{-4} mΩ/h), under the assumption that growth rates were identical. This serves to explain why the decreasing rate of electrical resistance at 3.8 MPa appeared to be high compared to the initial 4.0 MPa, which can be attributed to an increase in surface area. Consequently, it is likely that the surface area becomes a significant driver for the decrease in the rate of electrical resistance, particularly during the later stages of growth.

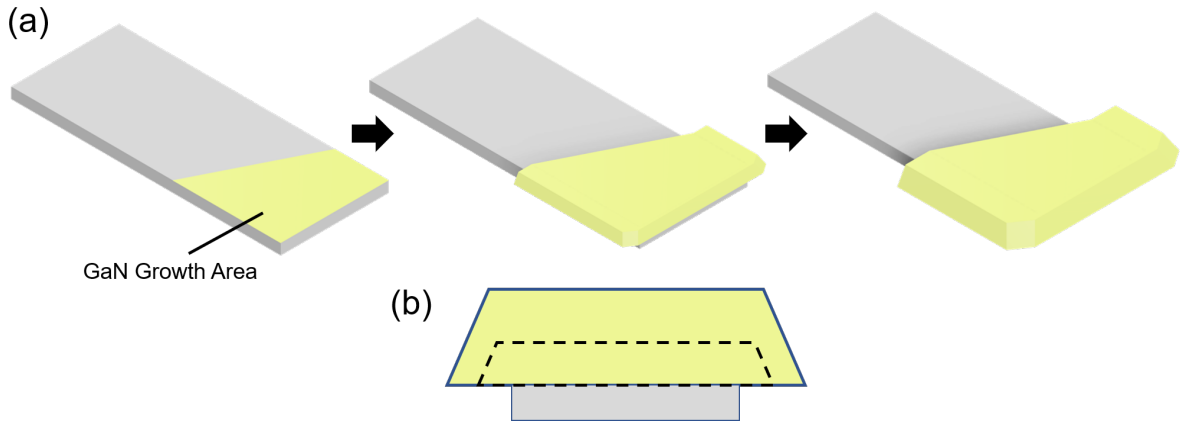

Figure 5.11: (a) Illustrative representation of the increasing growth surface area (indicated by the yellow region) due to the progression of both thick and lateral growth expansion, as modeled from the final crystal shape of the sample in Fig. 5.6e. (b) Cross-sectional representation of how the surface area estimation at a specific crystal thickness (indicated by the black dashed line) is scaled from the final crystal shape.

Post-run mass loss analysis

Finally, the author will discuss whether the amount of growth can be anticipated from the change in Ga/Na ratio and its electrical resistance. Post-run mass loss of Ga via incorporation as GaN was analyzed and verified whether it matches the change in composition as anticipated by electrical resistance. Table 5.2 summarizes the change in Ga fraction from the initial setup to the post-run measurement, and the estimated decrease in electrical resistance. Samples 1-3 correspond to GaN crystal sample shown in Fig. 5.5c (blue, red, green, respectively), and sample 4 corresponds to the crystal in Fig. 5.6e. Changes in Ga fraction, denoted as ΔR_{Ga}, were estimated based on the mass loss resulting from Ga incorporation into the GaN crystal. The decrease in electrical resistance was predicted by measuring the electrical resistance of the Ga-Na solution with the corresponding Ga/Na ratio in an Ar ambient. The actual decrease in electrical resistance was calculated from the difference between the electrical resistance value at the immersion of the crystal into the solution, and the final electrical resistance value at the end of the measurement. In all experiments, the electrical resistance seemed to decrease less than what the expected mass loss change of Ga (changes in Ga fraction only) would suggest. These discrepancies indicate that the total change in electrical resistance was not solely due to the change in the Ga/Na ratio. Here, it can be hypothesized that nitrogen continues to dissolve during growth and causes an increase in electrical resistance, counteracting the effect of the growth process. To account for this effect, the overall contribution of nitrogen dissolution to electrical resistance ΔR_N that has accumulated over the growth process was estimated. The amount of contribution was

determined based on the linear slope increase in electrical resistance R' in Eq. (4.6), associated with nitrogen dissolution, measured from the electrical resistance of Ga-Na solution at the anticipated Ga/Na ratio. R' values for Ga ratio of 27 %, 22 %, 21.4 %, and 20 % were 1.96×10^{-4} mΩ/h, 3.8×10^{-4} mΩ/h, 3.9×10^{-4} mΩ/h, 4.53×10^{-4} mΩ/h, respectively. Then, R' is assumed to linearly grade toward the R' of the final Ga/Na ratio and the increase in electrical resistance was accumulated over the growth period. If the contribution of nitrogen was considered, the total expected decrease in electrical resistance $\Delta R_{Ga} + \Delta R_N$ would become closer to the measured changes in electrical resistance. For sample no. 3 and 4, it appeared that ΔR_N was overestimated and the crystal growth run for both experiments were long. Presumably, the linearly graded assumption is not valid for such cases. For sample 4, the experiment underwent different growth pressure, and the effect was not accounted for in the estimation. Note that this is only an estimation. It is not precisely known whether the behavior of nitrogen dissolution with and without the presence of crystal growth. It is also important to note that the value of resistance has large uncertainty due to geometric factors. Nevertheless, accounting for nitrogen contribution ΔR_N is important in anticipating the growth amount in-situ.

Additionally, it is worth noting that the Ga/Na ratio of the solution was shifting throughout the growth process, and other physical phenomena may have come into play, such as the loss of Na due to vaporization (a result of increased Na activity), which may have also contributed to an increase in electrical resistance. It was estimated that the rise in the Ga/Na ratio due to Na vaporization is around 3.2 %, for a total increase of 0.02 mΩ (the difference between measured resistance and ΔR_{Ga}). However, the observed amount of vaporization in the system was not as high as projected, typically only 0.2 %, suggesting that nitrogen dissolution appears to be the contributing factor.

Table 5.2: Post-run analysis of compositional shift in comparison to electrical resistance.

No.	Changes in Ga fraction [mol %]	ΔR_{Ga} [mΩ]	ΔR_N [mΩ]	$\Delta R_{Ga} + \Delta R_N$ [mΩ]	Measured changes [mΩ]
1	27→22.0	-0.0316	0.0133	-0.0183	-0.0176
2	27→22.0	-0.0316	0.0132	-0.0184	-0.0184
3	27→21.4	-0.0354	0.0230	-0.0124	-0.0195
4	27→20.0	-0.0442	0.0260	-0.0182	-0.0245

5.5 Summary

In conclusion, the author designed and incorporated dipping technology for in-situ GaN monitoring utilizing electroresistometry. The in-situ monitoring approach has been effectively demonstrated and replicated on numerous occasions.

Through systematic and comparative analysis, the author identified that changes in the Ga/Na ratio of the Ga-Na solution play a crucial role in monitoring the GaN growth process. Electroresistometry provides indirect access to GaN growth through the tracking of Ga consumption. The shift in composition towards pure Na results in a decrease in residual alloy resistivity, serving as an important indicator for the GaN process.

It should be noted that this method measures the volumetric growth rate, which appears higher in the later stages of growth as Ga consumption increases due to the availability of more surface area. This understanding of the growth process allows for more effective monitoring and can potentially lead to more controlled and efficient GaN growth.

References

[1] R. Tandryo, K. Murakami, T. Kitamura, M. Imanishi, and Y. Mori, Appl. Phys. Express **12**, 065502 (2019).

[2] R. Tandryo, K. Murakami, K. Okumura, T. Yamada, T. Kitamura, M. Imanishi, M. Yoshimura, and Y. Mori, J. Cryst. Growth **535**, 125549 (2020).

[3] T. Sato, K. Nakamura, M. Imanishi, K. Murakami, H. Imabayashi, H. Takazawa, Y. Todoroki, D. Matsuo, M. Imade, M. Maruyama, M. Yoshimura, and Y. Mori, Jpn. J. Appl. Phys. **54**, 105501 (2015).

[4] F. Kawamura, M. Morishita, K. Omae, M. Yoshimura, Y. Mori, and T. Sasaki, J. Mater. Sci. Mater. Electron. **16**, 29 (2005).

[5] W. S. Cleveland and S. J. Devlin, J. Am. Stat. Assoc. **83**, 596 (1988).

[6] H. Yamauchi, R. Tandryo, T. Yamada, K. Murakami, S. Usami, M. Imanishi, M. Maruyama, M. Yoshimura, and Y. Mori, Jpn. J. Appl. Phys. **61**, 055505 (2022).

[7] T. Itami, M. Shimoji, J. Meijer, G. Vinke, C. Van Der Marel, and W. Van Der Lugt, Phys. B+C **142**, 145 (1986).

[8] L. Nordheim, Ann. Phys. **401**, 607 (1931).

[9] G. L. Hall, Phys. Rev. **116**, 604 (1959).

[10] C. Kittel, *Introduction to Solid State Physics*, Wiley, (2004).

[11] M. Morishita, F. Kawamura, M. Kawahara, M. Yoshimura, Y. Mori, and T. Sasaki, J. Cryst. Growth **270**, 402 (2004).

Chapter 6

Application of insights from in-situ electroresistometry

In Chapter 4, the author explored the fundamental properties and laid the foundation for interpreting the electrical resistance of the Ga-Na solution. By taking electrical resistance measurements, the author examined the behavior of the homogenization process, nitrogen dissolution, and the formation of CN^-. While some of these investigations resulted in unique and counter-intuitive findings, they demonstrated a strong correlation with crystal growth in Na-flux growth. Yamada *et al.* immediately applied the insights about the time-dependent nature of nitrogen dissolution to increase nitrogen concentration through an extended pre-growth holding period [1]. This approach facilitated the creation of a highly supersaturated solution in the Ga-Na-Li system and the selective dissolution of sapphire with Li addition [1]. Therefore, it is evident that electroresistometry constitutes a valuable investigative tool. However, the potential of this technology is not fully realized unless the insights obtained from in-situ monitoring studies are thoroughly applied.

In this chapter, we delve into the application of the insights gained from in-situ electroresistometry. One of these applications is the use of a novel temperature sequence, termed dynamic temperature growth. The author also employ electroresistometry as a means to investigate the impact of impurities. While the study presented here is not exhaustive, it provides readers with a sense of the potential applications for in-situ electroresistometry.

6.1 Dynamic temperature growth for enhanced nitrogen dissolution

In the research detailed in Chapter 4, the electroresistometry study of the Ga-Na solution suggested certain benefits associated with high-temperature processing. High

temperatures not only improve the homogenization process of the Ga-Na solution but also potentially enhance the nitrogen dissolution process, which is a crucial step in the Na-flux method for GaN growth.

However, a high-temperature environment is not necessarily beneficial for the actual crystal growth process of GaN. Specifically, high temperatures can reduce the supersaturation of the Ga-Na solution, which is essential for the formation of GaN crystals. Additionally, high temperatures can also increase the likelihood of GaN decomposition, further compromising the crystal growth process.

To utilize on the benefits of enhanced nitrogen dissolution at high temperatures while avoiding the drawbacks of GaN decomposition, the author proposes a novel temperature sequence, as illustrated in Fig. 6.1. In conventional temperature profiles, the temperatures remain constant throughout the entire process. However, in this dynamic temperature profile, the high-temperature phase is applied during the nitrogen dissolution process until the solution becomes supersaturated. Following this phase, the temperature is then lowered for the subsequent crystal growth process. This two-step temperature sequence seeks to take advantage of the beneficial aspects of both high and low-temperature processes, potentially optimizing the growth of GaN crystals.

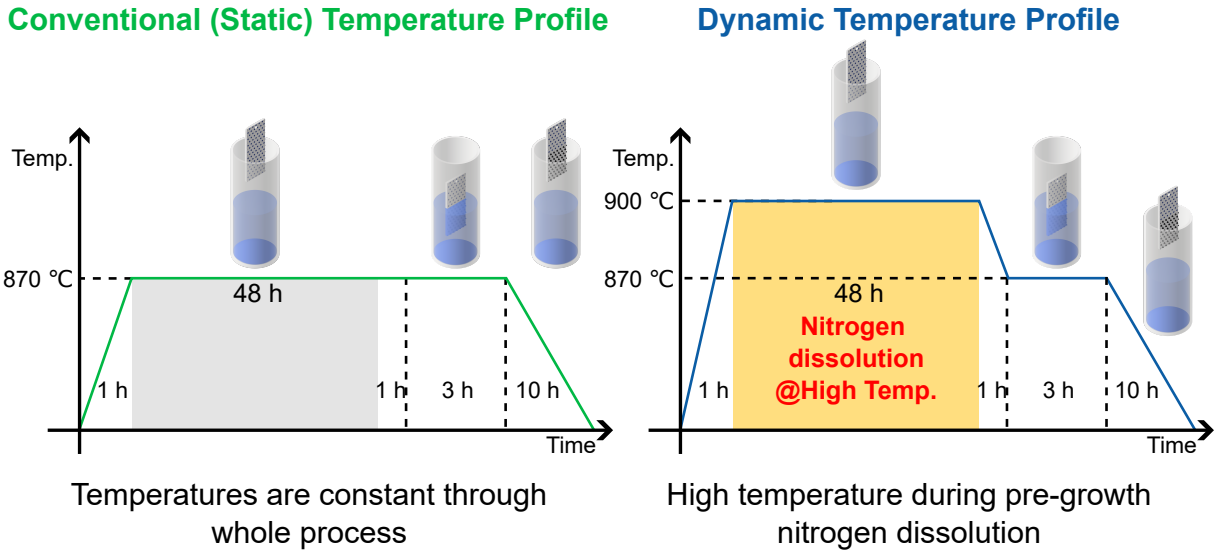

Figure 6.1: Temperature sequence of conventional static and dynamic temperature profile.

6.1.1 Improvement in growth rate

Crystal growth using dynamic temperature

To investigate the potential advantage of using the dynamic temperature profile, the author proceeds to carry out the crystal growth process, subsequently verifying the super-

saturation of the Ga-Na solution by evaluating the crystal size, following a similar method in Chapter 4. MPS substrate with the pattern outlined in Fig. 4.12a was utilized as the seed substrate and the temperature sequence presented in Fig. 6.1 was applied. Growth parameters were summarized as in Table 6.1.

Table 6.1: Growth parameters for dynamic temperature growth experiment.

PS Diameter [µm]	PS Pitch [µm]	Temperature [°C]	N_2 pressure [MPa]	Ga:Na:C [mol %]
250	550	Fig. 6.1	4.0	27:73:0.0
250	550	Fig. 6.1	4.0	27:73:0.5

Figure 6.2 shows the SEM images of the GaN crystal grown with dynamic temperature profile compared to that grown with conventional static temperature profile. The crystals grown in the Ga-Na solution have significant improvement in crystal size when applied with dynamic temperature profile.

Figure 6.3 provides a comparison of the crystal sizes grown with both the dynamic and conventional temperature profiles. A notable improvement is evident in the thickness of the crystal. The crystal grown under the conventional temperature profile measures 62.8 µm in thickness, while the one grown under the dynamic temperature profile is substantially thicker at 151.7 µm. This signifies an improved growth rate in the *c*-direction, achieving an enhancement of as much as 2.5 times. A similar improvement is also evident for the Ga-Na-C solution, though it is not as significant as with the Ga-Na solution.

Electrical resistance of Ga-Na solution with dynamic temperature profile

The growth rate improvement achieved by applying a dynamic temperature profile confirms that the nitrogen dissociation process is indeed enhanced at higher temperatures, as indicated by the electrical resistance shown in Fig. 4.20. The dissolution of gas in metals typically complies with Sievert's law and higher temperatures increase the solubility of gases. In the case of nitrogen, its dissolution into metal is an endothermic process, which is enhanced by increasing temperatures [2]. However, the seemingly high nitrogen concentration was also intriguing because the nitrogen might be desorbed back into gas upon lowering the temperature, given that its solubility will decrease. Nevertheless, the results of the crystal growth, which demonstrate an improvement in growth rate, suggest that the nitrogen concentration was indeed improved.

To further elucidate this mechanism, the author attempts to measure the electrical resistance of the Ga-Na solution using a dynamic temperature profile.

Figure 6.5 shows the changes in the electrical resistance ratio of the Ga-Na solution, measured at dynamic temperatures. The electrical resistance measured at 870 °C is also plotted here for comparison. For the dynamic temperature profile, the first 48 hours

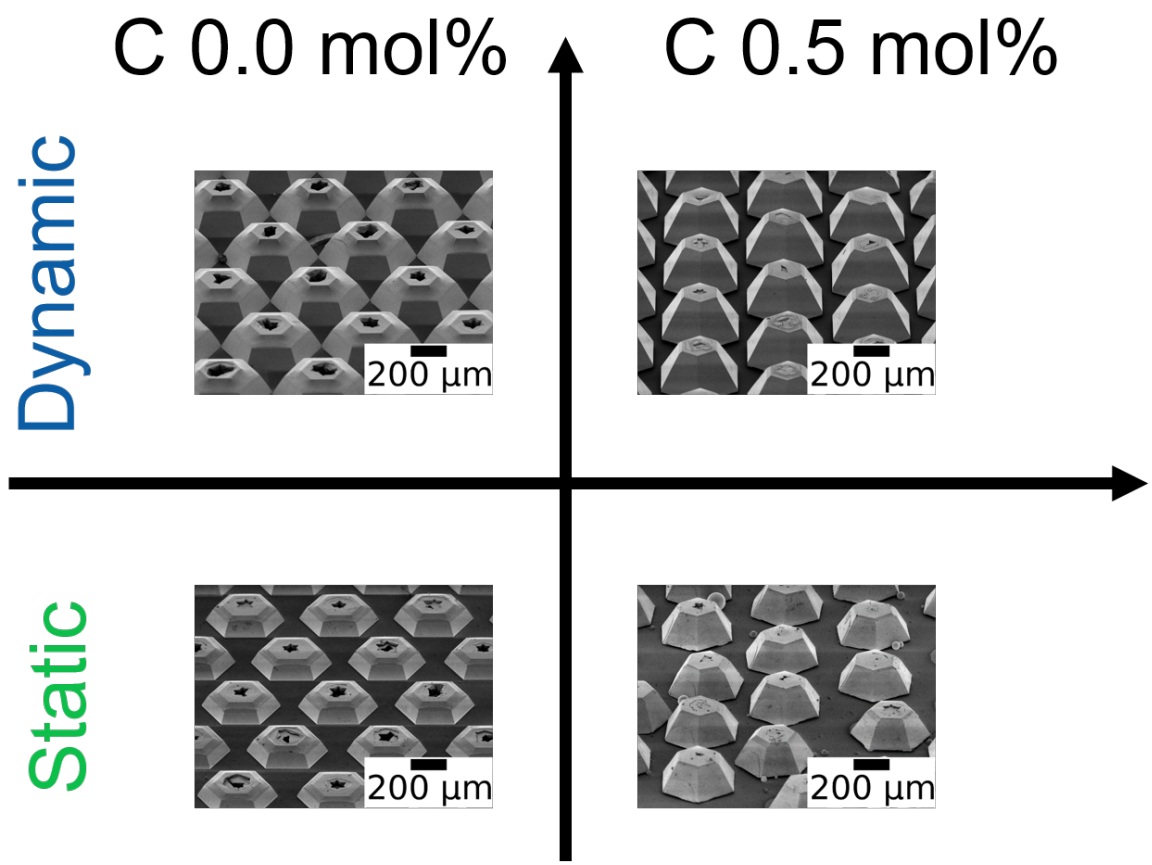

Figure 6.2: SEM images of GaN crystal grown with conventional and dynamic temperature growth.

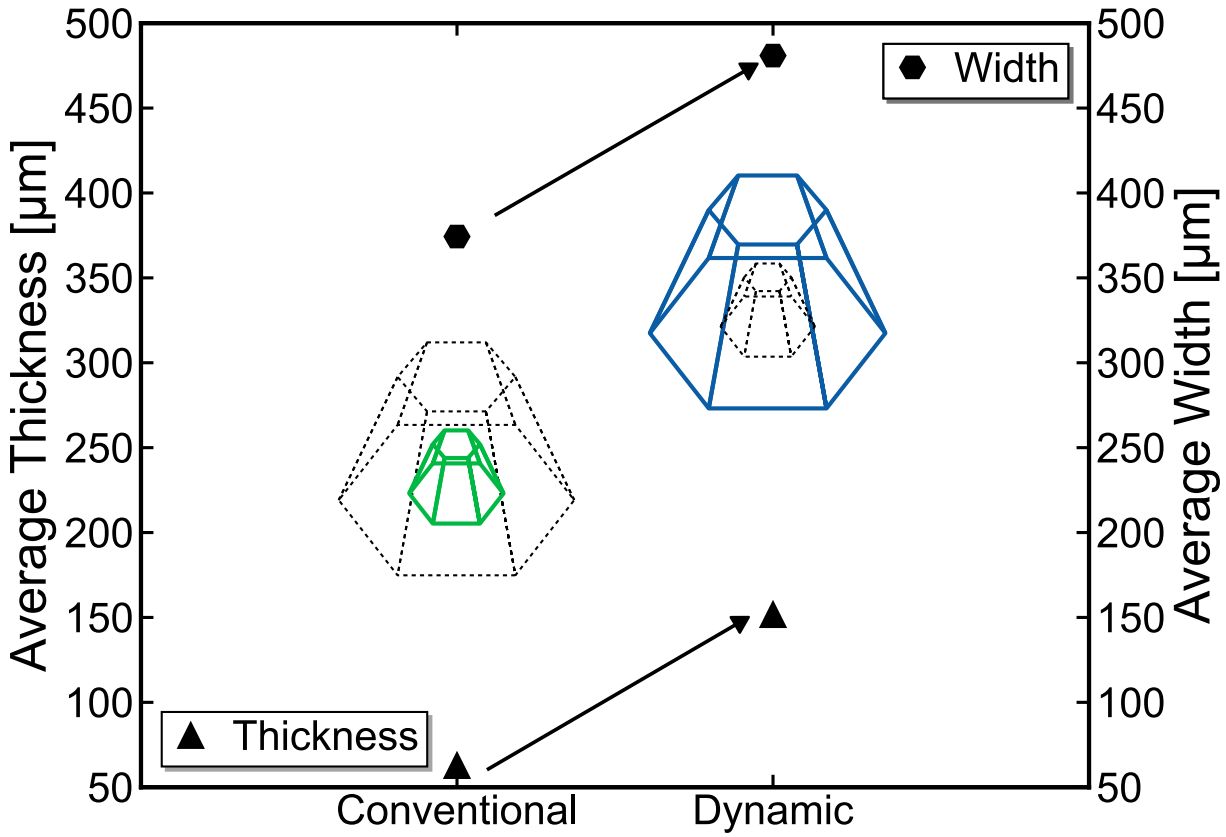

Figure 6.3: Evaluation of crystal size of GaN grown on point-seed in Ga-Na solution with conventional and dynamic temperature profile.

consisted of the high-temperature phase at 900 °C. During this phase, the electrical resistance significantly increased, consistent with the previous measurement at 900 °C in Fig. 4.20. The temperature was then lowered to 870 °C over one hour. The electrical resistance during this period experienced a decrease due to the temperature dependence of resistivity. However, the decrease in electrical resistance did not drop to the Ga-Na solution's electrical resistance measured at a constant 870 °C, but remained high.

Upon reducing the temperature to 870 °C, this temperature was maintained, and the electrical resistance measurement continued. During this phase, a decrease in electrical resistance was observed, but the degree of the decrease was small. Consequently, the electrical resistance undergoing the high-temperature phase remained high, compared to that maintained at a constant 870 °C.

The above results imply two crucial points. First, the significant increase in electrical resistance indeed resulted from the increased nitrogen concentration, not from the temperature coefficient of the electrical resistance. This conclusion can be drawn because the electrical resistance's drop due to decreased temperature was small. Second, the nitrogen concentration remained high, as indicated by the electrical resistance, which aligns with the crystal growth result. The reason for this can be deduced from the decreasing behavior of electrical resistance. If the decrease in electrical resistance can be interpreted as the desorption behavior, then the measurement had revealed a slow desorption property of the nitrogen from the Ga-Na solution.

6.1.2 Investigation of desorption properties

The measured electrical resistance intriguingly revealed the slow desorption properties of nitrogen upon lowering temperature being observed as a slight decrease. If the observed decrease in electrical resistance indicates an increase in nitrogen concentration, a reduction in crystal size would be an expected outcome. To verify this, a crystal growth experiment was executed employing the modified dynamic temperature profile shown in Fig. 6.5. Upon lowering the temperature, the crystal was not immediately immersed but held above the Ga-Na solution for a designated period. This period is referred to as the "second holding growth period". The duration of the second holding growth period was varied between 0 h, 1 h, and 5 h, with the hypothesis that the crystal would grow smaller with longer second pre-growth holding periods.

Figure 6.6 shows the relationship between the duration of the second pre-growth holding period and the size of the resulting GaN crystal. Crystals grown using the conventional static temperature profile are also plotted for comparison (marked in green).

Evaluations of both average thickness and width revealed that the crystals grown using the dynamic temperature profile (marked in blue) exhibits a higher growth rate. For the samples grown under the dynamic temperature profile, the crystal that was immediately

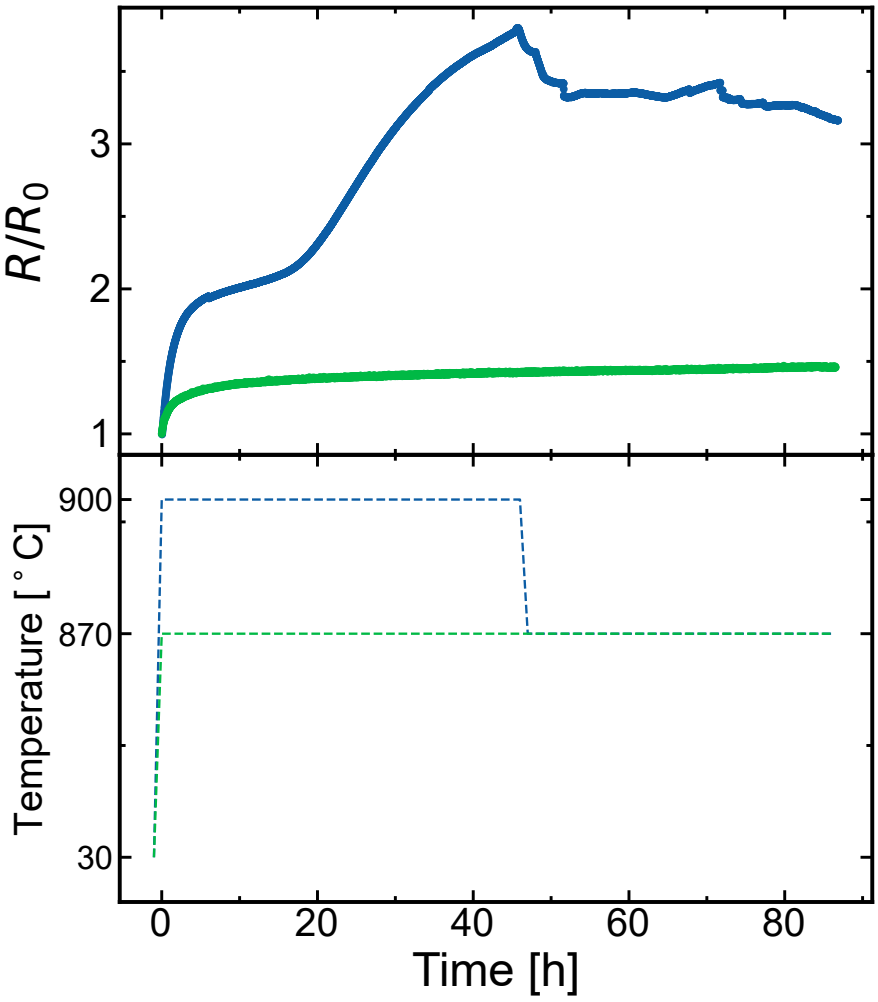

Figure 6.4: Changes of electrical resistance ratio of Ga-Na solution measured with conventional and dynamic temperature profile.

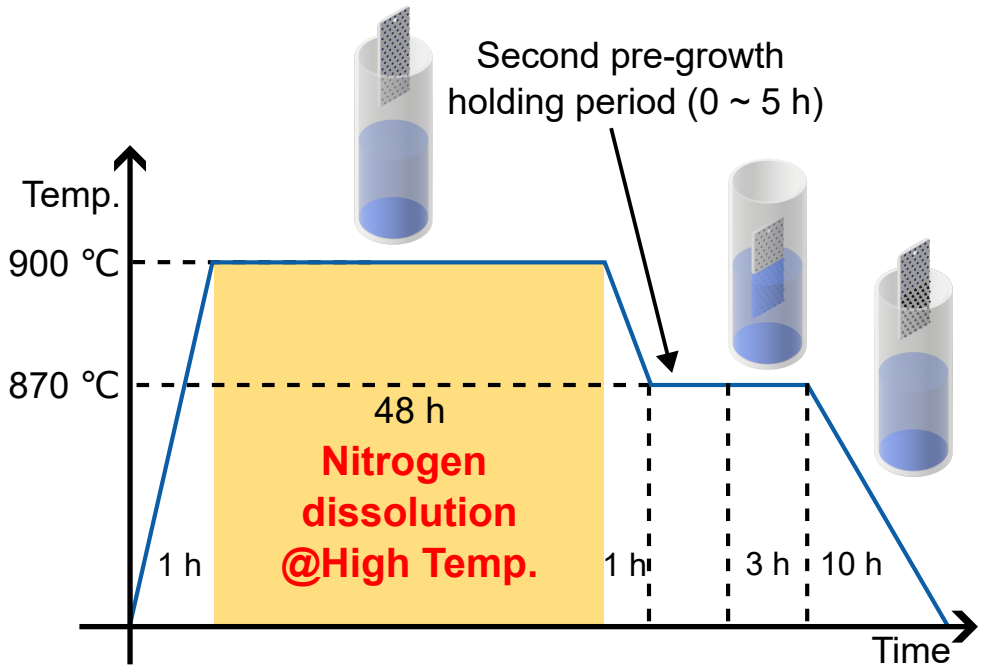

Figure 6.5: Schematic illustration temperature sequence to investigate desorption properties of nitrogen.

immersed (i.e., the second pre-growth holding period was zero) resulted in the largest size, while those that were immersed later yielded smaller crystals. Despite the desorption of nitrogen leading to a decrease in supersaturation, all crystals grown using the dynamic temperature profile demonstrated a higher growth rate, indicating that the desorption process is rather slow.

The process of nitrogen desorption happened while remaining in a nitrogen atmosphere, with the same pressure of 4 MPa as during the nitrogen dissolution. Nitrogen desorption was suppressed by the partial pressure of nitrogen in the gas [3]. Also, the process of nitrogen dissolution is preceded by the dissociation of nitrogen molecules into atoms. On the other hand, nitrogen desorption is preceded by the association (recombination) of nitrogen atoms [4]. This association requires two atomic nitrogen atoms to collide, which is a less likely occurrence.

6.1.3 Shortening the pre-growth holding period

The previous section outlined how the effectiveness of the dynamic temperature profile is attributed to two phenomena: the enhanced dissolution of nitrogen at high temperatures, and the slow desorption properties when the temperature is lowered. These characteristics can be exploited to achieve a highly supersaturated solution. Another possible application of these findings could be to accelerate the synthesis of GaN by achieving supersaturation more rapidly. In the growth process using the dipping technique, the Ga-Na solution typically requires a pre-growth holding period of approximately 15 hours before

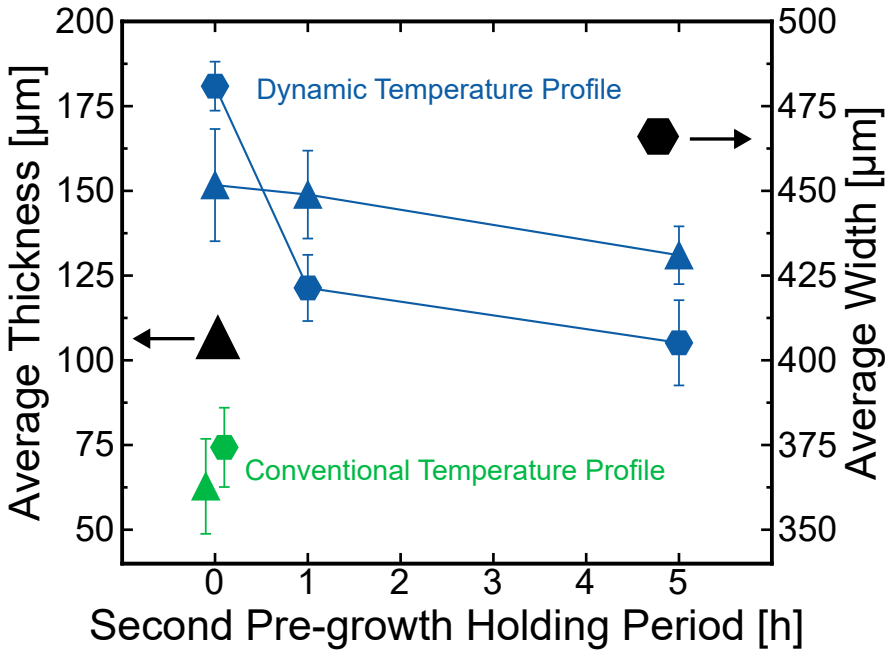

Figure 6.6: Average thickness and width of the grown GaN crystal as the function of second pre-growth holding period. Temperature sequence used for the corresponding growth is shown in Fig. 6.5.

the crystal growth can commence. As revealed in Section 4.3, this duration is determined by the time required for CN^- to form. To ensure crystal growth, the pre-growth holding period is usually set to 24 hours. However, a shorter process would be desirable from an economic and industrial standpoint.

The author sought to grow GaN crystals using the dynamic temperature profile, with the aim of investigating whether the crystals could be grown with a shorter pre-growth holding period.

Figure 6.7 shows the SEM images of the GaN crystals grown with a shortened pre-growth holding period of 10 hours, with a side-by-side comparison of crystals grown under a dynamic temperature profile and those developed under the conventional static temperature profile.

Crystal growth was not observed for either carbon-free or carbon-added Ga-Na solutions under the conventional temperature profile (maintained constant at 870 °C). However, when a dynamic temperature profile was introduced, crystal growth was made possible. With the carbon-free setup, the grown crystals were smaller and demonstrated inconsistent growth. In contrast, the carbon-added setup yielded more effectively grown crystals. These outcomes could suggest fundamental differences between carbon-free and carbon-added Ga-Na solutions. Ga-Na solution is slow in reaching equilibrium, and this process is expedited by the increased solubility of N_2 at higher temperatures. On the

other hand, the carbon-added solution reaches supersaturation significantly faster than its carbon-free counterpart, but the presence of carbon slows down the synthesis process, despite the rapid attainment of supersaturation. The high-temperature process permits a faster dissolution of carbon in sodium [5], which is likely also applicable to Ga-Na solutions. Given that the appearance of carbon-related resistance peaks relies on the presence of nitrogen, it is plausible that an accelerated nitrogen dissolution process could lead to a quicker dissolution of carbon itself.

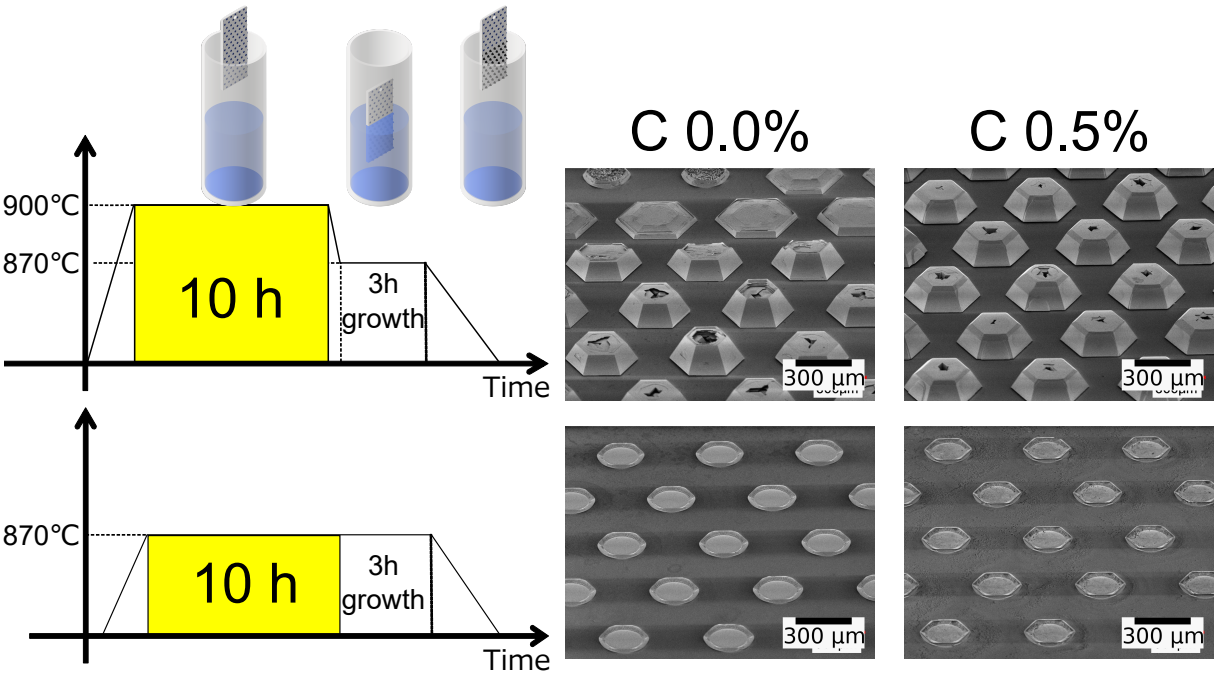

Figure 6.7: Scanning electron microscope images of GaN crystal grown with short pre-growth holding period.

6.1.4 Improvement in nucleation

Multi-point seed technology allows for the growth of GaN crystals through the coalescence process of small seed crystals. This method is effective for growing large-diameter GaN crystals while minimizing the number of pre-existing dislocations from the seed crystal. An obvious path to further reducing dislocations is to shrink the diameters even more. However, it has been empirically observed that GaN becomes more challenging to nucleate on a smaller point seed. The growth of GaN can be facilitated by adding Li into the Ga-Na solution, which significantly increases nitrogen solubility. Yet, as Li may incorporate into the crystal, an alternative approach is desired. Consequently, this study proposes the use of a dynamic temperature sequence as a means to achieve a highly supersaturated solution for the growth on small-diameter point seeds.

Experiments were conducted to grow crystals on seeds of diameters: 250 µm, 100 µm, and 50 µm. These were performed using the temperature sequence indicated in Fig. 6.1. Both carbon-free and carbon-added Ga-Na solutions were evaluated and compared.

The results of the crystal growth experiments are summarized in Fig. 6.8. Typically, a point seed with a diameter of 250 µm is used and has been found to grow stably. However, the growth of GaN on point seeds with diameters smaller than 100 µm proved to be extremely challenging using conventional growth conditions. When a dynamic temperature profile was employed, growth became possible on seeds with a 100 µm diameter. Despite this, crystal growth was still difficult with 50 µm-diameter seeds. Interestingly, during these crystal growth experiments, the author noticed that growth was possible even under the conventional temperature profile when using a carbon-free Ga-Na solution. This suggests that the presence of carbon could be the cause behind the difficulties experienced when growing on smaller point seeds.

The factors causing the inhibition of growth related to carbon remain somewhat mysterious. However, as growth difficulties increase in correlation with point seed size, there are two potential factors: interaction with the underlying sapphire substrate or issues related to a small *c*-plane.

Decreasing the diameter of the point seed results in an increase in the exposed area of the underlying sapphire. Albar *et al.* reported the formation of a series of pits on the sapphire surface due to etching by atomic carbon [6]. If this phenomenon also occurs in Ga-Na solution, then the etching of carbon contributes to the generation of impurities, which inhibit the growth of GaN crystals.

In carbon-added solutions, the formation of Ga-N is prevented as C-N exhibits stronger bonding energy. The bonding strength of C-N becomes weaker near the kink at the *c*-plane GaN surface [7]. From this, it can be deduced that the probability for GaN growth decreases as the *c*-plane GaN area becomes limited with smaller diameters. However, bond weakening is an atomic-scale phenomenon, and it seems implausible that changes on the micrometer scale could significantly impede growth.

The potential of carbon-free growth has often been neglected since the discovery of carbon addition. This is largely due to the slow process of nitrogen dissolution associated with carbon-free methods, which often leads to reduced growth rates. Moreover, controlling nucleation becomes challenging due to the excessive tendency at the liquid-gas interface in carbon-free systems. However, with a deeper understanding of the time-dependent and temperature-dependent characteristics of the carbon-free growth process, it is possible to optimize these process parameters for a more efficient and effective synthesis.

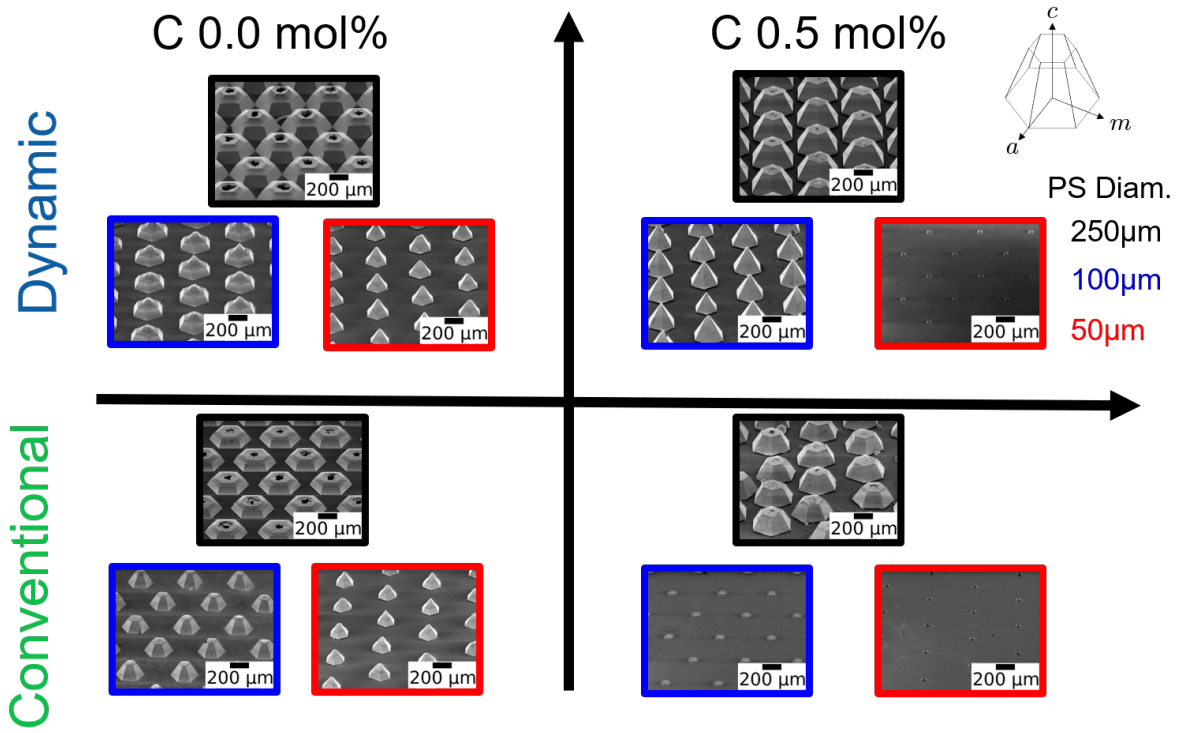

Figure 6.8: Scanning electron microscope images of GaN crystal grown on small point seed.

6.2 Inspection tool for impurity effect

Impurities can have various effects on the Ga-Na solution and the subsequent GaN synthesis process. Certain impurities can promote the process, such as the increased nitrogen solubility caused by the addition of Li [8] or C [9]. On the other hand, some impurities can be inhibitive, such as oxygen and moisture, as reported by Morishita [10].

Despite the significant impact of impurities, their effects are challenging to evaluate without the use of in-situ monitoring. As such, exploring the influence of impurities represents a potential area of interest for in-situ electroresistometry studies.

In this section, the author intentionally introduced impurities into the starting materials, Ga and Na, and measured the electrical resistance of the resultant Ga-Na solution. These experiments aimed to investigate the influence of various impurities on the electrical resistance of the solution, providing valuable insights into how these impurities may impact the GaN synthesis process. As noted in Chapter 3, it is important to emphasize that there's a significant degree of uncertainty in the resistance values due to dependencies on geometric factors, including the position of the probe in the current system. Therefore, while the exact resistance values carry a degree of uncertainty, our discussion will primarily focus on the observed trends and the behavior of these impurities.

6.2.1 Promotive impurity

Li has been reported to significantly enhance nitrogen solubility in Ga-Na solution, as observed by Morishita *et al.* [8]. If this is indeed the case, then a higher resistance value could be anticipated due to increased nitrogen incorporation in the Ga-Na solution. To investigate this effect, the author performed an experiment to measure the electrical resistance of a Ga-Na solution that was slightly doped with Li (0.02 mol %). This Li concentration was kept low to minimize any direct contribution of Li to the electrical resistance, which could potentially complicate the analysis.

Figure 6.9 shows the changes in electrical resistance of a Ga-Na solution with added Li. For comparison, the resistance of a Ga-Na solution both without any addition and with added carbon is also included in the plot. The electrical resistance of the Ga-Na solution with the addition of Li and C was higher compared to the Ga-Na solution without any additives, with the solution that included Li exhibiting the highest resistance.

Previous studies have noted an improved growth rate with the addition of either Li [11] or C [9], possibly due to enhanced nitrogen dissolution. It remains unclear, however, whether the increase in electrical resistance observed here can be directly linked to an increase in nitrogen concentration. Hubberstey and Roberts reported an increase in resistivity following the incorporation of nitrogen in a Li-Ba alloy [12]. In contrast, an increase in nitrogen concentrationled to a decrease in the residual resistivity when Ba was added into liquid Na [13]. It seems that changes in electrical resistivity behave differently, depending on the specific species involved.

6.2.2 Inhibitive impurity

Elements from Group IV such as silicon (Si) and germanium (Ge) are often introduced into the GaN layer to achieve and control the electrical properties of n-type GaN. In the Na-flux growth, crystal growth was observed with the addition of Ge or Sn, but the addition of silicon did not yield crystal growth. The reasons behind this discrepancy remain uncertain. For further insight, the author considered the inhibitive effect observed with oxygen, as reported by Morishita [10]. Oxygen is believed to decrease the solubility of nitrogen, a reduction that is accentuated with the incorporation of oxygen into the Ga-Na solution. This phenomenon might offer some understanding of the challenges encountered with silicon addition.

In this section, the author aims to investigate the underlying reasons for the inhibitive effects of these impurities by measuring the electrical resistance of Ga-Na solutions that contain these impurities.

To incorporate silicon (Si), the author used a Si single crystal wafer (111) which was cut into chips measuring 1 mm × 1 mm. The Si chip were added together with Ga and Na, and the amount of Si added was set to 1 mol %. For the inclusion of oxygen (O), gallium

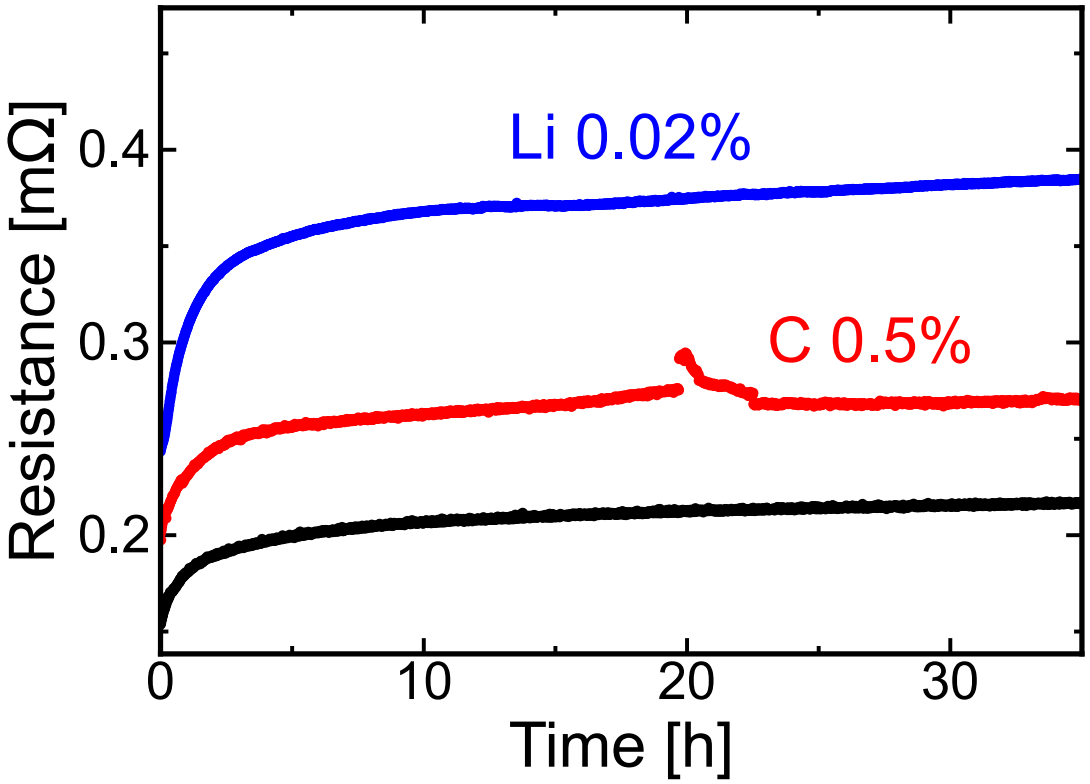

Figure 6.9: Changes of electrical resistance of the Ga-Na solution in comparison with the added with Li and C.

oxide (Ga_2O_3) powder was used. The weights of added Ga, Na, and Ga_2O_3 powder were adjusted such that the final molar ratio of Ga:Na was 27:73 mol % and the amount of added O was 1 mol %. Pressure decay experiments were also performed to examine any changes in nitrogen absorption behavior.

Figure 6.10a shows the electrical resistance of the Ga-Na solution, with incorporated Si, O, and a non-additive for comparison. Notably, for the Ga-Na solution containing Si, distinct differences were observed during the latter stages of measurement. The linear increase described in Eq. (4.6) with $R't$, which represents the nitrogen dissolution, was not observed. For the Ga-Na solution with incorporated O, the electrical resistance was also observed to behave differently. The electrical resistance of Ga-Na solution increased at the later stages, but the initial and overall increases in resistance were considerably small.

Pressure decay analysis indicated that the Ga-Na solution with incorporated Si demonstrated nitrogen absorption during the initial 15 hours, but this absorption ceased after approximately 20 hours. On the other hand, the Ga-Na solution with incorporated O did not exhibit any nitrogen absorption until around 30 h, at which point the decay began.

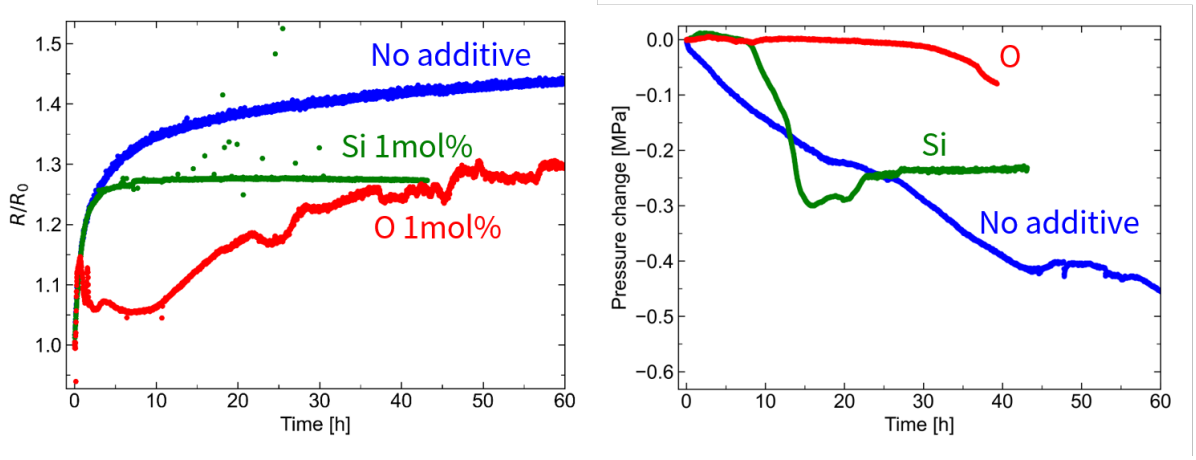

Figure 6.10: (a) Changes of electrical resistance ratio of Ga-Na solution incorporated with Si and O. (b) Pressure decay measurement on corresponding solution.

Discussion

The findings outlined above reveal distinct inhibitive effects induced by Si and O. In the Ga-Na solution incorporated with Si, nitrogen dissolution appeared to occur based on pressure decay measurements, however, the resistance did not exhibit a linear increase. According to the model illustrated in Fig. 4.15, the increase in electrical resistance is connected with the formation of Ga-N bonding. If this model is accurate, it would mean that the incorporation of Si hinders the formation of Ga-N bonds.

Figure 6.11 shows a photograph of the Ga-Na alloy post-measurement. The left-side photograph presents a typical Ga-Na solution alloy. For the Ga-Na-Si alloy in the right-side, black residues were seen precipitating above the Ga-Na alloy. Figure 6.11b shows the SEM image, indicating the crystalline plane of the residue. This residue was identified as sinoite (Si_2N_2O) via Powder X-ray Diffraction (PXRD) analysis (Fig. 6.12). This evidence suggests a reaction occurring between Si, nitrogen, and oxygen in the system. Consequently, it shows that nitrogen was absorbed into the solution despite of incorporation of Si. The inhibitive effect on Ga-N bonding might be associated with this reaction involving Si, or it could be due to the presence of sinoite; the exact reason is not clear as of now.

Conversely, oxygen did not appear to inhibit the formation of Ga-N bonding indirectly, but rather its presence seems to alter the nitrogen dissociation process. Nitrogen absorption in iron (Fe) and its alloys is known to be impeded by oxygen. This is attributed to the fact that oxygen, being a surface-active element, blocks surface sites where the nitrogen dissolution reaction could take place. Therefore, it is plausible to suggest that a similar mechanism might be at work in the Ga-Na system when oxygen is introduced.

Electroresistometry serves as a tool for evaluating the impact of impurities. However, its application within the current system used in this study was limited to the observation of trends. Determining the tolerable limits of impurity incorporation could be invaluable in an industrial setting, but such an endeavor necessitates a more quantitative approach, specifically with regard to assessing the impact of impurities on measurements. As a step towards addressing this limitation, future work should focus on converting resistance measurements to resistivity values, which would enable more in-depth investigations in this area.

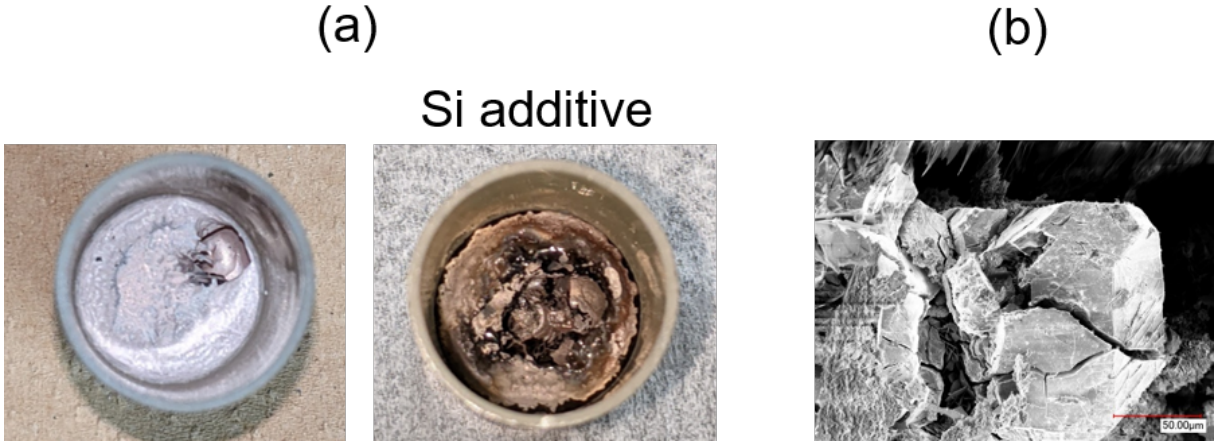

Figure 6.11: (a) Photograph of the Ga-Na alloy after measurement. Ga-Na solution incorporated with Si precipitated black residue on the surface of alloy. (b) Scanning electron microscope image of the black residue.

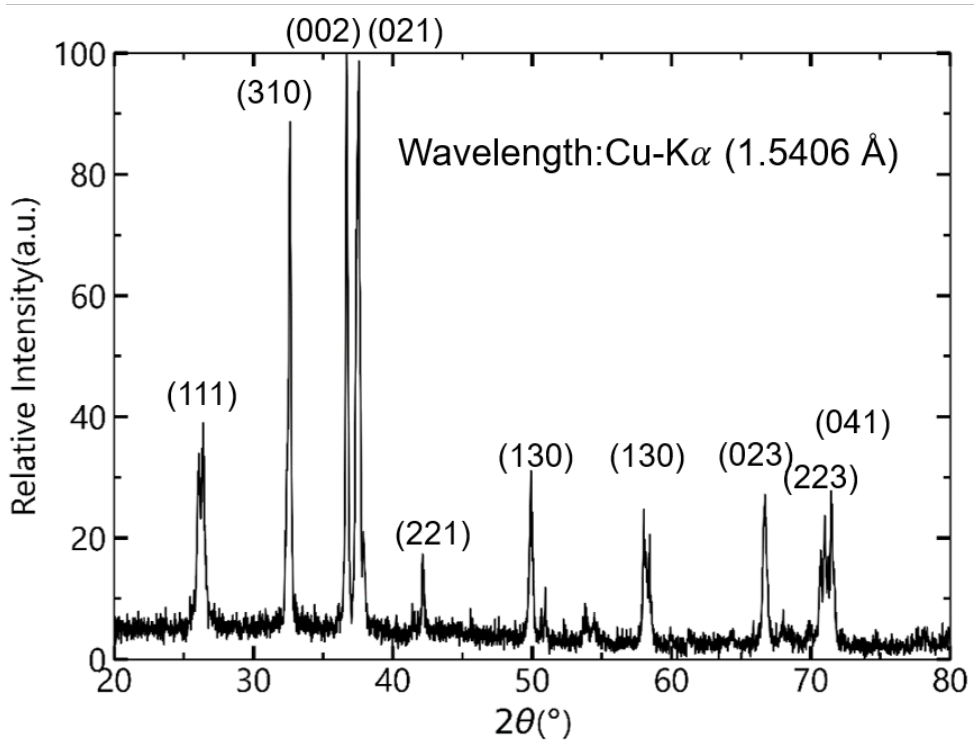

Figure 6.12: Powder X-ray Diffraction (PXRD) analysis of the residue collected from Fig. 6.11a. XRD matches with the pattern of Si_2N_2O.

6.3 Summary

In this section, the author demonstrated how insights obtained from electroresistometry studies can be applied for process optimization. This was accomplished by introducing a high-temperature nitrogen dissolution phase, referred to as the dynamic temperature profile. This temperature sequence enhances the synthesis process, resulting in improved growth rates, promoted nucleation, and shorter time required to create supersaturated solutions.

The utility of electroresistometry for investigating impurities was also demonstrated. It was found that adding promotive impurities such as Li resulted in an increase in electrical resistance, potentially indicative of improved nitrogen concentration. On the other hand, inhibitive impurities such as Si prevented the expected linear increase in resistance. This unusual behavior might suggest that Si interferes with the formation of Ga-N bonds. For a more in-depth analysis of the effects of impurities, it is recommended to convert the resistance measurements to resistivity values in future work.

References

[1] T. Yamada, M. Imanishi, K. Murakami, K. Nakamura, M. Yoshimura, and Y. Mori, J. Cryst. Growth **533**, 125462 (2020).

[2] G. Colonna, L. D. Pietanza, and M. Capitelli, J. Thermophys. Heat Transf. **22**, 399 (2008).

[3] K. Ito, K. Amano, and H. Sakao, Trans. Iron Steel Inst. Japan **28**, 41 (1988).

[4] C.-H. Eom, M.-H. Song, and D.-J. Min, ISIJ Int. **55**, 2694 (2015).

[5] R. Pulham and P. Hubberstey, J. Nucl. Mater. **115**, 239 (1983).

[6] J. D. Albar, A. Summerfield, T. S. Cheng, A. Davies, E. F. Smith, A. N. Khlobystov, C. J. Mellor, T. Taniguchi, K. Watanabe, C. T. Foxon, L. Eaves, P. H. Beton, and S. V. Novikov, Sci. Rep. **7**, 6598 (2017).

[7] T. Kawamura, Y. Yamada, H. Imabayashi, M. Maruyama, M. Imade, M. Yoshimura, Y. Mori, and Y. Morikawa, Jpn. J. Appl. Phys. **9**, 08JA04 (2010).

[8] M. Morishita, F. Kawamura, M. Kawahara, M. Yoshimura, Y. Mori, and T. Sasaki, J. Cryst. Growth **284**, 91 (2005).

[9] F. Kawamura, M. Morishita, M. Tanpo, M. Imade, M. Yoshimura, Y. Kitaoka, Y. Mori, and T. Sasaki, J. Cryst. Growth **310**, 3946 (2008).

[10] M. Morishita, PhD thesis (Osaka University, 2007).

[11] M. Morishita, F. Kawamura, T. Iwahashi, M. Yoshimura, Y. Mori, and T. Sasaki, Jpn. J. Appl. Phys. **42**, L565 (2003).

[12] P. Hubberstey and P. G. Roberts, J. Chem. Soc. Dalt. Trans., 667 (1994).

[13] C. C. Addison, G. K. Creffield, P. Hubberstey, and R. J. Pulham, J. Chem. Soc. Dalt. Trans. **2**, 1105 (1976).

Chapter 7

Conclusions

7.1 Conclusions

In this dissertation, in-situ electroresistometry of Ga-Na solution was proposed as a novel monitoring technology for Na-flux growth, whose in-situ monitoring is extremely difficult due to high temperature, high pressure, corrosive nature of Ga and Na. The basis for interpreting the electrical resistance data was established through systematic experiments and analysis. This in-situ monitoring technology offers to open new research opportunities on fundamental studies of Na-flux growth mechanism and both for industrial applications.

In Chapter 1, the author highlighted the growing concern of energy issues and the potential role of wide-bandgap semiconductor materials in solving these problems. Among these materials, Gallium Nitride (GaN) has shown exceptional promise, leading to high-performance devices across various applications. However, the availability of high-quality GaN material remains a significant bottleneck in the widespread development and application of GaN-based devices. Na-flux method has emerged as a promising technique for the crystallization of GaN. Nevertheless, one key element is still missing from Na-flux growth: in-situ monitoring. The ability to monitor the growth process in real-time provides invaluable insight into the growth dynamics, material quality, and overall process optimization. Incorporating this capability into Na-flux growth could revolutionize GaN synthesis, further accelerating the development of GaN-based devices and their applications in energy-saving technologies.

In Chapter 2, the author provided a comprehensive description of three major techniques used for the crystallization of bulk GaN: HVPE, ammonothermal method, and Na-flux method. The Na-flux method, compared to the other two methods, operates under milder process conditions and is advantageous for the growth of large-diameter GaN crystals. The author further discussed the technological progress made in Na-flux GaN growth. In recent years, improvements in crystal quality, growth rate, and size

have been achieved. However, many aspects of the Na-flux growth process remain poorly understood. There is a significant opportunity for further research into the fundamental mechanisms of Na-flux growth, which could lead to further enhancements in the technology. This includes in-depth studies of the solution behavior, the influence of various process parameters, and the development of in-situ monitoring techniques.

In Chapter 3, the author introduced electroresistometry as a potential in-situ monitoring technology for the Na-flux GaN growth process. This technique measures the electrical resistance of the solution over time, which can provide valuable insights into the various stages of the growth process. The basis for using electroresistometry lies in the fact that electrical resistivity is a structural-sensitive property that can reveal information about the chemical bonding state in the solution. The key components of the electroresistometry system designed by the author for monitoring the Na-flux growth process are as follows:

- The 4-point probe measurement technique is utilized to measure the low-resistive liquid metal of Ga and Na. This technique offers high accuracy, especially for low-resistance materials. High-temperature measurements, however, could introduce thermoelectric effects due to temperature differences between two dissimilar metal junctions. To cancel these effects, the author employs an offset-compensated method.

- Tantalum (Ta) wire is chosen as the electrode material for electrical resistance measurement of the Ga-Na solution in the Na-flux growth. Although Ta is known to react with Ga at high temperatures, in Ga-Na solutions with low Ga content, Ta does not exhibit corrosive reactions. Moreover, the successful growth of transparent GaN crystals was demonstrated even with the immersion of Ta in the Ga-Na solution.

- The electroresistometry setup also includes the monitoring of other growth parameters such as temperature and pressure (including back pressure). These additional measurements provide valuable data that can be used for correlation analysis with the electrical resistance data, which was discussed in detail in Chapter 4

The operational testing of the designed system was carried out by measuring the electrical resistance in liquid Ga and Na. The results successfully indicate the positive temperature coefficient and phase transformation, thus demonstrating the system's accuracy in measuring electrical resistance. However, the conversion from electrical resistance to resistivity presents challenges due to geometric factors in a crucible with a inner diameter of 17 mm. The effective current spreading area was approximated to be within a radius of 6 to 7 mm around the probe. The probe position in relative to the crucible become

sensitive. Consequently, the comparison of the resistance across the measurement is difficult. Nevertheless, the electroresistometry can still provides valuable insights from the measured electrical resistance behavior.

In Chapter 4, the author utilized in-situ electroresistometry to monitor the Ga-Na solution, establishing a basis for interpreting electrical resistance through systematic analysis and measurements in Ga-Na, Ga-Na-N, and Ga-Na-C-N systems. Key findings from this chapter include:

- Homogenization: Liquid-liquid transformation from Ga and Na to a homogeneous Ga-Na solution is reflected in increasing resistance curve observed in the early stages of measurement. The saturation of the electrical resistance indicate the complete homogenization process. Temperature and composition dependence of the homogenization velocity was investigated. From the arrhenius plot, the calculated activation energy for homogenization in Ga:Na 27:73 mol % Ga-Na solution was 68.34 kJ/mol which was typically high, indicating slow process of homogenization through.

- Nitrogen Dissolution: The nitrogen dissolution process was identified by a linear increase in electrical resistance. The increase in electrical resistance is attributed to the capture of free electrons carried by Ga atoms upon bonding with dissolved nitrogen. This model aligns well with the observed pressure decay curve, signifying nitrogen absorption. The continuous increase over an extended period of measurements revealed the time-dependent nature of nitrogen dissolution, which was further verified through crystal growth investigations. Electrical resistance measurements at 900 °C exhibited a significant improvement in the rate of electrical resistance increase.

- Formation of CN^-: The formation of CN^- was detected by electrical resistance measurements in the form of peaks and valleys. The reason for this phenomenon is unclear; however, the signaled peaks are significant as they indicate readiness for GaN synthesis. The timing of these peaks is influenced by volume and nitrogen pressure (concentration).

In Chapter 5, the author incorporated the dipping technology into the electroresistometry system, thus advancing towards in-situ monitoring of GaN growth. The crystal growth process of GaN was captured through the electrical resistance of the Ga-Na solution in the form of decreasing resistance. This decrease in electrical resistance was due to a decrease in the Ga/Na ratio as Ga atoms were consumed during the growth process. This growth monitoring measures the volumetric growth rate, which is strongly influenced by the surface area of the growth. This development represents a significant step forward in the ability to monitor and control the growth process of GaN crystals in real time.

In Chapter 6, the author applies the insights gained from the electroresistometry study of the Ga-Na solution described in Chapter 4. Electroresistometry study suggested the potential enhancement in both the homogenization process and nitrogen dissolution at high temperatures. The author proposes the use of a "dynamic temperature profile" as a novel temperature sequence for Na-flux growth. This approach temporarily utilizes a high-temperature process in the early stages of growth, and then performs subsequent crytal growth at lower temperatures. This technique yielded a 2.5 times improvement in the growth rate, demonstrating its potential for enhancing the efficiency of GaN crystal growth. Moreover, it could be utilized to improve nucleation on the growth of small diameter point seeds, as well as to shorten the overall growth process. Electrical resistance measurements were also utilized to observe the effects of impurities. With the addition of Li, the electrical resistance increased, indicating a possible enhancement in dissolved nitrogen content. However, the addition of Si seemed to inhibit the linear increase in the Ga-Na solution, which may explain the inhibitory effects due to Si. These results highlights the importance of understanding and controlling impurity effects in the Na-flux growth of GaN crystals.

7.2 Future outlooks

In-situ electroresistometry has proven to be an effective diagnostic tool in the Na-flux growth process, demonstrating its capabilities in real-time monitoring of the crystal growth. By accurately measuring changes in electrical resistance, it provides valuable insights into the processes of homogenization, nitrogen dissolution, and crystal growth.

However, this techniques are currently limited to semi-quantitative analysis, being measured as electrical resistance. The author recognized there is room for improvement in both technological aspects of in-situ electroresistometry and its correlating study. Here, the author descibes the future outlook and possible improvement:

- **Alternative electrode materials**

  Despite being corrosive-resistant and can be used for crystal growth, Ta wires form a nitride reaction at the surface. Change in contact resistance is not a concern with four-point probe, however the nitrogen in Ga-Na solution is inevitably consumed by the probes. Seek for alternative inert electrode is suggested.

- **Conversion to electrical resistivity**

  The current use of electrical resistance in run-to-run experiments offers limited comparison capabilities. If this technology can be expanded to provide qualitative analysis, it would considerably enhance its utility. To achieve this, it would be essential to convert the measured electrical resistance to electrical resistivity, a parameter that better reflects the material properties of the Ga-Na solution.

This conversion would allow a precise evaluation of the contribution of nitrogen and other elements, expressed through a resistivity coefficient ($\Delta\rho/c$). Additional parameters like temperature could also be accurately assessed. Once determined, the measured electrical resistivity could be further utilized to quantify the supersaturation levels of the solution, which has a direct influence on crystal growth. The ability to control these parameters could subsequently be employed to optimize the growth process, thereby enhancing reproducibility. Though this transition from electrical resistance to resistivity would require further research and technological development, the potential benefits it can bring to the process are significant.

- **Multi-probing**

  Heat and mass transport are fundamental to the crystal growth process, requiring an assessment that includes spatial information. Current electroresistometry techniques provide a holistic measurement of electrical resistance. While it is possible to shrink the probe for local measurements, this could complicate comparisons between different experimental runs.

  Therefore, future work could involve developing techniques for spatially resolved measurement, such as multi probing. Local measurement of resistance would correspond to local nitrogen concentration and the multi-probing allows the nitrogen concentration to be spatially resolved. This would not only permit a comprehensive mapping but could also provide insights into the movement and distribution of nitrogen in the liquid phase.

In conclusion, in-situ electroresistometry has opened up new opportunities for monitoring and controlling GaN crystal growth. The author hopes that further improvement with this technique and expansion in its applications, we can expect to see significant advancements in the production of high-quality GaN crystals.

Appendix A

Lesson from Innovation Design Course

In a world where technology is growing quickly, some new inventions still take time to be accepted and used widely. There are many examples of this slow progress in history. For example, Gallium Nitride (GaN) technology, which was key to making energy-saving LED lighting, was developed in the late 1990s. However, it took a while for this technology to become popular in the market. The big change came after the Tohoku earthquake when people realized the importance of saving energy. The market for LED lighting started to grow faster. The story is similar with video conferencing technology. This technology was not new when the COVID-19 pandemic hit, but the changes in society and immediate needs during that time made it more popular and widely used. Some technologies may be left behind if they do not meet the market's needs, but other new and innovative technologies can change the market's needs.

The author took part in an Innovation Design Course at Osaka University. In this course, the author learned how to analyze what the market needs, review his research topics, and understand how considering customer (industry) perspectives could help speed up the use of new technology. The course aimed to add new values to research technology and subsequently align it with future needs, or the prevailing market. The author had the opportunity to discuss the research topic with industry professionals who served as mentors. This chapter summarizes what the author learned from the Innovation Design Course.

A.1 Review on in-situ electroresistometry technology

The Innovation Design Course started with a review on in-situ electroresistometry technology with an active discussion and receiving feedback from industry professionals. The discussion focused on the following subsection.

A.1.1 Background

Semiconductor materials based on silicon have been the industry standard for creating electronic devices such as smartphones, computers, cameras, and televisions. However, the rate of innovation for silicon-based properties has seen a gradual decline, opening the door for Gallium Nitride (GaN) semiconductor devices. GaN devices are remarkable, as they offer performance improvements up to 100 times faster than their silicon counterparts. Some of the notable advantages provided by GaN over silicon include superior energy efficiency, increased device speed, miniaturization, and high operating voltage.

In 2015, world leaders met at the Paris Climate Conference (COP21) to tackle climate change problem. They agreed to aim for less than 2 °C increase in global warming. The origin of climate change is the greenhouse effect due to an unbalanced carbon cycle. Toward realization of carbon-neutral society, every member of society must have an opportunity to consciously use less energy and utilize it more wisely. GaN has a significant role to play here as it serves as the foundation for energy-saving devices, and is already being used in light-emitting diodes. The next goal for energy conservation lies in electric vehicles, and the rising number of such vehicles globally is anticipated to drive the market of GaN devices.

GaN has the potential to significantly impact the electric vehicle market, where high-quality GaN substrates become essential for robust device structures. However, the current state of GaN substrate technology struggles to produce high-quality substrates in large quantities. This leads to a high production cost for GaN substrates and associated device performance issues linked to reliability due to leakage currents originating from defects. As stated in Chapter 1, GaN devices are primarily manufactured on lower-cost foreign substrates such as Si, SiC, and sapphire, but this results in deteriorated performance. Therefore, innovation in GaN substrate technology is eagerly awaited to facilitate wider adoption of GaN devices.

GaN substrates have recently become more accessible largely due to active research and advance in three major growth techniques: HVPE, ammonothermal, and Na-flux, as detailed in Chapter 2. The Na-flux method is seen as having a significant economic advantage in producing GaN substrates, and it has been shown to produce high-quality, large-diameter GaN wafers. Even though the growth rate is slower with Na-flux, the resulting GaN wafer can serve as seed substrates for subsequent thick growth using HVPE. This collaborative approach paves the way for mass production of high-quality GaN wafers through slicing of thick bulk GaN as shown in Fig. A.1. However, significant challenges remain in the Na-flux synthesis process. The financial cost, time, and labor involved in producing Na-flux GaN wafers remain high. Additionally, reproducibility is a key issue that must be resolved before this technology can advance to the industrial production

stage. This highlights the need for ongoing research and development efforts to overcome these hurdles and realize the full potential of GaN substrates in various applications.

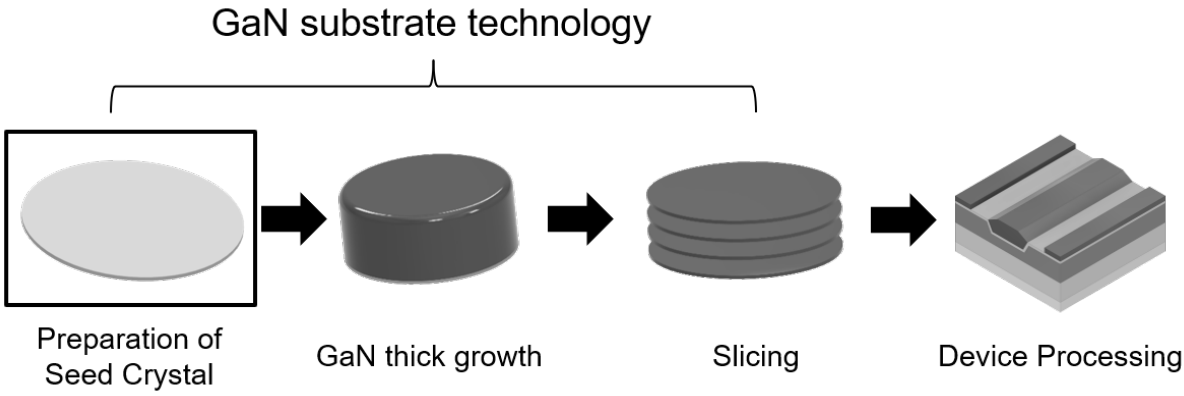

Figure A.1: Schematic illustration of the stages involved in mass production of GaN substrates for subsequent device processing.

In the semiconductor wafer production industry, achieving reproducibility is dependent on precise and real-time control of the synthesis process. This requires the capability to visualize or monitor critical parameters related to the synthesis process. However, monitoring the Na-flux process is complicated by high temperature and pressure conditions. Moreover, the corrosive nature of gallium and sodium further compounds these challenges. Given these constraints, the development of a novel in-situ monitoring approach is highly sought after. Such technology could significantly improve the reproducibility of the Na-flux growth process, effectively tackling one of the key obstacles in the mass production of high-quality GaN substrates.

A.1.2 Understanding the essence and application of the in-situ electroresistometry

The author has introduced in-situ electroresistometry in Ga-Na solutions as a novel approach for observing Na-flux growth. This proposition is based on the observed increase in electrical resistance in correlation with the rise in nitrogen concentration within the Ga-Na solution. Typical monitoring methods primarily depend on optical metrology, using reflectance to measure properties or aiding in visualizing the crystal growth process. However, electrical resistance offers a unique, highly sensitive means of observing changes in structure and chemical bonding states, as detailed in Chapter 3.

This method, with its sensitivity to chemical bonding states, offers a unique advantage in detecting the reaction of various species, including impurities within the Ga-Na solution. Given that the Na-flux growth process is highly sensitive to impurities, this unique aspect of the method is particularly beneficial. Furthermore, this approach yields

strong quantitative measurements, as electrical resistance inherently provides information about the materials involved. This, in turn, offers greater insight into the overall composition and quality of the materials being monitored, potentially enhancing the quality and efficiency of the Na-flux growth process.

In-situ electroresistometry technology as novel monitoring for Na-flux growth offers considerable advantages for both academic and industrial applications. For academia, it serves as an invaluable real-time diagnostic instrument, aiding in the exploration of the solution states used for GaN crystal growth. It facilitates a mechanistic study of GaN crystal growth through the Na-flux method, contributing to a deeper understanding of this vital process. Industries see the value in its ability to provide real-time data and insights into processes that were previously difficult to monitor. Its potential for improving efficiency, process optimization, and enhancing quality control is attractive for any sector where precision and accuracy are of importance.

A.1.3 Identifying the customers (user) of in-situ electroresistometry

The electroresistometry technique for crystal growth monitoring from the liquid phase is a new approach, unattempted in previous studies. The author's research focuses on its special design and development as a monitoring technique for Na-flux growth. Not surprisingly, the most significant interest in this in-situ technology comes from Na-flux growers themselves.

A.1.4 Potential Competitors

Potential competitors for the in-situ electroresistometry monitoring technology within the Na-flux method landscape could include optical visualization techniques. Such methods offer a straightforward, contactless monitoring capability. However, due to the high-temperature conditions of the Na-flux growth process, achieving effective visualization can be extremely challenging. In this scenario, in-situ monitoring with electroresistometry stands out as a unique technique with the capability to monitor the process and is sensitive to presence of chemical species. While advantageous in quantitative measurement, interpreting the value of electrical resistance is not straightforward, adding a layer of complexity to its practical use.

A.1.5 Vision and goal of in-situ electroresistometry

The ultimate aim of developing in-situ electroresistometry technology is its practical application in industrial-scale Na-flux growth reactors for the production of large-diameter GaN crystals.

To advance towards this objective, the Innovation Design Course introduced the concept of Objective and Key Results (OKRs) [1] as a framework for designing the research goal. This framework involves setting "key results" necessary for the realization of the "objective". The establishment of key results uses a measurable metric, providing a quantitative way to track progress and define success.

In the context of the development of in-situ electroresistometry technology, this framework can help set the course of action and provide a structure for achieving the final goal as indicated in Fig. A.2. The objective is the successful implementation of this technology in industrial Na-flux growth reactors. The key results include specific milestones such as demonstration of in-situ monitoring of GaN crystal growth (Chapter 5), scaling the electroresistometry technology to industry-scale size reactor, demonstrating its success control in industrial setting.

Objective and Key Results (OKRs)

Objective: In-situ electroresistometry for monitoring of industry-scale Na-flux growth reactor

KR1: Demonstrate in-situ monitoring of GaN crystal growth

KR2: Scaling electroresistometry measurement to industry-scale size reactor

KR3: Demonstrate improved reproducibility (to 90 %)

Figure A.2: Objective and Key Results for development of in-situ electroresistometry technology.

A.2 Direct discussion with industry professionals (mentors)

In the innovation design course, the author conducted mock presentations to industry professionals, including the Na-flux growers who serve as mentors. The author's proposal centered around the implementation of in-situ electroresistometry as an innovative technology within the Na-flux growth industry. The mentors provided feedback and further discussion about the proposed technology. These discussions enabled the author to gain valuable insights from an industry perspective, facilitating the reidentification of problems within the field. This section outlines the author's proposal for the application of in-situ electroresistometry.

A.2.1 Improving reproducibility: monitoring of impurity in Ga-Na solution

The author proposed the use of in-situ electroresistometry as a tool to address the reproducibility issue in the Na-flux growth. In Fig. A.3, previous studies have highlighted the problem of reproducibility in GaN crystal growth using Na-flux method. Despite using the same growth conditions, the yield of GaN crystals obtained varied significantly. This discrepancy suggests the presence of unaccounted parameters that influence crystal growth, in addition to the controlled factors such as temperature and pressure. The overall consistency of the crystal growth is only ~40 %.

Oxygen and moisture have been identified as impurities that hinder the nitrogen dissolution process [2]. Notably, sodium (Na) is prone to oxidation and could be a source of oxygen in the Na-flux solution. Furthermore, the use of alumina crucibles in the Na-flux growth also introduces oxygen into the system.

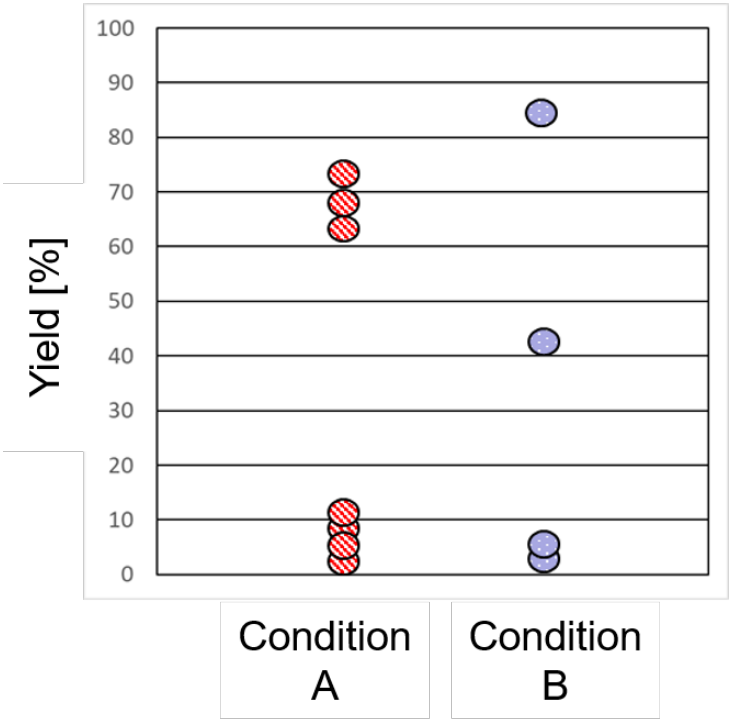

Figure A.3: Reproducibility in the Na-flux growth.

The electrical resistance of a Ga-Na solution reflects the nitrogen dissolution process, as detailed in Chapter 4. The influence of impurities was also discussed in Section 6.2. In the author's findings, with the addition of Si into the Ga-Na solution, the electrical resistance of the Ga-Na solution does not linearly increase and reflected the inhibitory effect of Si on Ga-N formation. This caused the electrical resistance to deviate from its expected linear increase, which would ordinarily result from the formation of Ga-N bonding upon nitrogen dissolution.

The author proposed in-situ electroresistometry as a method to monitor both the quantity of dissolved nitrogen and the influence of unintentionally incorporated impurities including commonly incorporated oxygen. Implementing this approach could lead to maintaining consistent nitrogen concentration levels—a crucial parameter that governs the supersaturation of the crystal growth. This could, in turn, offer better control and reproducibility in the growth process of GaN crystals. The author set the OKRs, which are outlined in Fig. A.4.

Objective and Key Results (OKRs)
Objective: Improve reproducibility of Na-flux growth (to 90 %)
KR1: Correlate the electrical resistance and the nitrogen concentration
KR2: Measure the influence of oxygen impurities on nitrogen dissolution
KR3: Demonstrate improved crystal growth reproducibility to 90 % by reducing oxygen source

Figure A.4: Objective and Key Results to achieve improved reproducibility in the Na-flux growth.

Feedback from mentors

The mentors expressed their appreciation for the importance of in-situ monitoring technology in improving reproducibility in growth processes. They have provided feedback and posed questions specifically related to the in-situ electroresistometry technique and its potential application in enhancing reproducibility. From their input, the author has gained valuable insights, which can be summarized as follows:

1. Questions: The mentors raised questions about the accuracy and reliability of the in-situ electroresistometry technique, particularly regarding the measurement of dissolved nitrogen concentration. They also inquired about the validity of using the increase in electrical resistance as an indication of nitrogen concentration, comparing it to other materials like Fe melt. These questions underscore how the industry values the importance of ensuring precise measurements and establishing a clear correlation between electrical resistance and nitrogen concentration. During this time, the author has yet to quantify the nitrogen concentration in current work.

2. Comments: The mentors commented that the author has not convincingly demonstrated the benefits of monitoring nitrogen concentration and impurities, such as oxygen. They suggest that the potential advantages of monitoring these parameters should be more explicitly highlighted. Furthermore, the mentors suggest that even

if oxygen levels could be monitored, it may not significantly change the approach to reducing oxygen incorporation. As a result, there may not be an immediate need for the utilization of this information.

Based on this feedback, one of the mentors recommended considering alternative applications and reconstructing the story of the presentation. They also suggested increasing the number of experiments to enhance the reliability of the results.

A.2.2 Other Applications

Following mentor feedback, the author reframed the presentation to highlight various potential applications of in-situ electroresistometry. Rather than hypothesizing future applications, the focus shifted towards introducing unique insights obtained from measuring the electrical resistance of the Ga-Na solution.

Enhanced growth rate through High-Temperature Solutions

The author discussed the potential for improving the Na-flux growth rate by leveraging high-temperature nitrogen dissolution phases, insights gained through the analysis of electrical resistance in the Ga-Na solution (Chapter 6). While the correlation with crystal growth was the primary focus of the presentation, some concerns were raised about the measurement's validity and accuracy.

Detection of CN^- Formation via Electrical Resistance

An intriguing observation was the identification of peaks and valleys related to the introduction of carbon into the Ga-Na solution, as outlined in Section 4.3. Although the implications of these findings are not yet fully understood, the mentors acknowledged this as a unique and interesting aspect of in-situ electroresistometry. The unexpected detection of these peaks underscores the potential of this method as a powerful real-time monitoring tool. This is especially relevant considering carbon's ability to suppress polycrystal formation and enhance GaN's growth rate, which is desirable in industrial applications.

Localized measurement of nitrogen concentration

Lastly, the author introduced a strategy for extending the use of electrical resistance measurements to capture localized nitrogen concentration by reducing the probe size. The mentors expressed interest in this in-situ monitoring approach, provided the author could convincingly demonstrate that the measurements indeed reflect the nitrogen concentration gradient. Additionally, the mentors recommended that the author provide a more convincing background for the necessity of measuring local nitrogen concentrations.

A.3 Summary

Through the Innovation Design Course work, the author endeavored to present a range of applications for in-situ electroresistometry technology. Engaging in discussions with the mentors provided valuable industrial perspectives and crucial lessons, including:

1. Customers purchase solutions, not products [3].

   What customers are seeking is not the in-situ electroresistometry technology in itself, but the solutions it can provide. Enhancing reproducibility is one of the key issues that needs addressing, and this does not necessarily mean that in-situ electroresistometry is the only viable solution. The author should consider alternative approaches that may also be available to tackle this problem. It's important that the focus remains on addressing the customer's needs rather than just promoting a specific technology. The author's work, then, is about demonstrating how technology can provide a superior solution to the problems customers face. The presentation and the research goal design should emphasize the necessity and urgency of the use of technology. Repeated and comprehensive discussions with the mentors have been instrumental in helping the author identify the solutions that are truly needed.

2. Unique and novel findings provide a strong asset

   Unique and unexpected findings are a powerful tool for innovation. In this case, the discovery of CN- related peaks and valleys not only emphasized the potential of electroresistometry as a tool sensitive to chemical bonding, but also underscored its innovative application in real-time monitoring of crystal growth processes. This intriguing finding sparked the interest of the mentors, highlighting the effectiveness of electroresistometry in revealing unexpected phenomena. The uniqueness of these results increases the perceived value of the technology and underscores the promise of its future applications.

3. Addressing the customer's concern

   Addressing the customer's concern is a crucial aspect in the promotion of a technology. In the case of in-situ electroresistometry, the validity and accuracy of measurements are key considerations for those planning to integrate this technology into their systems. During the discussions, the mentors raised questions about the validity and accuracy of nitrogen concentration measurements relative to electrical resistance, reflecting their concerns about the technology's ability to accurately quantify critical parameters. This highlights the industrial perspective in considering the in-situ monitoring technology - potential customers are looking for reliable metrics that can be used to achieve desired results. Therefore, it is important

to demonstrate the accuracy and reliability of the in-situ electroresistometry measurements, as this could substantially enhance its perceived value and promote its adoption in the industry.

4. Presenting in terms of customer's language

   Presenting the results in terms the customers can understand and relate to can greatly increase the value of the technology. In this case, translating the electrical resistance readings from in-situ electroresistometry into nitrogen concentration values may make the technology more understandable and relevant to potential users. This could prove to be more persuasive, as nitrogen concentration is directly related to the crystal growth process, whereas electrical resistance may not immediately convey its relevance and importance.

Future Outlooks

From the learning addressed above, the author has identified jobs-to-be-done to promote the adoption of in-situ electroresistometry. These tasks include the quantification of nitrogen concentration, clarification of mechanism and interpretation of the electrical resistance value, and demonstration of the measurement at an industrial scale reactor. Quantification of nitrogen concentration, for example, poses a significant challenge, as it would necessitate the conversion of the measurement into electrical resistivity. These tasks may not be achievable solely with the use of electroresistometry technology. It is essential to consider the integration of other methods and to explore potential collaborations that could help address these concerns. Simulation technologies or visual monitoring techniques could help in the interpretation of electrical resistance and quantification of the nitrogen concentration, which could substantially enhance the value and credibility of in-situ electroresistometry technology.

References

[1] J. Doerr, *Measure what matters: how Google, Bono, and the Gates Foundation rock the world with OKRs*, Portfolio/Penguin, (2018).

[2] M. Morishita, PhD thesis (Osaka University, 2007).

[3] C. M. Christensen, T. Hall, K. Dillon, and D. S. Duncan, *Competing against luck: the story of innovation and customer choice*, Harper Business, (2016).

List of Publication

Papers

[1] **Ricksen Tandryo**, Kosuke Murakami, Tomoko Kitamura, Masayuki Imanishi, Yusuke Mori,
"Monitoring of Ga-Na Melt Electrical Resistance and Its Correlation with Crystal Growth on the Na Flux Method"
Applied Physics Express Vol. 12, p. 065502 (2019).

[2] **Ricksen Tandryo**, Kosuke Murakami, Kanako Okumura, Takumi Yamada, Tomoko Kitamura, Masayuki Imanishi, Masashi Yoshimura, Yusuke Mori,
"Temperature Dependence of Nitrogen Dissolution on Na Flux Growth"
Journal of Crystal Growth Vol. 535, p. 125549 (2020).

[3] Hyoga Yamauchi, **Ricksen Tandryo**, Takumi Yamada, Kosuke Murakami, Shigeyoshi Usami, Masayuki Imanishi, Mihoko Maruyama, Masashi Yoshimura, Yusuke Mori,
"Suppression of Newly Generated Threading Dislocations at the Regrowth Interface of a GaN Crystal by Growth Rate Control in the Na-flux Method"
Japanese Journal of Applied Physics Vol. 61, p. 055505 (2022).

[4] **Ricksen Tandryo**, Koichi Itozawa, Kosuke Murakami, Hitoshi Kubo, Masayuki Imanishi, Shigeyoshi Usami, Mihoko Maruyama, Masashi Yoshimura, Yusuke Mori,
"Monitoring of GaN Crystal Growth Rate in the Na Flux Growth via Electroresistometry of Ga-Na Solution"
Journal of Crystal Growth Vol. 617, p. 127292 (2023).

International Conferences

[1] **Ricksen Tandryo**, Kosuke Murakami, Takumi Yamada, Tomoko Kitamura, Masayuki Imanishi, Masashi Yoshimura, Yusuke Mori,
"Monitoring of nitrogen content in Ga-Na melt by electrical resistance measurement on Sodium-Flux method"
The 7th International Conference on Light-Emitting Devices and Their Industrial Applications (LEDIA2019)

Pacifico Yokohama Conference Center, Japan, Apr. 25, 2019, LEDIA-6–02, Oral Presentation.

[2] **Ricksen Tandryo**, Kosuke Murakami, Kanako Okumura, Takumi Yamada, Tomoko Kitamura, Masayuki Imanishi, Masashi Yoshimura, Yusuke Mori,
"Temperature Dependence of Nitrogen Dissolution on Sodium Flux Growth"
19th International Conference on Crystal Growth and Epitaxy (ICCGE-19)
Keystone, Colorado, USA, July 29, 2019, Oral Presentation.

[3] Koichi Itozawa, **Ricksen Tandryo**, Kosuke Murakami, Masayuki Imanishi, Shigeyoshi Usami, Mihoko Maruyama, Masashi Yoshimura, Yusuke Mori,
"In-situ monitoring of GaN crystal growth by the Na-flux method via electrical resistance measurement"
The 40th Electronic Materials Symposium (EMS-40)
Online, Oct. 11, 2021, P1–B05, Poster Presentation.

[4] Bhavpreeta Pratap Charan, **Ricksen Tandryo**, Masayuki Imanishi, Kosuke Murakami, Shigeyoshi Usami, Mihoko Maruyama, Masashi Yoshimura, Yusuke Mori,
"Analysis of Helical Dislocations observed in HVPE GaN grown on Na-Flux GaN substrate"
The 9th International Conference on Light-Emitting Devices and Their Industrial Applications (LEDIA2022)
Pacifico Yokohama, Kanagawa, Japan & Online, Apr. 22, 2022, LEDIA6–05, Oral Presentation.

[5] Jumpei Fujiwara, Koichi Itozawa, **Ricksen Tandryo**, Kosuke Murakami, Masayuki Imanishi, Shigeyoshi Usami, Mihoko Maruyama, Masashi Yoshimura, Yusuke Mori,
"Effect of Ga/flux composition ratio and the amount of dissolved nitrogen on the growth habit of GaN crystal by the Na-flux point seed method"
The 9th International Conference on Light-Emitting Devices and Their Industrial Applications (LEDIA2022)
Pacifico Yokohama, Kanagawa, Japan & Online, Apr. 22, 2022, LEDIA6–03, Oral Presentation.

[6] **Ricksen Tandryo**, Kosuke Murakami, Hitoshi Kubo, Masayuki Imanishi, Shigeyoshi Usami, Mihoko Maruyama, Masashi Yoshimura, Yusuke Mori,
"Growth of small-diameter point seed GaN crystals in the Na-Flux method"
The 9th International Conference on Light-Emitting Devices and Their Industrial Applications (LEDIA2022)
Pacifico Yokohama, Kanagawa, Japan & Online, Apr. 22, 2022, LEDIA6–01, Oral Presentation , withdrawn.

[7] Shogo Washida, **Ricksen Tandryo**, Kosuke Murakami, Masayuki Imanishi, Shigeyoshi Usami, Mihoko Maruyama, Masashi Yoshimura, Yusuke Mori,
"Dependence of crystallinity of GaN crystals grown by the Na flux point seed technique on the off-angle of the seed substrate"

The 9th International Conference on Light-Emitting Devices and Their Industrial Applications (LEDIA2022)
Pacifico Yokohama, Kanagawa, Japan & Online, Apr. 22, 2022, LEDIA6–02, Oral Presentation.

[8] Hibiki Takahashi, **Ricksen Tandryo**, Kazuma Hamada, Shigeyoshi Usami, Masayuki Imanishi, Mihoko Maruyama, Masashi Yoshimura, Mori Yusuke,
"Surface planarization effect by Li addition on (20-21) GaN crystal growth in the Na-flux method"
International Workshop on Nitride Semiconductors (IWN2022)
Berlin, Germany, Oct. 11, 2022, PP 260, Poster Presentation.

[9] Bhavpreeta Pratap Charan, **Ricksen Tandryo**, Masayuki Imanishi, Kosuke Murakami, Shigeyoshi Usami, Mihoko Maruyama, Masashi Yoshimura, Yusuke Mori,
"Non-Destructive Characterization of Dislocations Observed in HVPE GaN Grown on Na-Fluxgrown GaN Substrate"
International Workshop on Nitride Semiconductors (IWN2022)
Berlin, Germany, Oct. 12, 2022, AT 145, Oral Presentation.

Domestic Conferences (Japan)

[1] Ricksen Tandryo, 村上 航介, 山田 拓海, 北村 智子, 今西 正幸, 吉村 政志, and 森 勇介
"Na フラックス法における 4 端子法抵抗測定を用いた窒素溶解量のモニタリング"
第 66 回応用物理学会春季学術講演会 (JSAP2019)
東京工業大学, 大岡山キャンパス, Mar. 12, 2019, 12a-W541–11, 口頭発表.

[2] 糸澤 孝一, Tandryo Ricksen, 村上 航介, 中村 幸介, 今西 正幸, 吉村 政志, and 森 勇介
"Na フラックス法における炭素添加の Na-Ga 融液電気抵抗に与える影響"
第 2 回結晶工学 ×ISYSE 合同研究会
東京大学本郷キャンパス, Nov. 20, 2019, 1P02, ポスター発表.

[3] Ricksen Tandryo, 糸澤 孝一, 村上 航介, 北村 智子, 山田 拓海, 今西 正幸, 吉村 政志, and 森 勇介
"Na フラックス法における GaN 結晶成長速度と Ga-Na 融液電気抵抗の関係"
第 2 回結晶工学 ×ISYSE 合同研究会
東京大学本郷キャンパス, Nov. 20, 2019, 1P03, ポスター発表.

[4] 糸澤 孝一, Ricksen Tandryo, 村上 航介, 今西 正幸, 吉村 政志, and 森 勇介
"Na フラックス法における電気抵抗測定を用いた結晶成長に伴う溶液状態変化のモニタリング"
第 67 回応用物理学会春季学術講演会
コロナウィルスのため未開催, Mar. 14, 2020, 14p-A302–5, 口頭発表.

[5] Ricksen Tandryo, 村上 航介, 山田 拓海, 北村 智子, 今西 正幸, 吉村 政志, and 森 勇介
“Dynamic 温度成長条件による Na フラックス中の窒素高濃度化”
第 67 回応用物理学会春季学術講演会
コロナウィルスのため未開催, Mar. 14, 2020, 14p-A302–6, 口頭発表.

[6] 糸澤 孝一, Ricksen Tandryo, 村上 航介, 今西 正幸, 丸山 美帆子, 吉村 政志, and 森 勇介
“Na フラックス法における電気抵抗変化と GaN 結晶成長の関連性”
第 3 回結晶工学 ×ISYSE 合同研究会
オンライン開催, Dec. 23, 2020, P–04, ポスター発表.

[7] 藤原 淳平, 糸澤 孝一, Ricksen Tandryo, 村上 航介, 今西 正幸, 丸山 美帆子, 吉村 政志, and 森 勇介
“Na フラックスポイントシード法における GaN 結晶成長形状の Ga 比率 _ 気相保持時間依存症”
第 3 回結晶工学 ×ISYSE 合同研究会
オンライン開催, Dec. 23, 2020, P–03, ポスター発表.

[8] Ricksen Tandryo, 村上 航介, 久保 等, 今西 正幸, 宇佐美 茂佳, 丸山 美帆子, 吉村 政志, and 森勇 介
“Na フラックス法における窒素溶解量促進に向けた窒素脱離特性評価”
第 82 回応用物理学会秋季学術講演会
オンライン開催, Sept. 12, 2021, 12p-N101–4, 口頭発表.

[9] 山内 彪我, Ricksen Tandryo, 山田 拓海, 村上 航介, 宇佐美 茂佳, 今西 正幸, 丸山 美帆子, 吉村 政志, and 森 勇介
“Na フラックス法を用いた GaN 結晶のホモエピタキシャル成長における転位挙動の調査”
第 82 回応用物理学会秋季学術講演会
オンライン開催, Sept. 12, 2021, 12p-N101–5, 口頭発表.

[10] 髙橋 響, 糸澤 孝一, Ricksen Tandryo, 宇佐美 茂佳, 今西 正幸, 丸山 美帆子, 吉村 政志, and 森 勇介
“Na フラックス法における Li 添加による (20-21) 面 GaN 単結晶の表面平坦化効果”
第 4 回結晶工学 ISYSE 合同研究会
オンライン開催, Dec. 23, 2021, P–02, ポスター発表.

[11] 鷲田 将吾, タンドリーヨ リクセン, 中島 達彦, 村上 航介, 今西 正幸, 宇佐美 茂佳, 丸山 美帆子, 吉村 政志, and 森 勇介
“Na フラックスポイントシード法における GaN 結晶品質の種結晶オフ角依存性”
第 69 回応用物理学会春季学術講演会 (The 69th JSAP Spring Meeting 2022)
神奈川県相模原市 (青山学院大学相模原キャンパス) &オンライン開催, Mar. 22, 2022, 22a-E202–4, 口頭発表.

[12] Ricksen Tandryo, 村上 航介, 久保 等, 今西 正幸, 宇佐美 茂佳, 丸山 美帆子, 吉村 政志, and 森 勇介
“Na フラックス法における窒素脱離特性を活用した微小 GaN 種結晶上の核発生成進”
第 69 回応用物理学会春季学術講演会 (The 69th JSAP Spring Meeting 2022)

神奈川県相模原市 (青山学院大学相模原キャンパス) &オンライン開催, Mar. 24, 2022, 24p-P04–1, ポスター発表（ポスター award).

[13] 高橋 響, Ricksen Tandryo, 濱田 和真, 村上 航介, 宇佐美 茂佳, 今西 正幸, 丸山 美帆子, 吉村 政志, and 森 勇介
“Na フラックス法を用いた Li 添加による {2021} 面 GaN 単結晶の平坦化”
第 83 回応用物理学会秋季学術講演会
東北大学川内北キャンパス (宮城県仙台市)+ オンライン, Sept. 21, 2022, 21a-C200–8, 口頭発表.

[14] 鷲田 将吾, Ricksen Tandryo, 濱田 和真, 中島 達彦, 村上 航介, 今西 正幸, 宇佐美 茂佳, 丸山 美帆子, 吉村 政志, and 森 勇介
“Na フラックス法における基板表面分解を起因としたファセット成長による転位減少効果”
第 83 回応用物理学会秋季学術講演会
東北大学川内北キャンパス (宮城県仙台市)+ オンライン, Sept. 21, 2022, 21a-C200–7, 口頭発表.

[15] Ricksen Tandryo, 糸澤 孝一, 村上 航介, 久保 等, 今西 正幸, 宇佐美 茂佳, 丸山 美帆子, 吉村 政志, and 森 勇介
“Na フラックス法における Ga-Na 融液の電気抵抗測定を用いた GaN 結晶成長速度のモニタリング”
第 83 回応用物理学会秋季学術講演会
東北大学川内北キャンパス (宮城県仙台市)+ オンライン, Sept. 21, 2022, 21a-C200–9, 口頭発表.

[16] Ricksen Tandryo, 糸澤 孝一, 村上 航介, 久保 等, 今西 正幸, 宇佐美 茂佳, 丸山 美帆子, 吉村 政志, and 森 勇介
“Na フラックス法における GaN 結晶成長速度の変化に伴う Ga-Na 融液の電気抵抗の変化”
第 5 回結晶工学 ISYSE 合同研究会
大阪大学吹田キャンパス銀杏会館, Nov. 18, 2022, P–02, ポスター発表 (講演奨励賞).

[17] 北野 春来, 髙橋 響, 中島 達彦, 濱田 和真, Tandryo Ricksen, 宇佐美 茂佳, 丸山 美帆子, 今西 正幸, 吉村 政志, and 森 勇介
“Na フラックス法を用いた半極性 (20-21) 面 GaN 結晶成長における結晶表面モルフォロジーの過飽和度依存性”
第 14 回ナノ構造エピタキシャル成長講演会
山口県宇部市（宇部市文化会館), Nov. 24, 2022, Th–P07, 口頭発表.

[18] 鷲田 将吾, 濱田 和真, Ricksen Tandryo, 中島 達彦, 村上 航介, 今西 正幸, 宇佐 美茂佳, 丸山 美帆子, 吉村 政志, and 森 勇介
“Na フラックス法における GaN 結晶表面のエッチピットを起因としたファセット成長による”
第 14 回ナノ構造エピタキシャル成長講演会
山口県宇部市（宇部市文化会館), Nov. 24, 2022, Th–P06, ポスター発表.

[19] 鷲田 将吾, 今西 正幸, 濱田 和真, Ricksen Tandryo, 村上 航介, 宇佐美 茂佳, 丸山 美帆子, 吉村 政志, and 森 勇介
“Na フラックス法におけるメルトバックを起因とするファセット成長を用いた GaN 結晶の転位減少効果”
第 15 回ナノ構造・エピキャピタル成長講演会
山形県山形市山形テルサ, June 16, 2023, Fr–P18, ポスター発表.